University of Massachusetts Amherst

ScholarWorks@UMass Amherst

October 2019

CHARACTERIZATION OF **β**-2-MICROGLOBULIN PRE-AMYLOID OLIGOMERS AND THEIR ROLE IN AMYLOID INHIBITION

Tyler M. Marcinko
University of Massachusetts Amherst

CHARACTERIZATION OF β-2-MICROGLOBULIN PRE-AMYLOID OLIGOMERS AND THEIR ROLE IN AMYLOID INHIBITION

A Dissertation Presented

by

TYLER M. MARCINKO

Submitted to the Graduate School of the
University of Massachusetts Amherst in partial fulfillment
of the requirements for the degree of

DOCTOR OF PHILOSOPHY

September 2019

Molecular and Cellular Biology

CHARACTERIZATION OF β-2-MICROGLOBULIN PRE-AMYLOID OLIGOMERS AND THEIR ROLE IN AMYLOID INHIBITION

A Dissertation Presented

by

TYLER M. MARCINKO

Approved as to style and content by:

_____
Richard W. Vachet, Chair

_____
Scott C. Garman, Member

_____
Peter Chien, Member

_____
Stephen J. Eyles, Outside Member

_____
Scott C. Garman, Graduate Program
Director

ACKNOWLEDGMENTS

ABSTRACT

CHARACTERIZATION OF β-2-MICROGLOBULIN PRE-AMYLOID OLIGOMERS
AND THEIR ROLE IN AMYLOID INHIBITION

SEPTEMBER 2019

TYLER MARTIN MARCINKO

B.Sc., LYCOMING COLLEGE

Ph.D., UNIVERSITY OF MASSACHUSETTS AMHERST

Directed by: Richard W. Vachet, Ph.D.

In dialysis patients, β-2 microglobulin (β2m) can aggregate and eventually form amyloid fibrils in a condition known as dialysis-related amyloidosis, which deleteriously affects joint, bone, and organ function, and eventually causes organ failure. To understand the early stages of the amyloid assembly process, we have employed a series of biophysical tools including chromatography, spectroscopy, and most especially, native electrospray ionization (ESI) together with ion mobility mass spectrometry (IM-MS) to study soluble pre-amyloid oligomeric species. We have also collaborated and integrated computational modeling to help better understand and rationalize the structural basis behind oligomerization.

Recently, several small molecules have been identified as potential inhibitors of β2m amyloid formation *in vitro*. In two chapters of this dissertation, we investigate if these molecules are more broadly applicable inhibitors of β2m amyloid formation by studying their effect on Cu(II)-induced β2m amyloid formation and examine their inhibitory mechanisms. We found that three molecules (doxycycline, rifamycin SV, and epigallocatechin gallate) can inhibit β2m amyloid formation *in vitro* by causing the

formation of amorphous, re-dissolvable aggregates. Rather than interfering with β2m amyloid formation at the monomer stage, we found that doxycycline and rifamycin SV exert their effect by binding to oligomeric species both in solution and in gas phase. Their binding results in a diversion of the expected Cu(II)-induced progression of oligomers toward a heterogeneous collection of oligomers, including trimers and pentamers, that ultimately matures into amorphous aggregates. EGCG is similar, generating a separate set of new oligomeric species that are ultimately off-pathway and distinctly non-fibrillar.

Using IM-MS, we show doxycycline and rifamycin promote the compaction of the initially formed β2m dimer, which causes the formation of other off-pathway and amyloid-incompetent oligomers that are isomeric with amyloid-competent oligomers in some cases. Epigallocatechin gallate appears to deplete an important tetrameric conformer. Overall, our results suggest that doxycycline, rifamycin SV, and epigallocatechin gallate are general inhibitors of Cu(II)-induced β2m amyloid formation. Interestingly, the putative mechanism of their activity is different depending on how amyloid formation is initiated with β2m which underscores the complexity of how these structures assemble with different methods *in vitro*.

With our ESI-IM-MS measurements, we revealed the presence of multiple conformers for the dimer, tetramer, and hexamer that precede the Cu(II)-induced amyloid assembly process, which is a brand new observation for this system. Experimental and computational results indicate that the predominant dimer is a Cu(II)-bound structure with an antiparallel side-by-side configuration. In contrast, tetramers exist in solution in both Cu(II)-bound and Cu(II)-free forms. Selective depletion of Cu(II)-bound species results in two primary conformers – one that is compact and another that is more expanded.

Molecular modeling and molecular dynamics simulations identify models for these two tetrameric conformers with unique interactions and interfaces that enthalpically compensate for the loss of Cu(II). Unlike with other amyloid systems, conformational heterogeneity seems to be an essential aspect of Cu(II)-induced amyloid formation by β2m. Moreover, the Cu(II)-free models represent a new advance in our understanding of this critical event in Cu(II)-induced amyloid formation, laying a foundation for further mechanistic studies as well as development of new inhibition strategies.

Finally, we end by presenting preliminary data on efforts that we have made in the lab to begin to better characterize the oligomeric conformers that we have detected. This is achieved primarily by performing tandem mass spectrometry experiments to study unfolding behavior/pathways, or by using solution phase labeling (i.e. deuterium) to enhance IM-MS.

TABLE OF CONTENTS

LIST OF TABLES

LIST OF FIGURES

LIST OF EQUATIONS

CHAPTER 1

INTRODUCTION

1.1 Protein folding, misfolding, and aggregation

For proper biological function, a newly synthesized polypeptide typically must fold into a defined three-dimensional structure. This is a process that is usually characterized by a series of dynamic chemical and physical events that are governed by thermodynamics and kinetics. The thermodynamics of the process is best illustrated by a protein folding landscape (Figure 1.1) [1]. Although this represents a general example, this three-dimensional landscape is unique to every single protein. Folding events typically lead to intermediate states, as molecules populate different states on the landscape from an unstructured ensemble at the top of the landscape to the lowest energy native state (N) at the bottom. It is important to note that this is an oversimplified *in vitro* example, and the folding process *in vivo* can be assisted by a class of proteins/enzymes known as molecular chaperones.
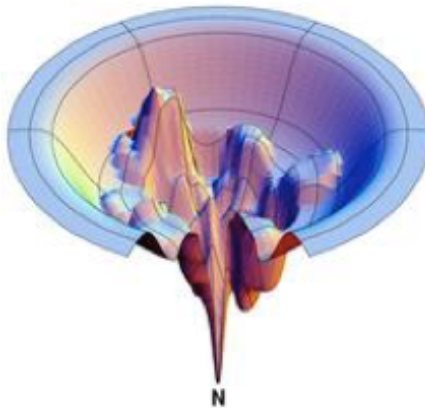
Figure 1.1: The general protein folding landscape (from ref. [1])

However, the same forces that allow proteins to eventually adopt their structure also allow for proteins to unfold or misfold (Figure 1.2) [2]. Although these misfolded species can diminish protein function, these states can also negatively impact cellular functions, and by extension, the health of the organism. Furthermore, some of these aberrant misfolded states are also capable of forming higher order oligomeric structures and aggregates (Figure 1.2). While there is a range of diverse structures that can emerge from misfolded proteins, they typically fall into either unstructured or structured states of varying stoichiometries. In this dissertation, we are specifically concerned with structured aggregates that form insoluble fibrillar deposits known as amyloids that have clear consequences on human health.
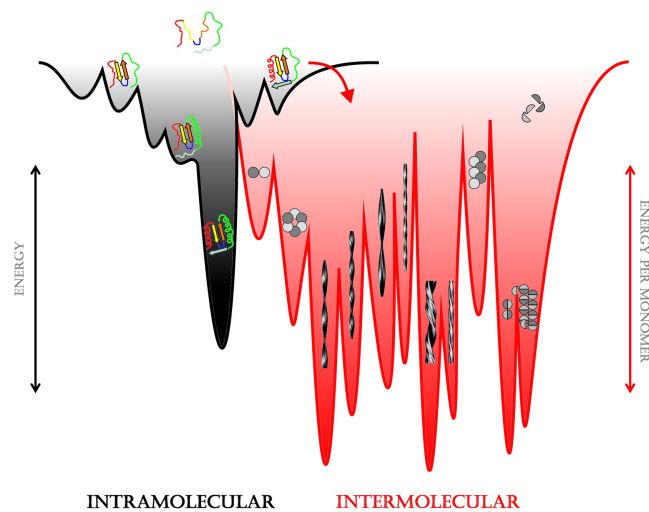
Figure 1.2: The misfolded/aggregation landscape (from ref. [2])

1.2 Amyloidosis and β-2 microglobulin

In general, amyloid fibrils are insoluble fibrils composed of protein that are deposited in organs and tissues [3]. They are characterized by a unique intermolecular β-sheet structure forming along an elongated axis that lends them their thermodynamic stability and characterizes their morphology [4]. There are several proteins that are

capable of forming amyloid fibrils, including amyloid β [5], tau [5], and α-synuclein [6]. Amyloid β and tau are implicated in Alzheimer's disease, while α-synuclein is associated with Parkinson's disease. A common feature amongst all amyloid-forming proteins is the similar morphology of the resulting fibrils despite them originating from differing proteins.

Although the general morphologies and structural characteristics of amyloid fibrils are similar, the pre-amyloid assembly process, especially the inducing mechanism, can be protein-dependent. Due to their nature, pre-amyloid oligomers are inherently transient, dynamic, and can be metastable. It has also become increasingly clear that these structures have heterogeneities that can influence the morphologies of the final aggregate structures [7,8]. These early steps of oligomerization, from induction to soluble aggregate formation, are critical to understanding the mechanisms of amyloid assembly.

Over the last decade or so, there has been emerging evidence that pre-amyloid oligomers can exhibit cytotoxicity [9]. This is apparently for multiple proteins and peptides that form amyloids, including Amyloid-β [10–14], α-synuclein [15], and IAPP [16], to name a few. This has recently shifted the paradigm (the so-called amyloid hypothesis) held by many in the field, as much of the surrounding biomedical dogma regarding amyloidoses has long held that the mature fibrils themselves are responsible for the symptoms of these diseases. Interestingly, there is also evidence for functional amyloids in bacteria and other microorganisms, which means classifying all amyloids as disease-causing is shortsighted as well [17]. For instance, there are reports that amyloids can function as a storage mechanism for protein toxins [18,19].

Furthermore, translational attempts at developing treatments that target the fibrils themselves have been met with many failures clinically, especially in the case of Alzheimer's [20,21]. This last fact alone should give both fundamental and applied/translational researchers pause when considering the development of new therapies for these diseases. While diagnostically challenging, the seemingly irreversible symptoms of amyloidoses often manifest over years, with fibril structures only detectable at later stages of the diseases, or more tragically, post-mortem. Based on these observations, it is not unreasonable to conjecture that these pre-amyloid oligomeric species play a critical role in early stages of these diseases. Thus, there is potentially great biomedical value in learning as much fundamental information about these structures as possible.

β-2 microglobulin (β2m) is a 99-residue protein composed of seven β-strands arranged in an anti-parallel β-sandwich motif tethered together by a lone disulfide bond (Figure 1.3) [22]. It is present on the surface of all nucleated cells [23]. Although it is normally a structural component of the class I major histocompatibility complex (MHC), elevated serum concentrations of β2m, as a result of long-term dialysis, result in deposition of β2m amyloid fibrils in patient joints and other organs [24,25]. The long-term consequences of these amyloid deposits are joint destruction and organ dysfunction, and this condition is known as dialysis-related amyloidosis (DRA) [26].

β2m's propensity to form amyloid fibrils has been studied extensively *in vitro*, and several conditions are capable of converting the protein from soluble to insoluble amyloids, which include, but are not limited to: low pH conditions [27], trifluoroethanol (TFE) [28], thermal denaturation [29], partial denaturation with lysophospholipids [30],

deletion of the first six amino acids [31], and incubation with catalytic amounts of Cu(II) [32–37]. Cu(II)'s potential importance to the manifestation of the disease is highlighted by a greater than 50% reduced incidence of DRA in dialysis patients treated with Cu(II)-free filter membranes [14]. However, Cu(II)-free membranes only prolong the onset of DRA and do not completely eliminate it.
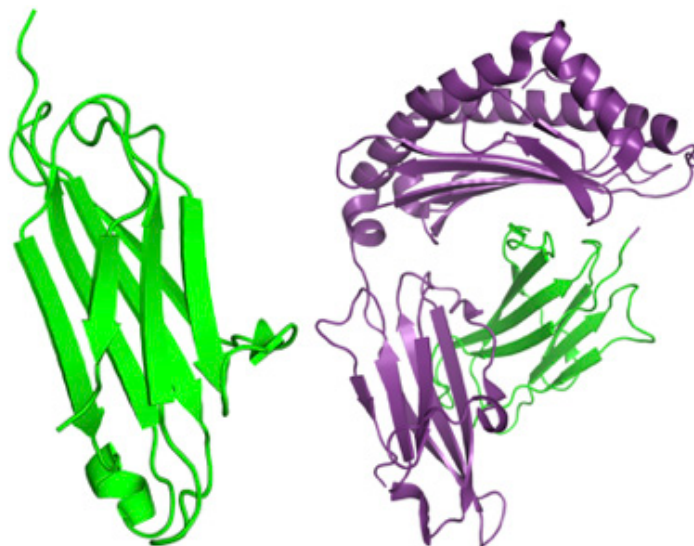
Figure 1.3: The structure of human β2m (shown in green) alone and in complex with the MHC (shown in purple) (PDB IDs: 1LDS and 4ZFZ, respectively)

We have previously studied in our group the *in vitro* Cu(II)-catalyzed oligomerization pathway that eventually results in the formation of amyloid fibrils [34,38]. This process begins with the binding of a single Cu(II) ion that destabilizes the native structure of monomeric β2m. Among the monomeric conformational changes, P32 importantly undergoes a *cis-trans* isomerization, F30 becomes solvent exposed, and R3 and D59 are repositioned to form intermolecular salt bridges that drive the formation of a dimer (Figure 1.4). The dimerization event then starts the formation of subsequent higher order oligomers (Figure 1.5). The dimer is capable of assembling with another dimer to form a tetramer. Notably, a second form of the tetramer is also detected where the Cu(II)

ions have been ejected. The newly liberated Cu(II) ions are then free to bind to new monomers, but they are not incorporated into the final amyloid fibril product, indicating that Cu(II) plays a catalytic role in the entire β2m amyloid formation process.
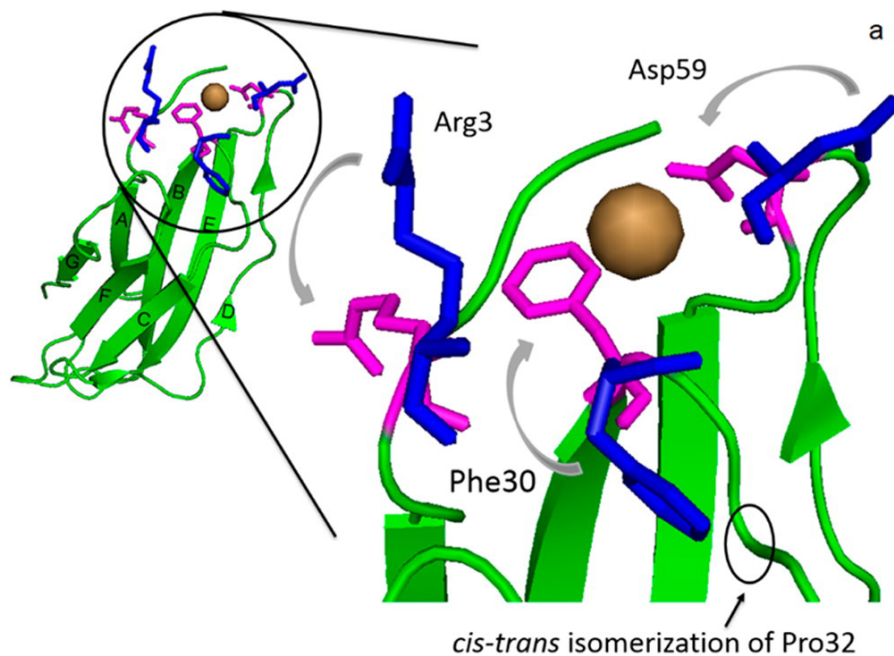
Figure 1.4: Conformational changes in the monomer upon Cu(II) binding that help facilitate dimer formation from ref. [24]

The ejection of Cu(II) from a form of the tetramer is a required step for amyloid formation, as the process up until that point is reversible with the addition of ethylenediaminetetraacetic acid (EDTA) [34]. A hexamer structure is eventually formed, and then presumably goes on to form larger n-mer structure that acts as a 'seed' that allows mature amyloid fibrils to be formed. The timescale for complete amyloid fibril formation can range from days to weeks, depending on conditions such as ionic strength and solution composition. In addition to these findings, we have also proposed the Cu(II) binding site [38], employed covalent labeling and docking experiments to generate

oligomeric models [35,36], evaluated the effects of other divalent metals [37], and found

new strand structural dynamics that contribute to oligomerization [39].
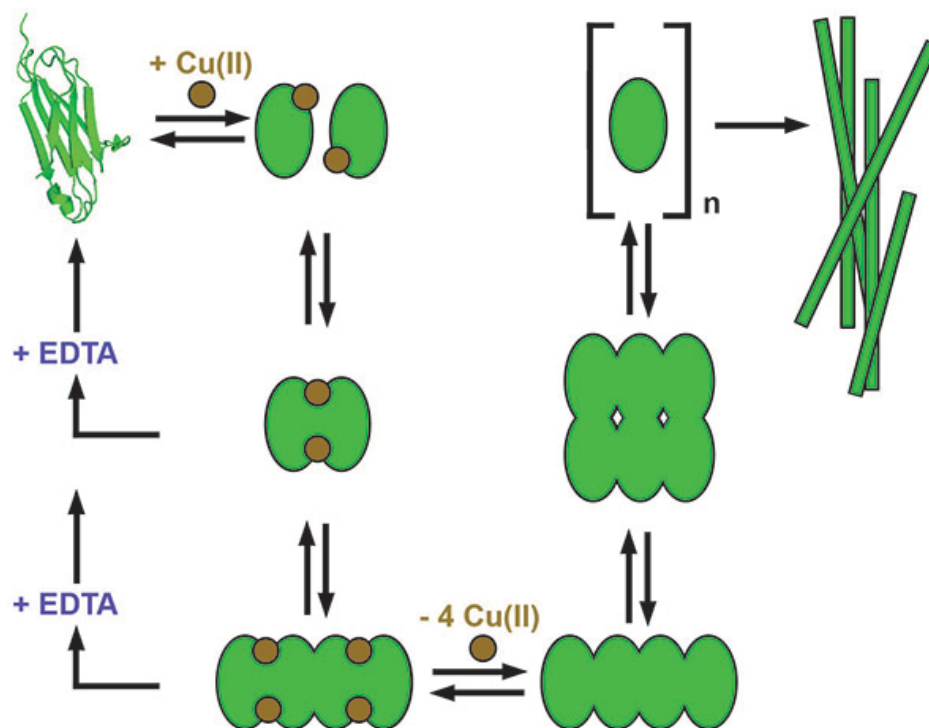
Figure 1.5: Proposed pathway for Cu(II)-catalyzed β2m amyloid formation

For some amyloid diseases such as Alzheimer's disease, cost of the disease is

staggering [40], but for DRA, the costs and incidence of the disease are not completely

clear. Some studies suggest that an incidence of >95% in patients on chronic long-term

dialysis (> 15 years) [41]. With no current treatments available, the only true cure is a

kidney transplant. With all amyloid forming proteins, understanding the fundamental

nature of this assembly process with molecular detail is integral to eventually developing

treatments for these diseases. For the purposes of β2m, the fact that the presence of Cu(II)

produces discrete oligomeric units that are observable and measurable make this a

valuable system for *in vitro* study. While Cu(II) and other divalent metal ions play important functional roles in biology, metal binding also has implications in amyloidoses like the aforementioned amyloid β and α-synuclein, as well as islet amyloid peptide, and Cu/Zn superoxide dismutase [42–44]. The commonality of Cu's involvement in amyloid formation means that not only does our work have importance for understanding amyloid formation with β2m system, but can also be broadly applicable to other systems and amyloidoses.

1.3 Amyloid inhibition

There is a significant interest in developing treatments for amyloid-related diseases. Due to the fact that our lab is mainly focused on bioanalytical chemistry, efforts to develop inhibitors from a translational perspective are outside the scope of our research. However, the value of studying amyloid inhibitors comes primarily from the fact that understanding the underlying molecular and structural mechanisms behind inhibition allows us to gain new fundamental understanding about amyloid formation. For example, parallel efforts to determine small molecule binding sites from another member in the lab have allowed us to develop a clearer rationale of inhibition [45].

One can envision several potential strategies for amyloid inhibition. For the purposes of our work, we elected to focus on small molecules specifically, although there is a large abundance of published examples of other modes of inhibition such as small peptides, biologics, or nanomaterials [46–48]. Potential outcomes from small molecule intervention could include stabilizing the native state of the target (thus preventing conversion to an aggregation-prone state), destabilizing or disrupting early oligomeric species, or promoting off-pathway (or non-productive) aggregates. Especially in cases

where aggregated species are still generated, it is important to evaluate whether or not

that these species are as harmful, or more harmful than actual pre-amyloid oligomers and

fibrils themselves [49].

Targeting the early stages of the disease (i.e. the pre-amyloid oligomers) is an

appealing one, as amyloid fibrils are remarkably stable and remain structured under

conditions that would denature most proteins [4,50]. The usage of small molecules as an

inhibition strategy at this stage of the process is a strategy that has been explored by other

research groups as well [51–54]. The work described in this dissertation is new in that we

have published the first efforts at investigating *in vitro* small molecule effects on Cu(II)-

catalyzed β2m amyloid formation.

1.4 Ion Mobility Spectrometry-Mass Spectrometry and its application to gas phase structural biology

Pre-amyloid oligomer precursors, like the ones explored in this dissertation, are of

keen interest to researchers, and there are many biophysical techniques, including mass

spectrometry (MS), that have been employed to study them *in vitro* [55–57]. Depending

on the application, MS has the ability to reveal both local information at the residue-level

but also give information about the overall protein structure. One of the many strengths

of MS in biomedical research is its versatility, and the main MS tool used in the work

described in this dissertation is ion mobility spectrometry-mass spectrometry (IM-MS).

IM-MS is a powerful technology to not only aid in studying amyloid forming

proteins, but also as a tool for structural biology in general. When coupled to a soft

ionization technique such as electrospray ionization (ESI), IM-MS has been increasingly

used to characterize protein complexes, as evidence shows that proteins maintain aspects

of their solution phase structures during the gas phase ion mobility measurements [58–65]. Numerous previous studies have demonstrated that ion mobility can provide useful insight into the stoichiometry and architecture of non-covalent complexes as well as the presence of conformational isomers for amyloid-forming proteins [51,65]. This information is in addition to the normal dimension of information given by mass spectrometry (i.e. molecular mass and abundance of the analyte in question). Collisional cross section (CCS) values, which are related to the molecular size of the protein, obtained from ion mobility measurements are found to correlate to solution-phase sizes.

Due to its usage in this dissertation, it is useful to understand how an IM separation occurs on a fundamental level. The particular version of IM used in this study is termed traveling wave-IMS (TWIMS) (Figure 1.6). Prior to IM separation, analyte ions are ionized under 'gentle' ESI source conditions to preserve their structure and assembly during the transfer from the solution phase to the gas-phase. This low energy transfer of protein ions to the gas phase gives us greater confidence in interpreting our results from a structural perspective.

Once ionized, analyte ions are focused into a beam and guided by optics through the rest of the instrument. Ions of specific m/z can be selected and isolated by quadrupole. After passing through a trapping region where collision energy can be applied, ions are introduced to the TWIMS cell. This cell is filled with a buffer gas, which is termed the drift gas, to a certain defined pressure.

For biological applications, the identity of the drift gas is usually nitrogen or helium [60]. An oscillating electric field of radio frequency (RF) and direct current (DC) voltages are applied to the cell via ring electrodes, and this field moves and propels ions

through the cell. Ions undergo collisions with the drift gas and are separated temporally based on differences in their collisional cross sections (CCS) (Figure 1.7) [66].
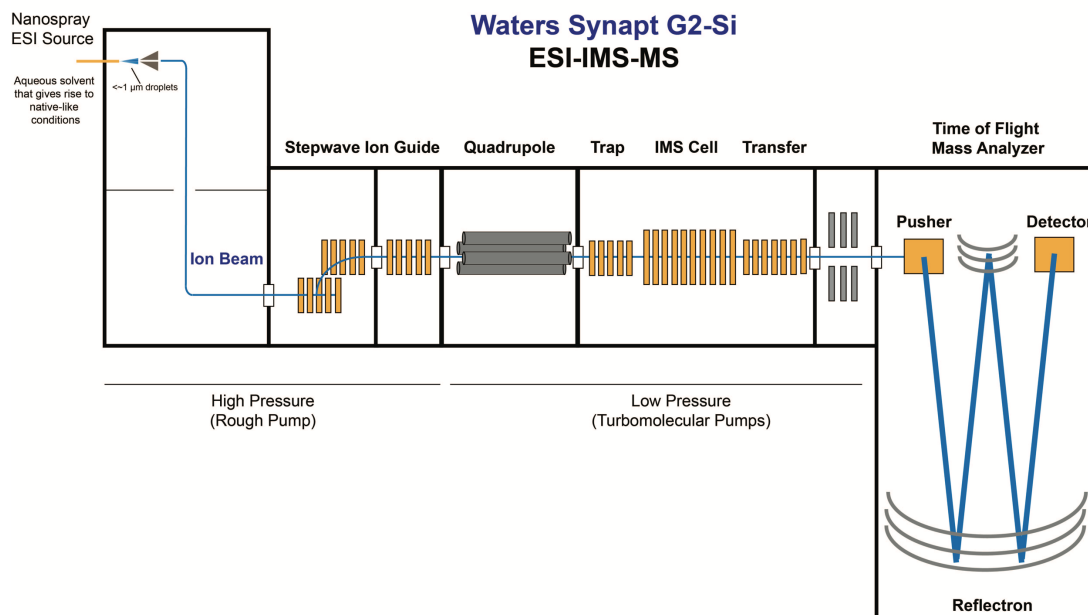
Figure 1.6: General diagram of the ESI-IM-MS instrument used in this dissertation

In Figure 1.6, the more compact (red) ion undergoes less collisions with the drift gas than the extended (blue) ion, and thus the red ion moves through the cell more rapidly. It is important to also note that IM is also useful for the multidimensional separation and differentiation of isobaric ions, which depicted in the bottom righthand corner of Figure 1.6. Overall, the main factors governing the TWIMS separation are the dependence of the drift time on the charge, CCS, and mass of the ion (in descending order). Due to the relatively higher field strength associated with TWIMS (relative to a lower strength field technique, like drift time-IMS), there is a much larger mobility dependence on charge.

Drift behavior is also influenced by the dynamic nature of TWIMS, as the electric field in the cell is dynamic by design. For example, the strong dependence of TWIMS mobility on charge means that a tetramer ion with eight charges will travel faster than a dimer with four charges or a monomer with two charges. Following an IM separation, ions are then pulsed into a time-of-flight (TOF) for mass analysis.
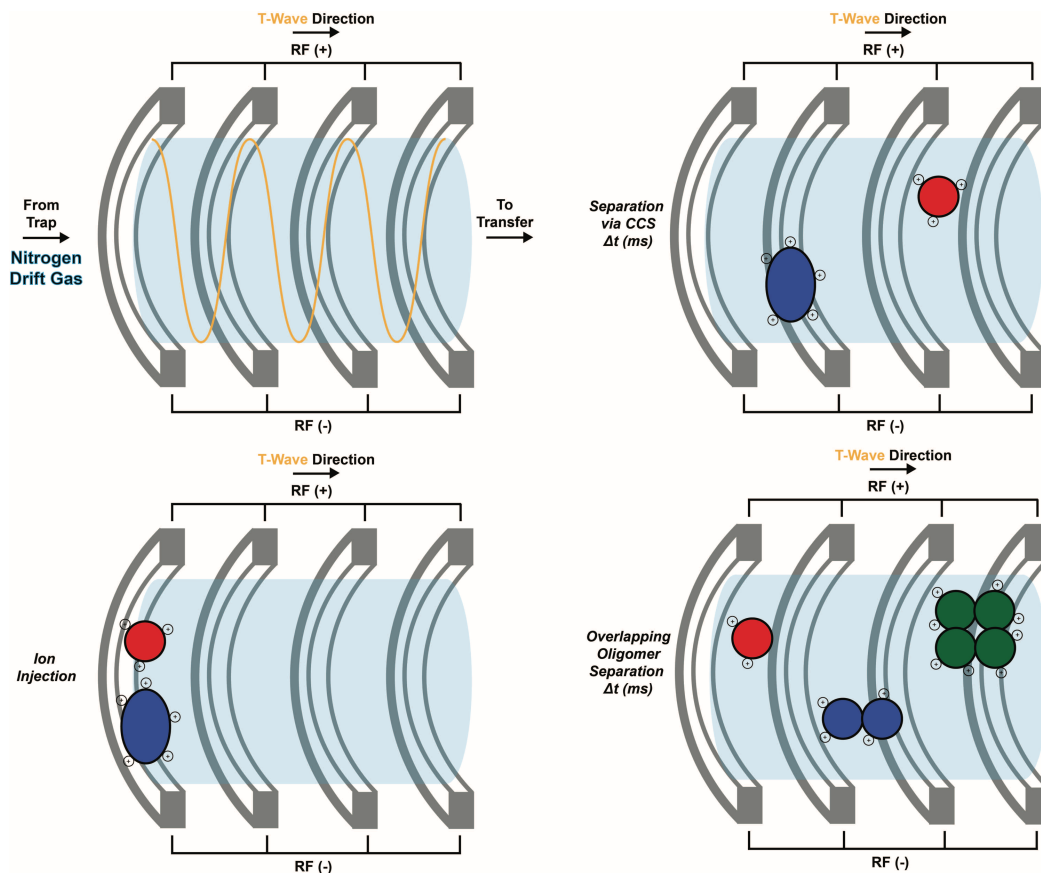
Figure 1.7: Example of a TWIMS cell, an IM separation of two molecules, and an IM separation of isobaric oligomer species

During the experiment, the *m/z*, abundance, and drift times of ions are measured. In order to relate drift time to structure, it is useful to convert drift time values to CCS values. The CCS value is a rotationally averaged cross-sectional area of the analyte. Experimental CCS values are determined from drift times through the IM cell via the construction of a calibration curve of known analytes. This calibration curve is obtained

using globular proteins whose CCS values have been directly determined by drift time-IMS (DTIMS) [67]. For these calibrants, the relationship between drift time and CCS in a TWIMS experiment is given by the Mason-Schamp equation (equation 1.1), where e is the elementary charge, N is the drift-gas number density, μ is the reduced mass of the ion and drift gas, k_b is the Boltzmann constant, T is the drift-gas temperature and K is the mobility of the ion [68,69]. Experimental CCS values are then estimated based on the calibration curve. CCS values can also be calculated from crystal structures and NMR ensembles via algorithmic methods such as projection approximation, trajectory, or exact hard sphere scattering, making it a valuable comparative structural tool [58].

$$\Omega = \frac{3e}{16N}\sqrt{\frac{2\pi}{\mu k_b T}}\frac{1}{K}$$

Equation 1.1: Mason-Schamp equation for calculation of CCS

One notable limitation of ESI-IM-MS is its structural resolution. Due to the nature of the technique, only coarse, low-resolution views of analyte structure are available. For example, residue positions (e.g. a sidechain becoming buried as part of a conformational change) are not resolvable in a typical ESI-IM-MS experiment. Generally, the consensus of the field seems be that differences in structure/CCS need to be on the order of a few (~2-3%) percent to be resolvable by TWIMS under the most optimal experimental conditions [70].

Despite the inherent low resolution nature of the technique, ESI-IM-MS can be utilized in concert with other techniques to obtain reliable structural information. For example, it has become common to complement ESI-IM-MS data with computational modeling via docking or molecular dynamics to propose structural models of proteins,

and in particular, non-covalent complexes [59,71–73]. This structural information available from ESI-IM-MS is further strengthened when other sources of structural data (e.g. nuclear magnetic resonance (NMR) distance constraints, or hydrogen-deuterium exchange (HDX) data) are included to constrain the number of possible structures generated during computational modeling and docking. This combination of techniques has allowed for greater structural insights into particularly challenging experimental systems, such as pre-amyloid oligomers, that seem to be resistant to traditional structural biology techniques like x-ray crystallization or NMR.

1.5 Conformational heterogeneity and analytical solutions

The primary analytical challenge with working with protein aggregates arises from the structural heterogeneity that seems to be inherent to amyloid systems. Pre-amyloid oligomers can co-exist as transient species in solution and can often be difficult to analyze. In the work described in this dissertation, heterogeneity is present in the pre-oligomers of β2m, which increasingly looks like a general feature of amyloid forming proteins rather than an exception to the rule [74–79]. This is especially surprising, as one might expect heterogeneity when the protein in question is intrinsically disordered, but it also occurs in structured proteins [76]. This only underlines the structural complexity behind amyloid formation.

Besides the oligomers, structural polymorphisms have also been reported for the mature fibrils as well [80]. For example, heterogeneities that are observable or measurable on mature fibrils are attributed to heterogeneities amongst oligomers [77]. This heterogeneity can be inherent or can be induced by factors as simple as subtle variations in solution conditions during oligomerization [81–83]. Traditional techniques

for characterizing protein structure and aggregation will typically only report on the global ensemble average of the molecules being analyzed (e.g. fluorescence or circular dichroism spectroscopy). There is a clear need for analytical techniques that can address these emerging challenges on important biomedical topics like amyloid formation.

To overcome this hurdle, ESI-IM-MS is unique in its ability to separate heterogeneous protein conformations that exist in solution [84]. The removal of water solvent and the evaporative cooling that occurs during ESI slows down interconversion processes between states. In addition, because separation and analysis time take place in milliseconds during ESI-IM-MS, conformations that formerly existed in solution can be separated and measured in the gas phase. Due to these advantages, there are numerous examples of ESI-IM-MS being used to study amyloid formation in the literature [55,56,85,86]. A recent example combined ESI-IM-MS and gas phase IR spectroscopy to measure β-sheet content in peptide amyloid assemblies, demonstrating that oligomeric species separated by IM had distinct structural features [86,87]

While an abundance of evidence indicates that these gas phase ions retain a 'memory' of their structures in solution, it is important to remember that energetics in the gas phase are vastly different to solution. For example, the hydrophobic effect is greatly diminished in the gas phase [88]. Ionic interactions are also strengthened due to the decrease in dielectric constant [89]. Although protein structures are able to evolve in the gas phase, these processes have been measured (or predicted) to take place on the seconds to minutes timescale, which is much longer than a typical mass spectrometry measurement [89]. The reliance of MS on solution phase memory is critical for assigning biological significance to measurements in the gas phase.

1.6 Summary

Amyloid formation is implicated in a number of diseases that adversely affect human health. While we still lack complete understanding about the underlying molecular mechanisms of this class of diseases, emerging biophysical tools, such as IM-MS, have allowed us greater insights into early stages of these diseases. Using these tools, we not only can evaluate the effect of small molecules, but also reveal previously unknown heterogeneous structures that underlines the complexity of amyloid formation.

In Chapter 2, we describe our efforts to evaluate and characterize the effects of small molecule inhibitors on β2m amyloid formation, with special focus on the pre-amyloid oligomers. We find that, in this case, effective small molecule inhibitors prefer to bind to oligomeric states and are capable of disrupting their structures such that the oligomers are not amyloid competent.

In Chapter 3, we reveal the presence of oligomeric conformational isomers, which suggests that Cu(II)-catalyzed amyloid formation is highly heterogeneous. Furthermore, we couple our IM experiments to computational experiments to construct plausible models of these heterogeneous oligomer structures and speculate on their importance to amyloid formation. We find these states are able to begin to structurally explain the crucial step of Cu(II) loss from the tetramer, which is a key step in amyloid formation.

In Chapter 4, we explore another example of small molecule inhibition, which has distinct mechanistic differences from the ones described in chapter 2. We find that off-pathway aggregates are rapidly generated, and a destabilization of the dimer is key to inhibitory activity.

Finally, Chapters 5 and 6 contains conclusions and future research directions.

1.7 References

[1] K.A. Dill, H.S. Chan, From Levinthal to pathways to funnels, Nature Structural & Molecular Biology. 4 (1997) 10–19.

[2] T. Eichner, S.E. Radford, A Diversity of Assembly Mechanisms of a Generic Amyloid Fold, Molecular Cell. 43 (2011) 8–18.

[3] R.N. Rambaran, L.C. Serpell, Amyloid fibrils: Abnormal protein assembly, Prion. 2 (2008) 112–117.

[4] R. Nelson, M.R. Sawaya, M. Balbirnie, A.Ø. Madsen, C. Riekel, R. Grothe, D. Eisenberg, Structure of the cross-β spine of amyloid-like fibrils, Nature. 435 (2005) 773–778.

[5] J.M. Nussbaum, M.E. Seward, G.S. Bloom, Alzheimer disease: A tale of two prions, Prion. 7 (2013) 14–19.

[6] A.T. Marvian, D.J. Koss, F. Aliakbari, D. Morshedi, T.F. Outeiro, *In vitro* models of synucleinopathies: informing on molecular mechanisms and protective strategies, Journal of Neurochemistry. 150 (2019) 535-565.

[7] J.D. Pham, B. Demeler, J.S. Nowick, Polymorphism of Oligomers of a Peptide from β-Amyloid, Journal of the American Chemical Society. 136 (2014) 5432–5442.

[8] D.P. Smith, S.E. Radford, A.E. Ashcroft, Elongated oligomers in β2-microglobulin amyloid assembly revealed by ion mobility spectrometry-mass spectrometry, Journal of the American Chemical Society. 136 (2010) 5432–5442.

[9] M.L. Choi, S. Gandhi, Crucial role of protein oligomerization in the pathogenesis of Alzheimer's and Parkinson's diseases, The FEBS Journal. 285 (2018) 3631–3644.

[10] J.C. Stroud, C. Liu, P.K. Teng, D. Eisenberg, Toxic fibrillar oligomers of amyloid-B have cross-B structure, Proceedings of the National Academy of Sciences. 109 (2012) 7717–7722.

[11] P. Cizas, R. Budvytyte, R. Morkuniene, R. Moldovan, M. Broccio, M. Lösche, G. Niaura, G. Valincius, V. Borutaite, Size-dependent neurotoxicity of β-amyloid oligomers, Archives of Biochemistry and Biophysics. 496 (2010) 84–92.

[12] M. Sakono, T. Zako, Amyloid oligomers: formation and toxicity of Aβ oligomers: Formation of toxic Aβ oligomers, FEBS Journal. 277 (2010) 1348–1358.

[13] U. Sengupta, A.N. Nilson, R. Kayed, The Role of Amyloid-β Oligomers in Toxicity, Propagation, and Immunotherapy, EBioMedicine. 6 (2016) 42–49.

[14] F. Bernini, D. Malferrari, M. Pignataro, C.A. Bortolotti, G. Di Rocco, L. Lancellotti, M.F. Brigatti, R. Kayed, M. Borsari, F. del Monte, E. Castellini, Pre-amyloid oligomers budding:a metastatic mechanism of proteotoxicity, Scientific Reports. 6 (2016) 35865.

[15] H. Mohammad-Beigi, F. Aliakbari, C. Sahin, C. Lomax, A. Tawfike, N.P. Schafer, A. Amiri-Nowdijeh, H. Eskandari, I.M. Møller, M. Hosseini-Mazinani, G. Christiansen, J.L. Ward, D. Morshedi, D.E. Otzen, Oleuropein derivatives from olive fruit extracts reduce α-synuclein fibrillation and oligomer toxicity, Journal of Biological Chemistry. 294 (2019) 4215–4232.

[16] N.B. Last, E. Rhoades, A.D. Miranker, Islet amyloid polypeptide demonstrates a persistent capacity to disrupt membrane integrity, Proceedings of the National Academy of Sciences. 108 (2011) 9460–9465.

[17] N. Shanmugam, M.O.D.G. Baker, S.R. Ball, M. Stein, C.L.L. Pham, M. Sunde, Microbial functional amyloids serve diverse purposes for structure, adhesion and defence, Biophysical Reviews. 11 (2019) 287-302.

[18] M. Shahnawaz, C. Soto, Microcin Amyloid Fibrils A Are Reservoir of Toxic Oligomeric Species, Journal of Biological Chemistry. 287 (2012) 11665–11676.

[19] S. Bieler, L. Estrada, R. Lagos, M. Baeza, J. Castilla, C. Soto, Amyloid Formation Modulates the Biological Activity of a Bacterial Protein, Journal of Biological Chemistry. 280 (2005) 26880–26885.

[20] S. Makin, The amyloid hypothesis on trial, Nature. 559 (2018) S4–S7.

[21] G.P. Morris, I.A. Clark, B. Vissel, Inconsistencies and Controversies Surrounding the Amyloid Hypothesis of Alzheimer's Disease, Acta Neuropathologica Communcations. 2 (2014) 135.

[22] H. Katou, T. Kanno, M. Hoshino, Y. Hagihara, H. Tanaka, T. Kawai, K. Hasegawa, H. Naiki, Y. Goto, The role of disulfide bond in the amyloidogenic state of β2-microglobulin studied by heteronuclear NMR, Protein Science. 11 (2009) 2218–2229.

[23] D.R. Madden, J.C. Gorga, J.L. Strominger, D.C. Wiley, The three-dimensional structure of HLA-B27 at 2.1 Å resolution suggests a general mechanism for tight peptide binding to MHC, Cell. 70 (1992) 1035–1048.

[24] F. Gejyo, S. Odani, T. Yamada, N. Honma, H. Saito, Y. Suzuki, Y. Nakagawa, H. Kobayashi, Y. Maruyama, Y. Hirasawa, M. Suzuki, M. Arakawa, β2-microglobulin: A new form of amyloid protein associated with chronic hemodialysis, Kidney International. 30 (1986) 385–390.

[25] T.B. Drüeke, Z.A. Massy, Beta2-Microglobulin, Seminars in Dialysis. 22 (2009) 378–380.

[26] F. Danesh, L.T. Ho, Dialysis-Related Amyloidosis: History and Clinical Manifestations, Seminars in Dialysis. 14 (2001) 80–85.

[27] V.J. McParland, N.M. Kad, A.P. Kalverda, A. Brown, P. Kirwin-Jones, M.G. Hunter, M. Sunde, S.E. Radford, Partially Unfolded States of β_2-Microglobulin and Amyloid Formation in Vitro, Biochemistry. 39 (2000) 8735–8746.

[28] E. Rennella, A. Corazza, S. Giorgetti, F. Fogolari, P. Viglino, R. Porcari, L. Verga, M. Stoppini, V. Bellotti, G. Esposito, Folding and Fibrillogenesis: Clues from β2-Microglobulin, Journal of Molecular Biology. 401 (2010) 286–297.

[29] K. Sasahara, H. Yagi, H. Naiki, Y. Goto, Heat-induced Conversion of β2-Microglobulin and Hen Egg-white Lysozyme into Amyloid Fibrils, Journal of Molecular Biology. 372 (2007) 981–991.

[30] T. Ookoshi, K. Hasegawa, Y. Ohhashi, H. Kimura, N. Takahashi, H. Yoshida, R. Miyazaki, Y. Goto, H. Naiki, Lysophospholipids induce the nucleation and extension of 2-microglobulin-related amyloid fibrils at a neutral pH, Nephrology Dialysis Transplantation. 23 (2008) 3247–3255.

[31] T. Eichner, S.E. Radford, Understanding the complex mechanisms of β2-microglobulin amyloid assembly: β2-microglobulin fibrillogenesis at physiological pH, FEBS Journal. 278 (2011) 3868–3883.

[32] C.J. Morgan, M. Gelfand, C. Atreya, A.D. Miranker, Kidney dialysis-associated amyloidosis: a molecular role for copper in fiber formation, Journal of Molecular Biology. 309 (2001) 339–345.

[33] C.M. Eakin, J.D. Knight, C.J. Morgan, M.A. Gelfand, A.D. Miranker, Formation of a Copper Specific Binding Site in Non-Native States of β-2-Microglobulin, Biochemistry. 41 (2002) 10646–10656.

[34] K. Antwi, M. Mahar, R. Srikanth, M.R. Olbris, J.F. Tyson, R.W. Vachet, Cu(II) organizes β-2-microglobulin oligomers but is released upon amyloid formation, Protein Science. 17 (2008) 748–759.

[35] V.L. Mendoza, K. Antwi, M.A. Barón-Rodríguez, C. Blanco, R.W. Vachet, Structure of the Preamyloid Dimer of β-2-Microglobulin from Covalent Labeling and Mass Spectrometry, Biochemistry. 49 (2010) 1522–1532.

[36] V.L. Mendoza, M.A. Barón-Rodríguez, C. Blanco, R.W. Vachet, Structural Insights into the Pre-Amyloid Tetramer of β-2-Microglobulin from Covalent Labeling and Mass Spectrometry, Biochemistry. 50 (2011) 6711–6722.

[37] J. Dong, C.A. Joseph, N.B. Borotto, V.L. Gill, M.J. Maroney, R.W. Vachet, Unique Effect of Cu(II) in the Metal-Induced Amyloid Formation of β-2-Microglobulin, Biochemistry. 53 (2014) 1263–1274.

[38] R. Srikanth, V.L. Mendoza, J.D. Bridgewater, G. Zhang, R.W. Vachet, Copper Binding to β-2-Microglobulin and Its Pre-Amyloid Oligomers, Biochemistry. 48 (2009) 9871–9881.

[39] N.B. Borotto, Z. Zhang, J. Dong, B. Burant, R.W. Vachet, Increased β-Sheet Dynamics and D–E Loop Repositioning Are Necessary for Cu(II)-Induced Amyloid Formation by β-2-Microglobulin, Biochemistry. 56 (2017) 1095–1104.

[40] Alzheimer's and Dementia: Facts and Figures, (n.d.). https://www.alz.org/alzheimers-dementia/facts-figures.

[41] R. Scarpioni, M. Ricardi, V. Albertazzi, S. De Amicis, F. Rastelli, L. Zerbini, Dialysis-related amyloidosis: challenges and solutions, International Journal of Nephrology and Renovascular Disease. Volume 9 (2016) 319–328.

[42] C.J. Sarell, S.R. Wilkinson, J.H. Viles, Substoichiometric Levels of Cu^{2+} Ions Accelerate the Kinetics of Fiber Formation and Promote Cell Toxicity of Amyloid-β from Alzheimer Disease, Journal of Biological Chemistry. 285 (2010) 41533–41540.

[43] R.M. Rasia, C.W. Bertoncini, D. Marsh, W. Hoyer, D. Cherny, M. Zweckstetter, C. Griesinger, T.M. Jovin, C.O. Fernandez, Structural characterization of copper(II) binding to -synuclein: Insights into the bioinorganic chemistry of Parkinson's disease, Proceedings of the National Academy of Sciences. 102 (2005) 4294–4299.

[44] S.S. Leal, H.M. Botelho, C.M. Gomes, Metal ions as modulators of protein conformation and misfolding in neurodegeneration, Coordination Chemistry Reviews. 256 (2012) 2253–2270.

[45] T. Liu, T.M. Marcinko, P.A. Kiefer, R.W. Vachet, Using Covalent Labeling and Mass Spectrometry To Study Protein Binding Sites of Amyloid Inhibiting Molecules, Analytical Chemistry. 89 (2017) 11583–11591.

[46] J. Lu, Q. Cao, C. Wang, J. Zheng, F. Luo, J. Xie, Y. Li, X. Ma, L. He, D. Eisenberg, J. Nowick, L. Jiang, D. Li, Structure-Based Peptide Inhibitor Design of Amyloid-β Aggregation, Frontiers in Molecular Neuroscience. 12 (2019) 1-10.

[47] M.A. Wälti, J. Steiner, F. Meng, H.S. Chung, J.M. Louis, R. Ghirlando, V. Tugarinov, A. Nath, G.M. Clore, Probing the mechanism of inhibition of amyloid-β(1–42)–induced neurotoxicity by the chaperonin GroEL, Proceedings of the National Academy of Sciences. 115 (2018) E11924–E11932.

[48] S. Sudhakar, E. Mani, Rapid dissolution of amyloid β fibrils by silver nanoplates, Langmuir. 35 (2019) 6962-6970.

[49] T. Härd, C. Lendel, Inhibition of Amyloid Formation, Journal of Molecular Biology. 421 (2012) 441–465.

[50] R. Tycko, R.B. Wickner, Molecular Structures of Amyloid and Prion Fibrils: Consensus versus Controversy, Accounts of Chemical Research. 46 (2013) 1487–1496.

[51] C. Bleiholder, T.D. Do, C. Wu, N.J. Economou, S.S. Bernstein, S.K. Buratto, J.-E. Shea, M.T. Bowers, Ion Mobility Spectrometry Reveals the Mechanism of Amyloid Formation of Aβ(25–35) and Its Modulation by Inhibitors at the Molecular Level: Epigallocatechin Gallate and *Scyllo* -inositol, Journal of the American Chemical Society. 135 (2013) 16926–16937.

[52] L.A. Woods, G.W. Platt, A.L. Hellewell, E.W. Hewitt, S.W. Homans, A.E. Ashcroft, S.E. Radford, Ligand binding to distinct states diverts aggregation of an amyloid-forming protein, Nature Chemical Biology. 7 (2011) 730–739.

[53] A. Nath, D.E. Schlamadinger, E. Rhoades, A.D. Miranker, Structure-Based Small Molecule Modulation of a Pre-Amyloid State: Pharmacological Enhancement of IAPP Membrane-Binding and Toxicity, Biochemistry. 54 (2015) 3555–3564.

[54] M.W. Beck, S.B. Oh, R.A. Kerr, H.J. Lee, S.H. Kim, S. Kim, M. Jang, B.T. Ruotolo, J.-Y. Lee, M.H. Lim, A rationally designed small molecule for identifying an in vivo link between metal–amyloid-β complexes and the pathogenesis of Alzheimer's disease, Chemical Science. 6 (2015) 1879–1886.

[55] L.A. Woods, S.E. Radford, A.E. Ashcroft, Advances in ion mobility spectrometry–mass spectrometry reveal key insights into amyloid assembly, Biochimica et Biophysica Acta (BBA) - Proteins and Proteomics. 1834 (2013) 1257–1268.

[56] D.M. Williams, T.L. Pukala, Novel insights into protein misfolding diseases revealed by ion mobility-mass spectrometry, Mass Spectrometry Reviews. 32 (2013) 169–187.

[57] N.E. Pryor, M.A. Moss, C.N. Hestekin, Unraveling the Early Events of Amyloid-β Protein (Aβ) Aggregation: Techniques for the Determination of Aβ Aggregate Size, International Journal of Molecular Sciences. 13 (2012) 3038–3072.

[58] F. Lanucara, S.W. Holman, C.J. Gray, C.E. Eyers, The power of ion mobility-mass spectrometry for structural characterization and the study of conformational dynamics, Nature Chemistry. 6 (2014) 281–294.

[59] S.-J. Hyung, B.T. Ruotolo, Integrating mass spectrometry of intact protein complexes into structural proteomics, Proteomics. 12 (2012) 1547–1564.

[60] B.T. Ruotolo, J.L.P. Benesch, A.M. Sandercock, S.-J. Hyung, C.V. Robinson, Ion mobility–mass spectrometry analysis of large protein complexes, Nature Protocols. 3 (2008) 1139–1152.

[61] B.T. Ruotolo, K. Giles, I. Campuzano, A.M. Sandercock, R.H. Bateman, C.V Robinson,, Evidence for Macromolecular Protein Rings in the Absence of Bulk Water, Science. 310 (2005) 1658–1661.

[62] C.A. Scarff, V.J. Patel, K. Thalassinos, J.H. Scrivens, Probing hemoglobin structure by means of traveling-wave ion mobility mass spectrometry, Journal of the American Society for Mass Spectrometry. 20 (2009) 625–631.

[63] J. Seo, W. Hoffmann, S. Warnke, M.T. Bowers, K. Pagel, G. von Helden, Retention of Native Protein Structures in the Absence of Solvent: A Coupled Ion Mobility and Spectroscopic Study, Angewandte Chemie International Edition. 55 (2016) 14173–14176.

[64] Y. Sun, S. Vahidi, M.A. Sowole, L. Konermann, Protein Structural Studies by Traveling Wave Ion Mobility Spectrometry: A Critical Look at Electrospray Sources and Calibration Issues, Journal of The American Society for Mass Spectrometry. 27 (2016) 31–40.

[65] M.M. Maurer, G.C. Donohoe, S.J. Valentine, Advances in ion mobility-mass spectrometry instrumentation and techniques for characterizing structural heterogeneity, The Analyst. 140 (2015) 6782–6798.

[66] A.A. Shvartsburg, R.D. Smith, Fundamentals of Traveling Wave Ion Mobility Spectrometry, Analytical Chemistry. 80 (2008) 9689–9699.

[67] M.F. Bush, Z. Hall, K. Giles, J. Hoyes, C.V. Robinson, B.T. Ruotolo, Collision Cross Sections of Proteins and Their Complexes: A Calibration Framework and Database for Gas-Phase Structural Biology, Analytical Chemistry. 82 (2010) 9557–9565.

[68] H.E. Revercomb, E.A. Mason, Theory of plasma chromatography/gaseous electrophoresis. Review, Analytical Chemistry. 47 (1975) 970–983.

[69] D.P. Smith, T.W. Knapman, I. Campuzano, R.W. Malham, J.T. Berryman, S.E. Radford, A.E. Ashcroft, Deciphering Drift Time Measurements from Travelling Wave Ion Mobility Spectrometry-Mass Spectrometry Studies, European Journal of Mass Spectrometry. 15 (2009) 113–130.

[70] V. Gabelica, A.A. Shvartsburg, C. Afonso, P. Barran, J.L.P. Benesch, C. Bleiholder, M.T. Bowers, A. Bilbao, M.F. Bush, J.L. Campbell, I.D.G. Campuzano, T. Causon, B.H. Clowers, C.S. Creaser, E. De Pauw, J. Far, F. Fernandez-Lima, J.C. Fjeldsted, K. Giles, M. Groessl, C.J. Hogan, S. Hann, H.I. Kim, R.T. Kurulugama, J.C. May, J.A. McLean, K. Pagel, K. Richardson, M.E. Ridgeway, F. Rosu, F. Sobott, K. Thalassinos, S.J. Valentine, T. Wyttenbach, Recommendations for reporting Ion Mobility Mass Spectrometry Measurements, Mass Spectrometry Reviews. 38 (2019) 291-320.

[71] S.L. Bernstein, N.F. Dupuis, N.D. Lazo, T. Wyttenbach, M.M. Condron, G. Bitan, D.B. Teplow, J.-E. Shea, B.T. Ruotolo, C.V. Robinson, M.T. Bowers, Amyloid-β protein oligomerization and the importance of tetramers and dodecamers in the aetiology of Alzheimer's disease, Nature Chemistry. 1 (2009) 326–331.

[72] N.F. Dupuis, C. Wu, J.-E. Shea, M.T. Bowers, The Amyloid Formation Mechanism in Human IAPP: Dimers Have β-Strand Monomer−Monomer Interfaces, Journal of the American Chemical Society. 133 (2011) 7240–7243.

[73] A. Politis, A.Y. Park, S.-J. Hyung, D. Barsky, B.T. Ruotolo, C.V. Robinson, Integrating Ion Mobility Mass Spectrometry with Molecular Modelling to Determine the Architecture of Multiprotein Complexes, PLoS ONE. 5 (2010) e12080.

[74] D. Matthes, V. Gapsys, J.T. Brennecke, B.L. de Groot, An Atomistic View of Amyloidogenic Self-assembly: Structure and Dynamics of Heterogeneous Conformational States in the Pre-nucleation Phase, Scientific Reports. 6 (2016) 33156.

[75] M. Stefani, Structural features and cytotoxicity of amyloid oligomers: Implications in Alzheimer's disease and other diseases with amyloid deposits, Progress in Neurobiology. 99 (2012) 226–245.

[76] L. Breydo, V.N. Uversky, Structural, morphological, and functional diversity of amyloid oligomers, FEBS Letters. 589 (2015) 2640–2648.

[77] A.T. Petkova, R.D. Leapman, Z. Guo, W.-M. Yau, M.P. Mattson, R. Tycko, Self-Propagating, Molecular-Level Polymorphism in Alzheimer's B-Amyloid Fibrils, Science. 307 (2005) 262–265.

[78] R. Tycko, Amyloid Polymorphism: Structural Basis and Neurobiological Relevance, Neuron. 86 (2015) 632–645.

[79] S.J.C. Lee, E. Nam, H.J. Lee, M.G. Savelieff, M.H. Lim, Towards an understanding of amyloid-β oligomers: characterization, toxicity mechanisms, and inhibitors, Chemical Society Reviews. 46 (2017) 310–323.

[80] R. Tycko, Physical and structural basis for polymorphism in amyloid fibrils: Amyloid Polymorphism, Protein Science. 23 (2014) 1528–1539.

[81] N.M. Kad, N.H. Thomson, D.P. Smith, D.A. Smith, S.E. Radford, β2-microglobulin and its deamidated variant, N17D form amyloid fibrils with a range of morphologies in vitro, Journal of Molecular Biology. 313 (2001) 559–571.

[82] N.M. Kad, S.L. Myers, D.P. Smith, D. Alastair Smith, S.E. Radford, N.H. Thomson, Hierarchical Assembly of β2-Microglobulin Amyloid In Vitro Revealed by Atomic Force Microscopy, Journal of Molecular Biology. 330 (2003) 785–797.

[83] W.S. Gosal, I.J. Morten, E.W. Hewitt, D.A. Smith, N.H. Thomson, S.E. Radford, Competing Pathways Determine Fibril Morphology in the Self-assembly of β2-Microglobulin into Amyloid, Journal of Molecular Biology. 351 (2005) 850–864.

[84] D.E. Clemmer, D.H. Russell, E.R. Williams, Characterizing the *Conformationome* : Toward a Structural Understanding of the Proteome, Accounts of Chemical Research. 50 (2017) 556–560.

[85] C. Bleiholder, M.T. Bowers, The Solution Assembly of Biological Molecules Using Ion Mobility Methods: From Amino Acids to Amyloid β-Protein, Annual Review of Analytical Chemistry. 10 (2017) 365–386.

[86] W. Hoffmann, G. von Helden, K. Pagel, Ion mobility-mass spectrometry and orthogonal gas-phase techniques to study amyloid formation and inhibition, Current Opinion in Structural Biology. 46 (2017) 7–15.

[87] J. Seo, W. Hoffmann, S. Warnke, X. Huang, S. Gewinner, W. Schöllkopf, M.T. Bowers, G. von Helden, K. Pagel, An infrared spectroscopy approach to follow β-sheet formation in peptide amyloid assemblies, Nature Chemistry. 9 (2017) 39–44.

[88] C.V. Robinson, E.W. Chung, B.B. Kragelund, J. Knudsen, R.T. Aplin, F.M. Poulsen, C.M. Dobson, Probing the Nature of Noncovalent Interactions by Mass Spectrometry. A Study of Protein−CoA Ligand Binding and Assembly, Journal of the American Chemical Society. 118 (1996) 8646–8653.

[89] K. Rajabi, A.E. Ashcroft, S.E. Radford, Mass spectrometric methods to analyze the structural organization of macromolecular complexes, Methods. 89 (2015) 13–21.

CHAPTER 2

SMALL MOLECULE-MEDIATED INHIBITION OF β-2 MICROGLOBULIN-

BASED AMYLOID FORMATION

This chapter is adapted from part of a paper published as: Marcinko, T.M.; Dong, J.; LeBlanc, R.; Daborowski, K.V.; and Vachet, R.W. Small Molecule-mediated Inhibition of β-2-Microglobulin-based Amyloid Formation. *J. Biol. Chem.* 2017, 292, 10630-10638.

2.1 Introduction

Given the prevalence of amyloid diseases, such as Alzheimer's, Parkinson's, and type II diabetes, there has been great effort put toward developing small molecule inhibitors of amyloid formation [1,2]. To properly employ such therapeutics, it is important to understand how potential candidates affect the amyloid assembly process. There are several potential strategies for disrupting amyloid formation, including stabilizing the native state of the protein, destabilizing or kinetically trapping early soluble oligomers, and/or promoting off-pathway aggregation.

In this study, we explore how several small molecules influence the amyloid fibril formation pathway of the protein β-2 microglobulin (β2m), which is the protein implicated in dialysis-related amyloidosis (DRA) [3,4]. β2m is a 99-residue protein composed of seven β-strands arranged in an anti-parallel β-sandwich motif held together a lone disulfide bond [5]. Although it is normally a structural component of the class I major histocompatibility complex, elevated serum concentrations of β2m, as a result of long-term dialysis, result in deposition of β2m amyloid fibrils in patient joints, ultimately resulting in joint destruction [6]. β2m amyloid fibril formation has been studied extensively *in vitro*, and several conditions can convert the protein from soluble to insoluble amyloids, including low pH conditions [7], trifluoroethanol (TFE) [8], thermal

denaturation [9], partial denaturation with lysophospholipids [9], deletion of the first six amino acids [10], and incubation with catalytic amounts of Cu(II) [11–13].

There has also been some preliminary work on identifying and studying potential inhibitors of β2m amyloid formation. Small molecules capable of binding to β2m, and in some cases inhibiting its amyloid formation, have been studied using surface plasmon resonance (SPR), capillary electrophoresis (CE), electrospray ionization mass spectrometry (ESI-MS), ion mobility spectrometry, and computational simulations [14–18]. A few small molecules have been found to inhibit β2m amyloid formation when initiated by acid or TFE addition [16,17]. These studies suggest that the effective inhibitors preferentially bind to partially- or natively-structured β2m and exert their inhibitory effect on the monomeric form of the protein, causing the formation of spherical instead of fibrillar aggregates. The impact of these molecules on the Cu(II)-catalyzed amyloid assembly pathway of β2m, however, has not been reported. Such studies represent an opportunity to determine if these molecules are more broadly capable of inhibiting β2m amyloid formation, especially under physiologically-relevant pH and ionic strengths (i.e. pH 7.4, 150 mM ionic strength). As previously reported by our group and others, Cu(II) binding to β2m causes several structural changes that allow β2m to oligomerize and eventual form amyloid fibrils. Oligomerization has been shown to proceed through discrete stages (i.e. formation of dimers, tetramers, and hexamers) which are necessary for amyloid formation *in vitro* [11–13,19–23]. Moreover, studying the effect of small molecules on the Cu(II)-catalyzed pathway provides an opportunity to investigate commonalities in the inhibition modes between different amyloid-forming conditions.

We explore in this work three small molecules, namely, doxycycline (Dox), rifamycin SV (Rif), and suramin (Sur), that are known to bind β2m and/or influence its amyloid assembly when initiated by acid or TFE. To more deeply understand how these molecules affect Cu(II)-induced β2m amyloid formation, we use a variety of biophysical techniques to study perturbations in the assembly of β2m oligomers and amyloid aggregates. We find that Dox and Rif inhibit amyloid formation by diverting β2m oligomers along a different pathway that leads to amorphous aggregates. Moreover, using ESI-MS and ion mobility spectrometry, we find that the inhibitors exert their influence by specifically perturbing the structures of β2m dimers and tetramers. Overall, our studies suggest that certain small molecules can generally inhibit β2m amyloid formation, but the mechanism is likely different depending on how amyloid formation is initiated.

2.2 Materials and methods

2.2.1 Materials

Human full-length β2m (Cat # 126-11) was purchased from Lee Biosolutions (Maryland Heights, MO). All chemicals and proteins, unless otherwise noted, were purchased from Sigma Aldrich (St. Louis, MO). Solid phosphotungstic acid (Cat#19500) was purchased from Electron Microscopy Services (Hatfield, PA).

2.2.2 Methods

2.2.2.1 Formation of β2m Oligomers and Amyloid Fibrils

For induction of β2m amyloid formation, a 1:2 molar ratio of protein to Cu(II) was used in a solution of 25 mM MOPS, 150 mM potassium acetate, and 500 mM urea,

at pH 7.4 as described in our previous work [11–13,22,23]. Protein concentrations ranged from 50 μM to 150 μM. Where applicable, Dox, Rif, or Sur were added to the above incubation mixture at a molar ratio of 1:2:1 protein:Cu(II):small molecule. A range of Dox, Rif, and Sur concentrations were explored, but a 1:1 ratio of protein:small molecule was found to be effective in all cases. Samples were incubated at 37 °C for varying time points (≤ 14 days) and were then analyzed using several different techniques.

2.2.2.2 Transmission Electron Microscopy

TEM images were obtained on a JEOL2000FX transmission electron microscope (Peabody, MA). Prior to imaging, incubated samples were spun at 14,000 RPM for 45 minutes. The supernatant was then removed and the pellet was re-suspended with 10 μL of deionized water. The samples were applied dropwise to 300-mesh carbon-coated copper grids (Cat#CF300-CU) obtained from Electron Microscopy Services and allowed to dry. The samples were then stained with a 1% (w/v) solution of phosphotungstic acid adjusted to pH 7.4 with potassium hydroxide. Following a water rinse, the samples were dried overnight and protected from ambient light until analysis.

2.2.2.3 Size Exclusion High Performance Liquid Chromatography (SEC-HPLC)

An HP Agilent 1100 series HPLC system fitted with a SuperSW2000 (Cat#18674) SEC column from Tosoh Bioscience, LLC (Tokyo, Japan) was used for all chromatographic analyses. The mobile phase consisted of 150 mM ammonium acetate at pH 6.9 and was used at a flow rate of 0.35 mL/min. For detection of proteins and β2m oligomers, the detector was set to 214 nm. For the detection of small molecules, the detector was set to 350 nm for Dox and 315 nm for Rif and Sur. A calibration standard

mixture of bovine serum albumin, ovalbumin, carbonic anhydrase, and β2m was used to estimate molecular weights from SEC elution times.

2.2.2.4 Electrospray Ionization Ion Mobility Spectrometry Mass Spectrometry (ESI-IM-MS)

A Waters Synapt G2-Si quadrupole time-of-flight (QTOF) mass spectrometer (Milford, MA) equipped with a nanospray source was used to collect all mass spectral data. The electrospray capillary voltage was set to 1.0 kV; the source temperature was set to 30°C; and the source offset and sampling cone were set at 20 V. All other source and instrumental parameters were optimized to maximize protein complex ion signals. Electrospray capillaries were prepared in-house, using established protocols by sputter-coating gold onto pulled borosilicate thin wall capillaries (Cat#30-0035) purchased from Harvard Apparatus (Holliston, MA) [24]. Immediately prior to analysis, samples were desalted from their incubation buffer into 100 mM ammonium acetate using a HiTrap desalting column from GE Healthcare (Chicago, Illinois). The *m/z* scale on the QTOF was calibrated from 500-8,000 using perfluoroheptanoic acid. CCS values were estimated from a calibration curve of native-like proteins using calibrants and methods that were previously described [25]. Data analysis was carried out using Waters MassLynx 4.1. Theoretical CCS values were calculated using Waters Driftscope.

2.2.2.5 Fluorescence Spectroscopy

To measure binding affinity of Cu(II) to β2m, a PTI Quantamaster 300 was used (Edison, NJ). Intrinsic fluorescence was monitored via excitation at 295 nm while emission was monitored from 300 to 400 nm. Prior to measurement, the samples were

equilibrated at ambient room temperature for 15 minutes. The fraction bound was

determined by measuring the average emission intensity ($<\lambda>$) via intrinsic Trp

fluorescence. Cu(II) concentrations were refined using the Hyperquad Simulation and

Speciation (HySS) software (Protonic Software). Solution conditions for the affinity

measurements were carried out using similar solution conditions to those described in the

main text. Data were plotted using Origin (Northampton, MA), and the titration data were

fitted using the Hill equation.

2.3 Results

2.3.1 The addition of doxycycline or rifamycin alters insoluble aggregate morphology in Cu(II)-catalyzed β2m amyloid formation

To test the ability of the small molecules to inhibit the amyloid assembly process

of β2m, we assessed the morphology of any resulting insoluble aggregates using TEM

(Figure 2.1). Following centrifugation, insoluble material was present in all sample tubes

after 14 days of incubation. Amyloid fibrils were observed in both the control (panel A)

and the Sur-treated samples (panel D). Some amorphous aggregates were also observed

in the TEM images of the Sur sample. In addition, a smaller insoluble pellet was

observed in the Sur sample as compared to the control, suggesting perhaps that Sur either

slows the fibrillization process or only partially affects it. The dimensions and

morphology of the fibrils observed in the control and Sur samples are consistent with

amyloid fibrils published previously [11,13]. Thioflavin T (ThT) fluorescence

experiments were also attempted, but the presence of the inhibitor molecules was found

to interfere with the spectral properties of ThT therefore compromising the results of the

assay. Such interferences were also observed for similar compounds by other groups [16,26].
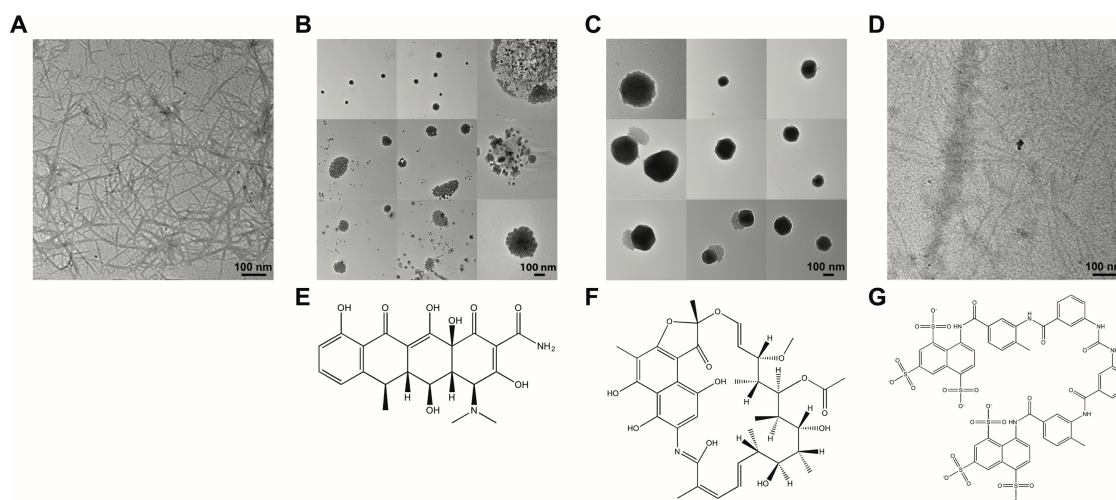
Figure 2.1: The addition of doxycycline or rifamycin alters insoluble aggregate morphology in Cu(II)-catalyzed β2m amyloid formation conditions after 14 days of incubation at 37°C. Samples contained 100 μM β2m, 200 μM Cu(II), and 100 μM of the corresponding small molecule. Panels A-D: TEM images at 25,000X magnification of the control (A), doxycycline (B), rifamycin (C), and suramin (D) samples. Panels E-G: Structures of doxycycline (Dox) (E), rifamycin (Rif) (F), and suramin (Sur) (G).

In the Dox (panel B) and Rif-treated (panel C) samples, the morphology of the insoluble aggregates is drastically different. Rather than elongated fibrils, we observed dense amorphous particles that appear to be evenly distributed with no evidence of fibrillar structures. When comparing Dox-treated aggregates to Rif-treated aggregates, the Dox-treated aggregates have a granular quality that either exists as discrete particles with diameters of approximately 5-10 nm or as part of larger aggregated clusters that range in size from about 200 to 500 nm. In contrast, the Rif-treated aggregates have larger amorphous structures with diameters that range from about 100 to 300 nm. In many cases, after resuspension of the insoluble material in 2% sodium dodecyl sulfate (SDS) and incubation at 37 °C for 24 hours, the Dox and Rif-treated samples were found to be completely re-dissolvable.

2.3.2 The presence of doxycycline and rifamycin causes the formation of new heterogeneous oligomeric states in solution and gas phase

We then assessed the impact of the small molecules on the oligomerization process that precedes fibril formation (Figure 2.2). Over the course of 6 days, peaks corresponding to dimers, tetramers, and hexamers are measured for both the control (panel A) and Sur-treated (panel D) samples. The soluble oligomer profiles for the
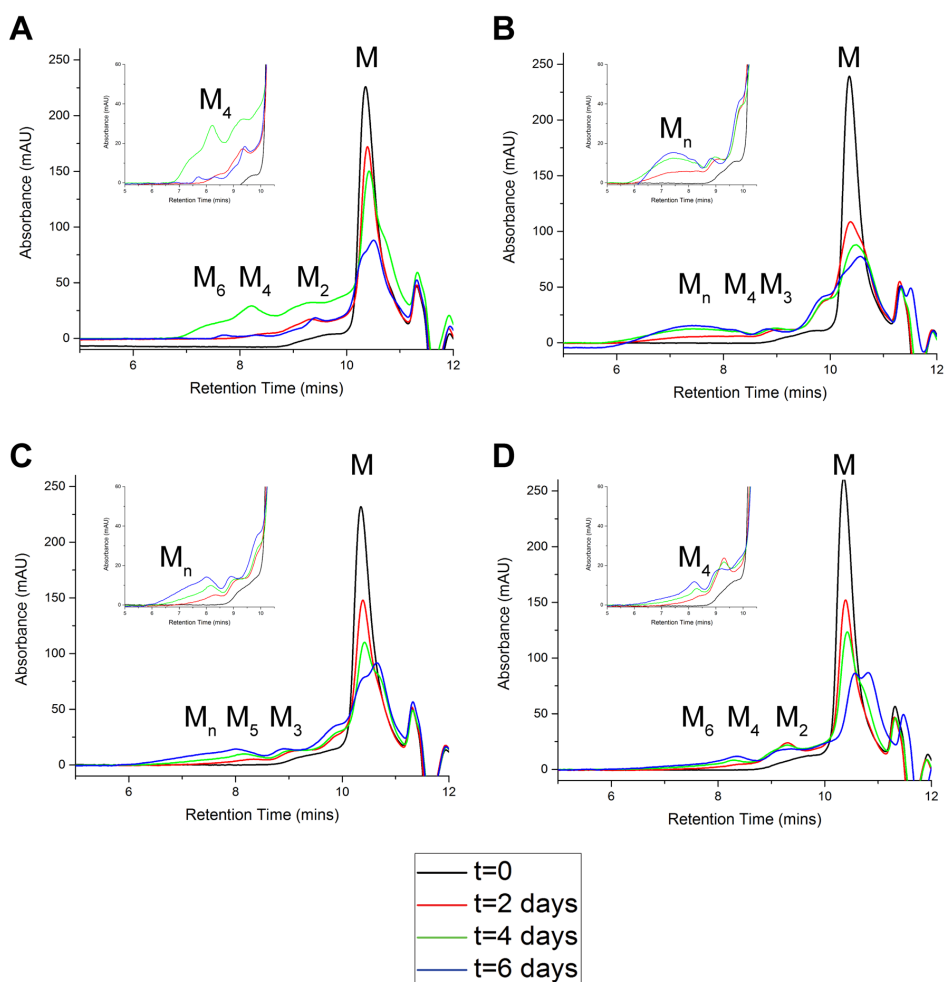
Figure 2.2: Doxycycline and rifamycin alter the soluble Cu(II) oligomerization profile and remain bound to oligomers in solution phase. Panels A-D: SEC results over the course of 6 days of incubation at 37°C for control (A), Dox (B), Rif (C), and Sur (D). Insets show expanded views of the oligomer elution region.

control and Sur-treated samples are consistent with previous work from our group [11,13]. The oligomeric species in the Sur samples tend to be less abundant than the control samples at the same time periods, which is consistent with Sur kinetically slowing but not inhibiting amyloid formation.

The presence of Dox (panel B) or Rif (panel C) changes the oligomerization profile. Rather than the formation of discrete even-numbered oligomers, peaks corresponding to a trimer are measured for both molecules. More interestingly, a large, broadly eluting peak is measured at higher molecular weights for both inhibitors. According to the calibration curve, species eluting during this range have estimated molecular weights ranging from a pentamer to octamer.
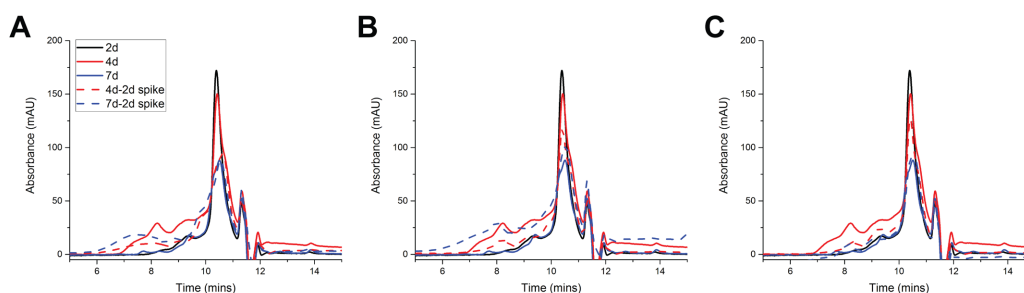
Figure 2.3: Mid-incubation conversion of amyloid formation by doxycycline and rifamycin. SEC-HPLC chromatograms for control samples (solid) over the course of 7 days. Inhibitors were introduced by spiking doxycycline (A), rifamycin (B), and suramin (C) in at 2 days and then monitoring the progression of oligomers at 4 days and 7 days (dashed).

Furthermore, there is a prominent tetrameric species that is observed in the Rif-containing sample. The oligomeric profiles observed with Dox and Rif are in contrast to the control and Sur-treated samples and are consistent with the altered aggregate morphologies observed with these two inhibitors. We also performed an experiment in which inhibitor addition was delayed until dimers (2 days) or tetramers (4 days) were

31

formed. For both Dox and Rif, the normal oligomer population was converted to an oligomer profile similar to the ones measured when the inhibitor is present from the start of the incubation (Figure 2.3).

To further investigate the identities of the oligomers that are present in the inhibitor (i.e. Dox and Rif) containing solutions, we employed native electrospray ionization mass spectrometry (Figure 2.4). Peak assignments are based on charge state
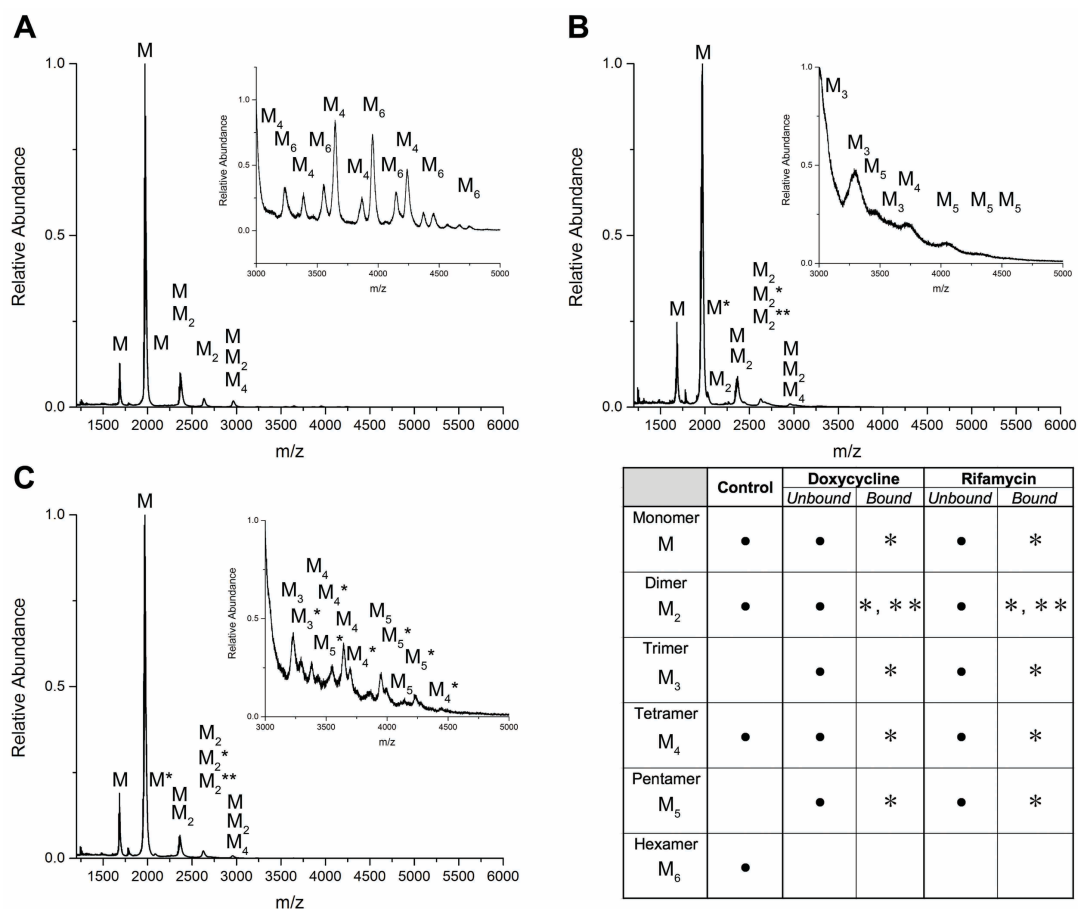
Figure 2.4: Nano-ESI-IM-MS reveals identities of soluble oligomeric species. Panels A-C: Native spray data after 6 days of incubation at 37°C for control (A), Dox (B), and Rif (C). Samples were desalted into 100 mM ammonium acetate prior to analysis. The samples contained 100 μM β2m, 200 μM Cu(II), and 100 μM of the corresponding small molecule. Sample concentration was 10 μM after desalting. Data for all samples were collected under identical instrumental conditions. In the associated table, a dot (●) signifies the confirmation of the presence of an oligomer while an asterisk (*) denotes the presence of a small molecule-bound adduct.

	Control	Doxycycline		Rifamycin	
		Unbound	Bound	Unbound	Bound
Monomer M	●	●	*	●	*
Dimer M_2	●	●	*, **	●	*, **
Trimer M_3		●	*	●	*
Tetramer M_4	●	●	*	●	*
Pentamer M_5		●	*	●	*
Hexamer M_6	●				

deconvolutions and CID data for each ionic species. For the control sample, even-numbered oligomers, but not odd-numbered ones, are observed at incubation times up to 6 days, which is consistent with both the SEC data (Figure 2.2) and previous results from our group [11,13]. In contrast to the control samples, the presence of Dox or Rif alters the oligomer profile by forming trimers and pentamers in addition to even-numbered oligomers.

2.3.3 Doxycycline and rifamycin are bound to oligomers in the solution and gas phase

Because each of the small molecules studied here absorbs at higher wavelengths than the protein, we can also separately detect when the small molecules are eluting and determine with which protein species they are associated. Overlays of the chromatograms showing the protein absorption and the small molecule absorptions indicate that both Dox and Rif elute primarily with the oligomeric species, suggesting preferential interactions with the β2m oligomers, while Sur does not (Figure 2.5). Blank solutions of each inhibitor dissolved in water at identical concentrations were also injected, and they were found to elute after the monomer peak, confirming that the small molecules only elute earlier because of interactions with β2m oligomers. Examination of the chromatograms displaying the entire elution profile show that Sur primarily elutes after the protein, indicating that it does not interact strongly with the monomer or any of the oligomers. Interestingly, after 14 days when the precipitates are formed, we found that all the small molecules (i.e. Dox, Rif, and Sur) are found free in solution, rather than

associated with the protein aggregates via UV-Vis spectroscopy with the assistance of a calibration curve.
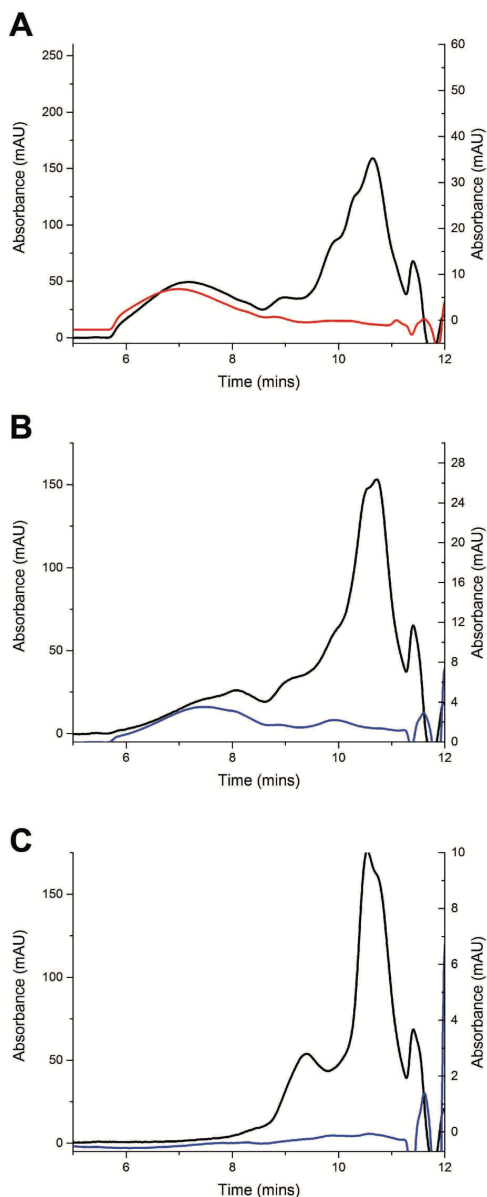
Figure 2.5: SEC-HPLC results with detector tuned to absorption of small molecules. For these panels, the black trace corresponds to the variable wavelength detector set to 214 nm whereas the colored trace corresponds to 350 nm (red) or 315 nm (blue) after 6 days of incubation for Dox (A), Rif (B), and Sur (C). Samples contained 100 μM β2m, 200 μM Cu(II), and 100 μM of the corresponding small molecule in panels A-D, and 150 μM β2m, 300 μM Cu(II), and 150 μM of the corresponding small molecule in panels E-G.

Furthermore, we also directly measured peaks corresponding to inhibitor-bound species are observed for both Dox and Rif bound several oligomeric charge states via ESI-IM-MS. Many of these oligomer-inhibitor complexes can be readily resolved in the mass spectra from the Rif samples, but in the Dox samples it is difficult to confirm the inhibitor-bound species in some cases. CID of the suspected inhibitor-bound oligomers, however, confirm that the inhibitors are bound to the oligomers, as a second charge-state distribution of inhibitor-adducted monomer ions are clearly observed (Figure 2.6). For Dox, this was the only confirmation of the ligands bound in the gas phase due to the poor resolution of the native mass spectra.
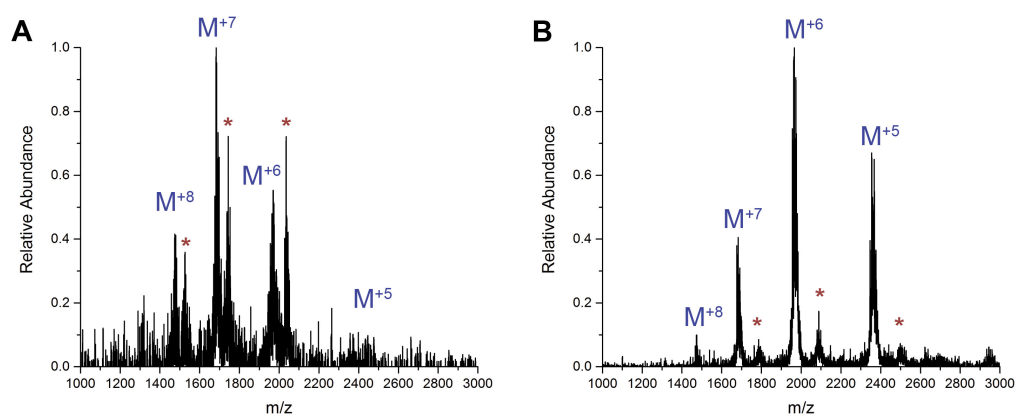
Figure 2.6: Collision-induced dissociation of oligomers confirm Dox and Rif are bound in gas phase. Spectra of activated monomer and small molecule adduct (*) dissociated from 13+ tetramer for Dox (A) and Rif (B).

2.3.4 Doxycycline and rifamycin alter oligomer structure in the gas phase

The β2m oligomers and their inhibitor complexes from the various samples were also monitored by ion mobility mass spectrometry to analyze for the presence of conformational isomers (conformers), as a way to assess the structural effects of the inhibitors on β2m and its oligomers. Numerous previous studies have demonstrated that ion mobility can provide useful insight into the stoichiometry and architecture of non-
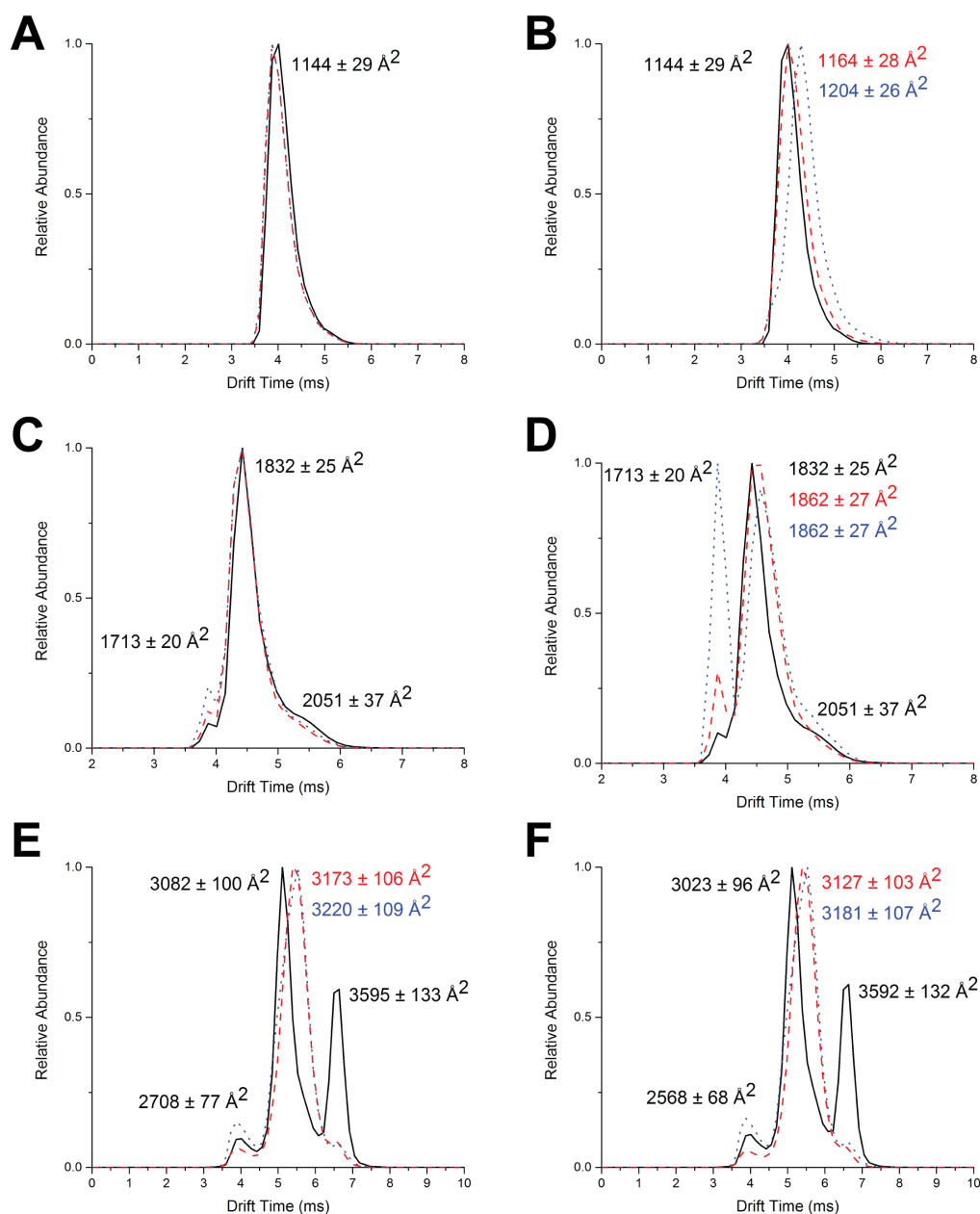
Figure 2.7: Arrival time distributions and collisional cross section (CCS) values reveal conformational and structural differences in oligomer populations. CCS values were estimated using a calibration curve and calculations as described in the materials and methods section. Panels A and B compare unbound 6+ monomer to the bound; panels C and D compare unbound 9+ dimer to the bound; panels E and F compare unbound 14+ tetramer to the bound. The control is shown in black, Dox in red dashes, and Rif in blue dots.

covalent complexes as well as the presence of conformational isomers [16,27,28]. Figure

4.7 illustrates the key differences that are observed between β2m oligomers formed in the

absence and presence of the inhibitors. The monomers, dimers, and tetramers of both control and inhibitor-containing samples were compared, as these β2m species are common to both sets of samples. For the monomer ions, only a single conformation is observed for the control or inhibitor-containing species, whether monitoring the ions without (Figure 2.7A) or with (Figure 2.7B) the inhibitor bound. In the presence of inhibitors, whether bound or un-bound, the predominant conformers (Figure 2.7C-F) show small increases in collision cross section (CCS) values when compared to the control samples, but these changes are insignificant in many cases.

When the inhibitors are present, though, differences in the number of conformers and the CCS values of the new conformers are apparent for the dimer and tetramer. For the dimer, a more compact conformer is present in both the inhibitor-free (Figure 2.7C) and inhibitor-bound (Figure 2.7D) complex ions. The compact dimer is much more abundant in the dimer-inhibitor complex ions (Figure 2.7D), especially for the Rif samples, suggesting that this dimer conformer is part of the effect that Rif has on the aggregation process. A more striking difference is seen in the arrival time distributions of the tetramer. The control sample indicates the presence of three conformers, including an expanded conformer with a CCS value of approximately 3600 $Å^2$ (Figure 2.7E). The more expanded conformer is absent in the inhibitor-containing samples (Figure 2.7E and F), indicating perhaps that the inhibitors influence the aggregation process by preventing the formation of this more expanded structure. There is also a small increase in the CCS value of the main conformer observed when Dox and Rif are present in the solution.

2.4 Discussion

The current study represents the first time that the effect of small molecule inhibitors on Cu(II)-catalyzed β2m amyloid formation has been investigated. The small molecules studied here were chosen because they are known to bind to β2m and/or inhibit β2m amyloid formation that is initiated by other means (e.g. with acid or 20% trifluoroethanol) [14–18]. In contrast to these previous studies, our experiments are conducted under physiologically relevant conditions (i.e. pH 7.4 and ionic strength of 150 mM). The fact that both Dox and Rif prevent amyloid formation that is initiated by Cu(II) *and* by other means further suggest the promise of these molecules as inhibitors of β2m amyloid formation. Our results also suggest some commonalities between the Cu(II)-induced amyloid pathway and the amyloid pathways induced by acid or TFE. Moreover, the fact that Sur does not prevent amyloid formation further connects the different modes of initiating β2m amyloid formation, as this molecule behaved similarly with amyloid-inducing conditions involving TFE [15].

The apparent commonalities in how Dox and Rif prevent β2m amyloid formation that is initiated by different means motivates our attempts to understand the molecular basis of this inhibition, although it appears that these molecules influence the pathways at different points. Previous work with TFE suggested that Dox inhibits β2m self-association while stabilizing native-like structures [17]. Under acidic conditions, Rif inhibits fibrillization via binding to specific conformations of the monomer and dimer and was capable of disassembling oligomers by favoring inhibitor-bound monomers [16]. In contrast, our results indicate that the inhibitors interact more favorably with larger oligomeric species (≥ dimer) thus diverting the amyloid-competent oligomerization

pathway (Figure 2.2) toward re-dissolvable aggregates with non-fibrillar morphologies (Figure 2.1). Dox and Rif divert the normal Cu(II)-induced oligomer assembly process, whether present at the beginning of the incubation or when added after the oligomers are already present, (Figure. 2.2, 2.3) such that more than just even-ordered oligomers are formed. The loss of an ordered oligomer assembly process might explain why amorphous aggregates are formed in the presence of the inhibitors.

The increased oligomer heterogeneity observed when the inhibitors are present indicate that these small molecules change the structures of the pre-amyloid oligomers and/or perturb the specific interactions that the pre-amyloid oligomers have that enable them to progress to a fibrillar morphology. The structural and oligomeric changes are presumably enforced by the preferential binding of the Dox and Rif to the higher-order oligomers, as revealed by the SEC data shown in Figure 2.5.

The inhibitors, however, are eventually released upon formation of the amorphous aggregates as indicated by their presence in the isolated supernatant. The exact molecular-level details of the structural changes are not known, but some insight into the structural differences between the on- and off-pathway oligomers is obtained using ion mobility and MS. Ion mobility has been increasingly used to characterize protein complexes, as evidence shows that proteins maintain aspects of their solution phase structures during the ion mobility measurements [29–31]. Moreover, in many cases CCS values obtained from ion mobility measurements are found to correlate to solution-phase conformations [32–36]. In the current context, ion mobility reveals the presence of isomeric protein oligomers (Figure 2.7). The appearance of a more compact conformer for the dimer when the inhibitors are present suggest that the inhibitors exert their effect

at this stage of the aggregation process, especially given the fact that CCS values for the inhibitor-bound and inhibitor-free monomers are essentially unchanged (Figure 2.7A and B).

Compaction of the dimer might cause key residues that are important for tetramer assembly to be inaccessible, thereby preventing proper tetramer assembly. Furthermore, the structural remodeling that the inhibitors exert on the dimer appears to be responsible for altering the oligomerization pathway, such that trimers and pentamers are formed. In previous work, we established a model of the pre-amyloid dimer based on covalent labeling/MS data and molecular dynamics simulations. This dimer, which has similar structural features to one of the dimer units in the crystallographic hexamer formed by the non-amyloidogenic H13F mutant (PDB ID: 3CIQ), is calculated to have a CCS of 1831 $Å^2$, which is in excellent agreement with the experimentally determined value of 1830 ± 30 $Å^2$ (Figure 2.7C) [22]. The more compact dimer, which is formed in the presence of the inhibitors (Figure 2.7C and D), has a CCS value that is 120 $Å^2$ smaller, representing a 6.6% decrease. This compaction would correspond to roughly 13 residues in the dimer, which is probably an extensive enough change to disrupt key residues involved in the amyloid-competent tetramer.

Compaction of the dimer in the presence of Dox and Rif not only indicates these molecules exert their effect at this stage of the aggregation process, but it may also explain the dramatic difference in the tetramer conformers when the inhibitors are present. The most notable change is the complete disappearance of the elongated conformer with a CCS value of 3600 ± 100 $Å^2$ (Figure 2.7E and F). In previous work, we found that two pre-amyloid tetramers are formed upon incubation with Cu(II), one

with Cu(II) bound and the other with Cu(II) absent, and formation of the Cu(II)-free

tetramer is necessary for eventual amyloid formation [11]. Based on this previous work,

it is reasonable to conclude that the elongated tetramer measured here is the Cu(II)-free

tetramer, and its disappearance in the presence of the inhibitors may explain why amyloid

formation is not possible in the presence of these molecules. A more open conformation

might be expected for the Cu(II)-free tetramer as residues previously constrained by

binding to Cu(II) are released. Interestingly, we previously reported a structural model of

the tetramer based on covalent labeling/MS measurements and molecular dynamics

simulations [23]. The calculated CCS value of this model is 2952 Å^2, which is

remarkably close to the measured CCS value (i.e. 3000 ± 100 Å^2) of the predominant

conformer, suggesting that our previous structural model is of the Cu(II)-bound tetramer.

In a separate parallel effort in the lab, Tianying Liu studied and determined the

binding site for Dox, Rif, and Sur on monomeric β2m using a combination of covalent

labeling-mass spectrometry (CL-MS) and docking [37]. In the context of our findings, it

is useful to summarize and discuss her findings here (Figure 2.8). On the monomer, Rif

was found to bind on the G β strand, while Dox was found to bind on the D β strand.

Notably, these sites form a critical interface for the Cu(II)-bound tetramer [23]. Binding

in these regions may be sufficient enough to disrupt a proper tetramer from forming. In

contrast, Sur binds at a completely different region, near the C β strand and C-D loop,

which have no known oligomeric interfaces. These data are internally consist with the

data laid out in this chapter.
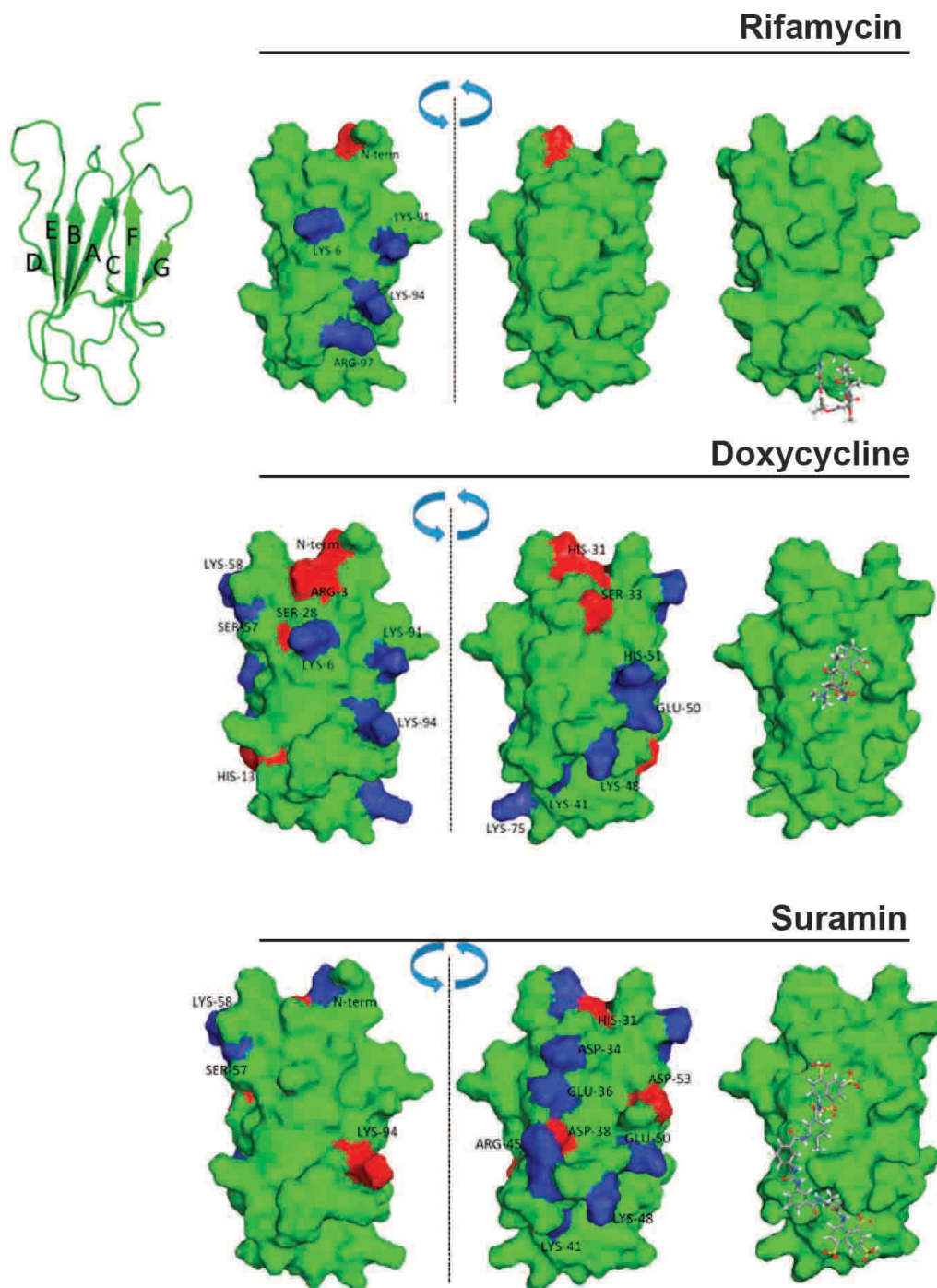
Figure 2.8: Covalent labeling results revealing putative small molecule binding sites. β2m is shown in cartoon structure in the upper left with β strand nomenclature. On the right, β2m is shown in surface models in two opposite 180° orientations. Colored in red on the surface models of β2m are residues that were measured to increase in covalent labeling percentage, while the blue residues indicate a decrease. The surface models on the far left indicate proposed binding sites, with the molecules shown as sticks. Data and figure from reference [37].

Overall, our results indicate that Dox and Rif perturb the Cu(II)-induced amyloid process by diverting pre-amyloid aggregation along a pathway that is less ordered in terms of oligomer sizes and more amorphous in terms of the final insoluble material (Figure 2.9).
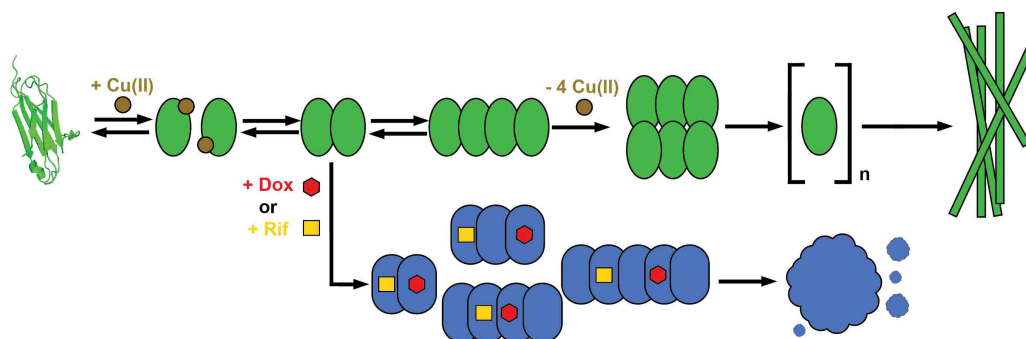
Figure 2.9: Proposed model for Dox and Rif-based inhibition. Dox and Rif alter the amyloid assembly pathway yielding stoichiometrically and structurally distinct soluble and insoluble oligomeric structures.

The process begins with compaction of the dimer that presumably enables the formation of trimers instead of the tetramers that are normally observed on the amyloid pathway. The inhibitors also appear to prevent the formation of an elongated tetramer, which may be the Cu(II)-free tetramer that is required to eventually form an amyloid-competent nucleus [11].

Interestingly, tetracyclines like Dox are known to bind divalent metals like Cu(II), suggesting that they might influence Cu(II)-β2m interactions [38,39]. The affinities of tetracyclines for Cu(II), however, are typically lower than the affinity of β2m for Cu(II) [38]. Moreover, Dox is known to precipitate readily upon binding to Cu(II) in aqueous solutions [39]. Because the only precipitation we observe is the formation of amorphous protein aggregates after 2+ weeks of incubation in the presence of Dox, we conclude that β2m-Cu(II) interactions remain mostly unaffected. The affinity of β2m for Cu(II)

changes in the presence of Dox ($K_d = 1.2$ μM without Dox and 30 μM with Dox), yet the Cu(II) concentrations used in this study are such that the majority of β2m is bound to Cu(II). Moreover, we have results that indicates that Dox binds to a site distant from the Cu(II) binding site, which likely explains the increase in K_d value observed in the presence of this small molecule [37]. From these considerations, we conclude that the observed effect of Dox is attributed to its interaction with the protein oligomers, as indicated by the ion mobility mass spectrometry data.

The observation that the inhibitors influence the β2m amyloid formation process at the oligomer stage rather than at the monomer stage is somewhat unexpected. Work on other amyloid systems, including amyloid β and transthyretin, have also concluded that small molecules can inhibit amyloid formation by working on oligomeric species rather than at the monomeric level, but our work is the first evidence of this occurring with β2m [40–42]. While amyloid inhibition is a desirable outcome in general, generating off-pathway aggregates during the process could lead to other undesired consequences, such as unexpected cellular toxicity [43–47]. Thus, studies like the ones described here, which seek to gain insight into the mechanism of inhibition, are important for understanding possible side effects of amyloid inhibition.

2.5 Conclusions

Dox and Rif inhibit the amyloid fibril formation of β2m by causing the establishment of an alternative oligomerization pathway that ultimately produces amorphous, re-dissolvable aggregates. Rather than interfering with the amyloid pathway at the monomer stage, these molecules initially exert their influence on the dimer, causing compaction of this oligomer, which leads to the formation of larger oligomers that are

incapable of forming amyloid fibrils. Dox and Rif also prevent the formation of an

amyloid-competent tetramer that was found previously to be an essential step along the

Cu(II)-induced amyloid pathway.

These inhibitors remain bound to the early oligomers that populate the alternate

aggregation pathway, suggesting that they reinforce the structural changes caused by their

binding; however, the molecules are released upon formation of the larger amorphous

precipitates that are eventually formed. Overall, the results from this study not only

describe molecules that can inhibit β2m amyloid formation but also reveal that inhibitors

can work by diverting, rather than preventing, the aggregation pathway of β2m by

causing somewhat subtle structural changes to pre-amyloid oligomers. Moreover, this

study demonstrates the value of native ESI-MS and ion mobility for revealing the β2m

oligomer structural changes that are associated with amyloid inhibition.

2.6 References

[1] A.J. Doig, P. Derreumaux, Inhibition of protein aggregation and amyloid formation by small molecules, Current Opinion in Structural Biology. 30 (2015) 50–56.

[2] B. Cheng, H. Gong, H. Xiao, R.B. Petersen, L. Zheng, K. Huang, Inhibiting toxic aggregation of amyloidogenic proteins: A therapeutic strategy for protein misfolding diseases, Biochimica et Biophysica Acta (BBA) - General Subjects. 1830 (2013) 4860–4871.

[3] T.B. Drüeke, Z.A. Massy, Beta2-Microglobulin, Seminars in Dialysis. 22 (2009) 378–380.

[4] F. Gejyo, S. Odani, T. Yamada, N. Honma, H. Saito, Y. Suzuki, Y. Nakagawa, H. Kobayashi, Y. Maruyama, Y. Hirasawa, M. Suzuki, M. Arakawa, β2-microglobulin: A new form of amyloid protein associated with chronic hemodialysis, Kidney International. 30 (1986) 385–390.

[5] H. Katou, T. Kanno, M. Hoshino, Y. Hagihara, H. Tanaka, T. Kawai, K. Hasegawa, H. Naiki, Y. Goto, The role of disulfide bond in the amyloidogenic state of β2-microglobulin studied by heteronuclear NMR, Protein Science. 11 (2009) 2218–2229.

[6] F. Danesh, L.T. Ho, Dialysis-Related Amyloidosis: History and Clinical Manifestations, Seminars in Dialysis. 14 (2001) 80–85.

[7] V.J. McParland, N.M. Kad, A.P. Kalverda, A. Brown, P. Kirwin-Jones, M.G. Hunter, M. Sunde, S.E. Radford, Partially Unfolded States of β $_2$ -Microglobulin and Amyloid Formation in Vitro, Biochemistry. 39 (2000) 8735–8746.

[8] E. Rennella, A. Corazza, S. Giorgetti, F. Fogolari, P. Viglino, R. Porcari, L. Verga, M. Stoppini, V. Bellotti, G. Esposito, Folding and Fibrillogenesis: Clues from β2-Microglobulin, Journal of Molecular Biology. 401 (2010) 286–297.

[9] T. Ookoshi, K. Hasegawa, Y. Ohhashi, H. Kimura, N. Takahashi, H. Yoshida, R. Miyazaki, Y. Goto, H. Naiki, Lysophospholipids induce the nucleation and extension of 2-microglobulin-related amyloid fibrils at a neutral pH, Nephrology Dialysis Transplantation. 23 (2008) 3247–3255.

[10] T. Eichner, S.E. Radford, Understanding the complex mechanisms of β2-microglobulin amyloid assembly: β2-microglobulin fibrillogenesis at physiological pH, FEBS Journal. 278 (2011) 3868–3883.

[11] K. Antwi, M. Mahar, R. Srikanth, M.R. Olbris, J.F. Tyson, R.W. Vachet, Cu(II) organizes β-2-microglobulin oligomers but is released upon amyloid formation, Protein Science. 17 (2008) 748–759.

[12] R. Srikanth, V.L. Mendoza, J.D. Bridgewater, G. Zhang, R.W. Vachet, Copper Binding to β-2-Microglobulin and Its Pre-Amyloid Oligomers, Biochemistry. 48 (2009) 9871–9881.

[13] J. Dong, C.A. Joseph, N.B. Borotto, V.L. Gill, M.J. Maroney, R.W. Vachet, Unique Effect of Cu(II) in the Metal-Induced Amyloid Formation of β-2-Microglobulin, Biochemistry. 53 (2014) 1263–1274.

[14] M. Quaglia, C. Carazzone, S. Sabella, R. Colombo, S. Giorgetti, V. Bellotti, E. De Lorenzi, Search of ligands for the amyloidogenic protein β2-microglobulin by capillary electrophoresis and other techniques, Electrophoresis. 26 (2005) 4055–4063.

[15] L. Regazzoni, R. Colombo, L. Bertoletti, G. Vistoli, G. Aldini, M. Serra, M. Carini, R.M. Facino, S. Giorgetti, M. Stoppini, G. Caccialanza, E. De Lorenzi, Screening of fibrillogenesis inhibitors of β2-microglobulin: Integrated strategies by mass spectrometry capillary electrophoresis and in silico simulations, Analytica Chimica Acta. 685 (2011) 153–161.

[16] L.A. Woods, G.W. Platt, A.L. Hellewell, E.W. Hewitt, S.W. Homans, A.E. Ashcroft, S.E. Radford, Ligand binding to distinct states diverts aggregation of an amyloid-forming protein, Nature Chemical Biology. 7 (2011) 730–739.

[17] S. Giorgetti, S. Raimondi, K. Pagano, A. Relini, M. Bucciantini, A. Corazza, F. Fogolari, L. Codutti, M. Salmona, P. Mangione, L. Colombo, A. De Luigi, R. Porcari, A. Gliozzi, M. Stefani, G. Esposito, V. Bellotti, M. Stoppini, Effect of Tetracyclines on the Dynamics of Formation and Destructuration of β2-Microglobulin Amyloid Fibrils, Journal of Biological Chemistry. 286 (2011) 2121–2131.

[18] C. Carazzone, R. Colombo, M. Quaglia, P. Mangione, S. Raimondi, S. Giorgetti, G. Caccialanza, V. Bellotti, E. De Lorenzi, Sulfonated molecules that bind a partially structured species of beta2-microglobulin also influence refolding and fibrillogenesis, Electrophoresis. 29 (2008) 1502–1510.

[19] C.J. Morgan, M. Gelfand, C. Atreya, A.D. Miranker, Kidney dialysis-associated amyloidosis: a molecular role for copper in fiber formation, Journal of Molecular Biology. 309 (2001) 339–345.

[20] C.M. Eakin, J.D. Knight, C.J. Morgan, M.A. Gelfand, A.D. Miranker, Formation of a Copper Specific Binding Site in Non-Native States of β-2-Microglobulin, Biochemistry. 41 (2002) 10646–10656.

[21] C.M. Eakin, F.J. Attenello, C.J. Morgan, A.D. Miranker, Oligomeric Assembly of Native-like Precursors Precedes Amyloid Formation by β-2 Microglobulin, Biochemistry. 43 (2004) 7808–7815.

[22] V.L. Mendoza, K. Antwi, M.A. Barón-Rodríguez, C. Blanco, R.W. Vachet, Structure of the Preamyloid Dimer of β-2-Microglobulin from Covalent Labeling and Mass Spectrometry, Biochemistry. 49 (2010) 1522–1532.

[23] V.L. Mendoza, M.A. Barón-Rodríguez, C. Blanco, R.W. Vachet, Structural Insights into the Pre-Amyloid Tetramer of β-2-Microglobulin from Covalent Labeling and Mass Spectrometry, Biochemistry. 50 (2011) 6711–6722.

[24] H. Hernández, C.V. Robinson, Determining the stoichiometry and interactions of macromolecular assemblies from mass spectrometry, Nature Protocols. 2 (2007) 715–726.

[25] M.F. Bush, Z. Hall, K. Giles, J. Hoyes, C.V. Robinson, B.T. Ruotolo, Collision Cross Sections of Proteins and Their Complexes: A Calibration Framework and Database for Gas-Phase Structural Biology, Analytical Chemistry. 82 (2010) 9557–9565.

[26] F. Meng, P. Marek, K.J. Potter, C.B. Verchere, D.P. Raleigh, Rifampicin Does Not Prevent Amyloid Fibril Formation by Human Islet Amyloid Polypeptide but Does Inhibit Fibril Thioflavin-T Interactions: Implications for Mechanistic Studies of β-Cell Death [†], Biochemistry. 47 (2008) 6016–6024.

[27] D.M. Williams, T.L. Pukala, Novel insights into protein misfolding diseases revealed by ion mobility-mass spectrometry, Mass Spectrometry Reviews. 32 (2013) 169–187.

[28] R. Beveridge, Q. Chappuis, C. Macphee, P. Barran, Mass spectrometry methods for intrinsically disordered proteins, The Analyst. 138 (2013) 32–42.

[29] F. Lanucara, S.W. Holman, C.J. Gray, C.E. Eyers, The power of ion mobility-mass spectrometry for structural characterization and the study of conformational dynamics, Nature Chemistry. 6 (2014) 281–294.

[30] S.-J. Hyung, B.T. Ruotolo, Integrating mass spectrometry of intact protein complexes into structural proteomics, Proteomics. 12 (2012) 1547–1564.

[31] B.T. Ruotolo, J.L.P. Benesch, A.M. Sandercock, S.-J. Hyung, C.V. Robinson, Ion mobility–mass spectrometry analysis of large protein complexes, Nature Protocols. 3 (2008) 1139–1152.

[32] B.T. Ruotolo, Evidence for Macromolecular Protein Rings in the Absence of Bulk Water, Science. 310 (2005) 1658–1661.

[33] C.A. Scarff, V.J. Patel, K. Thalassinos, J.H. Scrivens, Probing hemoglobin structure by means of traveling-wave ion mobility mass spectrometry, Journal of the American Society for Mass Spectrometry. 20 (2009) 625–631.

[34] J. Seo, W. Hoffmann, S. Warnke, M.T. Bowers, K. Pagel, G. von Helden, Retention of Native Protein Structures in the Absence of Solvent: A Coupled Ion Mobility and Spectroscopic Study, Angewandte Chemie International Edition. 55 (2016) 14173–14176.

[35] Y. Sun, S. Vahidi, M.A. Sowole, L. Konermann, Protein Structural Studies by Traveling Wave Ion Mobility Spectrometry: A Critical Look at Electrospray Sources and Calibration Issues, Journal of The American Society for Mass Spectrometry. 27 (2016) 31–40.

[36] M.M. Maurer, G.C. Donohoe, S.J. Valentine, Advances in ion mobility-mass spectrometry instrumentation and techniques for characterizing structural heterogeneity, The Analyst. 140 (2015) 6782–6798.

[37] T. Liu, T.M. Marcinko, P.A. Kiefer, R.W. Vachet, Using Covalent Labeling and Mass Spectrometry To Study Protein Binding Sites of Amyloid Inhibiting Molecules, Analytical Chemistry. 89 (2017) 11583–11591.

[38] M. Jezowska-Bojczuk, L. Lambs, H. Kozlowski, G. Berthon, Metal ion-tetracycline interactions in biological fluids. 10. Structural investigations on copper(II) complexes of tetracycline, oxytetracycline, chlortetracycline, 4-(dedimethylamino)tetracycline, and 6-desoxy-6-demethyltetracycline and discussion of their binding modes, Inorganic Chemistry. 32 (1993) 428–437.

[39] M. Brion, L. Lambs, G. Berthon, Metal ion-tetracycline interactions in biological fluids. Part 6. Formation of copper(II) complexes with tetracycline and some of its derivatives and appraisal of their biological significance, Inorganica Chimica Actra. 123 (1986) 61–68.

[40] C. Bleiholder, T.D. Do, C. Wu, N.J. Economou, S.S. Bernstein, S.K. Buratto, J.-E. Shea, M.T. Bowers, Ion Mobility Spectrometry Reveals the Mechanism of Amyloid Formation of Aβ(25–35) and Its Modulation by Inhibitors at the Molecular Level: Epigallocatechin Gallate and *Scyllo* -inositol, Journal of the American Chemical Society. 135 (2013) 16926–16937.

[41] Y. Liang, M.O. Ore, S. Morin, D.J. Wilson, Specific Disruption of Transthyretin(105–115) Fibrilization Using "Stabilizing" Inhibitors of Transthyretin Amyloidogenesis, Biochemistry. 51 (2012) 3523–3530.

[42] D.D. Soto-Ortega, B.P. Murphy, F.J. Gonzalez-Velasquez, K.A. Wilson, F. Xie, Q. Wang, M.A. Moss, Inhibition of amyloid-β aggregation by coumarin analogs can be manipulated by functionalization of the aromatic center, Bioorganic & Medicinal Chemistry. 19 (2011) 2596–2602.

[43] M.E. Larson, S.E. Lesné, Soluble Aβ oligomer production and toxicity: Soluble oligomeric Aβ production and toxicity, Journal of Neurochemistry. 120 (2012) 125–139.

[44] M. Fändrich, Oligomeric Intermediates in Amyloid Formation: Structure Determination and Mechanisms of Toxicity, Journal of Molecular Biology. 421 (2012) 427–440.

[45] K.E. Marshall, R. Marchante, W.-F. Xue, L.C. Serpell, The relationship between amyloid structure and cytotoxicity, Prion. 8 (2014) 192–196.

[46] U. Sengupta, A.N. Nilson, R. Kayed, The Role of Amyloid-β Oligomers in Toxicity, Propagation, and Immunotherapy, EBioMedicine. 6 (2016) 42–49.

[47] E. Cerasoli, M.G. Ryadnov, B.M. Austen, The elusive nature and diagnostics of misfolded Aβ oligomers, Frontiers in Chemistry. 3 (2015) 17.

CHAPTER 3

STRUCTURAL HETEROGENEITY IN THE PRE-AMYLOID OLIGOMERS OF

β-2-MICROGLOBULIN

This chapter is adapted from part of a manuscript to be submitted as: Marcinko, T.M.; Liang, C.; Savinov, S.; Chen, J.; and Vachet, R.W. Structural heterogeneity in the pre-amyloid oligomers of β-2-microglobulin.

3.1 Introduction

β-2-microglobulin (β2m) is a 99-residue structural protein non-covalently associated with major histocompatibility complex I, which is present on the surface of all nucleated cells [1]. β2m features a 7-membered anti-parallel beta-strand arrangement forming a beta-sandwich, which is connected by a single disulfide bond [2]. In chronic dialysis patients, it is known to form amyloid fibrils that deposit in joints and other organs [3,4]. The long-term consequences of these amyloid deposits are joint destruction and organ dysfunction [4].

β2m is capable of forming amyloid fibrils under a variety of conditions *in vitro* (e.g. incubation at low pH, addition of trifluoroethanol, presence of collagen, truncation of the first six amino acid residues, and incubation with Cu(II)), but the exact physiological mechanism(s) that triggers amyloid formation *in vivo* is unclear [5–12]. Preceding oligomer (and eventually, amyloid) formation, there are a series of known structural events that disrupt the native state of β2m. These events include the *cis-trans* isomerization of P32 leading to the repacking of the hydrophobic core of the protein, and the repositioning of other residues, such D59 and R3, depending on how amyloid formation is initiated [13–16].

While there are some common β2m structural changes caused by the different amyloid initiating conditions, oligomerization proceeds differently in many cases. For example, acid-induced amyloid formation proceeds via the sequential addition of monomeric units [6], whereas Cu(II)-catalyzed oligomerization generally proceeds through even numbered steps, with the dimer as a building block [11,12]. Moreover, the monomeric subunits in Cu(II)-catalyzed oligomers are thought to be native-like in their structures, while acid-induced oligomerization progresses through partially unfolded intermediates [17]. This apparent complexity and diversity underline the importance of studying amyloid formation, and comparing oligomeric structures generated by different mechanisms.

One particularly interesting feature of amyloid forming proteins that have been recently revealed in other amyloid systems is the presence of different conformational isomers(conformers) in higher-order oligomers that precede amyloid fibrils [17,18]. In fact, there is even evidence that the mature fibrils themselves can even be heterogeneous [19], suggesting that different oligomeric conformers might lead to different amyloid morphologies. This heterogeneity can manifest itself in many ways, such as through different oligomeric assembly states that may be off-pathway (i.e. not productive to further assembly and amyloid formation) [17,18]. Our group first gathered preliminary evidence of conformational heterogeneity for β2m pre-amyloid oligomers while using ion mobility-mass spectrometry (IM-MS) to understand small molecule inhibitors of β2m amyloid formation [20]. There is little information about such conformational heterogeneity for β2m pre-amyloid oligomers, prompting the study described here.

In this study, we characterize the heterogeneity present in Cu(II)-catalyzed β2m pre-amyloid oligomers and provide insight into the different structural forms that are present during amyloid formation. To do this, we primarily employ IM-MS, which separates protein complex ions based on their collisional cross section (CCS) [21–23]. To relate these measurements to solution-phase structures, the protein complex ions are generated under native-like conditions in which a memory of their solution-phase structures remains [21,24–30]. Computational modeling and other experimental constraints such as covalent labeling MS [24,31] can then be combined with the IM-MS measurements to build model structures of the pre-amyloid conformers. From our measurements, we find that oligomers generated in the presence of Cu(II) are structurally distinct when compared to β2m amyloids formed under different conditions (e.g. acid). In addition, we find unique heterogeneity in β2m tetramers that is associated with Cu(II) loss from the oligomers, which is an essential step in Cu(II)-induced amyloid formation by β2m. We propose that tetramer heterogeneity is an essential feature of Cu(II)-induced amyloid formation by β2m, which contrasts to conformational isomers in other amyloid systems that are typically thought to be associated with off-pathway products [32–34].

3.2 Materials and methods

3.2.1 Methods

3.2.1.1 β2m Oligomer Formation

Human, full-length wild type β2m (Cat #126-11) that is purified from urine was purchased from Lee Biosolutions (Maryland Heights, MO). Non-protein chemicals, unless otherwise noted, were purchased from Sigma-Aldrich (St. Louis, MO). The

solution conditions for the protein samples are similar to our previous work, which
included 25 mM MOPS, 150 mM potassium acetate, 500 mM urea at pH 7.4 [12,35].
Protein concentration of incubated samples ranged from 50-100 μM, and copper
concentrations were always kept at a 2:1 Cu:β2m ratio. Incubation conditions to form
β2m amyloids were carried out at 37°C, and under these conditions amyloids are fully
formed on the order of weeks (<1 month) [12,20,35]. The pre-amyloid oligomers of
interest in this study were sampled during days 1-10.

3.2.1.2 Electrospray Ionization Ion Mobility Spectrometry Mass Spectrometry (ESI-IM-MS)

Prior to analysis, samples were removed from the incubation chamber and
exchanged into 100 mM ammonium acetate through a GE HiTrap desalting column (Cat#
17140801) (Chicago, IL). Desalted fractions were then loaded into gold sputter-coated
glass borosilicate nanospray capillaries from Harvard Apparatus (Cat# 30-0035)
(Holliston, MA), whose preparation was described previously [36]. Mass spectral data
were collected on a Waters Synapt G2-Si (Milford, MA). Mass calibration of the
instrument from *m/z* 500-8000 was conducted with perfluoroheptanoic acid (PFHA). Our
nanospray ESI-IM-MS method was carefully optimized and performed under low energy
conditions to ensure the gentle transfer of protein complex ions from the solution phase to
the gas phase to minimize any unfolding or dissociation. No evidence of any highly
charged monomeric ions, which are a hallmark of oligomer unfolding and dissociation,
were noted during these experiments. Briefly, instrumental settings included 1 kV
capillary voltage, 20 V cone voltage, 20 V offset, and 30°C source temperature. The ion
mobility cell was operated at a wave height of 20 V, while the wave velocity was set to

300 m/s. Drift times were converted to CCS values via a calibration using proteins with known CCS values, which was described in theoretical and experimental detail elsewhere [37]. MS data were analyzed and exported with MassLynx and Driftscope. Final plots were made with OriginLab (Northampton, MA).

3.2.1.3 EDTA depletion of Cu(II)-bound species

The introduction of EDTA to deplete Cu(II)-bound species was carried out similar to prior work [12]. Briefly, prior to desalting, EDTA (500 mM) was added to incubated β2m samples to yield a final concentration of 10 mM. The added volume was approximately 2% of the total sample volume, in order to minimize dilution. The EDTA-doped samples were then allowed to remain at ambient room temperature for 10 minutes prior to desalting and ESI-IM-MS analysis. Data were analyzed as described above, but the signals shown in arrival time distribution plots were normalized by dividing the individual ion's signal by the total ion signals of all β2m peaks in the spectra in order to account for oligomer dissociation.

3.2.1.4 Collisional Cross Section calculations

The CCS value of each MD-calculated protein state was estimated using the IMPACT program that uses the projection approximation (PA) method [38]. For each configuration sampled by MD simulation, ten PA calculations were repeated and the average value was reported. The simulated CCS value for each β2m oligomer was determined by the peak position after fitting the CCS distribution that was calculated

from all possible configurations sampled by MD using a Gaussian function. All calculated values from crystal or NMR structures were treated identically.

3.2.1.5 Structure Excision and Protein-Protein Docking

Initial tetramer models of β2m were generated via protein-protein docking using dimeric subunits from the hexameric structure of the H13F mutant (PDB: 3CIQ). The subunit structures were transformed into protonation-state optimized all-atom models using the Schrödinger Maestro protein preparation wizard (Schrödinger, LLC, New York, NY). For each dimeric subunit, unconstrained protein-protein docking was performed with Schrödinger BioLuminate PIPER algorithm (Schrödinger, LLC, New York, NY). The 'homodimer' mode was implemented, probing 70,000 ligand rotations. The optimal oligomeric models were selected for further analysis via visual inspection and MD stability tests (see below), upon which symmetric docked structures have collapsed onto compact (TET3) or extended (TET4) forms persisting through simulations.

3.2.1.6 Molecular Dynamics Simulations

Classical MD simulations using atomistic models were performed using the GROMACS 2018 package [39]. The CHARMM36m force field and the TIP3P model were chosen for modeling human β2m and water molecules [40,41]. The protonation states of the titratable amino acid side chains and N-/C-terminus of β2m were chosen to reproduce the physiological condition at pH 7. The simulations of β2m monomer, dimers, tetramers were then performed to verify their stability maintaining by crucial interactions.

The detailed procedures for constructing different oligomer states and simulation parameters are summarized in Appendix A.

3.3 Results

3.3.1 β2m oligomers have characteristic structural heterogeneities present during amyloid formation

In the presence of stoichiometric amounts of Cu(II), we first performed native ESI-IM-MS experiments at several intervals during the early stages (≤ 7 days) of β2m oligomerization. Figure 3.1A shows representative mass spectral results from samples at day 6. These mass spectra reveal the presence of soluble even-ordered oligomers, including dimers, tetramers, and hexamers, whose stoichiometries are the same as measured previously for Cu(II)-induced β2m amyloid formation [11,12,15,42]. These oligomeric species populate over time, implying that specific assembly steps are occurring in solution in order to build them. For example, dimers are detected after a few hours to 10 days of incubation, while tetramers and hexamers require 1 and 2 days, respectively, to be detected.

Interestingly, upon examination of the IM data under native MS conditions, we detect multiple peaks in the arrival time distributions (ATDs) of the oligomers but not the monomer (Figure 3.1B), indicating that the oligomers have conformational isomers. The presence of multiple conformations is particularly striking for the tetramer and hexamer. The monomers with and without Cu(II) bound have identical ATDs, indicating that Cu(II) binding does not itself introduce this conformational heterogeneity at the monomer level (Figure 3.2). The multiple conformations for each oligomer are present as soon as

56

the oligomer is first detected by MS, and the centroids for these peaks also remain consistent.
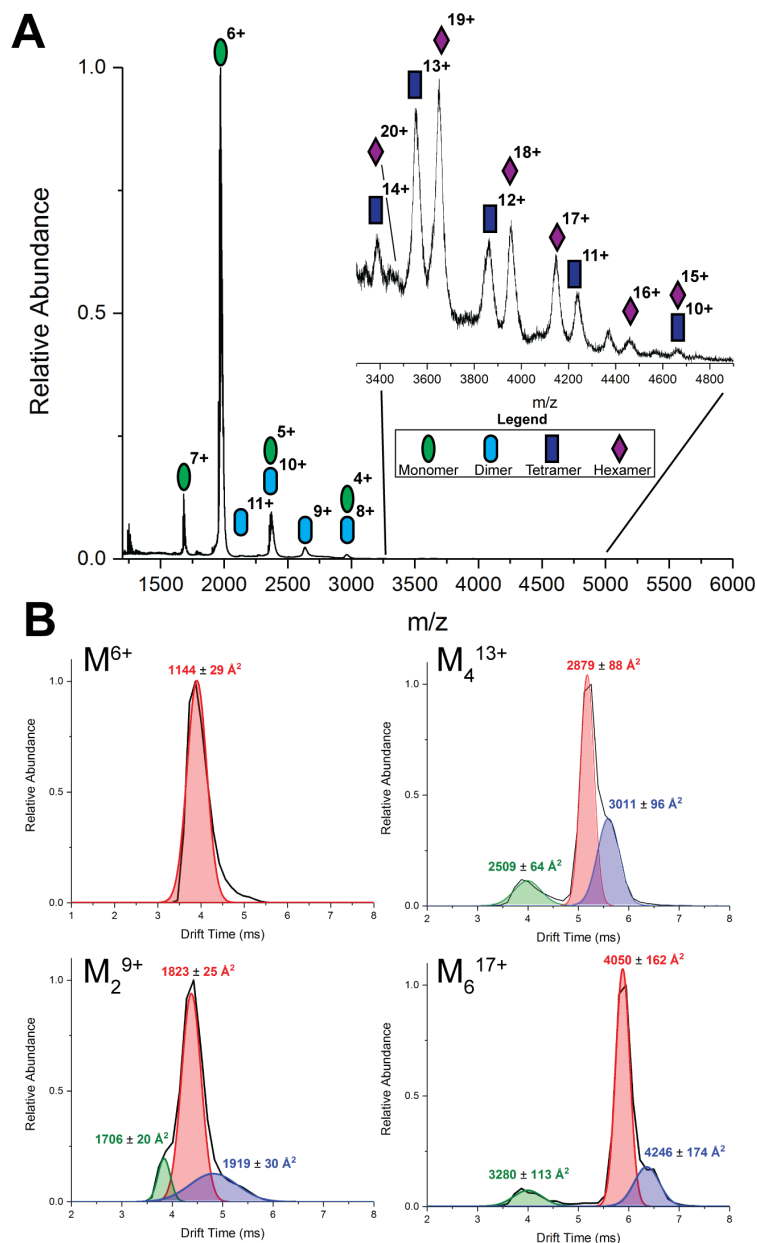
Figure 3.1: Mass spectra and extracted arrival time distributions of β2m oligomers after incubation in the presence of Cu(II) for 6 days. Panel A shows the mass spectrum collected over the full m/z acquisition range, while the inset shows an expanded view of the m/z region where tetramer and hexamer ions are detected. Panel B shows representative ATD plots, extracted from their corresponding mass spectral peaks. Peaks were fit using Gaussian distributions. The collisional cross section for the centroid of each peak is shown in corresponding color. The error values are from estimations of the random error of the CCS calibration curve. Odd charge states are chosen for each oligomer to ensure their unique identity.
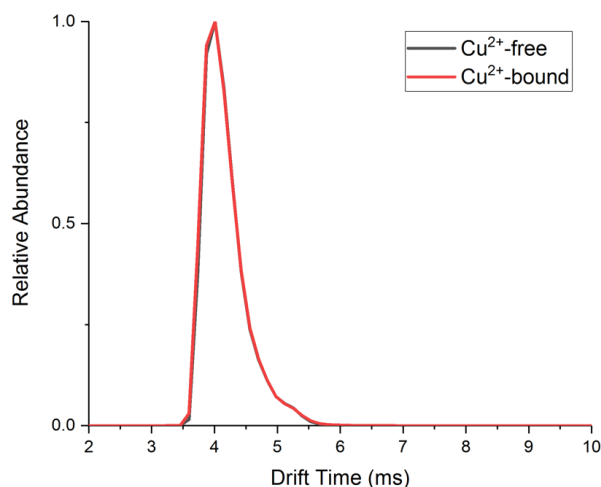
Figure 3.2: Extracted ATD of M^{6+} ion for Cu(II)-bound and Cu(II)-free β2m. Cu(II)-containing sample was loaded with >95% Cu(II) (red) versus no Cu(II) (black).

A summary of the oligomer collision cross sections (CCS) from measurements of different charge states as a function of oligomer stoichiometry is shown in Figure 3.3. These data demonstrate that the Cu(II)-induced oligomers are all more compact than simple 'beads on string,' immediately providing rough insight into the geometry of these species. Moreover, when the CCS values are compared to calculated and measured CCS values for other previously reported β2m and β2m mutant oligomers (Table 3.1), we find that the Cu(II)-induced oligomers are more compact in almost every case.

The measured monomer CCS value is consistent with the monomeric crystal/NMR structures for the wild-type protein and is more compact and less heterogeneous than the monomers measured upon amyloid initiation at low pH (Table 3.1). We also find that some of the Cu(II)-induced oligomers are more heterogeneous than corresponding oligomers produced at low pH [6,17]. The measured CCS values for the most abundant conformers for the Cu(II)-induced dimers and tetramers are in good agreement with calculated CCS values for the P32A mutant dimer structure (PDB:

2F8O), as well as dimers and tetramers excised from the Cu(II)-bound H13F hexamer

structure (PDB: 3CIQ) (Table 3.1) [13,43].
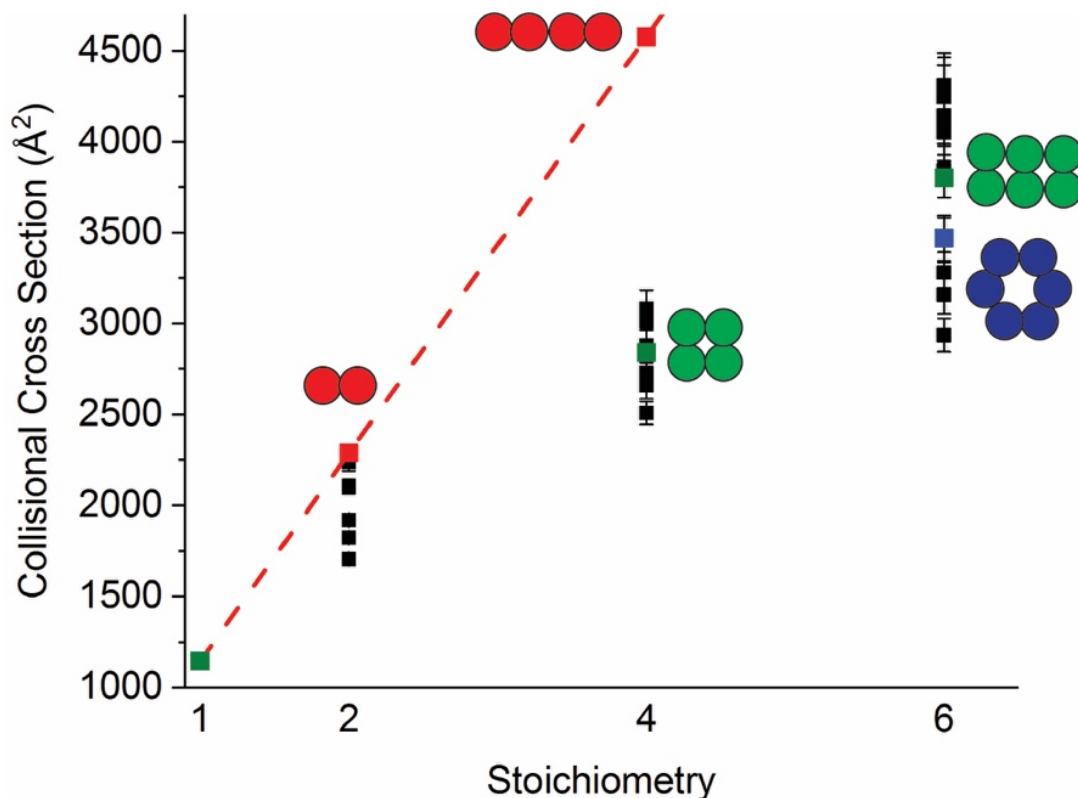
Figure 3.3: A scatter plot of experimentally determined CCS values for β2m conformers (black) and theoretical models (red & green). Black squares represent actual IM measurements. Error bars are from estimated random error of the calibration curve. Red models assume perfect spherical particles assembled as beads on a string. Green models also assume spherical monomers, but in a more compact configuration. The blue hexamer is a calculated CCS value for a hexagonal array of spheres.

3.3.2 Computational modeling coupled to ESI-IM-MS and covalent labeling reveals a side-by-side configuration for the β2m dimer

To further investigate the dimers measured with ESI-IM-MS, we used

computational modeling to generate potential candidate structures for comparison (Figure

3.4). Because the Cu(II)-induced dimers in our experiments have similar CCS values to

the calculated CCS values for the dimeric structures taken from the H13F hexamer (Table

Species	Amyloid inducing agent	CCS (Å²)	Method	PDB ID	Reference
Monomer (crystal)	None	1142	Calculated	1LDS	# (Radford 2002)
Monomer (2D NMR)	None	1153	Calculated	1JNJ	# (Esposito 2002)
Monomer	Cu(II)	1180	Measured	-	this work
Monomer (native-like)	Low pH	1325	Measured	-	# (Ashcroft 2010)
Monomer (partially unfolded)	Low pH	1768	Measured	-	# (Ashcroft 2010)
Monomer (unfolded)	Low pH	2093	Measured	-	# (Ashcroft 2010)
Monomer (reduced)	Low pH	2530	Measured	-	# (Ashcroft 2010)
Dimer	Cu(II)	1823	Measured	-	this work
Dimer	Low pH	2180	Measured	-	# (Ashcroft 2010)
Dimer (edge-to-edge)	Low pH	~2000	Measured	-	# (Ashcroft 2010)
Dimer (end-to-end)	Low pH	~2200	Measured	-	# (Ashcroft 2010)
Dimer P32A	Cu(II)	1829	Calculated	2F8O	# (Miranker 2006)
Tetramer P32A	Cu(II)	2997	Calculated	2F8O	# (Miranker 2006)
Dimer DIMC20	TFE	2015	Calculated	From 3TLR	# (Bolognesi 2012)
Dimer DIMC50	TFE	2024	Calculated	From 3TM6	# (Bolognesi 2012)
Dimer via H13F (position 1)	Cu(II)	1831	Calculated	From 3CIQ	# (Miranker 2008)
Dimer via H13F 2 (position 2)	Cu(II)	1964	Calculated	From 3CIQ	# (Miranker 2008)
Tetramer	Cu(II)	3080	Measured	-	this work
Tetramer	Cu(II)	3120	Calculated	From 3CIQ	# (Miranker 2008)
Tetramer	Low pH	3721	Measured	-	# (Ashcroft 2010)
Tetramer (DIMC20)	TFE	3278	Calculated	From 3TLR	# (Bolognesi 2012)
Tetramer (DIMC50)	TFE	3059	Calculated	From 3TM6	# (Bolognesi 2012)
H13F Hexamer	Cu(II)	3972	Calculated	3CIQ	# (Miranker 2008)
Hexamer	Cu(II)	4050	Measured	-	this work

Table 3.1: Survey of calculated and measured CCS values for various monomeric and oligomeric states of β2m

3.1), we used these structures as starting points for the calculations. We excised two

dimer configurations from the H13F crystal structure, mutated the F13 back to H,

subjected the structures to energy minimization, and then performed MD calculations in

explicit solvent. For each dimer, we also removed Cu(II) and did separate energy

minimization and MD calculations.

Of the four resulting dimer configurations, three were found to be stable during

the simulations for up to 1 µs. The three stable configurations can be categorized as either

having a head-to-head interaction involving the N-terminal region of the protein or a

side-by-side interaction involving the four-strand β-sheet (Figure 3.2A). The side-by-side

Cu(II)-free dimer is relatively unstable *in silico*, as it dissociated during the MD
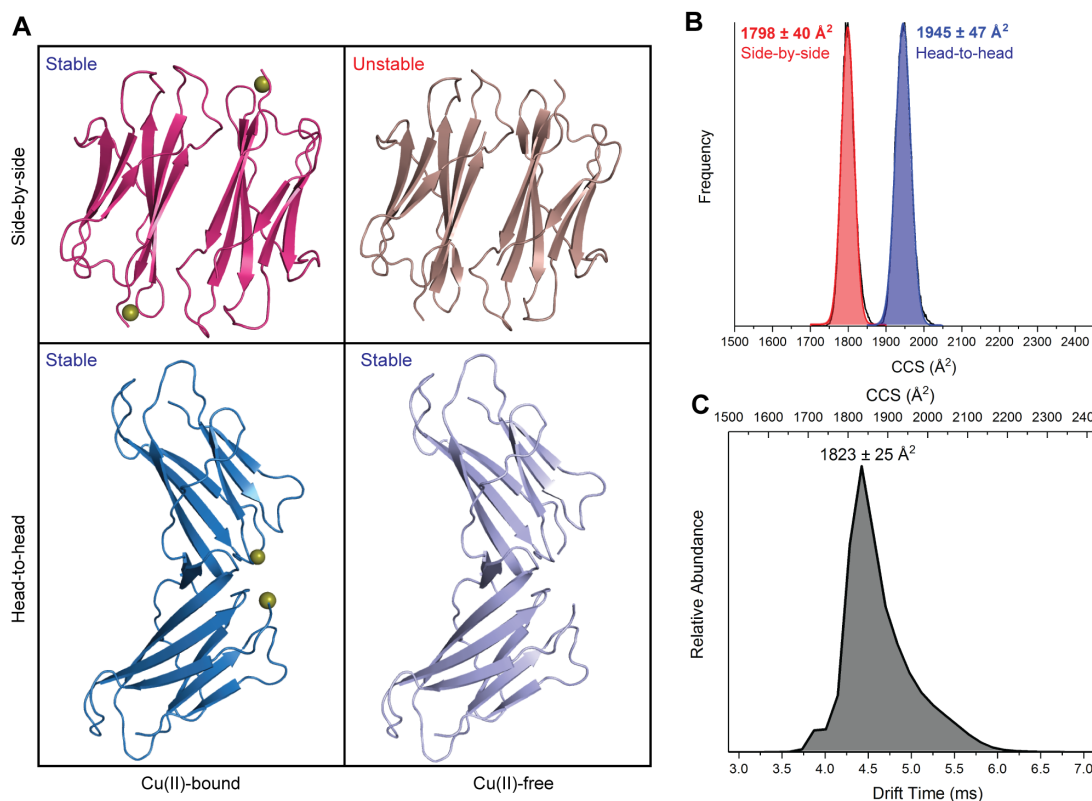
Figure 3.4: Different configurations of the β2m dimer in apo- and holo- forms from computational modeling. Panel A shows four different configurations of dimer in both apo- and holo-forms found following structure excision from H13F and MD simulations. Panel B shows calculated CCS centroid values and distributions for both dimer configurations across the MD trajectory. Panel C is an extracted ATD for the dimer[9+] ion with a centroid CCS value for the most abundant species.

simulation. Of the three stable configurations, solvent accessible surface area (SASA) calculations of the Cu(II)-bound side-by-side structure is more consistent with trends measured by covalent labeling-mass spectrometry data (Figure 3.3) [16]. Moreover, previous work has also show that Cu(II) remains bound to the dimer, suggesting that the modeling experiments are recapitulating the necessity of Cu(II) for dimer stability [15]. As a way to provide further support for the side-by-side dimer configuration, we then calculated the theoretical CCS values of the three stable configurations (Figure 3.2B). Comparison of these results to the experimentally measured CCS values (Figure 3.2C) reveals that the main conformer agrees well with the side-by-side dimer structure.
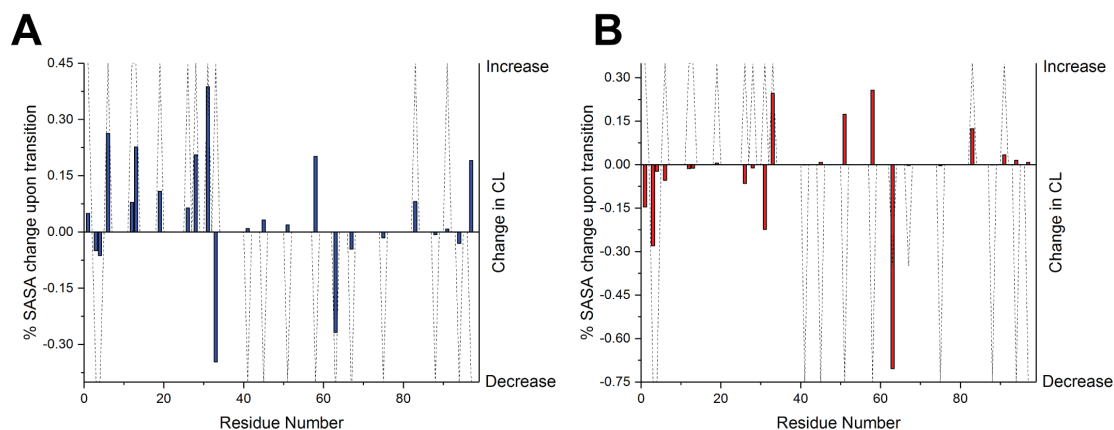
Figure 3.5: Comparison of covalent labeling trends with changes in solvent accessible surface area (SASA) for dimeric models. Panel A displays data for the monomer to side-by-side dimer transition, while panel B shows data for the head-to-head dimer transition. % change in SASA is expressed on the Y1 axis (bars), while the percentage covalent labeling change is displayed on Y2 (black dots). CL data from ref. [16].

Critical for the stabilization of the side-by-side dimer are the presence of intermolecular salt bridges (R3-E16, D59-K19) that are found in the modeled structure only when Cu(II) is present (Figure 3.4). Overall, these results are consistent with a previously reported model of the dimer [16].
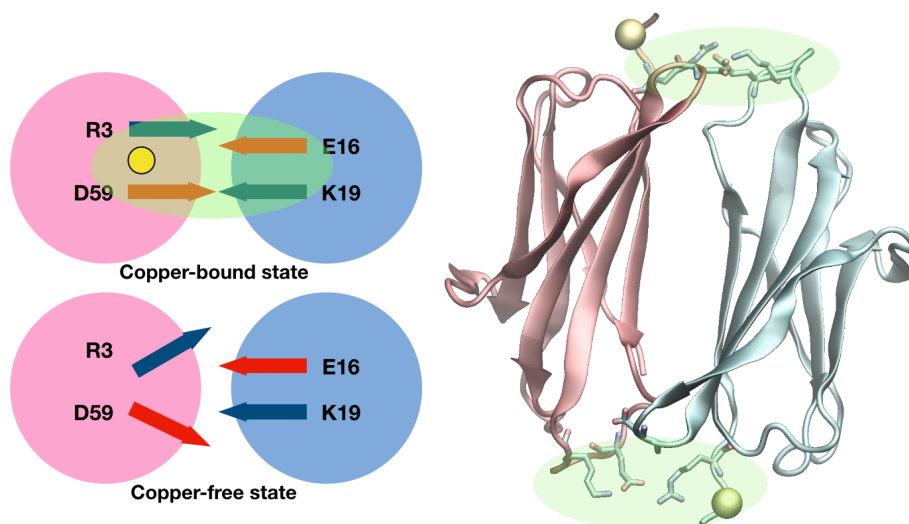
Figure 3.6: Important residues involved in salt bridges that stabilize the side-by-side dimer. The residues highlighted in green in the left hand cartoon are shown in sticks on the dimer structure at right. The orientations of these four residues are unique to the Cu(II)-bound state, as their geometries are different in the Cu(II)-free.

3.3.3 β2m tetrameric species are uniquely heterogeneous

Unlike the dimers, which have relatively little conformational heterogeneity, the tetramers have several conformers with a range of CCS values (Figure 3.1). Moreover, the tetramer ATD peak widths for all charge states narrow over time (Figure 3.5B) in contrast to the dimers (Figure 3.5A) and hexamers (Figure 3.5C) whose ATD peak widths remain constant during the course of the amyloid formation reaction. The peak widths for the tetrameric ions decrease an average of 45% from day 1 to day 10. The
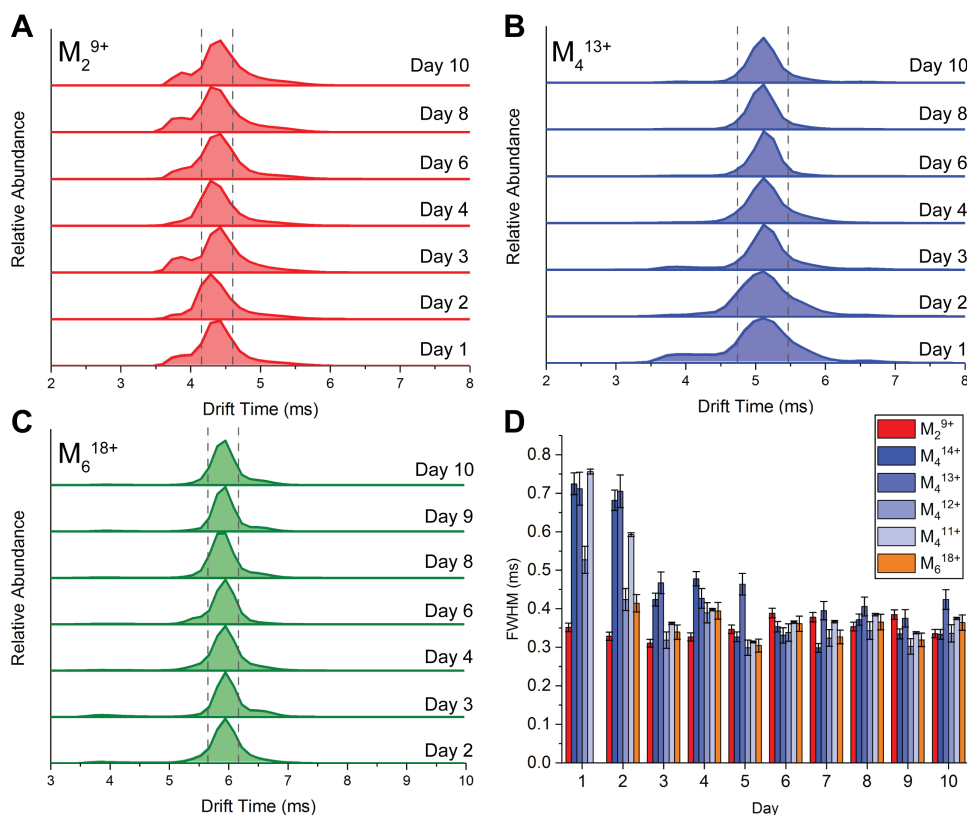
Figure 3.7: Extracted ATDs for oligomeric conformers during early amyloid formation. Panels A-C show extracted ATDs for dimer[9+], tetramer[13+], and hexamer[18+] ions over the early stages of amyloid formation, respectively. The width of the dashed lines are added to approximate the FWHM of the first day that the ion is detected and are for illustrative purposes only to guide the eye. Panel D shows calculated FWHM values of selected dimer, tetramer, and hexamer ions over the course of the experiment. Error bars reflect calculated percent variation based on standard deviations on replicate measurements of the corresponding ion ATDs on different days of analysis.

timeframe over which this structural heterogeneity evolves coincides with the emergence of the Cu(II)-free tetramer, which several studies have previously found to be a necessary step for Cu(II)-induced amyloid formation [12,44,45]. Structural information about this Cu(II)-free tetramer is largely absent; however, it is reasonable to hypothesize that some degree of structural transformation occurs to form this necessary oligomeric species because the Cu(II)-tetramer is resistant to dissociation upon the addition of EDTA, while the Cu(II)-bound tetramer dissociates into monomers [12]. An intriguing question is whether the presence of multiple tetrameric conformers are a prelude to the formation of the Cu(II)-free tetramer.

To address this question, we added EDTA once dimers, tetramers, and hexamers were present in solution, and then used ion mobility to measure the resulting oligomeric conformers (Figure 3.6). Consistent with previous observations, the addition of EDTA causes an increase in monomer signal (Figure 3.6A), dissociation of the dimer (Figure 3.6B), partial dissociation of the tetramer (Figure 3.6C), and no effect on the hexamer signal (Figure 3.6C). Interestingly, the ATDs of the EDTA-treated tetrameric ions result in the depletion of the most abundant conformer in each charge state, leaving the more compact and/or expanded conformer (Figures 3.6D & E). Given the high affinity of EDTA for Cu(II) and its excess concentration, we attribute these remaining peaks to the Cu(II)-free tetramer. Evidently, the Cu(II)-free tetramer has multiple conformations and is structurally different than the Cu(II)-bound version. It is possible that the decreased heterogeneity observed for the tetramer over time (i.e. Figure 3.6A and D) reflects the sampling of different conformational states to achieve tetramers that are stable in the absence of Cu(II).
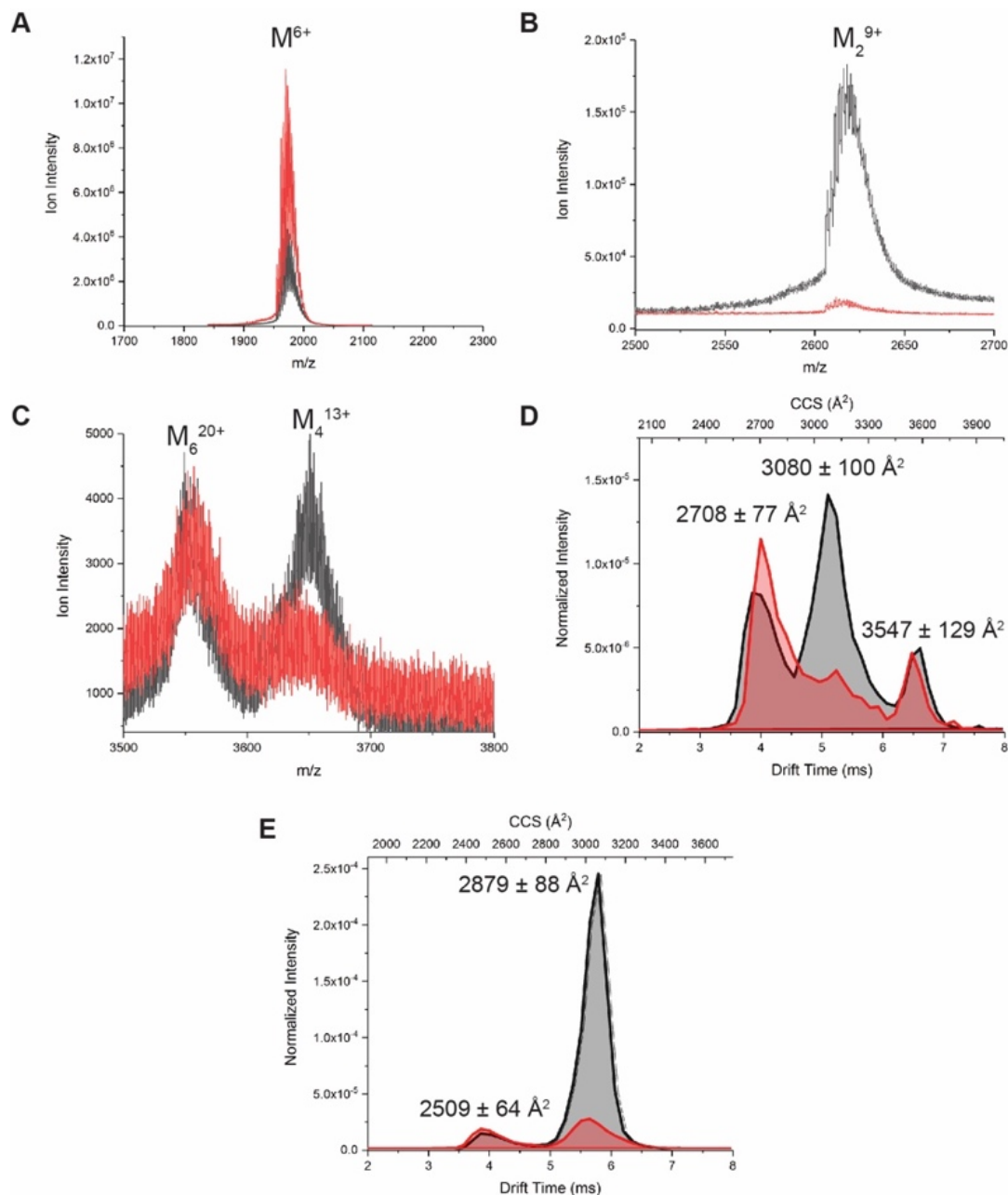
Figure 3.8: Treating oligomers with EDTA reveals structures of Cu(II)-free tetramer. Panels A, B, and C show mass spectra around selected ions from control (black) and EDTA-treated (red) samples of β2m incubated for 6 days in the presence of Cu(II). Panels D and E are extracted ATDs of the control (black) and EDTA-treated (red) for the tetramer[14+], and tetramer[13+] charge states, respectively. The associated CCS values are denoted adjacent to the corresponding peak. Ion intensity for panels D and E are normalized by dividing the individual ion intensity by the sum total of β2m intensity in the spectra.

3.3.4 Computational modeling coupled to ESI-IM-MS and covalent labeling reveals heterogeneous configurations for Cu(II)-bound and Cu(II)-free tetramers

To investigate plausible structures of both Cu(II)-bound and Cu(II)-free tetramers, we used computational modeling. Tetramer structures were formed by docking randomly oriented side-by-side dimers, and the resulting 10,000 structures were filtered and constrained via a scoring function that considered previous covalent labeling-MS data [46]. Five candidate structures survived this filtering, and their CCS values range from 2901 to 3136 $Å^2$. However, these structures are relatively unstable *in silico*, dissociating within 100 ns. While these structures might be consistent with the most abundant conformation of the Cu(II)-bound tetramer (Figure 3.6D and E), these structures are not consistent with the full range of CCS values measured by IM-MS, especially for the Cu(II)-free tetramers. Moreover, the instability of the five structures *in silico* caused us to conclude that the tetramers probably require very specific interactions not captured in the 10,000 structures from the docking experiments.

Considering the interactions observed in the H13F mutant crystal structure, we hypothesized that head-to-head contact may be another binding interface in the tetramer, and thus we generated two separate models via crystal structure excision. One model retained Cu(II) (TET1 in Figure 3.7A) and the other had Cu(II) removed (TET2 in Figure 3.7B). Both of these structures, which are very similar and have identical interfaces (Figure 3.7C), remain stable for 1 μs during MD simulations. The interface between the dimer of dimers is consistent with a prior Cu(II)-bound tetramer model obtained from covalent labeling-MS data (Figure S7) and features cation-π interactions between H51 and F56, as well as a van der Waals interaction between L54 of each dimer subunit (Figure 3.7D) [46]. The calculated CCS value of these two structures is 3150 ± 50 $Å^2$

(Figure 3.7C), which has reasonable agreement with the most abundant conformer

measured by IM (Figure 3.6D).
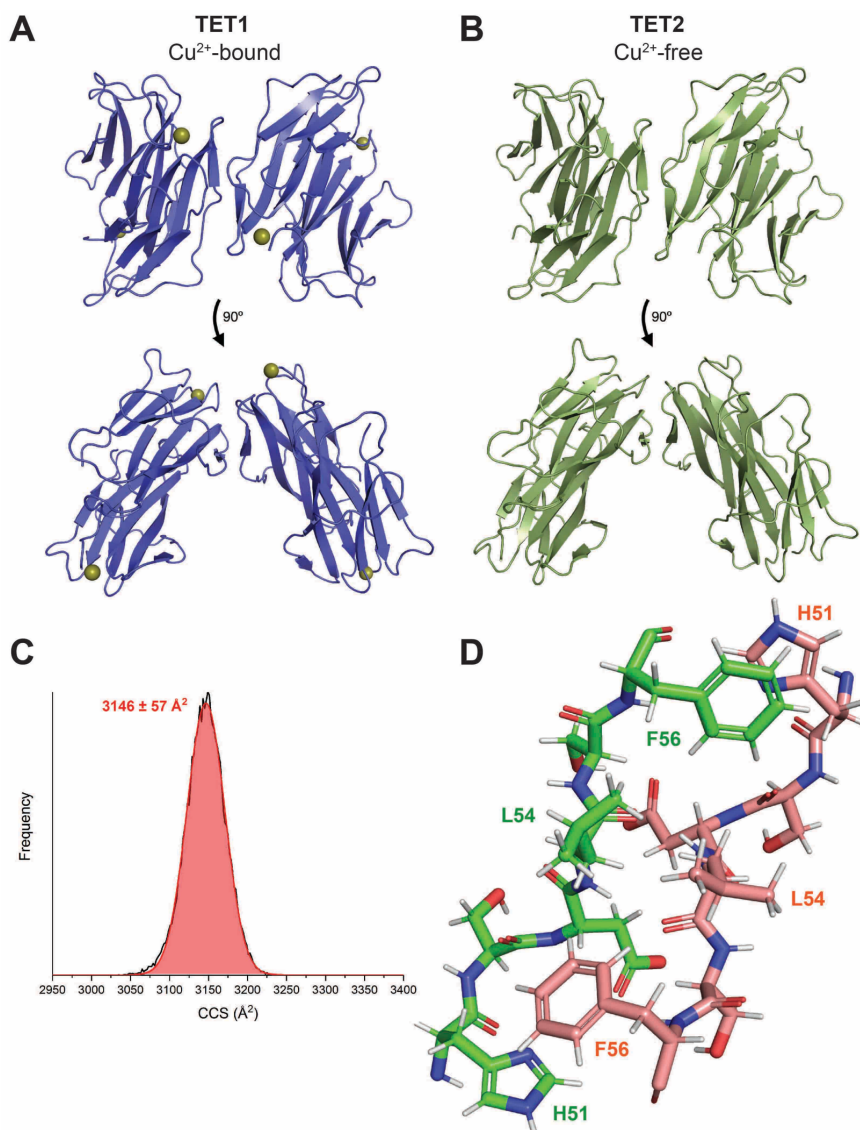
Figure 3.9: Computational models of similarly structured Cu(II)-bound and Cu(II)-free tetramers. Panel A shows a Cu(II)-bound while panel B shows a Cu(II)-free configuration of tetramer in found following excision and MD simulations in two orientations. Panel C is the calculated CCS distribution for the model, with the annotated value being the centroid of the Gaussian ± standard deviation. Panel D is a stick view of the interface between the dimer of dimers for both of these structures, where important interactions are denoted by residue letter and number.

Because this most abundant conformer disappears upon the addition of EDTA, we

further sought to identify models for the Cu(II)-free tetramers. Inspired by the *in silico*

stability of the Cu(II)-free head-to-head dimer (Figure 3.8A), we generated tetramer

structures by docking two Cu(II)-free monomers to the Cu(II)-free head-to-head dimer.

Emerging from these calculations was a structure referred to as TET3 (Figure 3.8A),

which is stable during MD simulations for 1 μs. Interestingly, TET3 has a calculated

CCS values of 2880 ± 60 Å^2, which is more compact than TET1 and TET2 and is more

consistent with the measured CCS value of the compact Cu(II)-free tetramer (Figure

3.6D). Another set of possible tetramers was also generated by docking two Cu(II)-free

head-to-head dimers via side-by-side interactions. The structure TET4 (Figure 3.8B)

arises from these docking experiments, and it is also stable for 1 μs *in silico*. Moreover, it

has a calculated CCS value of 3485 ± 56 Å^2, which is more extended than TET1, TET2,

and TET3, and is consistent with the measured CCS value of the larger Cu(II)-free

tetramer (Figure 3.6D).

Closer examination of the Cu(II)-free tetramer models reveal new interactions that

are important for its stability in Cu(II)'s absence. The central interface of the dimer-of-

dimers in TET3 is similar to that of TET1 and 2, where H51-F56, L54-L54, and E50-K58

are key interacting partners (Figure 3.8C). On the opposing side of the dimer of dimers,

salt bridges between K94-E77 and R81-E74 also form an interface (Figure 3.8C). An

important new interaction in TET3 within dimeric units involves the N-terminal amine,

whereupon removal of Cu(II), forms an electrostatic interaction with the sidechain of

D59 from the neighboring subunit. Lastly, H31, which is a key binding partner with

Cu(II), repositions itself in the absence of Cu(II) by drawing within approximately 5 Å of

W60 in a perpendicular orientation (Figure 3.8D) that is not observed in TET1 (Figure

3.8E). This non-native interaction is not observed for a representative Cu(II)-free
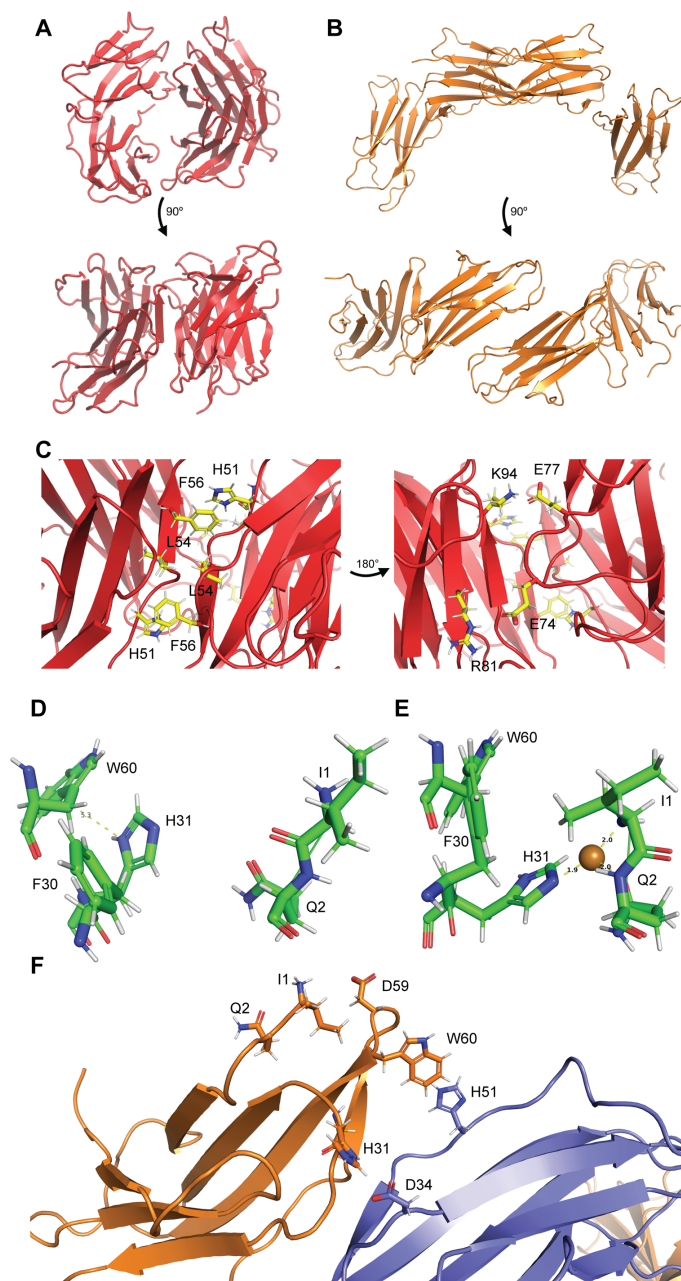
Figure 3.10: Computational models of compact and extended Cu(II)-free tetramers. Panel A shows the model of a proposed compact Cu(II)-free tetramer (TET3) structure in two orientations. Panel B shows the model of a proposed extended Cu(II)-free tetramer (TET4) structure in two orientations. Panel C highlights residues involved at interfaces of TET3 rotated about 180 degrees laterally. Panel D shows the Cu(II) binding site for TET3, while panel E shows the same region in Cu(II)-bound TET1. Residues highlighted, other than W60, are key interacting partners in Cu(II) binding. Distances that are measured in TET1 reflect the distance to the Cu(II) atom, while the one measured in TET3 reflects the distance to W60. Panel F shows Cu(II) binding site residues in orange that are now involved in interfacial contact (blue residues) in the TET4 structure.

structural ensemble measured by solution state NMR (Figure 3.9). Residues near the

Cu(II)-binding site are also repositioned in TET4, and some of them appear to help
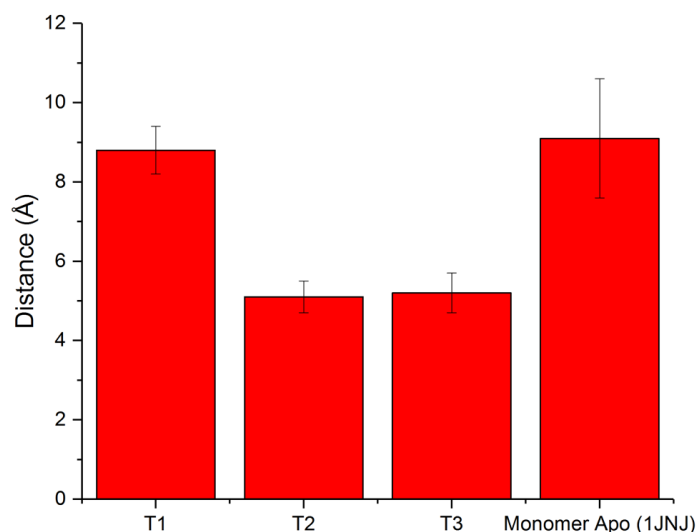
Figure 3.11: Calculated residues distances between H31 and W60 in β2m structures. Distances were calculated from an amide of His to the center of the planar benzyl ring of Phe. For T1-T3, 10 representative structures were selected from the MD trajectory. All structures from the NMR ensemble were used to calculate the distances for 1JNJ.

stabilize the tetramer interface. H31, in particular, forms a salt bridge with D34 from a

different subunit, and W60 forms a cation-π interaction with H51 (Figure 3.8F).

Calculated SASA values for these models tend to qualitatively agree to trends with

covalent labeling-MS data for the tetramer (Figure 3.10) [46]. It is important to note that

a weighting factor to account for heterogeneity is applied to the model SASA data, where

we estimated the abundances of TET1/2, TET3, and TET4 based on ion mobility data, as

the covalent labeling experiment would have likely captured all four species (if present).

3.3.5 The heterogeneity of the hexamer prevents structure assignment

In a manner similar to the tetramer, the hexamer has multiple conformations,

ranging from compact to less compact structures (Figures 3.1B and 3.3). Simple

geometric consideration assuming spherical subunits would indicate at least two possible
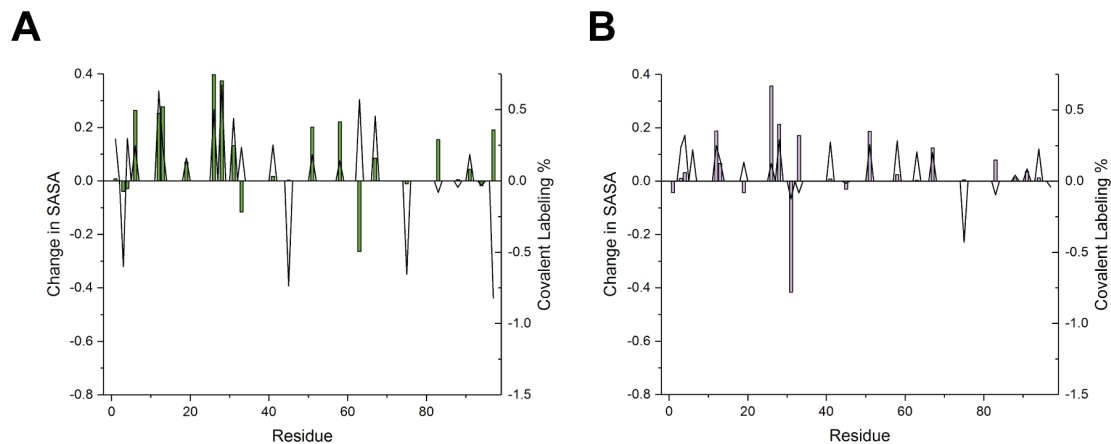
Figure 3.12: Comparison of covalent labeling trends with changes in SASA for tetrameric models. Panel A displays data for the monomer to heterogeneous tetramer transition, while panel B shows data for the dimer to heterogeneous tetramer transition. % change in SASA is expressed on the Y1 axis (bars), while the percentage covalent labeling change is displayed on Y2 (black lines). CL data from ref. [16].

topologies – a ring structure (i.e. blue structure in Figure 3.3) that is analogous to the

H13F mutant hexamer and a more extended structure (i.e. green structure in Figure 3.3).

Modeling the hexamer structures is beyond the scope of the current work as we do not

have any experimental data (e.g. residue-specific covalent labeling-MS results) other than

CCS values to help guide such experiments. It is worth noting, however, that the hexamer

is resistant to dissociation upon EDTA addition (Figure 3.6C), which suggests that Cu(II)

is not necessary for its stability. Its formation is therefore likely dependent on the

formation of a Cu(II)-free tetramer.

3.4 Discussion

β2m amyloid formation is fascinating because it can be induced under a variety of

conditions *in vitro*, and the oligomeric assemblies that precede the amyloids are different

[5,12,47–49]. Amyloid formation via Cu(II)-catalysis proceeds through discrete, even-

ordered oligomers, ranging from dimers to hexamers, [12], indicating that dimers are the

important building block. In contrast, β2m amyloid formation in low pH conditions proceeds via odd and even-ordered oligomeric states, ranging from dimers to tetradecamers, indicating that assembly occurs through the sequential addition of monomers [6].

Another difference between Cu(II)- and acid-induced β2m amyloid formation is the nature of the conformational heterogeneity. There is a notable level of monomer conformational heterogeneity at low pH, and oligomerization proceeds from partially unfolded states [17]. With Cu(II), however, the monomer appears to be one conformer, and heterogeneity emerges upon dimer formation, with the tetramers and hexamer having the most conformational heterogeneity. The partially unfolded monomeric states at low pH cause the acid-induced dimers and tetramers to be 16% (1823 Å^2 vs. 2180 Å^2) and 17% (3080 Å^2 vs. 3721 Å^2) larger than the most abundant Cu(II)-induced dimers and tetramers. This difference is large enough (e.g. 16% corresponds to roughly 32 residues on the dimer) to suggest that the oligomeric intermediates formed under each condition are quite distinct from one another, even though both conditions ultimately result in amyloid fibrils.

Our ESI-IM-MS and computational modeling results indicate that the predominant Cu(II)-bound dimer structure is in a side-by-side configuration, rather than a head-to-head or other configuration. Our experimental results suggest a significant burial of surface area, as the measured dimer CCS values are smaller than a simple beads-on-a-string model (Figure 3.3). Comparing the Cu(II)-dimer to acid-induced dimers and previously reported mutant DIMC constructs (Table 3.1), which are disulfide-bonded dimers assembled in a lateral (DIMC20) or laterally offset (DIMC50) manner, reveals

that the Cu(II)-induced dimer CCS values are also smaller [17,50]. These comparisons

further underline the importance of the large surface area buried by a side-by-side Cu(II)-

dimer with an anti-parallel arrangement of monomers (Figure 3.2). Other orientations are

incapable of producing such compact dimers, and other constructs (e.g. DIMC20 and

DIMC50) are inconsistent with covalent labeling MS data [16].

The Cu(II)-induced tetramer structures are especially unique due their

heterogeneity. The mobility distribution of the most abundant tetramer conformer is

initially very broad but gradually narrows over time (Figure 3.5). There are several

possible explanations for this behavior. Systematic factors like instrumental pressure

variation, gating timing, and ion diffusion in the IM cell could contribute to day-to-day

variability in measured drift times [51], but these factors would impact all oligomer ions

and not just the tetramers. Therefore, we conclude that the breadth of the mobility

distribution arises from multiple tetrameric conformers that have too similar CCS values

to be fully separated. The fact that this behavior coincides with the emergence of the

Cu(II)-free tetramer leads us to propose that some of these species are structures with

different degrees of Cu(II) loading that are transitioning to Cu(II)-free states (e.g.

TET1/TET2 → TET3 or TET4).

Measurements of CCS values before and after the addition of EDTA provide the

first experimental evidence for differences in the structures of the Cu(II)-bound and

Cu(II)-free tetramers. The most striking observation is that Cu(II)-free tetramers exist in

both more compact and extended states than the Cu(II)-bound tetramer (Figure 3.6D and

E). Computational efforts to build unbiased tetramer models through randomly oriented

dimers were somewhat unsuccessful. Although five tetramer models were found to be

consistent with covalent labeling MS data and the measured CCS value for the most abundant Cu(II)-bound tetramer, their instability *in silico* suggests that they may not be viable structures. The CCS values for these structures ranged from 2901 to 3136 Å^2, which is also insufficient to cover the spread of heterogeneity that we have measured for the tetramers. These results led us to hypothesize that specific contacts and interactions not captured via random docking are critical for tetramer stability.

TET1 was constructed considering the H13F crystal structure, specifically the head-to-head contacts between subunits, involving the cation-π interaction between H51-F56, a van der Waals interaction between L54-L54, and a salt bridge between E50-K58. Removal of Cu(II) from this structure yields TET2, which is stable *in silico*. Docking experiments were also used to construct Cu(II)-free tetramers. TET3 is a possible structure for the compact conformer, although its calculated CCS value is slightly higher than the experimentally measured CCS value for the compact Cu(II)-free tetramer.

New intramolecular and intermolecular interactions in TET3, like H31-W60, N-terminal amine, and new interfacial salt bridges, can possibly enthalpically compensate for the release of Cu(II). As noted above, comparison of TET3 SASA values to covalent labeling data generally agree. While TET3 compactness makes it a good candidate for the Cu(II)-free tetramer with the smaller CCS value, it is difficult to envision a structural transformation from TET1 to TET3 as it would necessarily involve an anti-parallel to parallel reconfiguration of the monomeric units in the dimers following Cu(II) removal

(Figure 3.11). Such a reconfiguration would require disruption of key salt bridges that stabilize the side-by-side dimer.

The other Cu(II)-free tetramer model, TET4, is consistent with the more extended conformer. TET4 not only agrees with covalent labeling-MS data, but also closely matches experimentally determined CCS values from ESI-IM-MS. There are new intermolecular interactions formed that explain its stability without Cu(II), most notably the dramatic repositioning of H31 and its involvement in interfacial interactions with D34 from another subunit. We propose that TET4 is good candidate model for the expanded Cu(II)-free tetramer. Importantly, the more expanded conformer assigned to TET4 was found to be a crucial species in previous β2m amyloid inhibition studies [20]. This tetramer conformer was found to disappear in the presence of molecules that prevented
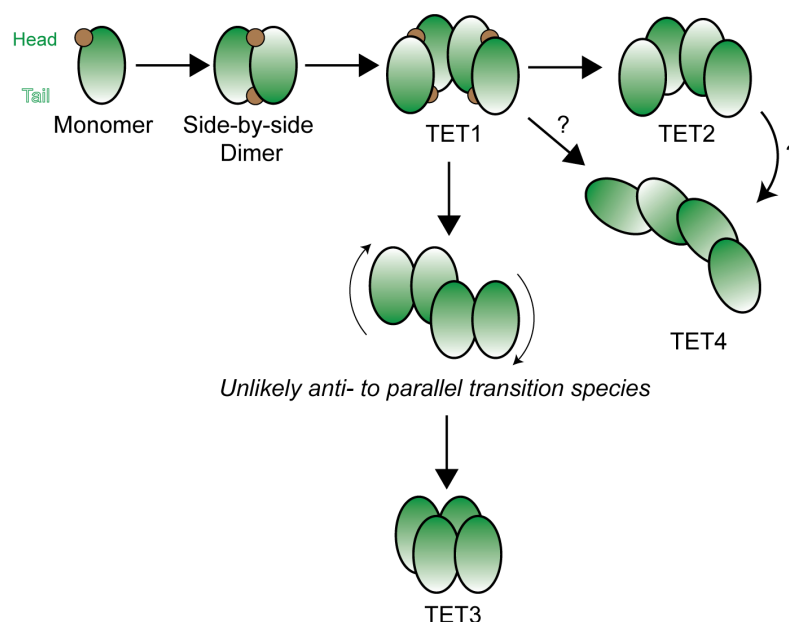
Figure 3.13: Possible schematic for Cu(II)-free tetramer conformer interconversions. Note the relative orientations of the poles (N-terminal head, C-terminal tail) of β2m, colored green and white.

the formation β2m amyloids, indicating that it is an important species on the pathway to β2m amyloid fibrils.

It is important to emphasize that TET3 and TET4 feature head-to-head interactions between subunits. Although we do not yet have direct experimental evidence for the presence of head-to-head interactions in Cu(II)-induced β2m oligomers, there are other examples of β2m oligomers having such interactions. These include mutant crystal structures [45] and the ΔN6 variant of β2m that is thought to 'transmit' its amyloidogenicity via a heterodimeric complex with the wild-type protein that is mediated by head-to-head interactions [52]. Moreover, in its normal biological context, bound to the MHC I receptor, β2m also interacts through residues located on loops near the head of the molecule [53]. Computational modeling and IM-MS results provide some evidence that head-to-head interactions could potentially play a role in Cu(II)-induced β2m amyloid formation.

Conformational heterogeneity in pre-amyloid oligomers is not exclusive to β2m, as such heterogeneity has been observed for amyloid-β and a-synuclein [54]. Unlike these previous amyloid systems in which heterogeneous structures are hypothesized to be off-pathway (non-productive) oligomers [55], heterogeneity in β2m oligomers might be a necessary feature of Cu(II) release. Cu(II) is required to initiate β2m oligomerization, but it is completely released upon formation of amyloid fibrils [12]. Given that Cu(II) is bound at a 1:1 stoichiometry in monomers, dimers, and some forms of the tetramers release of up to four equivalents of Cu(II) from the tetramer most likely occurs via multiple steps involving multiple conformers [12,15]. These findings also underline the complexity of this amyloid system.

3.5 Conclusions

In conclusion, we have found that structural heterogeneity is a key feature of Cu(II)-catalyzed amyloid formation with β2m. This heterogeneity manifests itself through the presence of multiple conformers, which are present in oligomeric states but absent in the monomer. This heterogeneity is the first time that these features have been described for the β2m-Cu(II) system. The conformational heterogeneity increases as the stoichiometry of the oligomers increase, as the dimer is the least heterogeneous, while the hexamer is the most. The most abundant conformer of the dimer, based on our evidence, is a side-by-side configuration of two anti-parallel monomers. We attribute the heterogeneity observed for the tetrameric species to arise from the transition from Cu(II)-bound to Cu(II)-free states, which is known to be a necessary step in Cu(II)-catalyzed β2m amyloid formation. We have generated models of these tetramer conformers that are consistent with IM-MS and covalent labeling-MS data and will be further validated in future experiments. Because one of the Cu(II)-free tetramers disappears in the presence of β2m amyloid inhibitors, these tetramers may serve as targets for the design of inhibitory molecules.

3.6 References

[1] D.R. Madden, J.C. Gorga, J.L. Strominger, D.C. Wiley, The three-dimensional structure of HLA-B27 at 2.1 Å resolution suggests a general mechanism for tight peptide binding to MHC, Cell. 70 (1992) 1035–1048.
[2] H. Katou, T. Kanno, M. Hoshino, Y. Hagihara, H. Tanaka, T. Kawai, K. Hasegawa, H. Naiki, Y. Goto, The role of disulfide bond in the amyloidogenic state of β2-microglobulin studied by heteronuclear NMR, Protein Science. 11 (2009) 2218–2229.
[3] F. Gejyo, S. Odani, T. Yamada, N. Honma, H. Saito, Y. Suzuki, Y. Nakagawa, H. Kobayashi, Y. Maruyama, Y. Hirasawa, M. Suzuki, M. Arakawa, β2-microglobulin: A new form of amyloid protein associated with chronic hemodialysis, Kidney International. 30 (1986) 385–390.

[4] T.B. Drüeke, Z.A. Massy, Beta2-Microglobulin, Seminars in Dialysis. 22 (2009) 378–380.

[5] V.J. McParland, N.M. Kad, A.P. Kalverda, A. Brown, P. Kirwin-Jones, M.G. Hunter, M. Sunde, S.E. Radford, Partially Unfolded States of β_2-Microglobulin and Amyloid Formation in Vitro, Biochemistry. 39 (2000) 8735–8746.

[6] D.P. Smith, L.A. Woods, S.E. Radford, A.E. Ashcroft, Structure and Dynamics of Oligomeric Intermediates in β2-Microglobulin Self-Assembly, Biophysical Journal. 101 (2011) 1238–1247.

[7] N.H.H. Heegaard, J.W. Sen, N.C. Kaarsholm, M.H. Nissen, Conformational Intermediate of the Amyloidogenic Protein β_2-Microglobulin at Neutral pH, Journal of Biological Chemistry. 276 (2001) 32657–32662.

[8] S. Giorgetti, S. Raimondi, K. Pagano, A. Relini, M. Bucciantini, A. Corazza, F. Fogolari, L. Codutti, M. Salmona, P. Mangione, L. Colombo, A. De Luigi, R. Porcari, A. Gliozzi, M. Stefani, G. Esposito, V. Bellotti, M. Stoppini, Effect of Tetracyclines on the Dynamics of Formation and Destructuration of β2-Microglobulin Amyloid Fibrils, Journal of Biological Chemistry. 286 (2011) 2121–2131.

[9] T. Eichner, S.E. Radford, Understanding the complex mechanisms of β2-microglobulin amyloid assembly: β2-microglobulin fibrillogenesis at physiological pH, FEBS Journal. 278 (2011) 3868–3883.

[10] C.J. Morgan, M. Gelfand, C. Atreya, A.D. Miranker, Kidney dialysis-associated amyloidosis: a molecular role for copper in fiber formation, Journal of Molecular Biology. 309 (2001) 339–345.

[11] C.M. Eakin, F.J. Attenello, C.J. Morgan, A.D. Miranker, Oligomeric Assembly of Native-like Precursors Precedes Amyloid Formation by β-2 Microglobulin [†], Biochemistry. 43 (2004) 7808–7815.

[12] K. Antwi, M. Mahar, R. Srikanth, M.R. Olbris, J.F. Tyson, R.W. Vachet, Cu(II) organizes β-2-microglobulin oligomers but is released upon amyloid formation, Protein Science. 17 (2008) 748–759.

[13] M.F. Calabrese, C.M. Eakin, J.M. Wang, A.D. Miranker, A regulatable switch mediates self-association in an immunoglobulin fold, Nature Structural & Molecular Biology. 15 (2008) 965–971.

[14] G.W. Platt, S.E. Radford, Glimpses of the molecular mechanisms of β_2-microglobulin fibril formation in vitro: Aggregation on a complex energy landscape, FEBS Letters. 583 (2009) 2623–2629.

[15] R. Srikanth, V.L. Mendoza, J.D. Bridgewater, G. Zhang, R.W. Vachet, Copper Binding to β-2-Microglobulin and Its Pre-Amyloid Oligomers, Biochemistry. 48 (2009) 9871–9881.

[16] V.L. Mendoza, K. Antwi, M.A. Barón-Rodríguez, C. Blanco, R.W. Vachet, Structure of the Preamyloid Dimer of β-2-Microglobulin from Covalent Labeling and Mass Spectrometry, Biochemistry. 49 (2010) 1522–1532.

[17] D.P. Smith, S.E. Radford, A.E. Ashcroft, Elongated oligomers in β2-microglobulin amyloid assembly revealed by ion mobility spectrometry-mass spectrometry, Proceedings of the National Academy of Sciences. 107 (2010) 6794–6798.

[18] J.D. Pham, B. Demeler, J.S. Nowick, Polymorphism of Oligomers of a Peptide from β-Amyloid, Journal of the American Chemical Society. 136 (2014) 5432–5442.

[19] W.S. Gosal, I.J. Morten, E.W. Hewitt, D.A. Smith, N.H. Thomson, S.E. Radford, Competing Pathways Determine Fibril Morphology in the Self-assembly of β2-Microglobulin into Amyloid, Journal of Molecular Biology. 351 (2005) 850–864.

[20] T.M. Marcinko, J. Dong, R. LeBlanc, K.V. Daborowski, R.W. Vachet, Small molecule-mediated inhibition of β-2-microglobulin-based amyloid fibril formation, Journal of Biological Chemistry. 292 (2017) 10630–10638.

[21] B.T. Ruotolo, J.L.P. Benesch, A.M. Sandercock, S.-J. Hyung, C.V. Robinson, Ion mobility–mass spectrometry analysis of large protein complexes, Nature Protocols. 3 (2008) 1139–1152.

[22] C. Bleiholder, N.F. Dupuis, T. Wyttenbach, M.T. Bowers, Ion mobility–mass spectrometry reveals a conformational conversion from random assembly to β-sheet in amyloid fibril formation, Nature Chemistry. 3 (2011) 172–177.

[23] J.L. Benesch, B.T. Ruotolo, Mass spectrometry: come of age for structural and dynamical biology, Current Opinion in Structural Biology. 21 (2011) 641–649.

[24] S.-J. Hyung, B.T. Ruotolo, Integrating mass spectrometry of intact protein complexes into structural proteomics, Proteomics. 12 (2012) 1547–1564.

[25] F. Lanucara, S.W. Holman, C.J. Gray, C.E. Eyers, The power of ion mobility-mass spectrometry for structural characterization and the study of conformational dynamics, Nature Chemistry. 6 (2014) 281–294.

[26] B.T. Ruotolo, K. Giles, I. Campuzano, A.M. Sandercock, R.H. Bateman, C.V Robinson, Evidence for Macromolecular Protein Rings in the Absence of Bulk Water, Science. 310 (2005) 1658–1661.

[27] C.A. Scarff, V.J. Patel, K. Thalassinos, J.H. Scrivens, Probing hemoglobin structure by means of traveling-wave ion mobility mass spectrometry, Journal of the American Society for Mass Spectrometry. 20 (2009) 625–631.

[28] J. Seo, W. Hoffmann, S. Warnke, M.T. Bowers, K. Pagel, G. von Helden, Retention of Native Protein Structures in the Absence of Solvent: A Coupled Ion Mobility and Spectroscopic Study, Angewandte Chemie International Edition. 55 (2016) 14173–14176.

[29] Y. Sun, S. Vahidi, M.A. Sowole, L. Konermann, Protein Structural Studies by Traveling Wave Ion Mobility Spectrometry: A Critical Look at Electrospray Sources and Calibration Issues, Journal of The American Society for Mass Spectrometry. 27 (2016) 31–40.

[30] M.M. Maurer, G.C. Donohoe, S.J. Valentine, Advances in ion mobility-mass spectrometry instrumentation and techniques for characterizing structural heterogeneity, The Analyst. 140 (2015) 6782–6798.

[31] A. Politis, A.Y. Park, S.-J. Hyung, D. Barsky, B.T. Ruotolo, C.V. Robinson, Integrating Ion Mobility Mass Spectrometry with Molecular Modelling to Determine the Architecture of Multiprotein Complexes, PLoS ONE. 5 (2010) e12080.

[32] R. Kodali, R. Wetzel, Polymorphism in the intermediates and products of amyloid assembly, Current Opinion in Structural Biology. 17 (2007) 48–57.

[33] G. Bellesia, J.-E. Shea, Diversity of kinetic pathways in amyloid fibril formation, The Journal of Chemical Physics. 131 (2009) 111102.

[34] A.E. Ashcroft, Mass spectrometry and the amyloid problem—How far can we go in the gas phase?, Journal of the American Society for Mass Spectrometry. 21 (2010) 1087–1096.

[35] J. Dong, C.A. Joseph, N.B. Borotto, V.L. Gill, M.J. Maroney, R.W. Vachet, Unique Effect of Cu(II) in the Metal-Induced Amyloid Formation of β-2-Microglobulin, Biochemistry. 53 (2014) 1263–1274.

[36] H. Hernández, C.V. Robinson, Determining the stoichiometry and interactions of macromolecular assemblies from mass spectrometry, Nature Protocols. 2 (2007) 715–726.

[37] M.F. Bush, Z. Hall, K. Giles, J. Hoyes, C.V. Robinson, B.T. Ruotolo, Collision Cross Sections of Proteins and Their Complexes: A Calibration Framework and Database for Gas-Phase Structural Biology, Analytical Chemistry. 82 (2010) 9557–9565.

[38] E.G. Marklund, M.T. Degiacomi, C.V. Robinson, A.J. Baldwin, J.L.P. Benesch, Collision Cross Sections for Structural Proteomics, Structure. 23 (2015) 791–799.

[39] M.J. Abraham, T. Murtola, R. Schulz, S. Páll, J.C. Smith, B. Hess, E. Lindahl, GROMACS: High performance molecular simulations through multi-level parallelism from laptops to supercomputers, SoftwareX. 1–2 (2015) 19–25.

[40] J. Huang, S. Rauscher, G. Nawrocki, T. Ran, M. Feig, B.L. de Groot, H. Grubmüller, A.D. MacKerell, CHARMM36m: an improved force field for folded and intrinsically disordered proteins, Nature Methods. 14 (2017) 71–73.

[41] W.L. Jorgensen, J. Chandrasekhar, J.D. Madura, R.W. Impey, M.L. Klein, Comparison of simple potential functions for simulating liquid water, The Journal of Chemical Physics. 79 (1983) 926–935.

[42] C.M. Eakin, J.D. Knight, C.J. Morgan, M.A. Gelfand, A.D. Miranker, Formation of a Copper Specific Binding Site in Non-Native States of β-2-Microglobulin, Biochemistry. 41 (2002) 10646–10656.

[43] C.M. Eakin, A.J. Berman, A.D. Miranker, A native to amyloidogenic transition regulated by a backbone trigger, Journal of Molecular Biology. 13 (2006) 202-208.

[44] M.F. Calabrese, A.D. Miranker, Formation of a Stable Oligomer of β-2 Microglobulin Requires only Transient Encounter with Cu(II), Journal of Molecular Biology. 367 (2007) 1–7.

[45] M.F. Calabrese, C.M. Eakin, J.M. Wang, A.D. Miranker, A regulatable switch mediates self-association in an immunoglobulin fold, Journal of Molecular Biology. 18 (2008) 965-971.

[46] V.L. Mendoza, M.A. Barón-Rodríguez, C. Blanco, R.W. Vachet, Structural Insights into the Pre-Amyloid Tetramer of β-2-Microglobulin from Covalent Labeling and Mass Spectrometry, Biochemistry. 50 (2011) 6711–6722.

[47] E. Rennella, A. Corazza, S. Giorgetti, F. Fogolari, P. Viglino, R. Porcari, L. Verga, M. Stoppini, V. Bellotti, G. Esposito, Folding and Fibrillogenesis: Clues from β2-Microglobulin, Journal of Molecular Biology. 401 (2010) 286–297.

[48] K. Sasahara, H. Yagi, H. Naiki, Y. Goto, Heat-induced Conversion of β2-Microglobulin and Hen Egg-white Lysozyme into Amyloid Fibrils, Journal of Molecular Biology. 372 (2007) 981–991.

[49] T. Ookoshi, K. Hasegawa, Y. Ohhashi, H. Kimura, N. Takahashi, H. Yoshida, R. Miyazaki, Y. Goto, H. Naiki, Lysophospholipids induce the nucleation and extension of 2-microglobulin-related amyloid fibrils at a neutral pH, Nephrology Dialysis Transplantation. 23 (2008) 3247–3255.

[50] M. Colombo, M. de Rosa, V. Bellotti, S. Ricagno, M. Bolognesi, A recurrent D-strand association interface is observed in β-2 microglobulin oligomers: β-2 microglobulin oligomeric interface, FEBS Journal. 279 (2012) 1131–1143.

[51] A.A. Shvartsburg, R.D. Smith, Fundamentals of Traveling Wave Ion Mobility Spectrometry, Analytical Chemistry. 80 (2008) 9689–9699.

[52] T.K. Karamanos, A.P. Kalverda, G.S. Thompson, S.E. Radford, Visualization of Transient Protein-Protein Interactions that Promote or Inhibit Amyloid Assembly, Molecular Cell. 55 (2014) 214–226.

[53] N.L. La Gruta, P.G. Thomas, A.I. Webb, M.A. Dunstone, T. Cukalac, P.C. Doherty, A.W. Purcell, J. Rossjohn, S.J. Turner, Epitope-specific TCR repertoire diversity imparts no functional advantage on the CD8+ T cell response to cognate viral peptides, Proceedings of the National Academy of Sciences. 105 (2008) 2034–2039.

[54] B.H. Toyama, J.S. Weissman, Amyloid Structure: Conformational Diversity and Consequences, Annual Review of Biochemistry. 80 (2011) 557–585.

[55] W.M. Tay, D. Huang, T.L. Rosenberry, A.K. Paravastu, The Alzheimer's Amyloid-β(1–42) Peptide Forms Off-Pathway Oligomers and Fibrils That Are Distinguished Structurally by Intermolecular Organization, Journal of Molecular Biology. 425 (2013) 2494–2508.

CHAPTER 4

EFFECT OF EPIGALLOCATECHIN-3-GALLATE ON β-2 MICROGLOBULIN AMYLOID FORMATION

4.1 Introduction

In terms of molecules with anti-amyloid properties, epigallocatechin-3-gallate (EGCG) may have the longest standing record *in vitro*. The earliest report of EGCG's properties in PubMed was published in 2001, where researchers reported observations that it could decrease Amyloid-β (Aβ) toxicity in cultured neuronal cells [1]. As of this writing, there are now over 206 entries for "EGCG amyloid" in PubMed. By our estimation, this means that this may be the most popular anti-amyloid agent in the literature.

In Chapter 2, we detailed the study behind the usage of doxycycline and rifamycin as amyloid inhibitors in Cu(II)-catalyzed β2m amyloid formation. The foundational work behind our study was the previously published information about doxycycline and rifamycin binding to β2m and their capabilities to inhibit acid- and trifluoroethanol (TFE)-induced amyloid formation [2,3]. However, the current motivation for investigating EGCG is born out of reports of its broad effectiveness in a number of amyloid systems, and our desire to evaluate its impact on the β2m-Cu(II) system. This work represents the first efforts to characterize EGCG's effect on β2m-Cu(II) amyloid formation.

EGCG itself is a 458 Da polyphenol catechin flavonoid that is highly abundant in green tea leaves [4]. It is notable for its anti-oxidant properties and other biological activities [5–7]. The chemical structure of EGCG is shown below in Figure 4.1B. Outside

of anti-amyloid properties, it also has the apparent property of having relatively promiscuous binding properties, as it seems able to interact with a number of different proteins and peptides both structured and unstructured [8–12].

Since the reports of EGCG's properties are numerous, it is useful to review and summarize some of the literature for other amyloid forming proteins. As alluded to earlier, EGCG has been evaluated extensively both *in vitro* and *in vivo* in perhaps the most infamous (and widely published) amyloid forming peptide, Aβ [13–17]. The reported observations with Aβ range from remodeling of the mature fibrils, redirecting aggregation away from fibrils, or even disrupting oligomeric precursor structures. In addition to Aβ, there have been reports for other amyloid forming systems such as α-synuclein (αS), huntingtin, immunoglobulin light chain (IG LC), and islet amyloid polypeptide (IAPP), to name a few [13,18–21].

For β2m specifically, EGCG has been previously evaluated in the same study that reported rifamycin as an effective amyloid inhibitor [3]. The primary focus of this study was assessing small molecule effects specifically at low pH conditions using a number of biophysical tools like thioflavin t (ThT) fluorescence, circular dichroism (CD), multidimensional nuclear magnetic resonance (NMR), and electrospray ionization ion mobility spectrometry-mass spectrometry (ESI-IM-MS). Although the focus of the latter half of the work is specifically focused on the effects of rifamycin, EGCG is screened under low pH (2.5) amyloid forming conditions. Interestingly, they found that in the presence of EGCG, β2m amyloid fibrils were still able to form at low pH, with no evidence of any other heterogeneous aggregates [3].

In a separate work, EGCG was evaluated with fully formed β2m amyloid fibrils disrupting cellular membranes [22]. Here, EGCG was added to cellular cultures alongside pre-formed low pH β2m fibrils. EGCG was reported to apparently strongly attenuate lipid bilayer disruption. This conclusion was arrived at by evaluating vesicle leakage, cellular morphology, and membrane fluidity measurements [22]. The authors conclude that EGCG has direct interactions with β2m fibrils that decrease their disruptive properties, although the exact mechanism and binding site(s) are unclear [22].

Overall, these reports highlight the apparent complexity of small molecule interactions with amyloid forming proteins like β2m and a ligand like EGCG that is seemingly capable of interacting with a slew of different proteins involved in a wide variety of biological roles. In the context of amyloid formation, there is a significant amount of heterogeneity present during the process and there are clearly multiple routes of small molecule anti-amyloid effects, whether it be by interfering with the formation of oligomeric precursors or by reducing the biological effect of mature aggregates. Our findings described here suggest that EGCG causes the formation of non-amyloid off-pathway aggregates which diverts oligomerization away from product on-pathway states.

4.2 Materials and methods

4.2.1 Materials

Human wild type β2m (Cat #126-11) was purchased from Lee Biosolutions (Maryland Heights, MO). Prior to use, it was reconstituted with water, and buffer exchanged into 10 mM ammonium acetate prior to a second lyophilization. Phosphotungstic acid (Cat #19500) was purchased from Electron Microscopy Services

(Hatfield, MA). All other chemicals were purchased from Sigma Aldrich (St. Louis, MO).

4.2.2 Methods

4.2.2.1 Oligomer and amyloid formation

β2m was incubated with 2 molar equivalents of Cu(II)SO$_4$ in 25 mM 3-(N-morpholino)propanesulfonic acid (MOPS) with 150 mM potassium acetate, 500 mM urea at pH 7.4 in a manner described previously [23,24]. Depending on the experiment, the β2m concentrations used in this study typically ranged from 50-500 μM. Following compounding, samples were sealed with parafilm and placed into a 37°C chamber for specified time points (≤1 month).

4.2.2.2 Transmission Electron Microscopy

Prior to analysis, samples were removed from the incubation chamber and centrifuged at 14,000 RPM for 45 minutes to isolate the insoluble aggregate material. The supernatant was then decanted and discarded. The pellet was then resuspended with 10 μL of MilliQ water. 2 μL of this slurry was then applied to 300-mesh carbon-supported copper grids (Cat #CF300-CU) (Electron Microscopy Services, Hatfield, MA). Once applied, the samples were allowed to dry overnight. The dried samples were then stained with by adding drop-wise a 1% (w/v) solution of phosphotungstic acid adjusted to pH 7.4 with potassium hydroxide (prior to sample application). Excess stain was rinsed away with water and were then allowed to dry overnight. TEM images were collected on a JEOL2000FX transmission electron microscope (Peabody, MA).

4.2.2.3 Size Exclusion High Performance Liquid Chromatography (SEC-HPLC) and Multi-Angle Light Scattering (MALS)

SEC-HPLC data was collected on an Agilent 1100 series HPLC that was outfitted with a SuperSW2000 column purchased from Tosoh Bioscience (Tokyo, Japan). The mobile phase consisted of 150 mM ammonium acetate. The mobile phase was filtered through a 0.22 μm filter prior to use. The flow rate, unless otherwise specified, was 0.35 mL/min. The detector was set to 214 nm. For estimation of molecular weight, a calibration standard consisting of bovine serum albumin, ovalbumin, carbonic anhydrase, and β2m was used.

For SEC-MALS, an Agilent 1240 HPLC was coupled to an 18-angle light scattering detector (DAWN-HELEOS-II), a dynamic light scattering detector (QELS), and a differential refractometer (Optilab T-rEX), all manufactured by Wyatt Technology (Goleta, CA). ASTRA software was used to analyze the data, specifically, for molar mass determination.

4.2.2.4 Electrospray Ionization Ion Mobility Spectrometry Mass Spectrometry (ESI-IM-MS)

Following removal from the incubation chamber at defined timepoints, samples were desalted and fractionated into 100 mM ammonium acetate using a GE Hi-Trap column (Cat #17-1408-01) (Chicago, IL). The fractions were then loaded into gold sputter coated borosilicate glass capillaries (Cat# 30-0035) from Hardvard Apparatus (Holliston, MA) that were pulled in-house to form tapered tips. The tips were prepared similarly to established protocols [25]. The tips were then loaded into a Waters Synapt G2-Si quadrupole time-of-flight mass spectrometer (QTOF), equipped with a traveling wave ion mobility cell (TWIMS) (Milford, MA). Instrument parameters were carefully

optimized to keep energy levels as low as possible to avoid potential

unfolding/dissociation of ion structures. Important source instrumental settings included:

1.0 kV capillary voltage, 30°C source temperature, 20 V source offset, and 20 V cone

voltage. The *m/z* scale was calibrated from 500-8,000 using perfluoroheptanoic acid.

Collisional cross section (CCS) values were estimated from ion drift times via by

calibration using proteins of known CCS previously measured using a drift time-IM

instrument described here [26]. Data were analyzed using MassLynx and plotted in

Origin (Northampton, MA).

4.2.2.5 Circular Dichroism (CD)

CD data were acquired on a Jasco J-1500 spectrophotometer. Data were collected

by scanning from 250 to 195 nm with a data pitch of 0.5 nm using a scan rate of 20

nm/min. Three total scans were averaged to generate the final results shown here.

Solution conditions were similar to the ones described above, but contained 25 μM β2m,

50 μM Cu(II), and 25 μM EGCG. Urea was omitted from the sample in order to generate

a higher quality spectra. Samples were equilibrated and measured at 20°C. Data were

analyzed using Spectra Analysis.

4.2.2.6 Reverse Phase (RP) Liquid Chromatography-Mass Spectrometry (LC-MS)

Reverse phase LC-MS was carried out on an Agilent 1100 HPLC fitted with a

OPTI-TRAP Micro column (Cat# 10-04816-TM) (Optimize Technologies, Oregon City,

OR) which was interfaced with a Bruker Amazon (Billerica, MA) quadrupole ion trap

mass spectrometer fitted with an electrospray ionization source. RP separation was

performed using a binary mobile phase system that consisted of water with 0.1% acetic

acid (A), and the second consisting of acetonitrile with 0.1% acetic acid (B). The flow

rate was 0.2 mL/min. Following injection, the column was equilibrated at 5%B for 3

minutes, then moved to 90% over the next 5 minutes. The column was then at 100%B for

5 minutes, and then returned to 5% for column equilibration. The electrospray needle

voltage was kept at 3.9 kV, and the capillary temperature was set to 250°C. Mass spectra

were acquired from *m/z* 300-2200.

4.3 Results

4.3.1 The presence of EGCG alters insoluble aggregate morphology
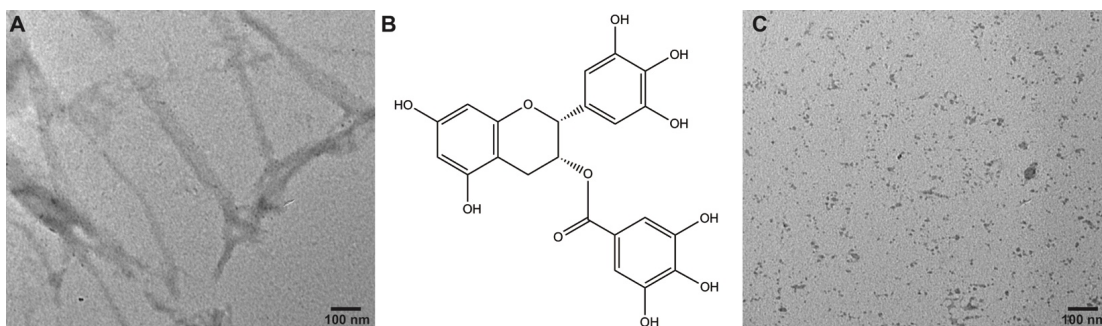
Figure 4.1: Transmission Electron Microscopy of EGCG-treated amyloid samples. Imaging performed after 1 month of incubation at 37°C. Panel A shows a representative non-EGCG treated control amyloid fibrils which shows classic amyloid morphology. Panel B shows the chemical structure of EGCG, was added to the solution at the beginning of the incubation. Panel C shows a representative image of the aggregates resulting from EGCG treatment in a solution of β2m:Cu(II):EGCG.

We first evaluated the effect of EGCG on the mature aggregate structures in a time

frame that is similar to normal amyloid formation with Cu(II). The control sample,

containing β2m and Cu(II), shown above in Figure 4.1A, produced amyloid fibrils that

have characteristic elongated fibril structures. These structures do not branch and are on

the order of several hundreds of nanometers in length. Overall, these structures are

consistent with our past observations [23,24,27]. In the EGCG-treated sample, shown in

Figure 4.1C, the results were markedly different. Rather than fibrils, we observed smaller

amorphous (or roughly spherical particles), which ranged from 5 to 25 nanometers

(individually). These particles were also apparently capable of forming higher order

aggregates, forming heterogeneous structures that were on the order of a few hundred

nanometers.

Another hallmark test of mature β2m amyloid fibrils is resistance to dissolution

with sodium dodecyl sulfate (SDS) [23,24,27]. Specifically, we have historically found

that β2m fibrils do not dissolve in a solution containing 2% SDS at 37°C. Following

centrifugation and decanting the supernatant, the aggregate pellets that produced the

TEM images shown above were both subjected to resuspension in 2% SDS and incubated

at 37°C. We found that the amyloid-containing control still contained observable

precipitate after 3 days of incubation, but the EGCG-containing sample had completely

dissolved. Taken together, we concluded that the introduction of EGCG successfully

inhibits the formation of amyloid fibrils and turned our focus to examining its impact on

the early steps of the oligomerization process to better rationalize the inhibitory activity.

4.3.2 EGCG promotes the formation of new species in the soluble oligomerization profile

We then turned our attention to determining the effect of EGCG on the earliest

stages of the amyloid formation process, which is the evolution of soluble β2m oligomers

that form on the scale of days. We monitored this process using SEC-HPLC to determine

both the stoichiometry of these complexes, and their abundance over time. Figure 4.2
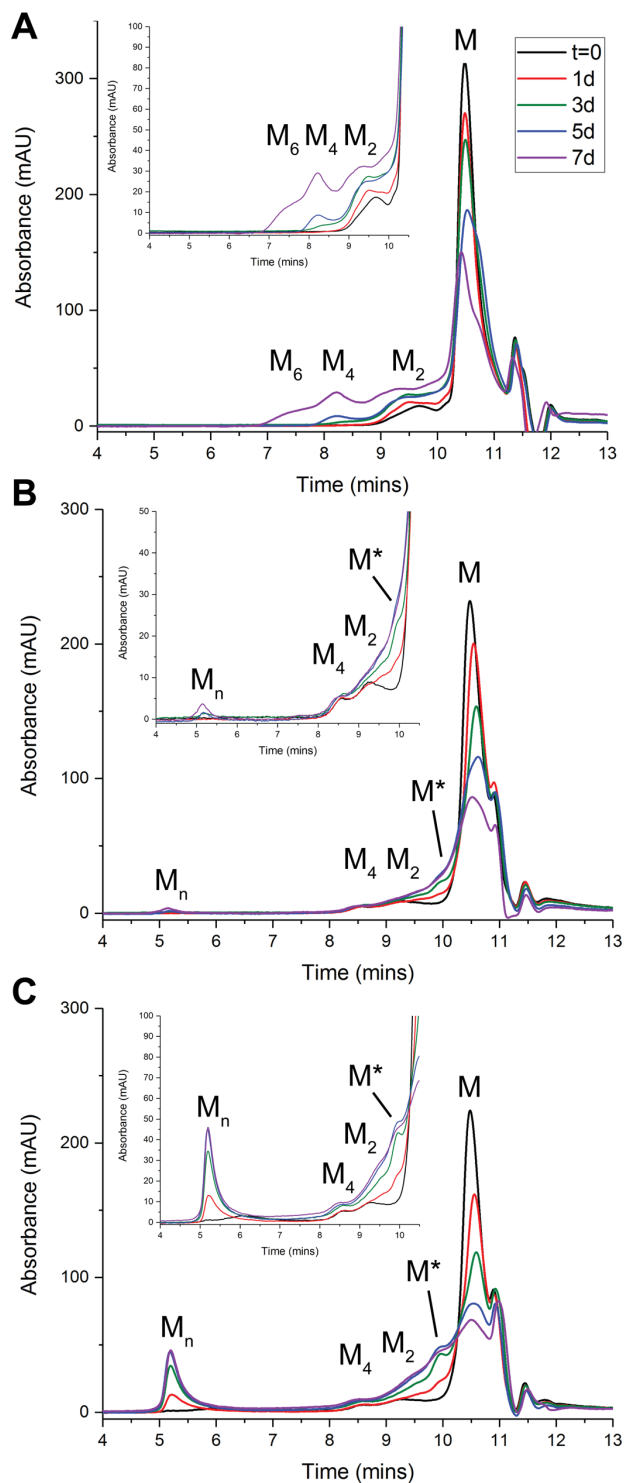
Figure 4.2: SEC-HPLC results of soluble oligomer content in the presence of EGCG. The insets showing an expanded region where oligomers typically elute. β2m monomer is denoted as M with subsequent numbering for oligomers. Panel A is the control that 1:2 β2m:Cu(II) but no EGCG. Panel B contains EGCG at a ratio of 1:2:0.1 β2m:Cu(II): EGCG, while panel C contains EGCG at a ratio of 1:2:0.3 β2m:Cu(II):EGCG.

(panels B and C).

Over the course of a week, the control sample shown in Figure 4.2A shows the presence of dimers, tetramers, and hexamers coupled to a corresponding decrease in monomer peak area. The loss in peak area is correlated with the formation of soluble oligomers, and eventually insoluble aggregates. Interestingly, the presence of EGCG in panel B reveals that there are two new species present. The first, eluting near the exclusion limit of the column around day 3, is denoted as M_n. The stated exclusion limit on this particular column, according to the manufacturer, is 150,000 Daltons (Da). Due to the limit, this means that we cannot accurately estimate the molecular weight of Mn, but it must be at least 150 kDa. There is no evidence of hexamers formed in the presence of EGCG.

The second new feature in the EGCG-containing samples is an intermediate peak that appears to elute between the dimer and monomer peaks (~10.6 mins), deemed M*. Based on the calibration curve, M* would correspond to a molecule that is approximately 16.7 kDa, which is larger than a monomer (11.7 kDa), but smaller than a dimer (23.4 kDa). Based on testing two EGCG concentrations, both M_n and M* appear to have a dose dependence, as their abundance increases when EGCG concentration increases (panel C) when compared to the lower EGCG concentration (panel B). This implies a causal link between these two species and EGCG.

Due to the limitation in molecular weight information from these experiments, we adapted our SEC method for further study of M_n. We used a column with an increased molecular weight range (exclusion limit: 7 mDa), and included a multi-angle light

91

scattering (MALS) detector in addition to normal ultraviolet absorbance. The results for

these SEC-MALS experiments are shown in Figure 4.3.
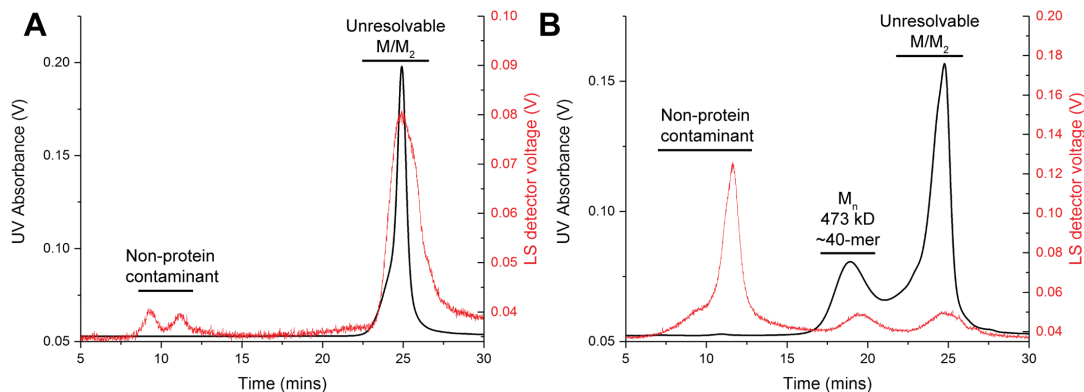
Figure 4.3: Comparison of SEC-MALS data for a Cu(II)-containing control (A), and a Cu(II)-containing sample with EGCG (B). The black data is UV absorbance at 214 nm, while the red is light scattering data from one of the detectors.

When comparing the Cu(II)-containing control to the EGCG-treated sample, there

is one main peak (~24 mins) that appears to have multiple species contained within in

both the UV absorbance (black) and the light scattering data (red). We attribute this peak

to primarily monomer, but also likely contains dimer, and in the case of the EGCG-

treated sample, M*. On the opposite end of chromatogram, there is also light scattering

response, but a negligible response from the UV absorbance. We attribute these peaks to

non-protein related contaminants that scatter light. An intermediate peak (~18 mins)

between these two regions is present in the EGCG containing sample (panel B) that is not

present in the control (panel A). This peak both absorbs UV light, and scatters light. The

molecular weight of this peak, determined by MALS, is approximately 473 kDa. When

considering the molecular weight of β2m, this corresponds to roughly a 40-mer

(assuming globular structure), which is the largest soluble β2m oligomer that we have

measured.

The above experiments indicate that EGCG is capable of altering the soluble oligomerization pathway from the beginning of the incubation with Cu(II). However, we also wondered if it was capable of altering the process mid-incubation. Figure 4.4 shows SEC-HPLC data for this experiment, where the addition of EGCG was delayed from t=0.
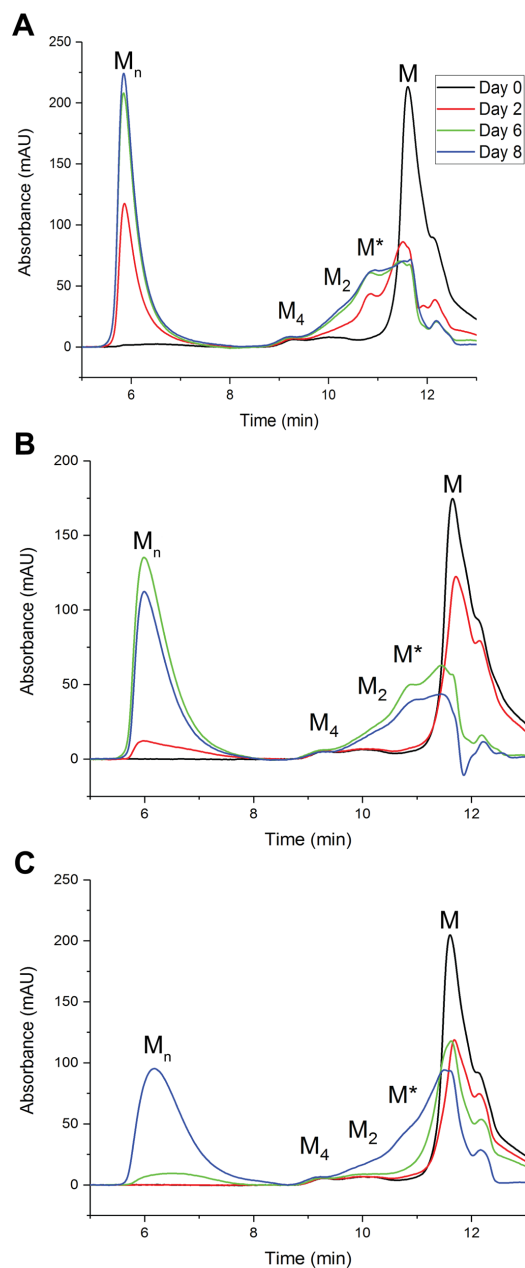
Figure 4.4: SEC-HPLC results for delayed introduction of EGCG. Analysis performed over 8 days of β2m-Cu(II) when the addition of EGCG is delayed by 5 hours (A), 2 days (B), and 6 days (C).

In all three cases tested (5 hours, 2 days, and 6 days), adding EGCG resulted in the evolution of M_n and M* species. At 5 hours, we expect that dimers are present, while at 2 days and 6 days there should be dimers and tetramers present. We interpret this to mean that EGCG's effect is not necessarily dependent on monomeric β2m, but will rather work when heterogeneous species are present.

4.3.3 Dose dependent effects of EGCG

Based on the results for two different EGCG concentrations in Figure 4.2, we sought to further characterize the dose dependent properties of EGCG (Figure 4.5). Here, we measured chromatographic peak height on chromatograms on day 5. Panel A, for the monomer, shows a steep dependence on the concentration of EGCG as it dramatically
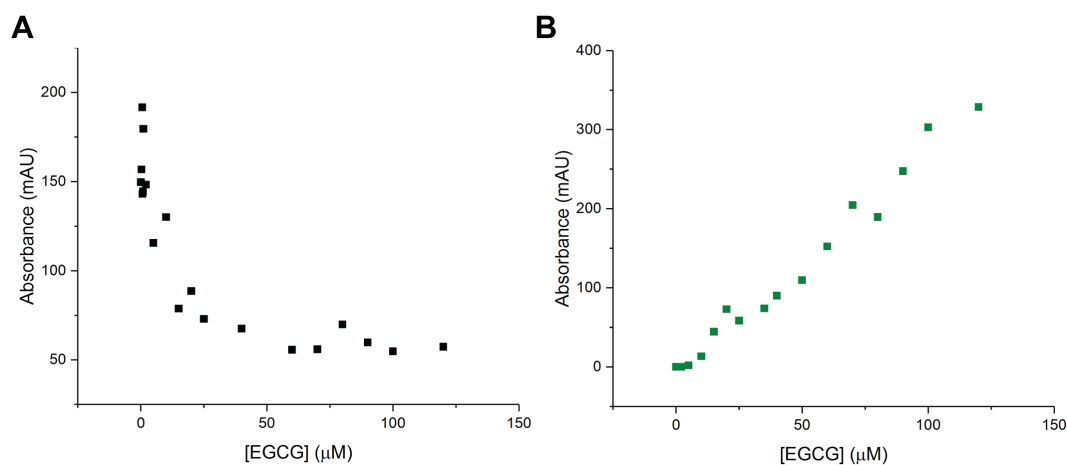
Figure 4.5: Dose dependent effects of EGCG. Individual points determined by quantifying chromatographic SEC peak height at day 5 for the monomer (A) and M_n (B) species.

decreases the amount of monomer present, plateauing around a 1:1 ratio of β2m:EGCG (50 μM). This suggests that EGCG, presumably binding to β2m, rapidly forces the monomer population to other species. We attribute this mostly to M_n, as it appears to growth in peak area to a much greater extent than M_2 or M_4. Indeed, plotting the dose dependent data for M_n yields a linear increase with no plateau (Figure 4.4B).
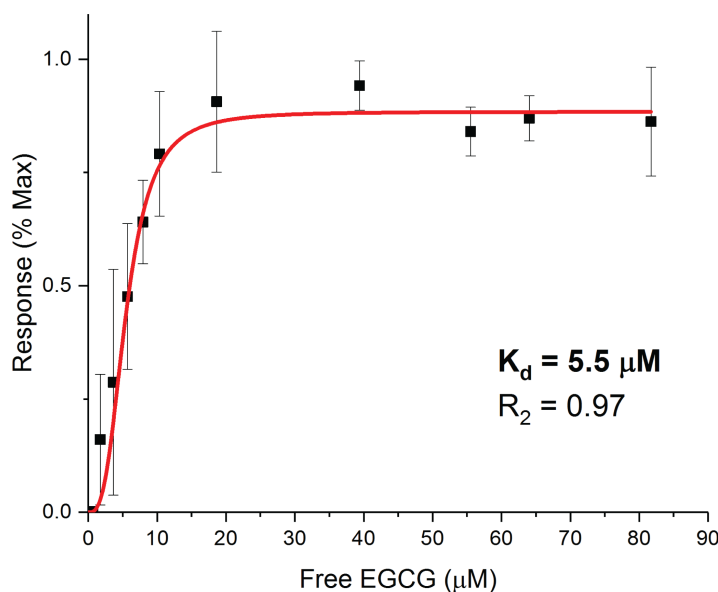
Figure 4.6: Estimation of K_d of EGCG for β2m. Results for fitting size exclusion response from dose dependent data to the Hill equation to estimate K_d (n=3). Error bars are standard deviation. The R^2 value for the fit is shown on the plot.

Based on the hyperbolic shape of the dose dependence data of the monomer, we sought to extract an effective dissociation constant. Figure 4.6 shows the results of fitting these data to the Hill equation in Origin. Interestingly, EGCG appears to have a much lower K_d value than other small molecules that we have worked with in the past [28], which is evident from the potent effect on altering oligomerization.

One outstanding question about EGCG's effect on amyloid formation is its impact when no Cu(II) is present. We previously discussed some of the structural details of Cu(II) unique effect on the monomer's structure in Chapter 1. When bound to Cu(II), the overall fold and tertiary structure of β2m is not perturbed, but there are a number of local and residue specific changes to β2m's structure, rendering it non-native. To determine if M_n and M* are generated by Cu(II)-free β2m, we did an identical SEC-HPLC experiment to the ones detailed above, only this time omitted Cu(II) from the incubated sample. To

our surprise, neither M_n or M^* are generated when Cu(II) is not present (Figure 4.7). This

result speaks to the specificity of EGCG's potent effect on Cu(II)-bound β2m.
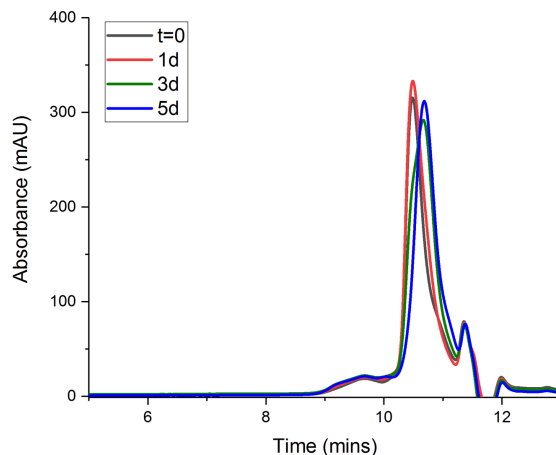
Figure 4.7: EGCG has no effect on oligomerization of β2m in the absence of Cu(II). SEC-HPLC chromatogram time course for incubated samples that contained β2m and EGCG, but no Cu(II).

4.3.4 Effect of EGCG on β2m oligomer stoichiometry and structure in the gas phase

We previously utilized ESI-IM-MS to characterize the stoichiometry of β2m

oligomers in the gas phase, alongside the structural effects of inhibitory molecules [27].

For EGCG, we once again turned to ESI-IM-MS to evaluate its effect on structures in the

gas phase. Figure 4.8 shows the results for a Cu(II)-containing control sample with β2m

(black), and a EGCG-treated sample (red) under the same incubation conditions.

This analysis yields a similar profile of oligomeric species in terms of

stoichiometry where we detect a heterogeneous mixture of monomers, dimers, tetramers,

and hexamers for the control (Figure 4.8A), and only dimers and tetramers are clearly

discernable with EGCG (Figure 4.8B) There was no evidence of larger mass species (≥

m/z 10,000) that would correspond to M_n. The EGCG-β2m complex was challenging to

preserve and detect in the gas phase, despite many attempts at trying to optimize

experimental conditions. Two different desalting methods prior to analysis yielded similar results, so we likely attribute it to incompatibility in the gas phase. The quality of spectra also suffers with increasing EGCG concentrations, in order to saturate β2m (in an effort to generate ligand-bound peaks). However, the overall increase in baseline noise and decrease in resolution due to spectra broadening hampered our efforts.
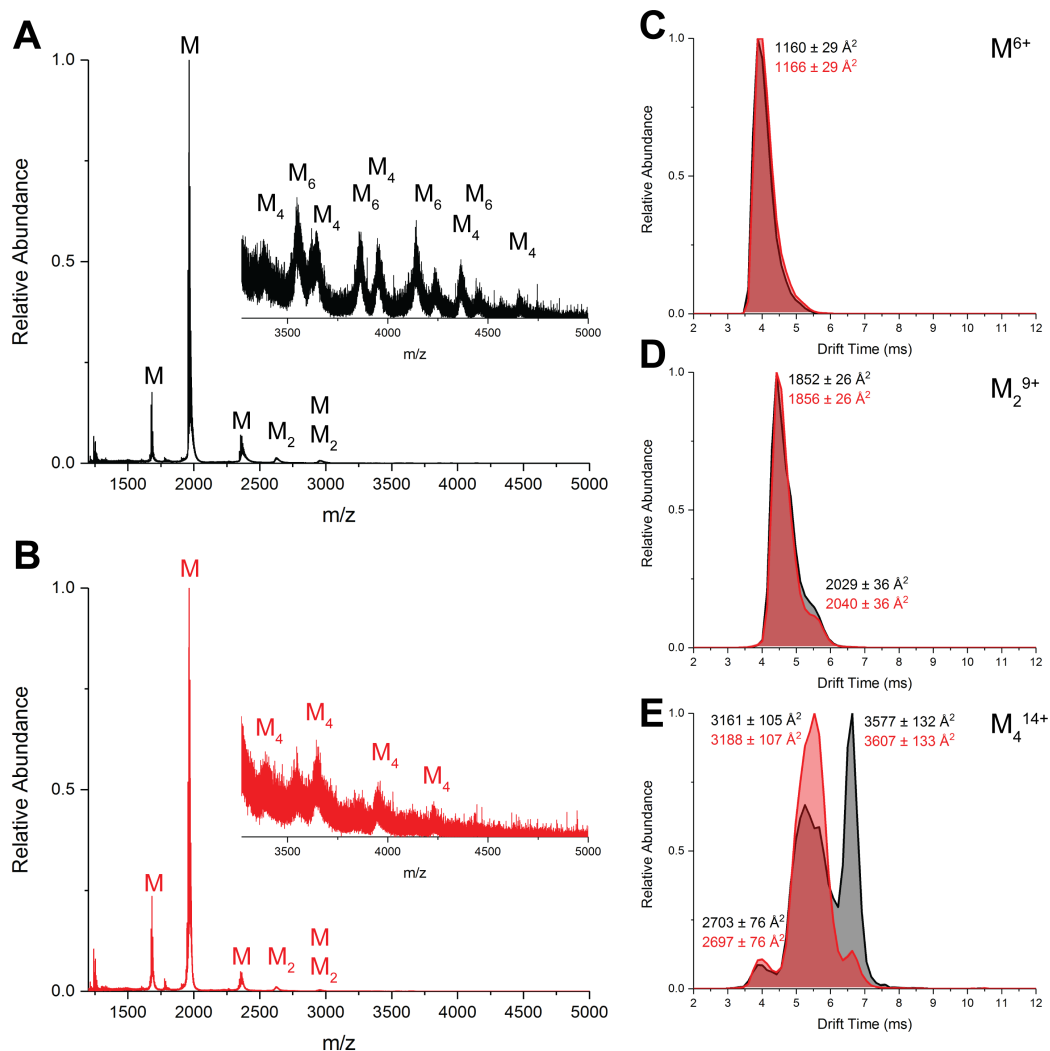
Figure 4.8: EGCG exerts unique effect on tetrameric conformer by ESI-IM-MS. ESI-IM-MS data for 1:2 β2m:Cu(II) (A), and 1:2:0.1 β2m:Cu(II):EGCG (B) after 6 days of incubation. Panels C-E show extracted arrival time distributions for selected denoted ions for the aforementioned control (black) and the EGCG-containing samples (red).

The best-case scenario for studying the protein structure in the gas phase is to compare a control oligomer with one that is bound to a small molecule(s) (assuming it occupies the same charge state). Due to the inability to capture the EGCG complexes, we then rely on 'solution memory' effects instead to rationalize any structural changes when comparing IM data (Figure 4.8C-E). Both the monomer and dimer for the selected charge states have similar centroid CCS values, and virtually identical arrival time distributions (panels C and D).

Interestingly, the expanded peak of the tetramer[14+] ion has an apparent decrease in abundance (panel E). This finding echoes back to our previous inhibitor work (chapter 2), where we found that was a key feature of effective small molecule inhibitors [27]. Furthermore, based on our results from chapter 3, this feature may also reflect a Cu(II)-free tetrameric state, which is a crucial transition point for Cu(II)-catalyzed amyloid formation. The apparent lack of this conformer, in addition to the diversion of the oligomerization pathway, may contribute to the observed effects of EGCG.

4.3.5 Characterization and putative identity of M*

The identity of M* is a more complex mystery than M_n. We first hypothesized that the presence/binding of EGCG was destabilizing to the point of unfolding β2m's structure. Thus, the increased hydrodynamic radii of these unfolded molecules were then causing the shift in retention time that we observed using SEC-HPLC. This hypothesis was also convenient because it could then be easily rationalized that these unfolded molecules were easily aggregating during the incubation and generating species like M_n.

We first assessed the secondary structure of β2m in the presence of Cu(II) and EGCG via circular dichroism. Figure 4.9 shows an overlay of these two spectra. There is

a global minima in the spectra at about 218 nm, which is the classic signature of β-sheet structure.

Due to an increase in the photomultiplier voltage because of non-optimal (i.e. high background absorption) solution conditions, the positive peaks below ~205 nm should not be interpreted. Both the control (black) and EGCG-containing samples yielded virtually indistinguishable spectra in both feature and ellipticity that is consistent with a folded protein containing a majority of β-sheet for its secondary structure.

We also have probes of monomer protein structure from other sources. The ESI-IM-MS data, shown about in Figure 4.8A and B, exhibit narrow charge state distributions for the monomer in both the Cu(II)-containing and EGCG-treated samples centered
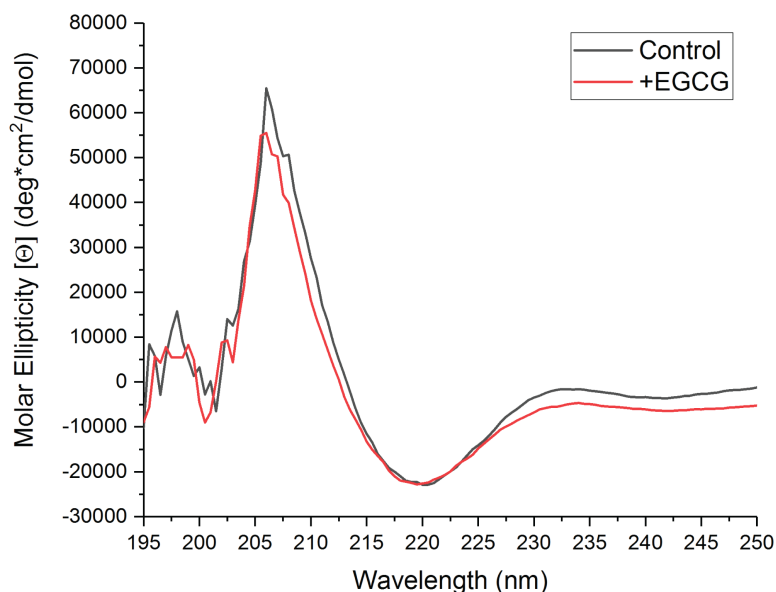
Figure 4.9: EGCG does not disturb the secondary structure of β2m. Circular dichroism spectra comparing a control sample of β2m in oligomerization conditions with Cu(II) (black) to an identical sample that contained EGCG (red). The ratio of β2m:Cu(II) was 1:2 for both samples. The EGCG sample contained a ratio of 1:2:1 β2m:Cu(II):EGCG.

around the 6+ ion. It has been documented that charge state distributions for proteins that arise during ESI are related to the total surface area, and are indicative of structural

heterogeneity [29]. We measure no such evidence during ESI. Furthermore, IM allows another dimension of analysis, as we can measure and compare the CCS of individual ions. Once again, the main (6+) ion for both the control (black) and EGCG-treated (red) sample shown in Figure 4.8C exhibits no significant difference in terms of the arrival time distribution, nor in its centroid CCS value. Based on these data, we therefore concluded that M* is not an unfolded monomer.

A second hypothesis regarding the identity of M* was a destabilized dimer that dissociates during SEC-HPLC analysis due to the perturbation of equilibria during the measurement [30]. Dissociation of dimer into monomeric units inside the column would effectively change the velocity of the individual subunits, which would retard their elution relative to dimer species that remain intact throughout analysis. If this hypothesis is correct, we expect that altering the flow rate during SEC-HPLC will alter the abundance of M*. Namely, decreasing the flow rate will cause longer residence times in column, and show lead to greater amounts of dimer dissociation. Data for these experiments are shown in Figure 4.10. We found no relationship between changing the flow rate and the abundance of M*, either by quantifying M* (via peak height) on its own (B) or in relative ratios to the other species in solution (panel C).

We also considered EGCG making chemical modifications to β2m that could potentially influence its behavior during SEC-HPLC. We collected fractions using the above SEC methods described above, and then subjected the monomer fraction to reverse phase (RP) liquid chromatography-mass spectrometry (LC-MS) (Figure 4.11). The LC-MS method involves the usage of a short (12 mm) desalting column with a rapid gradient, so only one peak is observed chromatographically. The extracted mass spectra from this

peak for both a Cu(II)-containing control (panel A) and the same condition plus EGCG

(panel B) show identical charge state distributions that lead to deconvoluted masses that

are not significantly different.
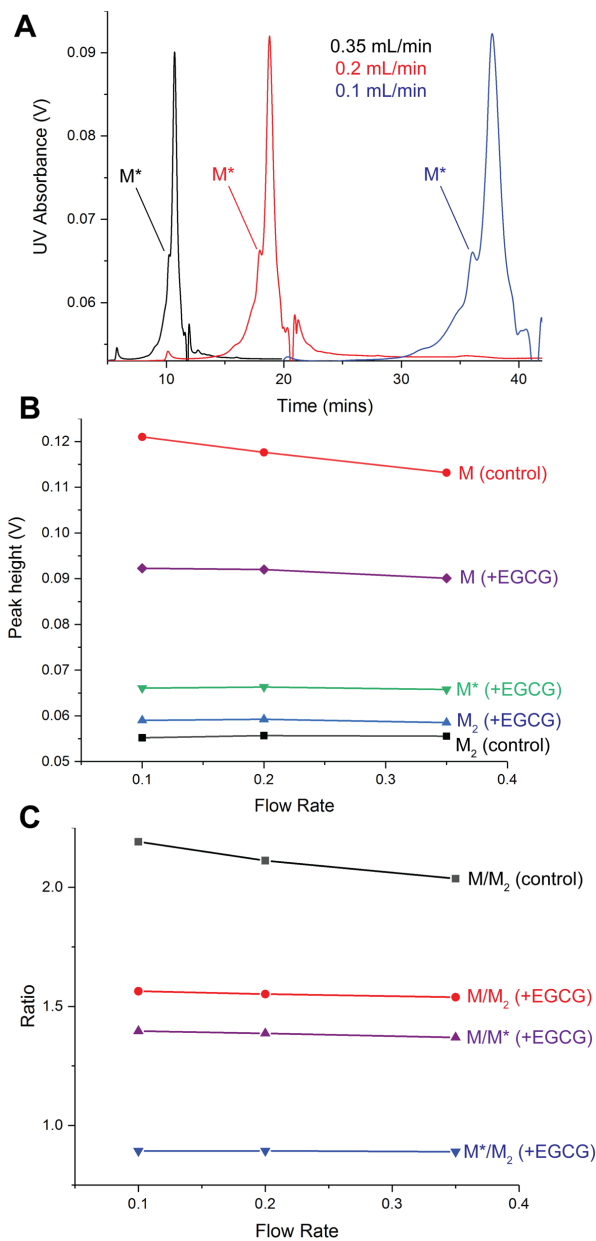
Figure 4.10: Effect of changing flow rate on abundance of M*. Panel A shows example SEC-HPLC chromatograms, with the M* species annotated. Panel B shows the quantification of M, M*, and M_2 species for both a control and EGCG-containing sample based on peak height. Panel C shows calculated ratios of M, M*, and M_2 species based on those peak heights.

There is also the presence of minor secondary peaks that appear to center near *m/z* 1100, but these species appear to be unrelated to β2m, and are also present in the baseline. There is no difference between panels A and B regarding these species. We also find no evidence of ions corresponding to EGCG in the major chromatographic peak alone or in complex with any of the β2m peaks. There is also no evidence of EGCG in the void volume peak. We conclude from these experiments that EGCG is not chemically modifying β2m to a detectable degree.
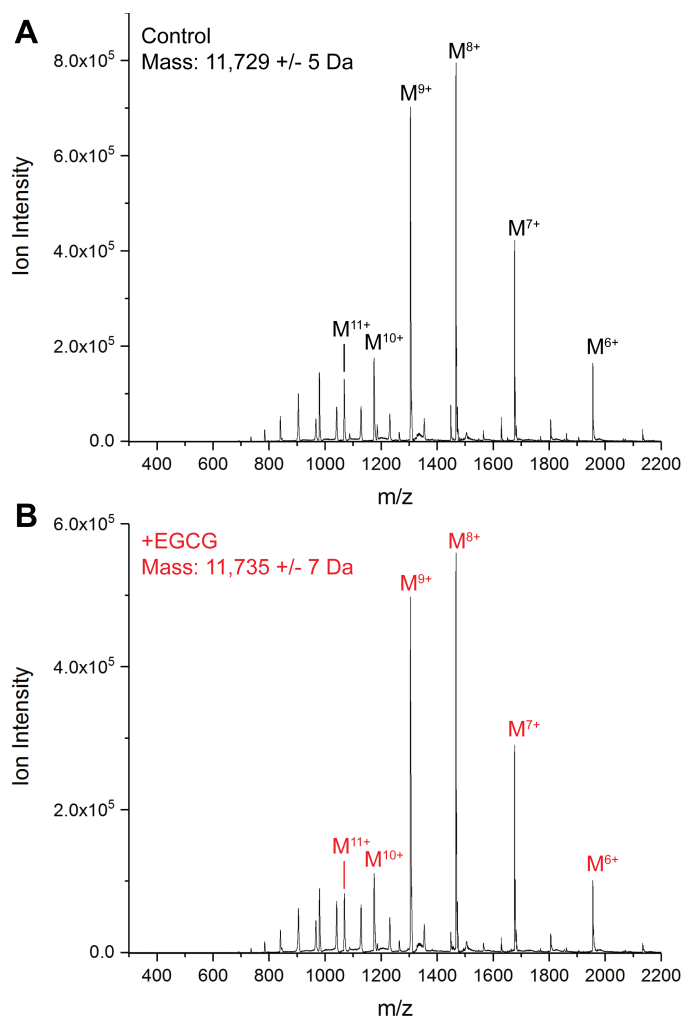
Figure 4.11: Reverse phase LC-MS of monomer fractions. Panel A is the extracted mass spectra for a Cu(II)-containing control, while panel B reflects a sample incubated with both Cu(II) and EGCG. The annotated peaks refer to β2m-related peaks and associate charge states. The deconvoluted mass for each sample is shown in the upper left hand corner, ± standard deviation.

4.4 Discussion

This chapter reflects the first efforts at assessing the effects of a popular anti-amyloid small molecule, EGCG, in the context of Cu(II)-catalyzed amyloid formation with β2m. EGCG was chosen for study due to its prevalence in the literature and its apparent ability to broadly affect amyloid formation amongst many different proteins [13,18–21]. It also serves as a natural extension of prior small molecule inhibition work that we recently reported [27,28]. Overall, our results suggest some important commonalities to other amyloid forming proteins, as well as unique Cu(II)-only mechanisms with regards to β2m.

TEM analysis of the mature aggregates generated in the presence of EGCG revealed no evidence of amyloid fibrils, or any fibril-like structures at all. Instead, we found the presence of amorphous, roughly globular aggregates by TEM. The morphologies that we observed are very similar to morphologies observed by other groups, namely Aβ1-40, IG LC, and αS [14,15,20]. This is especially interesting in the context of AβThe dimensions of these aggregates are similar to ones that we observed in our study. This suggests that although the mechanisms and early pre-amyloid events are different, there are similarities when it comes to assembly processes for higher order oligomers that manifest in changes to the mature insoluble aggregates.

The insoluble aggregates are also apparently reversible, as strong solubilizing agents like SDS are able to dissolve them. This finding also speaks to their structure, as amyloid fibrils are typically resistant to SDS which is attributed to the thermodynamic stability of the intermolecular β-sheet structure [31]. Other studies of EGCG-induced aggregates suggest a lack of regular ordered structure in these higher order species [15].

Closer investigation of secondary structure of the insoluble aggregates of β2m and EGCG using a technique like infrared spectroscopy would be informative to determine what structure, if any, these species have [32–35].

Interestingly, the other report of EGCG with β2m is from the context of low pH as the amyloid inducing stimulus [3]. Despite the large excess (~22:1) ratio of EGCG:β2m, amyloid fibrils are still formed [3]. This stands in contrast to our results, as we found that EGCG exerts an effect on Cu(II)-catalyzed β2m amyloid formation at much lower concentrations/ratios. While there are notable mechanistic differences between low pH and Cu(II)-catalysis, the general consensus is that β2m must adopt an amyloidogenic conformation which involves the *cis-trans* isomerization of P32, amongst other conformational changes [36,37]. Perhaps EGCG exerts its apparent effects at one of these points of mechanistic diversion.

A similar dichotomy was documented with $A\beta_{1-40}$, where EGCG was shown to have a specific inhibitory effect when the Aβ amyloids were formed with $CuCl_2$ and $ZnCl_2$ [14]. When Aβ was allowed to spontaneously form amyloids in the absence of Cu(II) with EGCG, no inhibition occurred. The authors also found evidence for ternary complex formation between Aβ, Cu(II)/Zn(II), and EGCG [14]. Indeed, in the absence of Cu(II), EGCG does not appear to promote the formation of M* or M_n with β2m. This is suggestive of a unique mechanism regarding EGCG's interactions with amyloid forming proteins and divalent metal systems.

The generation of new off-pathway oligomeric species is a common theme not only for EGCG [15,38], but also for other small molecules. These off-pathway aggregates may even lack defined structures, which is directly opposite of structured fibrils linked by

intermolecular β-sheets [37,39]. We previously found that this was a contributing factor

with β2m with two other effective small molecule inhibitors, doxycycline and rifamycin

[27]. For EGCG and β2m-Cu(II), this manifested in the generation of two new species,

which we deemed M_n and M*.

Comparing the large molecular weight of M_n (approximately 470 kD) to the

dimensions of aggregates that observed with TEM, it is geometrically feasible that a 40-

mer of β2m (whose longest dimension is ~4.5 nm with an area of 114 nm^2) would have a

spherical diameter that is roughly 65 nm. This approximation considers isotropic growth

of a globular oligomer [40,41]. Our microscopy results show aggregates on the order of

this diameter, so we infer that there are likely insoluble M_n species as well. As we do not

observe any oligomeric species that large by β2m with Cu(II), we can safely conclude

that Mn is off-pathway, and is thus detrimental to amyloid formation.

Assigning an exact identity of M* is much more difficult. Analytically, our efforts

to characterize it have largely been met with challenges. The first major hypothesis put

forth in this work was that M* is an unfolded state of β2m. Our CD, MS, and IM

evidence do not indicate any evidence of unfolding in solution or gas phase to a

detectable degree.

The second hypothesis that it was originally a dimeric species that is destabilized

in the presence of β2m, and due to the upset equilibria of oligomeric species in the

sample during SEC-HPLC analysis. This problem is inherent to SEC-HPLC, especially

when the solution of the incubation condition and the HPLC mobile do not match. As

mentioned above, dynamic dissociation and association of oligomers can occur during

size exclusion, which can result in altered peak shape or altogether unexpected peaks

[30]. Our efforts to change the flow rate to manipulate the abundance of M* showed no differences amongst the different conditions tested, despite drastically different residence times on the column. We also found that using SEC-MALS to calculate a molecular weight for M* is not feasible either, as the overlapping nature of the M_2, M*, and M peaks prevents accurate determination. Lastly, coupling SEC to MS (for detection) was inconclusive as well. This was due to poor chromatographic resolution coupled to low abundance of M_2 and M*.

The specific effect of EGCG when Cu(II) is present may be a hint that allows us to speculate on M*'s identity. If we assume that Cu(II) binds to β2m and is able to adopt the amyloidogenic conformation in the presence of EGCG, then perhaps EGCG is able to interact with the amyloidogenic β2m-Cu(II) complex, and divert oligomerization away from forming amyloid competent species. The altered structure of the β2m-Cu(II)-EGCG complex causes its apparent change in elution behavior on SEC. However, this structural difference is not preserved in the gas phase and may not have a major impact on secondary structure which is why our CD and ESI-IM-MS have revealed no differences between control and EGCG-treated samples. Although we lack direct evidence for it, there may be the possibility of this ternary complex in solution, much like the Aβ example cited earlier [14].

We also measured the apparent perturbance of one of the major tetrameric conformers in the presence of EGCG using ESI-IM-MS. Both doxycycline and rifamycin, which we discussed in chapter 2, also shared this characteristic [27]. In that case, we found that when the expanded conformer was depleted in abundance that there was a corresponding increase in the compact conformer. In EGCG's case, we only

measured a depletion of the expanded conformer. The missing Cu(II)-free tetramer

conformer may be one of the reasons why hexamers are curiously absent in the presence

of EGCG. We speculate that due to the hexamer's Cu(II)-free nature, it is dependent on

Cu(II)-free tetramer formation. This finding may have implications on how β2m forms

hexamers during amyloid formation. Armed with our new findings regarding the Cu(II)-

free tetramers that we built in chapter 3, it would be informative to determine the binding

site of EGCG on β2m to be able to extrapolate it obstructing an interface in an oligomeric

context.

4.5 Conclusions

Figure 4.12 is a summary of our findings with EGCG and Cu(II)-catalyzed

amyloid formation with β2m. We find that the addition of EGCG generates two new

species, M_n and M*. This effect is dose dependent and is more potent than inhibitors that

we have evaluated in the past. The lack of temporal separation between the

oligomerization steps prevents us from assigning an exact stepwise mechanism to

EGCG's effect (e.g. M* species generated in the presence of EGCG go on to
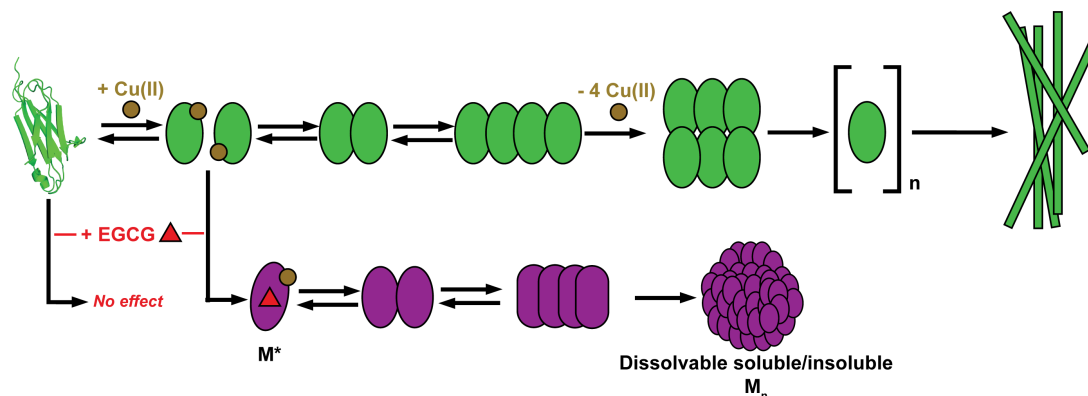
Figure 4.12: Proposed model for EGCG inhibition of Cu(II)-catalyzed amyloid formation with β2m.

form/compose M_n). The presence of M* and M_n can apparently divert β2m from forming

amyloid competent oligomers. The mature aggregates formed in the presence of EGCG

are morphologically distinct from amyloid fibrils and are dissolvable. The effect of

EGCG is also apparently Cu(II) specific, as adding EGCG with no Cu(II) present has no

impact on β2m oligomerization. We also note the apparent lack of hexamer formation in

the presence of EGCG, which has been a hallmark oligomers transitioning to Cu(II)-free

states during amyloid formation. The exact identity of M* is not clear at this time, but

with the hypotheses that we have tested, we speculate that it may be related to a β2m-

Cu(II)-EGCG ternary complex that our methods have not been able to distinguish.

4.6 References

[1] Y.-T. Choi, C.-H. Jung, S.-R. Lee, J.-H. Bae, W.-K. Baek, M.-H. Suh, J. Park, C.-W. Park, S.-I. Suh, The green tea polyphenol (-)-epigallocatechin gallate attenuates beta-amyloid-amyloid-induced neurotoxicity in cultured hippocampal neurons, Life Sciences. (2001) 603-614.

[2] S. Giorgetti, S. Raimondi, K. Pagano, A. Relini, M. Bucciantini, A. Corazza, F. Fogolari, L. Codutti, M. Salmona, P. Mangione, L. Colombo, A. De Luigi, R. Porcari, A. Gliozzi, M. Stefani, G. Esposito, V. Bellotti, M. Stoppini, Effect of Tetracyclines on the Dynamics of Formation and Destructuration of β2-Microglobulin Amyloid Fibrils, Journal of Biological Chemistry. 286 (2011) 2121–2131.

[3] L.A. Woods, G.W. Platt, A.L. Hellewell, E.W. Hewitt, S.W. Homans, A.E. Ashcroft, S.E. Radford, Ligand binding to distinct states diverts aggregation of an amyloid-forming protein, Nature Chemical Biology. 7 (2011) 730–739.

[4] N. Khan, F. Afaq, M. Saleem, N. Ahmad, H. Mukhtar, Targeting Multiple Signaling Pathways by Green Tea Polyphenol (−)-Epigallocatechin-3-Gallate, Cancer Research. 66 (2006) 2500–2505.

[5] T. Ozdal, E. Capanoglu, F. Altay, A review on protein–phenolic interactions and associated changes, Food Research International. 51 (2013) 954–970.

[6] T. Tanaka, T. Ishii, D. Mizuno, T. Mori, R. Yamaji, Y. Nakamura, S. Kumazawa, T. Nakayama, M. Akagawa, (−)-Epigallocatechin-3-gallate suppresses growth of AZ521 human gastric cancer cells by targeting the DEAD-box RNA helicase p68, Free Radical Biology and Medicine. 50 (2011) 1324–1335.

[7] H. Tachibana, K. Koga, Y. Fujimura, K. Yamada, A receptor for green tea polyphenol EGCG, Nature Structural & Molecular Biology. 11 (2004) 380–381.

[8] G. Fusco, M. Sanz-Hernandez, F.S. Ruggeri, M. Vendruscolo, C.M. Dobson, A. De Simone, Molecular determinants of the interaction of EGCG with ordered and disordered proteins, Biopolymers. 109 (2018) e23117.

[9] T. Takahashi, S. Nagatoishi, D. Kuroda, K. Tsumoto, Thermodynamic and computational analyses reveal the functional roles of the galloyl group of tea catechins in molecular recognition, PLOS ONE. 13 (2018) e0204856.

[10] A. Negri, V. Naponelli, F. Rizzi, S. Bettuzzi, Molecular Targets of Epigallocatechin—Gallate (EGCG): A Special Focus on Signal Transduction and Cancer, Nutrients. 10 (2018) 1936.

[11] K. Saeki, S. Hayakawa, S. Nakano, S. Ito, Y. Oishi, Y. Suzuki, M. Isemura, In Vitro and In Silico Studies of the Molecular Interactions of Epigallocatechin-3-O-gallate (EGCG) with Proteins That Explain the Health Benefits of Green Tea, Molecules. 23 (2018) 1295.

[12] S. Nakano, S. Megro, T. Hase, T. Suzuki, M. Isemura, Y. Nakamura, S. Ito, Computational Molecular Docking and X-ray Crystallographic Studies of Catechins in New Drug Design Strategies, Molecules. 23 (2018) 2020.

[13] J. Bieschke, J. Russ, R.P. Friedrich, D.E. Ehrnhoefer, H. Wobst, K. Neugebauer, E.E. Wanker, EGCG remodels mature α-synuclein and amyloid-β fibrils and reduces cellular toxicity, Proceedings of the National Academy of Sciences. 107 (2010) 7710–7715.

[14] S.-J. Hyung, A.S. DeToma, J.R. Brender, S. Lee, S. Vivekanandan, A. Kochi, J.-S. Choi, A. Ramamoorthy, B.T. Ruotolo, M.H. Lim, Insights into antiamyloidogenic properties of the green tea extract (-)-epigallocatechin-3-gallate toward metal-associated amyloid- species, Proceedings of the National Academy of Sciences. 110 (2013) 3743–3748.

[15] D.E. Ehrnhoefer, J. Bieschke, A. Boeddrich, M. Herbst, L. Masino, R. Lurz, S. Engemann, A. Pastore, E.E. Wanker, EGCG redirects amyloidogenic polypeptides into unstructured, off-pathway oligomers, Nature Structural & Molecular Biology. 15 (2008) 558–566.

[16] T. Zhang, J. Zhang, P. Derreumaux, Y. Mu, Molecular Mechanism of the Inhibition of EGCG on the Alzheimer Aβ $_{1-42}$ Dimer, The Journal of Physical Chemistry B. 117 (2013) 3993–4002.

[17] C. Bleiholder, T.D. Do, C. Wu, N.J. Economou, S.S. Bernstein, S.K. Buratto, J.-E. Shea, M.T. Bowers, Ion Mobility Spectrometry Reveals the Mechanism of Amyloid Formation of Aβ(25–35) and Its Modulation by Inhibitors at the Molecular Level: Epigallocatechin Gallate and *Scyllo* -inositol, Journal of the American Chemical Society. 135 (2013) 16926–16937.

[18] N. Lorenzen, S.B. Nielsen, Y. Yoshimura, B.S. Vad, C.B. Andersen, C. Betzer, J.D. Kaspersen, G. Christiansen, J.S. Pedersen, P.H. Jensen, F.A.A. Mulder, D.E. Otzen, How Epigallocatechin Gallate Can Inhibit α-Synuclein Oligomer Toxicity *in Vitro*, Journal of Biological Chemistry. 289 (2014) 21299–21310.

[19] D.E. Ehrnhoefer, M. Duennwald, P. Markovic, J.L. Wacker, S. Engemann, M. Roark, J. Legleiter, J.L. Marsh, L.M. Thompson, S. Lindquist, P.J. Muchowski, E.E. Wanker, Green tea (−)-epigallocatechin-gallate modulates early events in huntingtin misfolding and reduces toxicity in Huntington's disease models, Human Molecular Genetics. 15 (2006) 2743–2751.

[20] M. Hora, M. Carballo-Pacheco, B. Weber, V.K. Morris, A. Wittkopf, J. Buchner, B. Strodel, B. Reif, Epigallocatechin-3-gallate preferentially induces aggregation of amyloidogenic immunoglobulin light chains, Scientific Reports. 7 (2017) 41515.

[21] F. Meng, A. Abedini, A. Plesner, C.B. Verchere, D.P. Raleigh, The Flavanol (−)-Epigallocatechin 3-Gallate Inhibits Amyloid Formation by Islet Amyloid Polypeptide, Disaggregates Amyloid Fibrils, and Protects Cultured Cells against IAPP-Induced Toxicity, Biochemistry. 49 (2010) 8127–8133.

[22] T. Sheynis, A. Friediger, W.-F. Xue, A.L. Hellewell, K.W. Tipping, E.W. Hewitt, S.E. Radford, R. Jelinek, Aggregation Modulators Interfere with Membrane Interactions of β2-Microglobulin Fibrils, Biophysical Journal. 105 (2013) 745–755.

[23] K. Antwi, M. Mahar, R. Srikanth, M.R. Olbris, J.F. Tyson, R.W. Vachet, Cu(II) organizes β-2-microglobulin oligomers but is released upon amyloid formation, Protein Science. 17 (2008) 748–759.

[24] J. Dong, C.A. Joseph, N.B. Borotto, V.L. Gill, M.J. Maroney, R.W. Vachet, Unique Effect of Cu(II) in the Metal-Induced Amyloid Formation of β-2-Microglobulin, Biochemistry. 53 (2014) 1263–1274.

[25] H. Hernández, C.V. Robinson, Determining the stoichiometry and interactions of macromolecular assemblies from mass spectrometry, Nature Protocols. 2 (2007) 715–726.

[26] M.F. Bush, Z. Hall, K. Giles, J. Hoyes, C.V. Robinson, B.T. Ruotolo, Collision Cross Sections of Proteins and Their Complexes: A Calibration Framework and Database for Gas-Phase Structural Biology, Analytical Chemistry. 82 (2010) 9557–9565.

[27] T.M. Marcinko, J. Dong, R. LeBlanc, K.V. Daborowski, R.W. Vachet, Small molecule-mediated inhibition of β-2-microglobulin-based amyloid fibril formation, Journal of Biological Chemistry. 292 (2017) 10630–10638.

[28] T. Liu, T.M. Marcinko, P.A. Kiefer, R.W. Vachet, Using Covalent Labeling and Mass Spectrometry To Study Protein Binding Sites of Amyloid Inhibiting Molecules, Analytical Chemistry. 89 (2017) 11583–11591.

[29] I.A. Kaltashov, A. Mohimen, Estimates of Protein Surface Areas in Solution by Electrospray Ionization Mass Spectrometry, Analytical Chemistry. 77 (2005) 5370–7379.

[30] I.A. Kaltashov, J.W. Pawlowski, W. Yang, K. Muneeruddin, H. Yao, C.E. Bobst, A.N. Lipatnikov, LC/MS at the whole protein level: Studies of biomolecular structure and interactions using native LC/MS and cross-path reactive chromatography (XP-RC) MS, Methods. 144 (2018) 14–26.

[31] T. Eichner, S.E. Radford, A Diversity of Assembly Mechanisms of a Generic Amyloid Fold, Molecular Cell. 43 (2011) 8–18.

[32] Ruysschaert, J.M., Raussens, V., ATR-FTIR Analysis of Amyloid Proteins, Methods in Molecular Biology. 1777 (2018) 69–81.

[33] Cristovao, J.S., Henriques, B.J., and Gomes, C.M., Biophysical and Spectroscopic Methods for Monitoring Protein Misfolding and Amyloid Aggregation, Methods in Molecular Biology. 1873 (2019) 3–18.

[34] T.O. Zhang, A.M. Alperstein, M.T. Zanni, Amyloid β-Sheet Secondary Structure Identified in UV-Induced Cataracts of Porcine Lenses using 2D IR Spectroscopy, Journal of Molecular Biology. 429 (2017) 1705–1721.

[35] L.E. Buchanan, M. Maj, E.B. Dunkelberger, P.-N. Cheng, J.S. Nowick, M.T. Zanni, Structural Polymorphs Suggest Competing Pathways for the Formation of Amyloid Fibrils That Diverge from a Common Intermediate Species, Biochemistry. 57 (2018) 6470–6478.

[36] C.M. Eakin, A.J. Berman, A.D. Miranker, A native to amyloidogenic transition regulated by a backbone trigger, Nature Structural & Molecular Biology. 13 (2006) 202–208.

[37] T. Eichner, S.E. Radford, Understanding the complex mechanisms of β2-microglobulin amyloid assembly: β2-microglobulin fibrillogenesis at physiological pH, FEBS Journal. 278 (2011) 3868–3883.

[38] X.R. Cheng, B.Y.H. Hau, A.J. Veloso, S. Martic, H.-B. Kraatz, K. Kerman, Surface Plasmon Resonance Imaging of Amyloid-β Aggregation Kinetics in the Presence of Epigallocatechin Gallate and Metals, Analytical Chemistry. 85 (2013) 2049–2055.

[39] M.G. Iadanza, M.P. Jackson, E.W. Hewitt, N.A. Ranson, S.E. Radford, A new era for understanding amyloid structures and disease, Nature Reviews Molecular Cell Biology. 19 (2018) 755–773.

[40] J. Seo, W. Hoffmann, S. Warnke, X. Huang, S. Gewinner, W. Schöllkopf, M.T. Bowers, G. von Helden, K. Pagel, An infrared spectroscopy approach to follow β-sheet formation in peptide amyloid assemblies, Nature Chemistry. 9 (2017) 39–44.

[41] C. Bleiholder, N.F. Dupuis, T. Wyttenbach, M.T. Bowers, Ion mobility–mass spectrometry reveals a conformational conversion from random assembly to β-sheet in amyloid fibril formation, Nature Chemistry. 3 (2011) 172–177.

CHAPTER 5

CONCLUSIONS

5.1 Conclusions

From the work described in this dissertation, there are several emerging themes to consider. Our furthered understanding about the nature of β2m amyloid formation, primarily through the study of early pre-amyloid oligomers, primarily stems from two approaches. The first is a more applied approach through the usage of small molecule inhibitors to study their impact on amyloid formation. The second approach is a more fundamental study via coupling electrospray ionization ion mobility spectrometry-mass spectrometry (ESI-IM-MS) with computational modeling to generate model oligomer structures that extend our knowledge about a previously uncharacterized species, the Cu(II)-free tetramer(s). The common thread that runs through each of these stories is how structural heterogeneity amongst these oligomeric species factors into amyloid formation and inhibition thereof.

Combining studies of the effects of the small molecules alongside determining binding site information have given our lab a platform for future studies of small molecules, either from a drug design perspective or for testing new hypotheses about oligomeric structures or conformational isomers (conformers). We rationalized the inhibitory nature of these small molecules due to the apparent differences in both abundance and structure of ions that we measured using ESI-IM-MS. As discussed in previous Chapters, ESI-IM-MS is uniquely suited for exploring these aspects of amyloid forming proteins due to its ability to analyze heterogeneous, lowly abundant, and

transient species like pre-amyloid oligomers. Our implementation and usage of IM-MS has subsequently provided a new dimension of information about β2m amyloid formation.

With regards to the inhibitors, it is clear that molecules identified as effective in other amyloid systems, like amyloid-β, have inhibitory effects on β2m. Epigallocatechin-3-gallate (EGCG), rifamycin, and doxycycline have all been demonstrated to be effective *in vitro*, and the results from these studies share similarities with our own findings [1–7]. Generally, a recurring theme amongst anti-amyloid small molecule research usually involves generating new oligomers that are unique either in stoichiometry or their structure. We found this to be true in β2m's Cu(II)-catalyzed context.

Classically, our group has always observed even-numbered oligomers with Cu(II)-catalyzed amyloid formation. In the context of effective small molecule inhibitors, we measured a range of new oligomeric states, including trimers, pentamers and a heterogeneous population of states approximating a 40-mer. While the mechanistic pathway to form these structures in unclear, their formation is undoubtedly caused by the presence of small molecule inhibitors like doxycycline, rifamycin, and EGCG due to their unique occurrences only specific inhibitory contexts. Presumably, these structures are capable of further oligomerization into the mature insoluble aggregates that we measured via electron microscopy. Due to the inherent low resolution of IM-MS, we have no data regarding structural details of these species, only a rough idea of their topology via collisional cross sectional areas.

In addition to new off-pathway oligomers, we also found evidence of perturbed structures in Chapters 2 and 4. We conclude that in the case of structural perturbance,

these affected oligomers are generally structurally changed in such a way that they are no longer amyloid competent (i.e. able to assemble/elongate into higher order fibrillar structures). More specifically, we found evidence of structural perturbance in both dimers and tetramers with regards to doxycycline and rifamycin. Assuming that tetramers assemble from dimers in this context, our results indicate that interfering with the conformational ensemble of the dimer has an effect on higher order structures (i.e. the altered dimer conformers cannot form amyloid tetramers, but nevertheless oligomerize).

Structural perturbance and off-pathway oligomerization may in truth go hand-in-hand. For example, structural perturbance could potentially expose hydrophobic residues that seek to be thermodynamically satisfied via oligomerization. These interactions on the new oligomers could also be largely nonspecific, as the broadly eluting peaks on size exclusion high performance liquid chromatography (SEC-HPLC) would indicate that these species are polydisperse. In contrast, we know that normal Cu(II)-catalyzed amyloid formation with β2m is highly specific in terms of early oligomers, as there are particular interactions that are necessary like the intramolecular salt bridge between D59-K19. This salt bridge, along with other interactions, was a critical feature of the Cu(II)-bound dimer, as we later found in our simulation work in Chapter 3. As noted above, the generation of new off-pathway oligomers with small molecule inhibitors have also been observed in other amyloid systems as well [8–11].

Curiously, we also found that there were instances of differences in covalent labeling percentages on residues that are distal from the presumed binding site in the monomer context [12]. These changes, although small, were statistically significant. We posit that these changes may be due to long range allosteric effects due to the binding of

inhibitor molecules. If residues that are critical for oligomerization are altered in their positioning due to allostery, then this can also account for inhibitory behavior. Looking forward, it is therefore not only possible to possibly design a small molecule inhibitor that occludes critical binding interfaces but can also change the structure of β2m such that is no longer capable of oligomerizing in an amyloid-productive manner. We have not explored the same approach with the oligomers, but allosteric changes in oligomeric states is within the realm of possibility and would require similar experiments that we have carried out on the monomer.

By comparing and contrasting our results with other reports, our work has allowed us to more deeply understand our amyloid system of choice. Even amongst β2m alone, there are key differences amongst inhibitors with different amyloid formation conditions. For example, we found that rifamycin was preferentially interacting with Cu(II)-catalyzed oligomers, while it preferred to bind to partially folded monomeric species at low pH [4,13]. This observation underscores important structural and mechanistic distinctions between β2m under different amyloid forming conditions. Some early features of amyloid formation with Cu(II)-catalysis and low pH are shared (e.g. the *cis-trans* isomerization of P32), but different (e.g. conformational heterogeneity of the monomer and a more diverse set of oligomer stoichiometries) [14–17]. For EGCG, it was not found to be an effective inhibitor at low pH, but appears to have unique effects on amyloid formation when the amyloid stimulus is a divalent metal [4,18].

An important point to note about the molecules that we have evaluated in the lab appear to have relatively low affinities for β2m (from a medicinal chemistry perspective). These range from the hundreds of micromolar for doxycycline and rifamycin to the low

single digit micromolar for EGCG. Neither of these cases would be ideal for actual therapeutic treatment, which would ideally desire affinities in the nanomolar range with exquisite specificity. Furthermore, EGCG might also make an exceedingly poor choice for a high fidelity binder due to its apparent promiscuous binding properties [19]. However, even with their low affinities, these molecules still exert surprisingly potent effects on inhibiting amyloid formation *in vitro.* Armed with our new knowledge about effective molecules, their structures, and their binding sites, we are poised to either build upon these molecules, or design new ones with effective structures and functional groups already in mind. As we are not a translational lab, the real value from our perspective is the new fundamental understanding that we gain from interfering with amyloid assembly. Developing a molecule for therapeutic use would require much more effort, and likely require industrial or clinical collaborations.

In a global sense, the behavior of these molecules in terms of how they inhibit amyloid formation suggests there must be some commonalities across different amyloid forming proteins despite having diverse sequences and structures (or in some cases, the lack thereof). The most obvious shared feature amongst amyloid forming proteins is the characteristic intermolecular β-sheet hydrogen bonding networks that stabilize these oligomeric structures [20–22]. Assuming the small molecules have direct interactions with either the oligomers or fibrils, it is reasonable to surmise that the specific structural requirements of the constellation of hydrogen bond donors/acceptors at the interfaces of these proteins is sufficiently disrupted by these inhibitors such that amyloid formation cannot proceed. It is also possible that these disruptions could be the results of long-range allosteric effects as well. Nevertheless, it seems that there still must be underlying

thermodynamic or kinetic factors for still oligomerizing, despite not being able to form a fibril structure.

One significant analytical challenge standing in the way of further investigation of these oligomeric species is the lack of higher resolution structural details of pre-amyloid oligomers, whether they be on-pathway or off (or in complex with small molecules). This is primarily due to the inherent polydispersity in oligomerizing samples. Isolating oligomers (e.g. through fractionation by SEC-HPLC) is not always feasible, as they are prone to dissociation when equilibria are necessarily disturbed by the collection/isolation process. β2m oligomers are also in low abundance, at the soluble stages of the amyloid formation process. For example, in the above case of using allostery to inhibit amyloid formation, it is not only difficult to predict allosteric effects, but also to discern structural effects of inhibitor binding.

These initial observations of conformeric species begged for further fundamental investigation. β2m was not unique in this regard, as there have been increasing mentions of structural heterogeneity amongst amyloid forming proteins in recent years [23]. While the implications and consequences of polymorphisms during amyloid formation are not completely understood (for one protein, let alone the entire family of amyloid forming proteins), the development of analytical tools like ESI-IM-MS have allowed us to make new measurements which permits new biological understanding.

IM is a valuable comparative technique as well. We are able to compare our measurements to other published results which has provided insight into the differences in oligomeric structures that β2m adopts whether the induction mechanism is Cu(II)-catalysis or low pH. Our ESI-IM-MS measurements led us to search for plausible

structural models for these complexes that would transform collisional cross section values to protein structures. While ESI-IM-MS provides inherently low resolution structural information, we were able to combine it with covalent labeling data to help assist our computational efforts in finding structures, which we described in Chapter 3.

One significant finding from the work described in Chapter 3 was the realization of the conformational heterogeneity exhibited by oligomers during amyloid formation with β2m and Cu(II). Prior to this work, our group had derived a structural model of both the Cu(II)-bound dimer and Cu(II)-bound tetramer [24,25]. Outside of our group, the structure of P32A mutant variant of β2m dimer was solved via x-ray crystallography by Andrew Miranker's group at Yale [14]. The configuration of this dimer is similar to our previous model in that it is anti-parallel and the central interface is composed of the ABED β-strands of β2m. Furthermore, there are also notably a hexameric structure where β2m appears to also retain a native-like structure as well [26]. In all cases that have been documented so far, β2m remains in a mostly native-like structure when incorporated as part of an oligomer.

This fact makes our findings regarding heterogeneity particularly surprising. Based on some of the above evidence, amyloid formation with β2m and Cu(II) does not appear to require a great deal of unfolding in order to oligomerize, at least at the early stages. Despite this, our new measurements have revealed that β2m can nevertheless be heterogeneous during early oligomeric formation. It is important to point out that our usage of conformational isomer or heterogeneity can either refer to differences within the tertiary structure of β2m (that may result in altered oligomeric structures) or at the quaternary level (which would be exhibited through configurational differences of

subunits within an oligomer). From our work, it is not yet clear which category our conformers fall into but either example (or even a combination of both) is possible.

Using our combined ESI-IM-MS, covalent labeling, and computational modeling approach, one of the most obvious directions to move in was learning more information about the Cu(II)-free tetramer which both our group and others have found to be an essential step in amyloid formation. The unique heterogeneous behavior of tetrameric ions during ESI, coupled with the ability to selectively deplete Cu(II)-bound species in solution using ethylenediaminetetraacetic acid (EDTA), allowed us to examine Cu(II)-free species exclusively.

Prior to this dissertation, our structural work had ended with a Cu(II)-bound tetrameric model [25]. However, as described in this dissertation and elsewhere, the Cu(II)-bound structure is not the only tetramer in solution. Based on our findings, we propose that the Cu(II)-bound to Cu(II)-free transition is likely complex (i.e. involving multiple conformers), which we attribute to the release of multiple Cu(II) ions. The exact structural transitions or interconversions of these conformers are not yet clear, but we have nevertheless detected each conformer's presence via ESI-IM-MS. We generally attribute this to the fact that ESI-IM-MS is effectively capable of 'freeze-drying' structures in the gas phase, whether they be independent or interconverting between one another [27].

The new models of Cu(II)-free oligomers have unique interactions and interfaces that will provide foundations for future study. The overall topology of the three different tetramers is quite different, with the most drastic being the extended conformation of TET4. The important thread that cements TET4's relevance to amyloid formation is its

apparent depletion prevents amyloid formation, as noted above and in Chapter 2. In an

extension of our inhibitor work, preliminary *in silico* evidence has pointed to a possible

binding site of rifamycin near the central interface of one of the Cu(II)-free conformers,

which may explain its decreased abundance, and thus, inhibition of amyloid formation.

Having this information may now allow us to potentially develop new molecules for

amyloid inhibition, whether it is derivatizing existing molecules or designing them *de

novo*.

It is important not to overinterpret data provided by computational models. As

such, it will be necessary in the future to perform validation experiments on the newly

discovered heterogeneous species to determine if the computational models are

representative of the pre-amyloid species in solution. This is a tall order, as obtaining

higher resolution structural data of aggregated/aggregating species can be challenging

even under the most optimal conditions. It may be feasible to perform covalent labeling

experiments, similar to the ones performed previously, on EDTA-treated Cu(II)-free

species. This would reveal residue solvent accessibility and would provide insight

whether the interactions shown by the model are present in solution or not.

This approach is not without its difficulties however, as having heterogeneous

species present when covalent labeling presents a challenge for data interpretation, as the

total labeling reflects the average population in the solution. It may be possible to work

around obstacle by either isolating tetrameric species, or by enriching them. A possible

method to achieve this would be through ion exchange chromatography, which would

separate species based on their surface charge, which would be different between the

conformers. This would also hopefully maintain a native-like structure and assembly of

the conformers, although dilution and disturbance of the normal equilibria would likely be an obstacle.

Although we have learned more about dimers and tetramers during this period, the hexameric oligomeric species that populate during β2m amyloid formation with Cu(II) are the least understood. Previously, we knew that hexamer formation does not depend on Cu(II) [28]. This means that sequentially the formation of hexamer is preceded by the formation of Cu(II) species (i.e. tetramers) in solution. Although a putative structure of the hexamer has been published, there are a few important caveats to consider [26]. The first is that a mutant variant of β2m is used to generate it. Interestingly, it also does not form amyloid fibrils, and the hexamer itself is bound to Cu(II) ions in the structure. Our experiments with EDTA further suggests that sequestering Cu(II) has no effect on hexamer stability.

In terms of the overall structure, the hexamer mutant crystal structure is arranged as a trimer of dimers in a doughnut shaped circular fashion. Comparing this structure to our ESI-IM-MS data reveals that an arrangement like this could indeed be possible, but the variation in the data means that multiple configurations are possible. Furthermore, it is possible to theoretically construct hexamers that also fit within the spread of the data, which further convolutes the problem. At this stage, with no other supporting data, it is difficult to assign a structure to the hexamer.

With regards to amyloid inhibition, no hexameric species were observed or measured in the presence of doxycycline, rifamycin, or EGCG. We concluded that the lack of hexamer is due to non-amyloid competent tetramers, which can apparently not assemble into hexamers. This fact further underlines the importance of the structural

requirements of these oligomeric species have in order to form amyloids. With little structural data, it is difficult to specifically say which region(s) are responsible, but the β2m subunits of the aforementioned crystal structure are native-like, so it is reasonable to assume that they are similar with a wild type hexamer. Nevertheless, the prevention of the formation of the hexamer, whether directly or indirectly, is noticeably deleterious to amyloid formation.

The primary mission of our group when it comes to our group's β2m research is gaining new fundamental understanding of the structural complexities of amyloid formation via the development of new analytical tools. We have coupled traditional biophysical tools with the usage of ESI-IM-MS in various applications to study pre-amyloid oligomers. Our efforts at using ESI-IM-MS represents the first of their kind in our lab. Natural extensions and variations of this technique to further investigate pre-amyloid oligomers are currently underway, and we present some of those preliminary results in Chapter 6.

The approaches used in this dissertation have also proven useful as a way to evaluate small molecule inhibition of amyloid formation. The effective small molecule inhibitors that we have evaluated so far apparently impact conformational distributions of pre-amyloid oligomers, which results in the generation of off pathway oligomers. Overall, the results in this dissertation have provided critical new insight into the early fundamental mechanisms behind the assembly of Cu(II)-induced β2m amyloids, and revealed the presence of heretofore unidentified heterogeneous structures that contribute to amyloid formation.

5.2 References

[1] T. Tomiyama, A. Shoji, K. Kataoka, Y. Suwa, S. Asano, H. Kaneko, N. Endo, Inhibition of Amyloid Protein Aggregation and Neurotoxicity by Rifampicin: its possible function as a hydroxyl radical scavenger, Journal of Biological Chemistry. 271 (1996) 6839–6844.

[2] A. Napp, V. Houbart, A. Demelenne, M. Merville, J. Crommen, M. Dumoulin, G. Garraux, A. Servais, M. Fillet, Separation and determination of alpha-synuclein monomeric and oligomeric species using two electrophoretic approaches, Electrophoresis. 39 (2018) 3022–3031.

[3] J. Li, M. Zhu, S. Rajamani, V.N. Uversky, A.L. Fink, Rifampicin Inhibits alpha-Synuclein Fibrillation and Disaggregates Fibrils, Chemistry & Biology. 11 (2004) 1513–1521.

[4] L.A. Woods, G.W. Platt, A.L. Hellewell, E.W. Hewitt, S.W. Homans, A.E. Ashcroft, S.E. Radford, Ligand binding to distinct states diverts aggregation of an amyloid-forming protein, Nature Chemical Biology. 7 (2011) 730–739.

[5] L. Regazzoni, R. Colombo, L. Bertoletti, G. Vistoli, G. Aldini, M. Serra, M. Carini, R.M. Facino, S. Giorgetti, M. Stoppini, G. Caccialanza, E. De Lorenzi, Screening of fibrillogenesis inhibitors of β2-microglobulin: Integrated strategies by mass spectrometry capillary electrophoresis and in silico simulations, Analytica Chimica Acta. 685 (2011) 153–161.

[6] S. Giorgetti, S. Raimondi, K. Pagano, A. Relini, M. Bucciantini, A. Corazza, F. Fogolari, L. Codutti, M. Salmona, P. Mangione, L. Colombo, A. De Luigi, R. Porcari, A. Gliozzi, M. Stefani, G. Esposito, V. Bellotti, M. Stoppini, Effect of Tetracyclines on the Dynamics of Formation and Destructuration of β2-Microglobulin Amyloid Fibrils, Journal of Biological Chemistry. 286 (2011) 2121–2131.

[7] C. Bleiholder, T.D. Do, C. Wu, N.J. Economou, S.S. Bernstein, S.K. Buratto, J.-E. Shea, M.T. Bowers, Ion Mobility Spectrometry Reveals the Mechanism of Amyloid Formation of Aβ(25–35) and Its Modulation by Inhibitors at the Molecular Level: Epigallocatechin Gallate and *Scyllo* -inositol, Journal of the American Chemical Society. 135 (2013) 16926–16937.

[8] D.E. Ehrnhoefer, J. Bieschke, A. Boeddrich, M. Herbst, L. Masino, R. Lurz, S. Engemann, A. Pastore, E.E. Wanker, EGCG redirects amyloidogenic polypeptides into unstructured, off-pathway oligomers, Nature Structural & Molecular Biology. 15 (2008) 558–566.

[9] X.R. Cheng, B.Y.H. Hau, A.J. Veloso, S. Martic, H.-B. Kraatz, K. Kerman, Surface Plasmon Resonance Imaging of Amyloid-β Aggregation Kinetics in the Presence of Epigallocatechin Gallate and Metals, Analytical Chemistry. 85 (2013) 2049–2055.

[10] T. Eichner, S.E. Radford, Understanding the complex mechanisms of β2-microglobulin amyloid assembly: β2-microglobulin fibrillogenesis at physiological pH, FEBS Journal. 278 (2011) 3868–3883.

[11] M.G. Iadanza, M.P. Jackson, E.W. Hewitt, N.A. Ranson, S.E. Radford, A new era for understanding amyloid structures and disease, Nature Reviews Molecular Cell Biology. 19 (2018) 755–773.

[12] T. Liu, T.M. Marcinko, P.A. Kiefer, R.W. Vachet, Using Covalent Labeling and Mass Spectrometry To Study Protein Binding Sites of Amyloid Inhibiting Molecules, Analytical Chemistry. 89 (2017) 11583–11591.

[13] T.M. Marcinko, J. Dong, R. LeBlanc, K.V. Daborowski, R.W. Vachet, Small molecule-mediated inhibition of β-2-microglobulin-based amyloid fibril formation, Journal of Biological Chemistry. 292 (2017) 10630–10638.

[14] C.M. Eakin, A.J. Berman, A.D. Miranker, A native to amyloidogenic transition regulated by a backbone trigger, Nature Structural & Molecular Biology. 13 (2006) 202–208.

[15] J. Dong, C.A. Joseph, N.B. Borotto, V.L. Gill, M.J. Maroney, R.W. Vachet, Unique Effect of Cu(II) in the Metal-Induced Amyloid Formation of β-2-Microglobulin, Biochemistry. 53 (2014) 1263–1274.

[16] D.P. Smith, S.E. Radford, A.E. Ashcroft, Elongated oligomers in β2-microglobulin amyloid assembly revealed by ion mobility spectrometry-mass spectrometry, Journal of the American Chemical Society. 136 (2010) 5432–5442.

[17] D.P. Smith, L.A. Woods, S.E. Radford, A.E. Ashcroft, Structure and Dynamics of Oligomeric Intermediates in β2-Microglobulin Self-Assembly, Biophysical Journal. 101 (2011) 1238–1247.

[18] S.-J. Hyung, A.S. DeToma, J.R. Brender, S. Lee, S. Vivekanandan, A. Kochi, J.-S. Choi, A. Ramamoorthy, B.T. Ruotolo, M.H. Lim, Insights into antiamyloidogenic properties of the green tea extract (-)-epigallocatechin-3-gallate toward metal-associated amyloid- species, Proceedings of the National Academy of Sciences. 110 (2013) 3743–3748.

[19] B.N. Singh, S. Shankar, R.K. Srivastava, Green tea catechin, epigallocatechin-3-gallate (EGCG): Mechanisms, perspectives and clinical applications, Biochemical Pharmacology. 82 (2011) 1807–1821.

[20] R. Kodali, R. Wetzel, Polymorphism in the intermediates and products of amyloid assembly, Current Opinion in Structural Biology. 17 (2007) 48–57.

[21] L.E. Buchanan, M. Maj, E.B. Dunkelberger, P.-N. Cheng, J.S. Nowick, M.T. Zanni, Structural Polymorphs Suggest Competing Pathways for the Formation of Amyloid Fibrils That Diverge from a Common Intermediate Species, Biochemistry. 57 (2018) 6470–6478.

[22] R. Nelson, M.R. Sawaya, M. Balbirnie, A.Ø. Madsen, C. Riekel, R. Grothe, D. Eisenberg, Structure of the cross-β spine of amyloid-like fibrils, Nature. 435 (2005) 773–778.

[23] B.H. Toyama, J.S. Weissman, Amyloid Structure: Conformational Diversity and Consequences, Annual Review of Biochemistry. 80 (2011) 557–585.

[24] V.L. Mendoza, K. Antwi, M.A. Barón-Rodríguez, C. Blanco, R.W. Vachet, Structure of the Preamyloid Dimer of β-2-Microglobulin from Covalent Labeling and Mass Spectrometry, Biochemistry. 49 (2010) 1522–1532.

[25] V.L. Mendoza, M.A. Barón-Rodríguez, C. Blanco, R.W. Vachet, Structural Insights into the Pre-Amyloid Tetramer of β-2-Microglobulin from Covalent Labeling and Mass Spectrometry, Biochemistry. 50 (2011) 6711–6722.

[26] M.F. Calabrese, C.M. Eakin, J.M. Wang, A.D. Miranker, A regulatable switch mediates self-association in an immunoglobulin fold, Nature Structural & Molecular Biology. 15 (2008) 965–971.

[27] D.E. Clemmer, D.H. Russell, E.R. Williams, Characterizing the *Conformationome* : Toward a Structural Understanding of the Proteome, Accounts of Chemical Research. 50 (2017) 556–560.

[28] K. Antwi, M. Mahar, R. Srikanth, M.R. Olbris, J.F. Tyson, R.W. Vachet, Cu(II) organizes β-2-microglobulin oligomers but is released upon amyloid formation, Protein Science. 17 (2008) 748–759.

CHAPTER 6

FUTURE DIRECTIONS

6.1 Future research directions

This chapter discusses several different avenues of possible future research into β2m amyloid formation, building off of the findings and conclusions from chapters 2-5 of this dissertation. Where applicable, preliminary data is shown.

6.1.1 Using collision-induced unfolding and dissociation to distinguish conformational heterogeneity

6.1.1.1 Background

Collision-induced dissociation (CID) is a versatile technique has a long history of use in conjunction with biological mass spectrometry, especially in tandem MS experiments [1–3]. As the name implies, it relies on the deposition of kinetic energy into the structure of analyte ions via collisions with (typically) inert gas molecules inside the mass spectrometer [1,2]. Depending on the experiment, the range of energies experienced by precursor analyte ions can disrupt non-covalent interactions all the way to the breaking of covalent bonds (as CID is probably most commonly known for peptide sequencing and protein identification during proteomics experiments) [4,5]. The products generated from CID experiments result in unique spectra that can lend additional confidence in the identification of analytes (beyond the initial mass measurement of the precursor).

In this dissertation, we are solely concerned with non-covalent complexes, so it is useful to discuss a typical CID experiment in that context (both in terms of information gained, as well as the instrumental setup). Here, ions are typically first selected using the quadrupole. These selected ions then enter the trap cell, which is filled with the collision gas (in this case, argon). The energetics of the collisions inside the trap cell are effectively modulated by an accelerating voltage applied by instrument at the point of injection into the cell. For our experiments, this is typically on the order of 10-150 V. Ions that are accelerated by this energy undergo more energetic collisions with the argon gas, leading to the aforementioned deposition of kinetic energy into the ion's structure [3].

A generalized example of a tandem CID experiment for a non-covalent complex (a β2m pre-amyloid tetramer) is shown below in Figure 6.1.1. The blue box highlights the isolated precursor ion. Following CID, monomeric (blue annotations) and trimeric
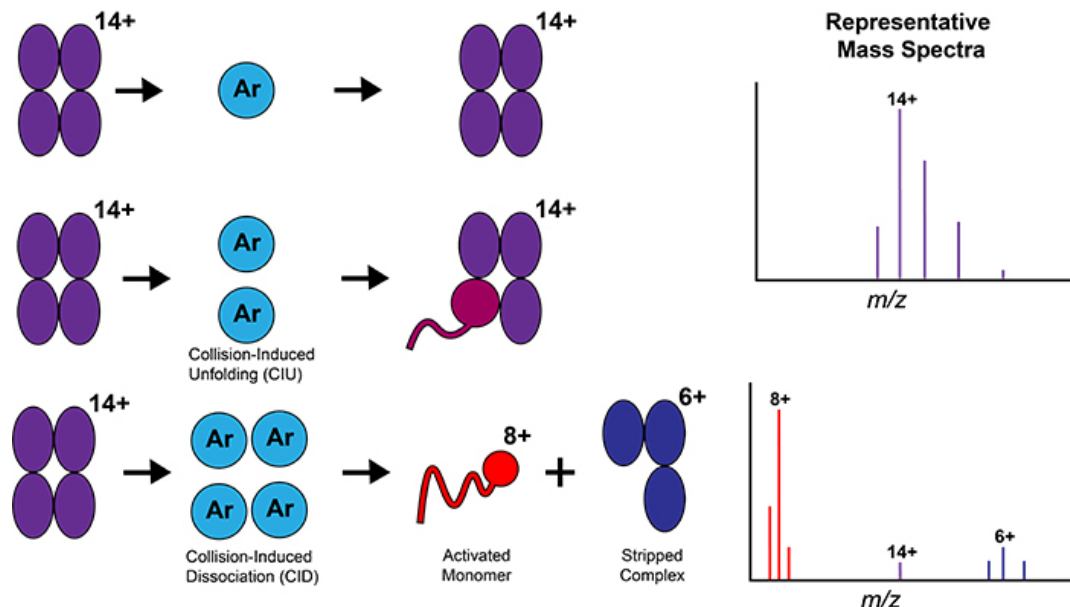
Figure 6.1: Generalized example of a CID experiment on a non-covalent complex with expected structure behavior and resulting mass spectra.

(orange annotations) product ions are observed in the spectra (Figure 6.1.2). This

asymmetric phenomenon of not only the dissociated monomer, but also charge, is
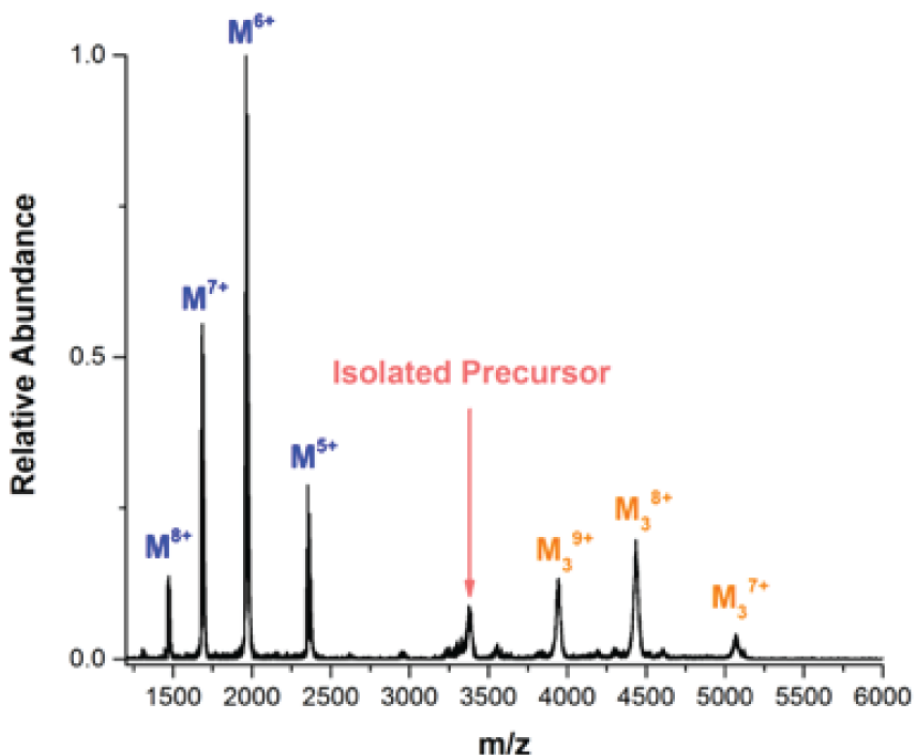
Figure 6.2: Example tandem MS CID mass spectra of a tetrameric ion. The asymmetric dissociation behavior of the complex is given by the presence of highly charged monomers, and 'stripped' trimers.

classical behavior of a non-covalent complex during CID, which was first identified and

documented in the mid-1990's [6,7]. In this example, we now not only have the *m/z* of

the ion to identify it (through its mass), but now also have an additional confirmation that

it is a tetramer through this tandem MS experiment.

The unique asymmetric dissociation behavior of protein complexes during CID

begs deeper fundamental questions about the underlying mechanisms of the process. The

prevailing mechanistic understanding and evidence suggests that as kinetic energy is

deposited in the ion's structure, it is unevenly distributed into one monomeric unit of the

complex. Given sufficient energy, this energized monomer begins to unfold (i.e. non-

covalent intramolecular interactions are disrupted). This unfolding coincides with the migration of charges (in this case, protons), to the newly unfolded surface area on the unfolding monomer [8,9]. Eventually, the unfolded monomer is ejected from the complex, taking an asymmetric number of charges, leaving a 'stripped' low charge complex (in the example above, trimer) [8,9].
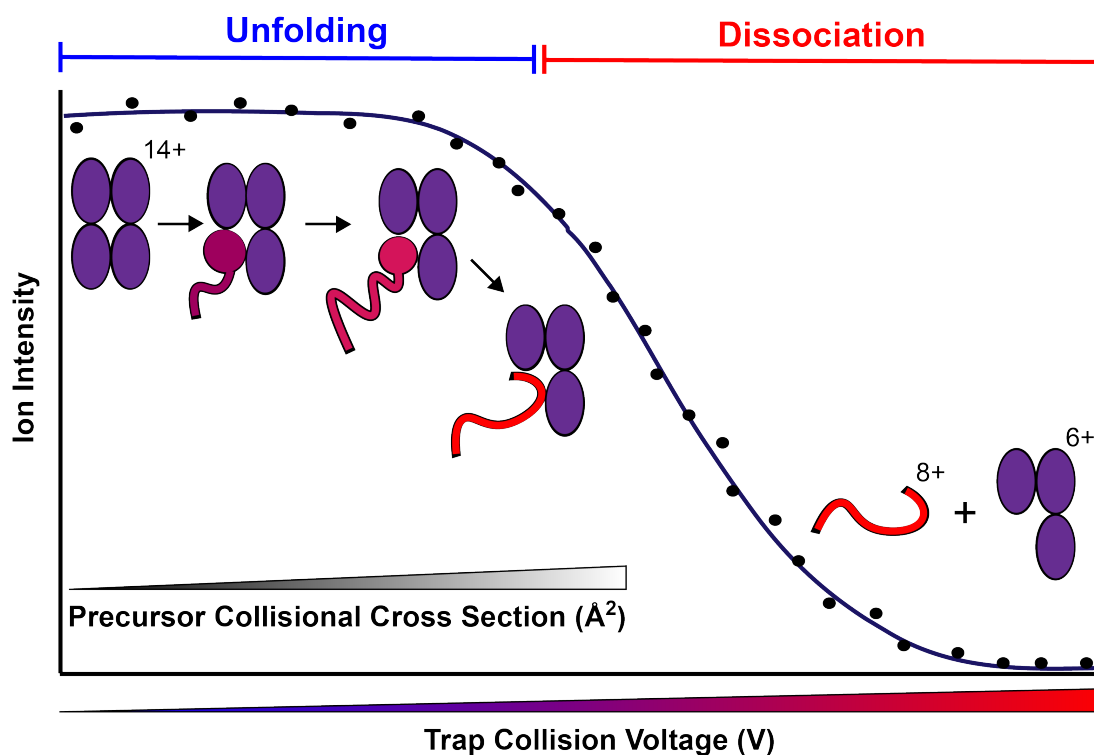
Figure 6.3: Generalized scheme for a CIU/CID experiment, showing the expansion and eventual dissociation of the precursor ion upon activation.

The entrance of ion mobility into understanding CID fundamentals have provided new views and methodologies to study this process. The period of time that precedes dissociation has been termed collision-induced unfolding (CIU), and in concert with ion mobility, has spun off into its own method to study protein complex structure (Figure 6.1.3) [10–12]. Not only can we gain insight into the gas phase stability of the precursor ion, but we can also study protein unfolding pathways in the gas phase. Ion mobility

plays a key role here, as the CIU/CID process occurs in the trap cell, which is upstream

of the ion mobility cell in the mass spectrometer. This allows us to separate and monitor

the structure (via CCS) of the unfolding precursor complex and products in addition to

the usual *m/z* and abundance given by the mass analyzer and detector. Monitoring the

drift times (and thus, CCS) of the unfolding species gives rise to what is referred to as the

CIU fingerprint (Figure 6.1.4) [13], which is a represented three-dimensionally and is

reminiscent of a classical transition plot generated during an equilibrium unfolding

experiment. These plots are generated by a specialized software called CIU Suite [13,14].

CIU studies have been documented for many different types of systems, including

differentiating protein isoforms, studying non-covalent complex architecture, protein-
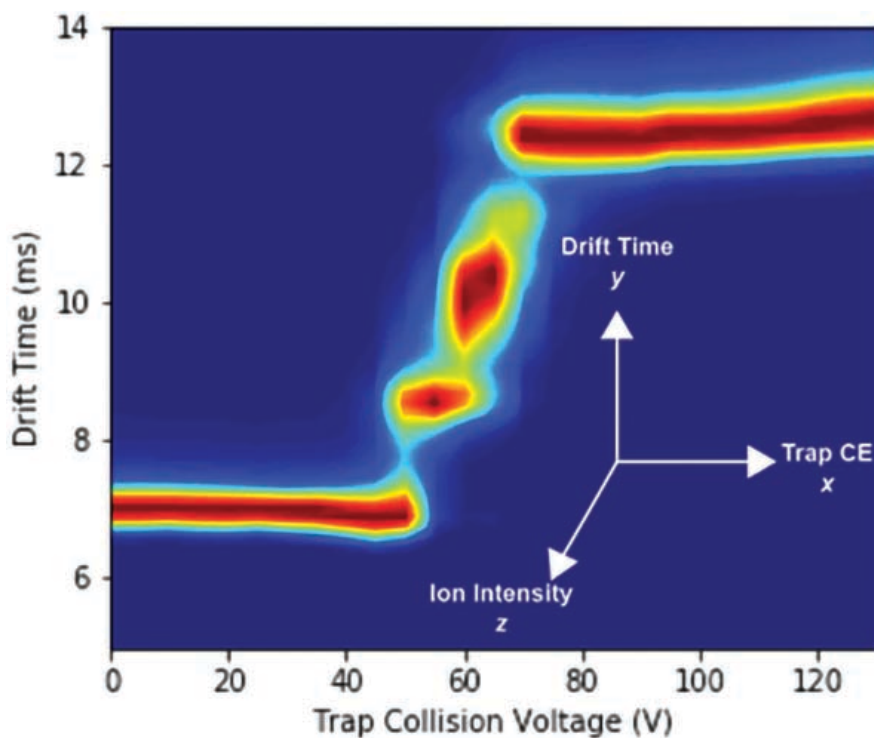
Figure 6.4: Example CIU fingerprint of tetrameric Concanavalin A[20+] with inset orienting the three-dimensional axes.

ligand interactions, and fundamental gas unfolding of proteins, amongst other examples

[15–18]. For our application, we particularly focused on the impact of conformational isomers on CIU behavior. The general hypothesis behind this work is that if the conformational isomers of β2m oligomers are truly different under native spray conditions, then their subsequent unfolding pathways (and CIU fingerprints) will also be different. The differences that we detect in terms of unfolded intermediates and their pathways implies intramolecular structural differences. This may also be manifested through differences of gas phase stability, which we infer from measuring abundance of precursor and product ions and reflects loss of the complex signal as a function of energy. Overall, these experiments add another layer of confidence to our growing list of evidence of the structurally distinct nature of β2m conformational heterogeneities.

6.1.1.2 Preliminary Results

To begin, we first built off of results that we described as part of chapter 3, where we noticed that ion mobility measurements of the tetramers uniquely narrowed in their distributions over time, which suggests the presence of multiple unresolved conformers. Other oligomers, like the dimer and hexamer, had no such behavior. Figure 6.1.5 shows a CIU experiment of the 9+ dimer charge state on two separate days following incubation with Cu(II). 2 day data is shown in red, while 6 day is shown in blue.

There are no obvious differences qualitatively from the CIU fingerprints, nor any significant differences in stability given by relative precursor stability, which have similar offsets and midpoints. These normalized values are calculated by integrating the precursor ion's mass spectral peak area and dividing by the precursor ion's peak area plus all of the product ion peak areas. The righthand panel shows a difference plot between the 2 day and 6 day data, which calculates an RMSD value based on how distinct two CIU

fingerprints are. The low RMSD value indicates the fingerprints are similar. For a frame

of reference, replicate experiments in our experience yielded around 5% RMSD.

Extraction of the actual arrival time distribution data for each of the ions are various

collision energies along the bottom row also reveals no significant differences. Taken

together, this is consistent with our previous conclusion that there are likely no

temporally dependent structural differences for the dimer (or at least, none that are

detectable by our methods).
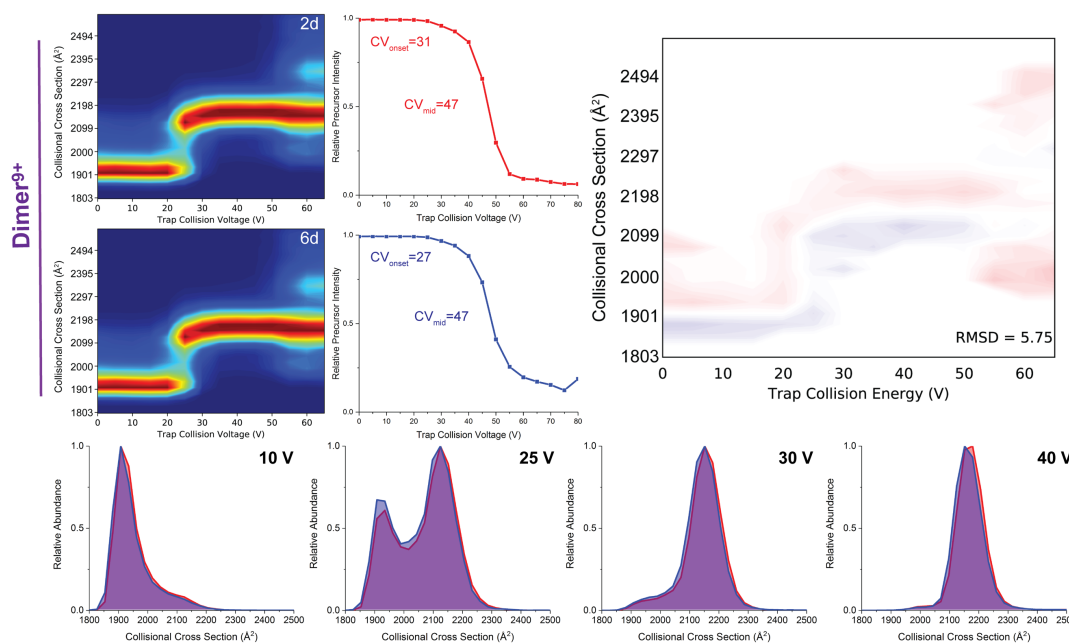
Figure 6.5: CIU data comparing the β2m dimer on two different days.

However, when a similar experiment is carried out on two tetrameric ions on

different days, a different result emerges. Figure 6.1.6 shows data for the 14+ charge

state, while Figure 6.1.7 shows data for the 13+ charge state. Here, we observe that the

tetramer exhibits differences in CIU, primarily through the presence of new

intermediates, which are most clearly shown on the bottom row of extracted arrival time

distributions. There is no clear difference between the gas phase stabilities of these populations (or is not sufficiently sensitive to detect these heterogeneities). The CIU differences appear to be more compact at lower voltages, but eventually extend to more expanded species at later timepoints. The RMSD difference between the two sets of data is 22.6, which is roughly 4 times larger than the dimer, indicating that there are significant differences present. We attribute these new unfolding intermediates to the likely presence of the Cu(II) tetramer.

In pursuit of more information on the Cu(II)-free tetramer, we conducted a similar Cu(II)-bound tetramer depletion experiment to the one described in chapter 3. Here we show results for the two most abundant charge states of the tetramer (14+ and 13+). The experimental conditions with regards to the concentration of EDTA and the pre-ESI incubation times were identical. The CIU fingerprints and stability plots are found in Figure 6.1.8, while the difference plots and extracted ATDs are found in Figure 6.1.9.
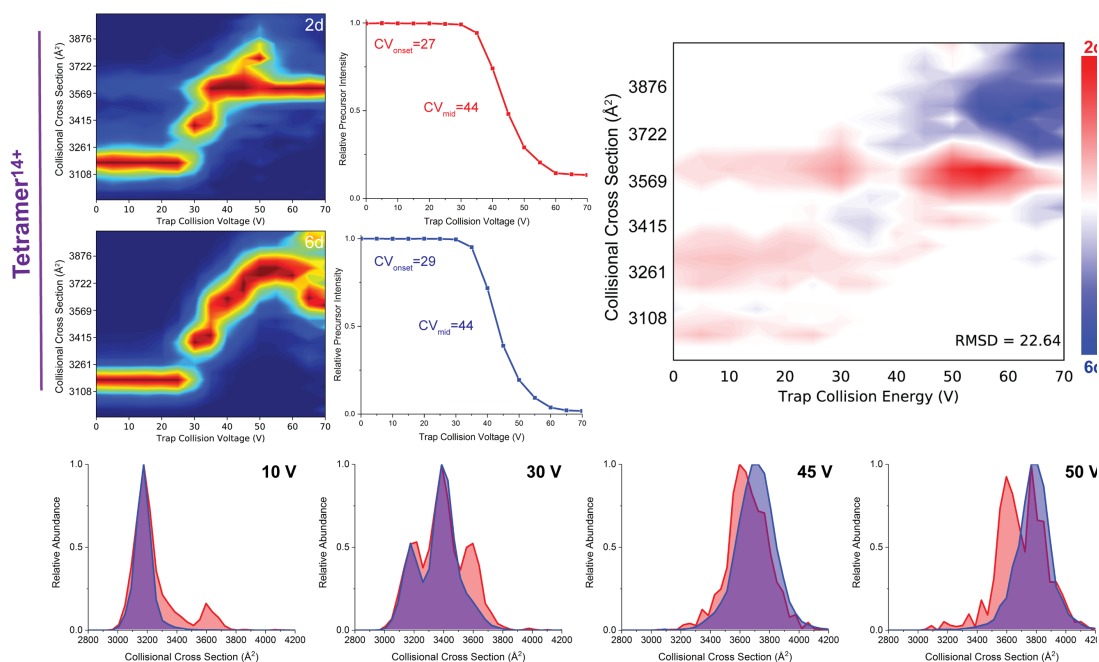
Figure 6.6: CIU data comparing the β2m tetramer[14+] ion on two different days.
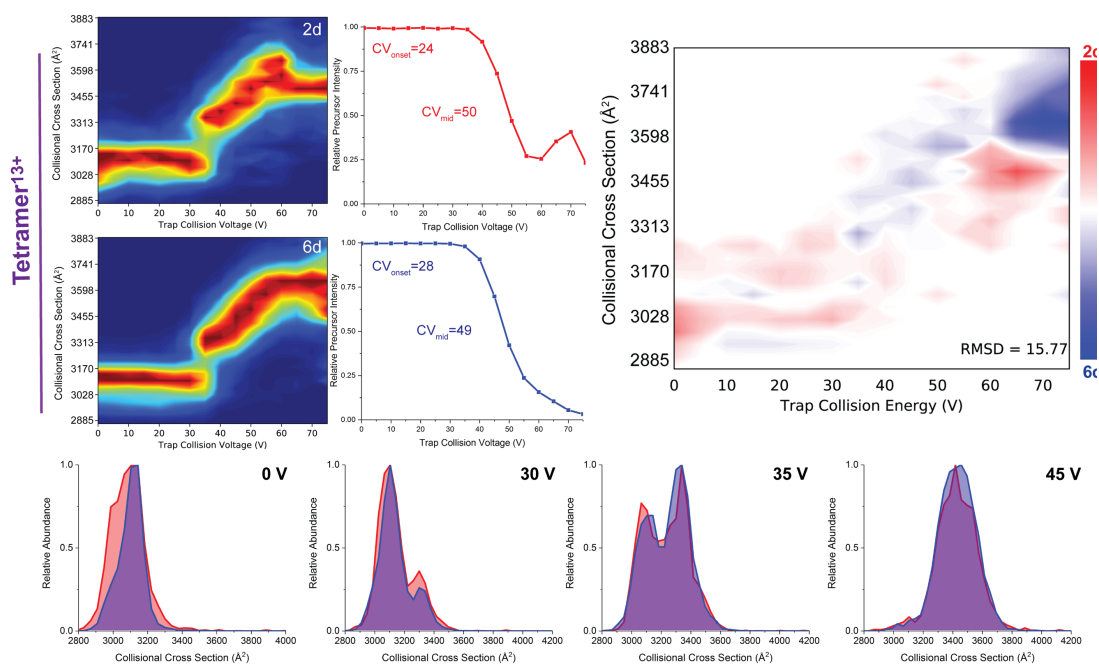
Figure 6.7: CIU data comparing the β2m tetramer[13+] ion on two different days. From the fingerprints themselves, there is an loss of spectral quality due to the loss of ion signal from Cu(II)-bound species dissociating. Interestingly, there is an apparent stabilization effect, where the offset slightly increases, but the midpoint shifts 7 V higher, which indicates that the Cu(II)-free tetramer is more stable than the Cu(II)-bound. This stability trend is also true for the 13+ tetramer.

When comparing the EDTA-treated to the control, difference plots reveal that there are regions with new unfolded species, and large RMSD values indicate that significant differences are present (Figure 6.1.9). Closer examination of the extracted arrival time distributions for both ions indicate that more expanded species are favored at low collision energies (10 and 35 V), while more compact species are present at higher energies (45 and 50 V). This overall trend appears to be reversed for the 13+ ion. We interpret this data to mean that the Cu(II)-free tetramer is more stable than the Cu(II)-

bound, and that Cu(II)-free tetramer unfold differently. Even amongst Cu(II)-free tetramers, there are clearly differences in trends amongst charge states, which might indicate that there is a further level of heterogeneity even amongst Cu(II)-free species, as we concluded in Chapter 3.
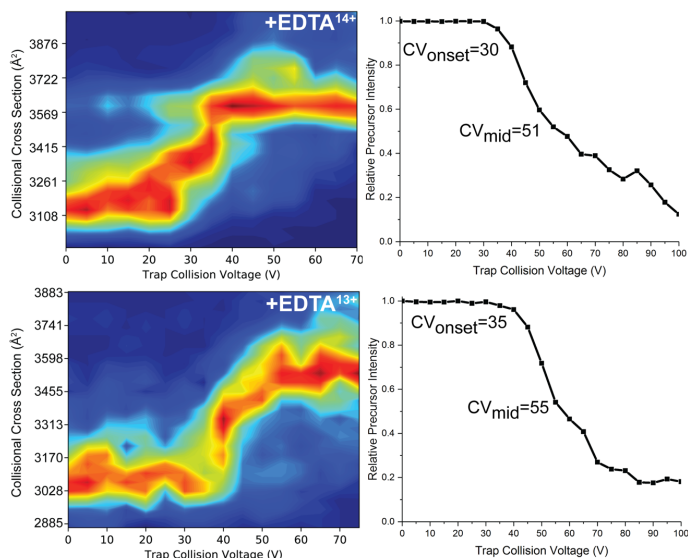
Figure 6.8: CIU fingerprint and gas phase stability of Cu(II)-free tetramers.

We also used CIU to study the effect of two small molecules that we described in chapter 2, rifamycin and suramin, to examine their effect on oligomer structure (Figure 6.1.10). Here, we are specifically performing CIU on ions that are clear peaks that correspond to a mass of oligomer plus that of the ligand. These data can then be compared back to the control data shown earlier. For both the rifamycin- and suramin-bound dimer, we measured a large increase in complex stability, as the midpoint increases (+14 V for rifamycin, and +17 V for suramin), indicating that both ligands stabilize the dimer in the gas phase. Interestingly, only rifamycin stabilizes the tetramer, as suramin doesn't appear to have a significant impact on the midpoint (+13 V for rifamycin). Comparison of the CIU fingerprints using difference plots more clearly shows

the stability increase indicated by the shift of the signal to the right, as well as reveals the presence of new intermediates (Figure 6.1.11). In all cases, RMSD values are greater than 15%, which suggests real difference in the unfolding intermediates detected.
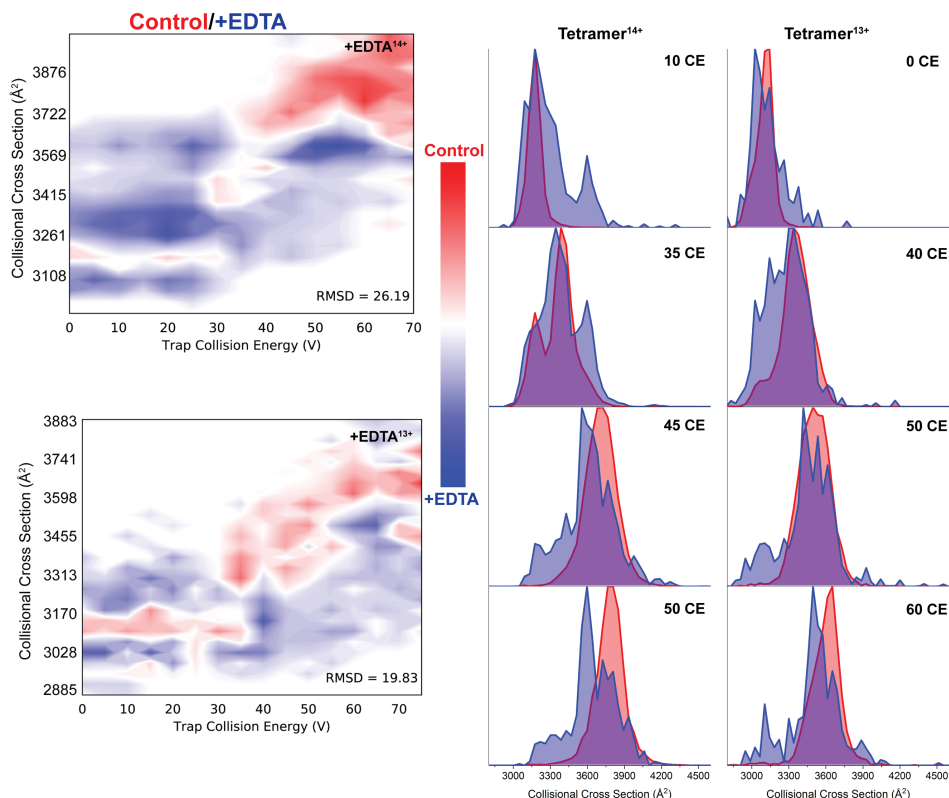
Figure 6.9: CIU difference plots and arrival time distribution comparison of Cu(II)-free tetramers.
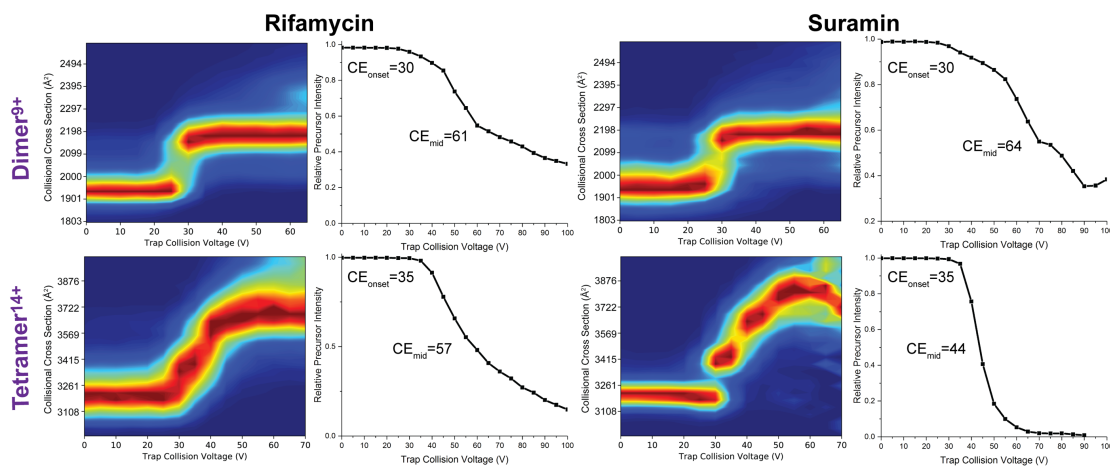
Figure 6.10: CIU fingerprints and stability plots of inhibitor-bound β2m dimers and tetramers.
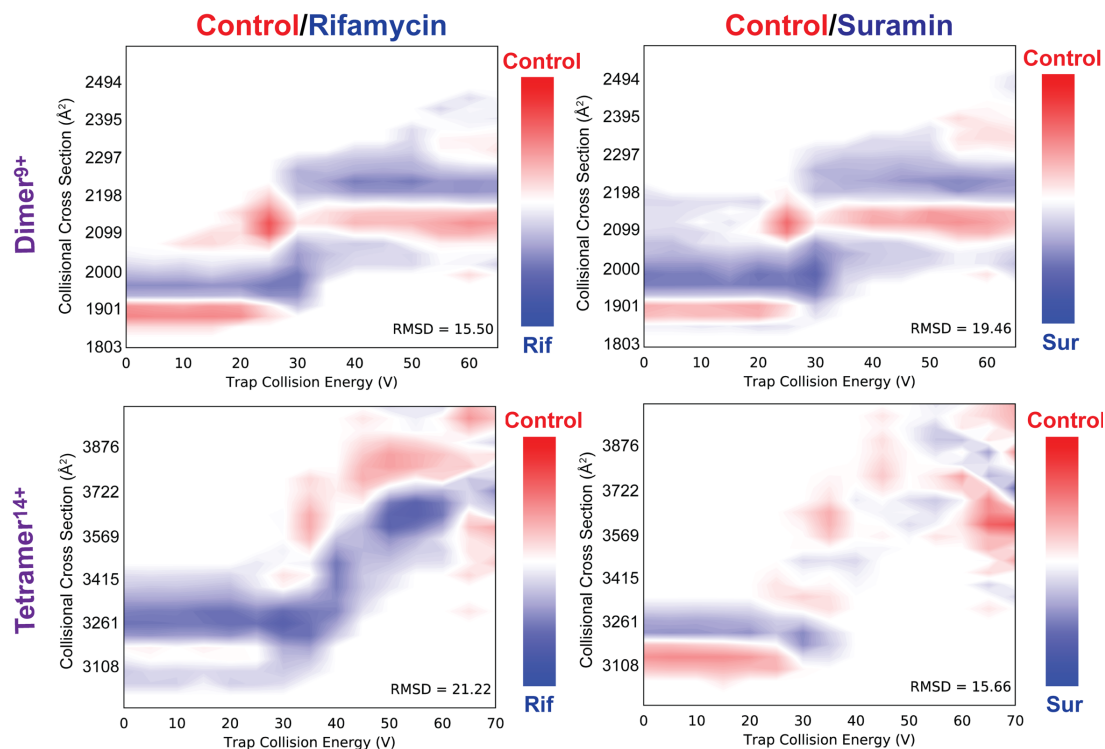
Figure 6.11: CIU difference plots of inhibitor-bound β2m dimer and tetramer.

Overall, we found that CIU and CID coupled with IM-MS to be a promising tool to further differentiate structural disparities amongst heterogeneous pre-amyloid oligomers. Differences that we detected using CIU in terms of unfolding intermediates and gas phase stabilities suggest intramolecular structural changes such as new protein-protein interaction sites and/or domain restructuring amongst oligomers, which supports our initial hypotheses that these conformers are structurally distinct. Like our experiments under native-like conditions, there is a temporal difference between tetramers, and an apparent stability and structure difference between Cu(II)-bound and Cu(II)-free tetramers.

The structural perturbance of oligomers caused by rifamycin appears to stabilize oligomers in the gas phase, and most, importantly the tetramer. In chapter 2, we attributed the ability of rifamycin's ability to inhibit amyloid formation to intervene at the tetramer,

possibly preventing the transition of Cu(II)-bound to Cu(II)-free. This stands in contrast to suramin, which does not stabilize the tetramer. The stabilizing effect of rifamycin may have an impact in redirecting the aggregation pathway, and helps explain why amyloid-competent oligomers are not produced in its presence.

As of this writing, these are the first studies of pre-amyloid oligomers that explores heterogeneity with CIU. An important limitation of the above data is that although we know that ions are unfolding, we cannot determine specific regions that are unfolding in sequence in an attempt to assign structures to the intermediates. This type of experiment has been reported for multi-domain monomeric proteins (or covalently linked ones) but remains elusive for non-covalent complexes ([18,19]. As such, interpreting our data in this manner is currently outside the scope of our work. Although the above data is encouraging, further experiments are also being conducted, specifically into model proteins with known structural heterogeneity where more in-depth structural data exists (i.e. NMR, x-ray crystallography) as a proof of principle.

6.1.2 Development of a HDX-enhanced IM-MS method to study protein conformational isomers

6.1.2.1 Background

As discussed above, IM-MS is a powerful technique for characterization of protein structure in the gas phase, but it also has its own share of drawbacks. Most notably, there are possibilities of gas phase conformer artifacts introduced by system parameters even under the gentlest of instrument conditions. These artifacts are especially possible for travelling wave ion mobility spectrometry (TWIMS) due to its relatively higher energies compared to other IM methods like DT-IMS [20]. Deposition of this

energy into the ion's structure results in unfolding, which complicates IM results. Furthermore, conformers detected and measured in the mass spectrometer following ESI are gas phase structures, and are believed to be representative of those in solution, as discussed in previous chapters [10,21–24]. Therefore, it is desirable to develop a novel orthogonal method to validate these structures measured during ESI-IM-MS by encoding the protein structure with a non-perturbing mass label (deuterium) in solution prior to ESI-IM-MS, and then measuring the resulting resolved conformers in both *m/z* and mobility space (Figure 6.2.1).
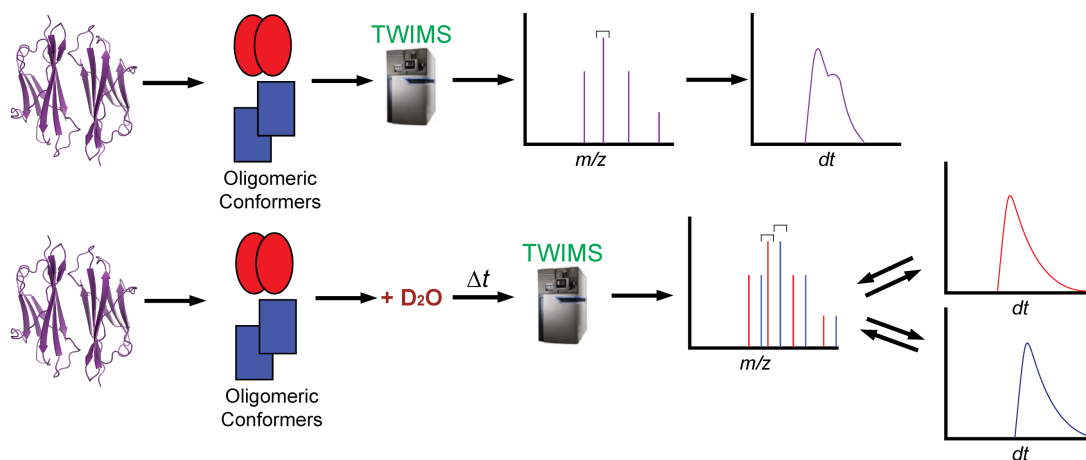
Figure 6.12: Generalized schematic of a HDX-enhanced IM experiment for oligomeric conformers.

Hydrogen-deuterium exchange (HDX) is an attractive candidate for enhancing IM due to its widespread use in probing protein structure and dynamics [25–28]. Deuterium is incorporated into the protein chemical structure at exchangeable hydrogens on a protein, most notably on residue sidechains, termini, and at backbone amides. Rates of exchange for HDX are structure sensitive in that a solvent-exposed hydrogen on the hydroxyl of tyrosine will exchange must faster than one buried in the hydrophobic core of the protein sequestered away from water. The same trend is observed for an exposed

backbone amide versus an amide engaged in a hydrogen bond in a secondary structure element such as a β-sheet, for example. HDX has also been extensively applied to studying amyloid systems such as amyloid β, tau, and α-synuclein to explain structural details of oligomerization processes [29–35]. Notably, one study was able to identify different populations of α-synuclein oligomers based on their incorporation of deuterium detected both globally and locally [29].

In the context of MS, HDX is most powerfully applied to studying protein structure by using a bottom-up (enzyme digested) approach to gain residue-level information about the incorporation of deuterium. However, there is also value in analyzing global exchange patterns of proteins by measuring the masses of intact protein ions [28,36–38]. Herein, we will apply global HDX patterns coupled with IM to be able to analyze and comment on protein structure both in solution phase and in the gas phase (Figure 6.2.2). Our experiments will likely not be able to capture kinetically capture the behavior of fast exchangers (i.e. sidechains, solvent-exposed backbone amides), the value
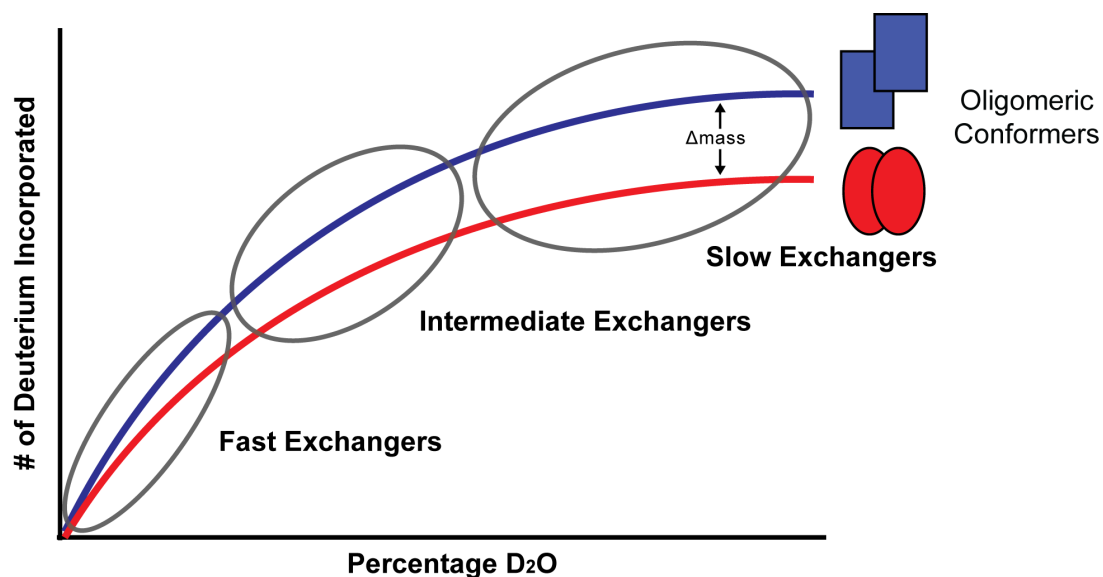
Figure 6.13 Global deuterium uptake as a function of co-incubated deuterium oxide percentage.

of the method will likely depend on intermediate and slow exchangers, like those involved in secondary structure elements and in the core of the conformers. The central hypothesis behind this work is that conformational isomers that exist in solution will incorporate deuterium differentially in a structure-dependent manner, and that detection of these conformers can be enhanced by resolving them in m/z space, structurally characterizing them using IM-MS, and using global exchange as a fingerprint.

It is also theoretically possible to monitor interconversion between different solution structures using HDX-IM-MS as well. If we consider a single mass spectral peak that gives rise to three different conformers in the presence of D_2O, extracting drift time information across sections of that mass spectral peak will reflect the different conformer populations (Figure 6.2.3, top). Extracting data from the leading edge of the mass spectral peak would reveal that if these structures are in slow equilibrium with each other, we would expect to see more abundant populations of the faster drifting (more compact) conformer, and minor amounts of the intermediate conformer (Figure 6.2.3, middle). However, if structures are in fast equilibrium, extracting the drift time information would reveal that the intermediate species is the predominant population within the peak and reflects the conversion occurring between the compact and expanded conformers (Figure 6.2.3, bottom).

Therefore, we propose that we can enhance the use of IM-MS by combining it with HDX, another popular technique that is often coupled with MS to study protein structure and dynamics. According the results described in chapter 3, we have found that β2m oligomers do exist with structural heterogeneities and we would like to investigate this further. While gas phase HDX coupled to ESI-IM-MS has been published previously

[39,40], the pairing of solution phase HDX and IM-MS would represent the first example of this type of study for any protein, not only for amyloid-forming proteins. Furthermore, this will also us to also further strengthen the link between solution phase and gas phase protein structures, which still remains an important caveat to consider when analyzing protein structure in the gas phase.

Before moving to the preliminary results, it is useful to understand how the data is practically handled and analyzed (Figure 6.2.4). The blue example spectra show a typical native spray experiment conducted under normal solution conditions (i.e. 100 mM
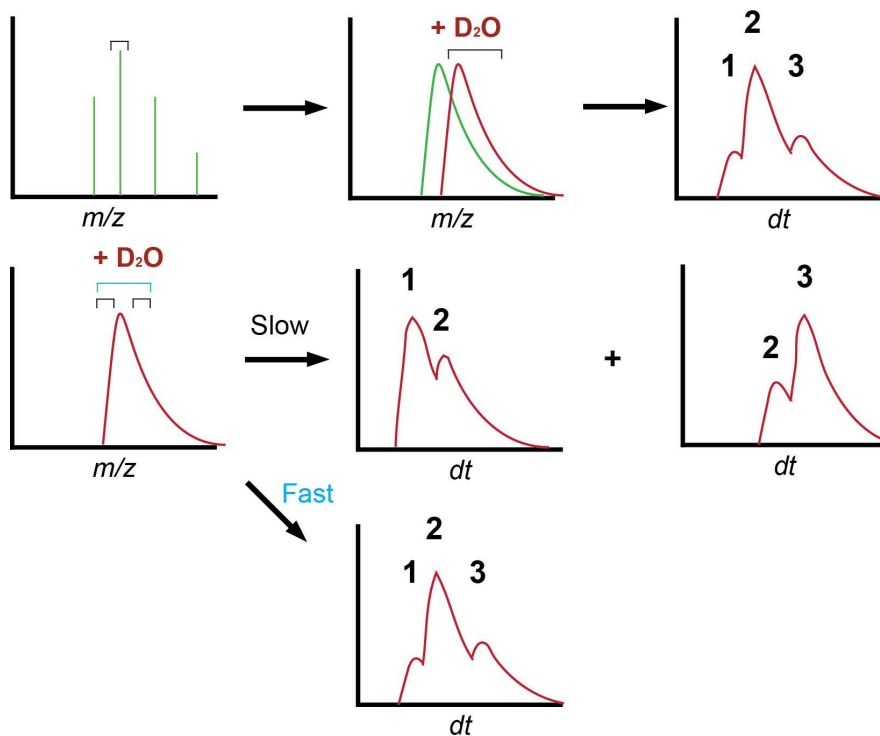
Figure 6.14: Interconversion of conformeric structures separated in *m/z* space while assessing conversion equilibrium in mobility (dt) space.

ammonium acetate). However, for HDX enhancement, solution components (i.e. the two proteins, ammonium acetate are mixed into a volume of deuterium oxide to yield a final desired percent (volume/volume). Following mixing, samples are immediately loaded into the ESI source, and analyzed. Note that the actual exchange process happens inside

the nanospray capillary that is loaded in the source of the instrument. Mass and ion mobility spectra are then acquired in a time dependent manner (e.g. intervals of 1 minute were typically feasible). This process was repeated over the course of the experiment (moving from the orange example spectra to the red spectra) which the total time varied from minutes to hours.

From Figure 6.2.4, we predict that the mass spectral peak will widen due to the differential uptake in deuterium of the conformeric species (in this case, three states). We expect that the extended conformer will migrate to the tail quicker and in higher abundances than the relatively more compact species. In order to analyze this data, we extract arrival time distribution from the mass spectral peaks at each timepoint, and then fit gaussian distributions to each mobility peak in order to calculate peak area, and thus abundance.
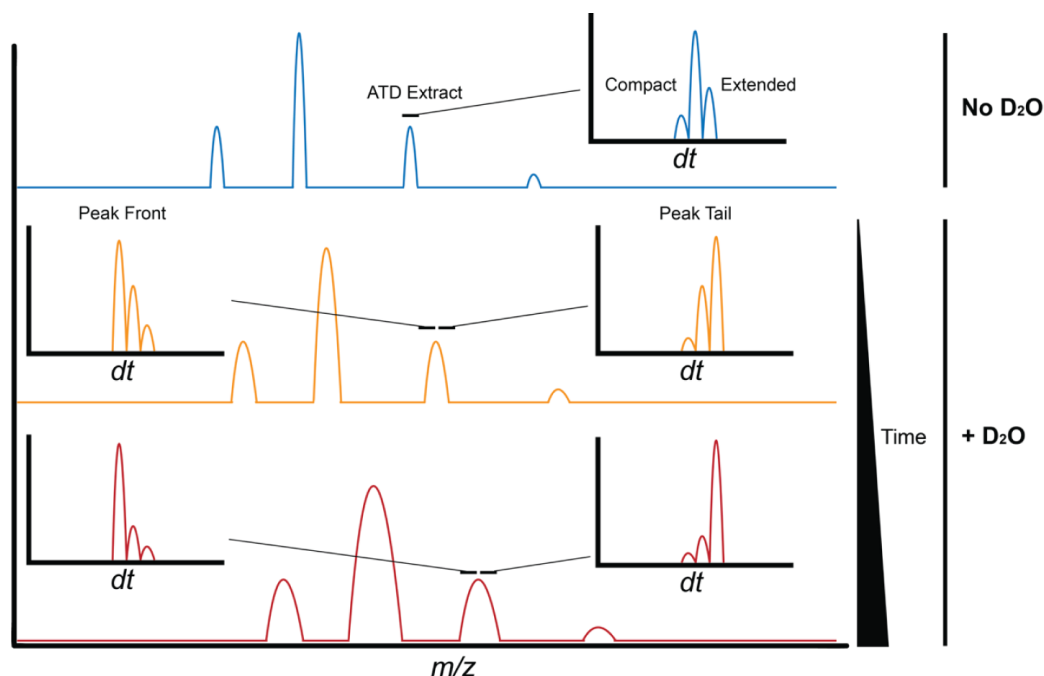
Figure 6.15: A typical HDX-IM-MS experiment time course. Blue is a no D_2O control, versus D_2O-containing samples in orange and red at two timepoints, with associated predicted extracted arrival time distributions.

6.1.2.2 Preliminary results

When beginning method development for HDX-enhanced IM, there were several potential avenues that were considered. One was to use the model monomeric proteins myoglobin and ubiquitin. Both proteins have long histories for use with mass spectrometry, and have been studied extensively especially from a structural point of view [22,23,41–44]. Most notably however, they both exhibit solution-dependent behavior that gives rise to multiple conformers during that have been detected using biophysical techniques like ESI-MS, IM-MS, fluorescence spectroscopy, and circular dichroism. These structural heterogeneities are exacerbated by acidifying the environment as well the presence of mild denaturants like methanol. For example, myoglobin is known to copopulate more compact states alongside expanded states in a single charge state in water:methanol mixtures [22].

Due to the fact that our end goal was to apply this technique to multimeric proteins, we eventually settled on models that were observed to have overlapping charge states during ESI-IM-MS analysis. This strategy also takes advantage of larger mass differences between the two molecules for easier demonstration of the proof of concept. We eventually settled on comparison of bovine serum albumin and enolase as our model proteins (Figure 6.2.5). Although the molecular weights of each molecule are vastly different (enolase exists primarily as a dimer in solution, with each monomer weighing roughly 46 kD), the CCS values of these two molecules are very similar (roughly 5%). This similarity is largely attributed to the large burial of surface area at the interface of the two enolase monomers. We predicted that the similarity in CCS would yield charge

state distributions at similar *m/z* values, due to the observed relationship between protein surface area and proton charging during positive mode ESI [45].

From a method development prospective, we had several parameters to consider for optimization. The first was the deuterium oxide percentage to use.

Bovine Serum Albumin (PDB ID: 4F5S)   Enolase (PDB ID: 1P43)

MW: ~66 kD
CCS ($Å^2$): 4490 (measured)
Theo. ΔMass: 1080 Da

MW: ~93 kD
CCS ($Å^2$): 4283 (calculated)
Theo. ΔMass: 1484 Da
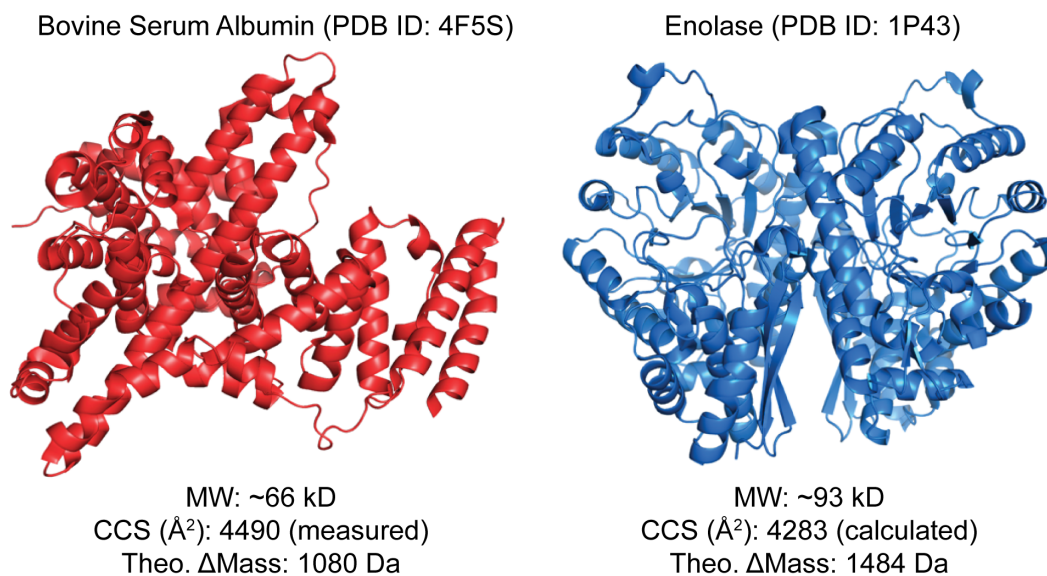
Figure 6.16: Example crystal structures of BSA and Enolase, with CCS values and total number of exchangeable sites.

One of our early concerns was D_2O suppressing ion signals during ESI. However, we found that using D_2O concentrations up to and including 95% did not reduce ion signal to an unusable degree. For experimental purposes, we aimed to use as high of a D_2O percentage as possible, as this would yield the greatest mass difference between structures (for a given kinetic timepoint).

The total exchange time was also a concern. There is pre-analysis time that is not captured on the preliminary data shown below. In these experiments, D_2O is the last component of the solution added prior to analysis. Following this addition, the samples are pipette mixed, loaded into nanospray capillaries, and then the capillary tips are then

trimmed to open an orifice. The trimmed capillary is then loaded into the instrument, the capillary voltage is applied, and then the source is physically adjusted relative to the instrument orifice to begins analysis. This entire process, from mixing to the beginning of the first acquisition timepoint takes anywhere from 1 to 5 minutes typically, where exchange is happening, but is not being detected or accounted for. Tip to tip variability is also an issue (yielding different spectral resolutions/quality) and capillary clogging at later timepoints can effectively ruin a kinetic experiment. Gas phase back exchange of deuterated protein ions is also a concern, due to water vapor present ambiently in the source, as well as the supplied gases further on in the instrument.

Experimentally, our expectation about the charge state overlap proved to be true (Figure 6.2.6). Proteins that were analyzed individually with ESI-IM-MS for BSA (red) and Enolase (blue), yielded charge state distributions centered around $\sim m/z$ 4500. Also note the presence of a bimodal charge state distribution in the enolase spectra, which may indicate conformational heterogeneity. The peaks observed at lower m/z values corresponded to enolase monomers. When mixed together in a 1:1 equimolar ratio, a complex spectrum is produced (purple), an important mass spectral overlap occurs at $\sim$ m/z 4500, which corresponds to BSA[15+] and Enolase[21+] ions. Instrument parameters used in this experiment are comparable to prior native spray experiments. Finally, extraction of the arrival distributions of both the BSA[15+] and Enolase[21+] ions revealed reasonable resolution between the two species, but were not quite baseline resolved. This allowed for less ambiguous data analysis (i.e. gaussian fitting). Note that enolase drifts faster than BSA despite similar CCS values, likely due to the TWIMS field effect on the extra charges of the 21+ ion.
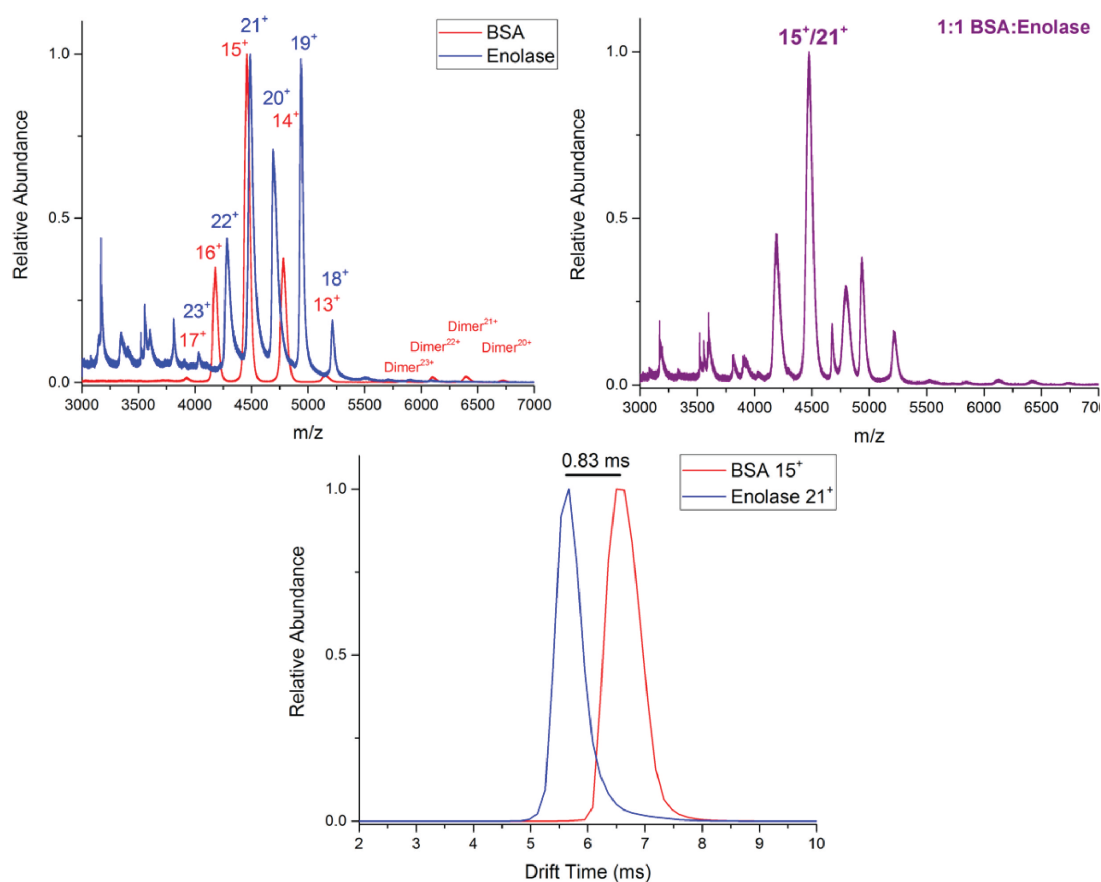
Figure 6.17: Representative mass spectra of BSA (red) and Enolase (blue) analyzed separately, and when combined in solution (purple). Extracted arrival time distributions for the overlapping mass spectral peak for each protein are shown on the bottom panel.

While we conducted HDX-IM-MS experiments at different D_2O concentrations and for different lengths of time, a representative experiment containing 85% D_2O for 10 minutes is shown in the left panel Figure 6.2.7. The inset panel shows an example gaussian fitting of the arrival time distributions that was used to generate the peak area values for the y-axis. The righthand panel is an identical control experiment but the electrospray solution contained no D_2O (i.e. was solely composed of 100 mM ammonium acetate). The instrument parameters were also identical. It takes approximately 6 minutes of exchange time to begin to measure a significant difference between the two species.
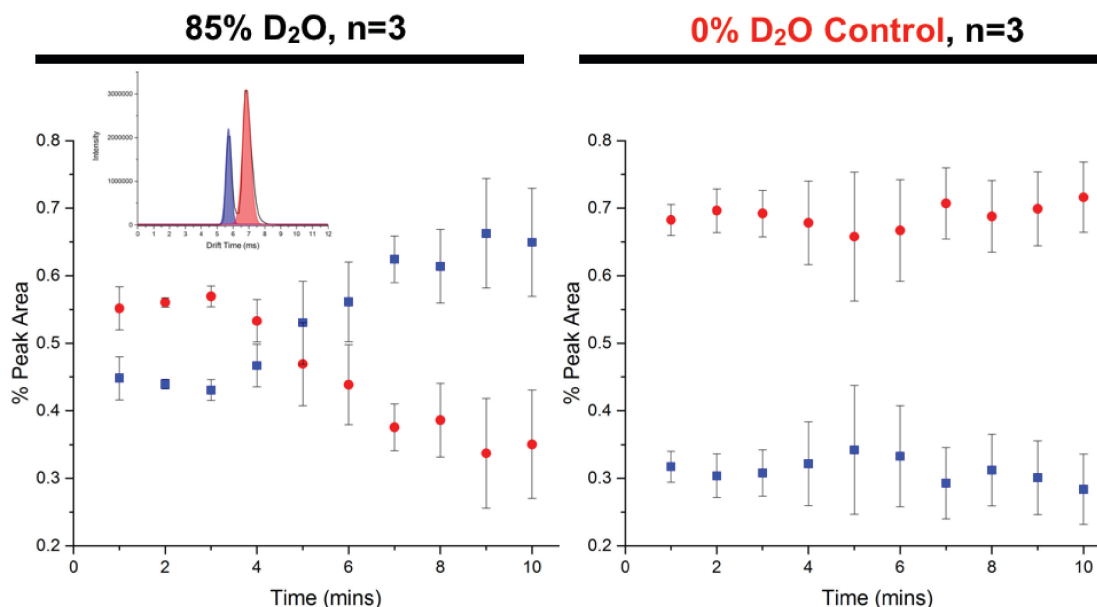
Figure 6.18: HDX-enhanced IM-MS for a mixed sample of BSA and Enolase while monitoring the BSA^{15+}/Enolase^{21+} charge state overlap.

This does not imply that exchange is not taking place, but it rather represents the limitation of resolution of using broad native mass spectral peaks to detect the mass difference. For example, the in order to shift the peak position 1 *m/z* larger, we must incorporate 15 deuteriums for BSA or 21 deuteriums for Enolase (due to the charge state). The 15+/21+ charge state in and of itself is approximately 190 *m/z* wide at 1 minute into an 85% D2O experiment, and thus it requires a substantial shift to begin detecting a difference. The control peaks, as expected, do not change over the course of the experiment. The global mass increase of the two proteins during the course of the experiment, calculated by averaging the mass of all charge states at each time point, is shown in Figure 6.2.8. It is important to note the dimensions of the y-axis, as the majority of the exchangeable sites on both proteins has already occurred by the time the samples are loaded and begun to be analyzed after the first minute.
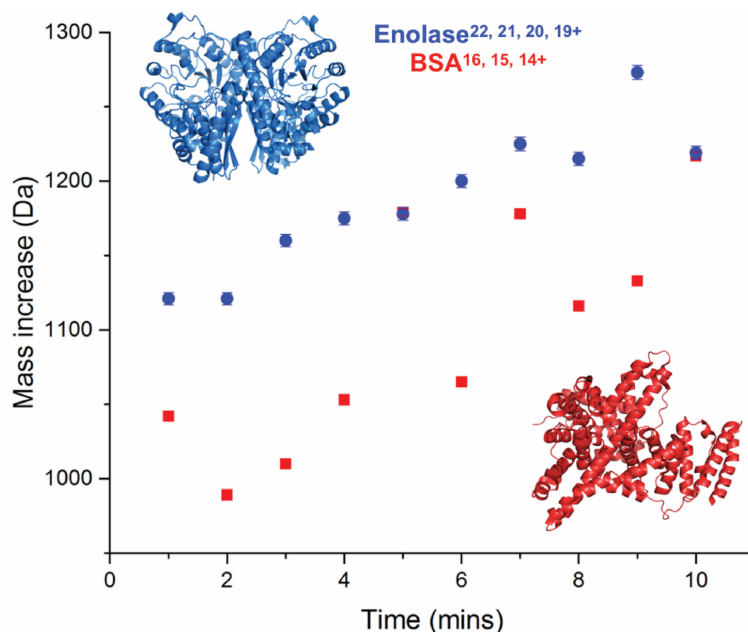
Figure 6.19: Global mass increase for BSA and Enolase during HDX-enhanced IM-MS experiment with 85% D_2O.

Overall, these preliminary results proved promising, but difficult to reproduce on multiple days. HDX is somewhat notorious for issues with reproducibility, especially for small changes in pH, time, age of deuterium oxide stock, and temperature, not to mention accounting for back exchange [46–48]. We contended with some of the practical issues detailed earlier. Although we chose these model proteins based on a large difference in exchangeable sites, monomeric β2m only has 191 exchangeable sites which is considerably less than BSA or Enolase. For example, the most abundant β2m dimer charge state (9+), we would need to exchange 9 sites to shift the mass spectral peak 1 *m/z* higher.

As alluded to earlier, the relatively broad peaks of native spray spectra mean that choosing the appropriate peak extraction window is critical for data analysis. Selecting this extraction in the absence of other data is difficult, at best, and likely requires further experiments to fully characterize rates of exchangers on the species being tested. This is

feasible for model proteins such as BSA or Enolase, but significantly more difficult for oligomeric conformers of β2m. Prediction of these rates without empirical data are also not trivial [46], although computational simulation efforts have been reported [49–51].

6.1.3 Small molecule screening of Cu(II)-catalyzed amyloid inhibitors

Despite our success with characterizing small molecule-based strategies for amyloid inhibition, the molecules in this dissertation represent an incredibly small portion of chemical space. In order to gain a deeper understanding of effective chemistries that prevent amyloid formation, a broader exploration is necessary. There are a number of options available to us at UMass, including the Small Molecule Screening Facility (SMSF) at UMass Medical. The SMSF hosts several options, including libraries that range from 240-30,000 compounds.

In terms of deciding where to focus efforts on intervening for β2m amyloid formation, three main avenues, which are also general enough to work for other amyloid forming proteins [52–56]. The first avenue would be to search for candidates that bind to monomeric β2m and inhibits the formation of soluble oligomers. The second strategy would be to search for molecules that intervene by binding to oligomeric structures, and prevent higher order aggregation (e.g. by destabilizing structures, or blocking interfaces). The third strategy, and possibly the least likely to succeed, would be to search for molecules that are able to dissemble or dissolve the fibrils themselves. For β2m, we would propose that the most prudent and realistic strategy would be to search for molecules that are capable of binding β2m, and inhibit the formation of amyloid-competent dimers (whether that be by preventing the formation of a dimer in the first

place, or perturbing the dimer's structure such that it cannot form a competent higher order oligomer).

In designing a small molecule screen, it is critical to consider the design of the primary screening assay. For amyloid formation and protein aggregation, this is a challenging prospect, as these phenomena can complicate the interpretation of results when screening for non-aggregation related indications. There are a number of potential strategies for screening small molecule interactions with amyloid forming proteins that have been reported, which include fluorescence, nuclear magnetic resonance, atomic force microscopy, surface plasmon resonance, isothermal calorimetry, and antibody binding assays [56]. For β2m, using capillary electrophoresis has also been reported [57].

For the purposes of β2m, we would propose screening assay strategies that are similar to the methodologies reported by the Vendruscolo, Knowles, and Dobson labs [58]. While this work focuses on amyloid β inhibitors, both *in vitro* and *in vivo*, we would only be interested in *in vitro* experiments, to keep the scale realistic, as well as play to our lab's analytical chemistry strengths. More specifically, we propose that the primary screening assay would consist of a Thioflavin T (ThT) fluorescence kinetics experiment. The structure of ThT is shown in Figure 6.3.1. We propose that a specific primary assay, like ThT fluorescence, would be preferable to a more general technique like light scattering, as we know from this dissertation and other works that small molecules can often still create aggregates. These aggregates, while not amyloidogenic, still scatter light and thus will show up as false positives.

ThT has a long history of use to detect not only the presence of amyloid-like precursors, but also to study the kinetics of early oligomerization [59–61].When in the
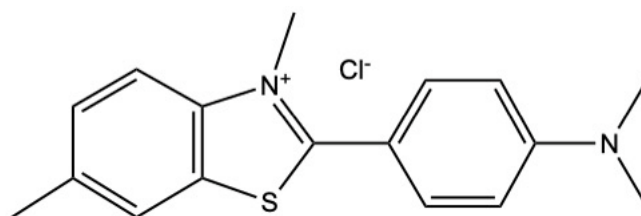
Figure 6.20: Structure of Thioflavin T.

presence of amyloid-like structures in an aqueous solution, ThT has a primary absorption

wavelength of 440 nm, and a large increase in quantum yield (intensity) at approximately

480 nm. Biophysically, the evidence and current understanding of ThT as a specific

probe for detecting amyloid structures is that it is capable of intercalating between the

characteristic intermolecular β-sheet structures [61]. This intercalation restricts ThT's

ability to rotate about the central bond present in the structure and lends it its unique

photophysical characteristics [61].

For the purposes of β2m, because the first emergence of intermolecular β-sheet

occurs with the formation of a dimer, we believe that the characteristic increase in

fluorescence intensity of ThT kinetically reflects the formation of dimers in solution. This

is also relatively time efficient, as we typically see ThT responses on the order of hours

with β2m and Cu(II) in our lab. Therefore, we expect that small molecules that can

effectively prevent dimer formation either by blocking interfacial regions, or by

disturbing the monomer structure will likely manifest in results similar to Figure 6.3.2.

Here, compared to the control, positive hits could potentially be identified by changes in

rate of formation or kinetic stability (molecule A), changes in rate as well as reduction in

abundance of oligomers at steady state (molecule B), or a complete inhibition of oligomer

formation (molecule C).
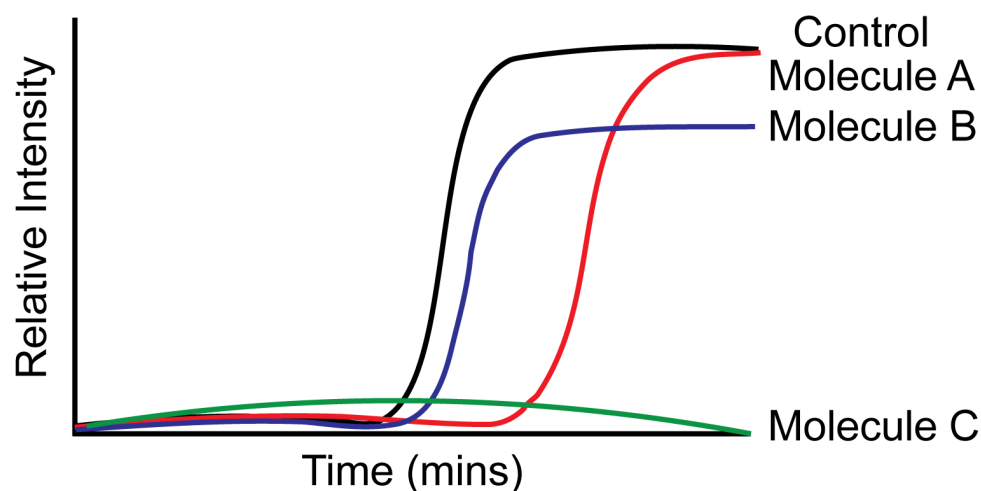
Figure 6.21: Example data for a Thioflavin T screening assay. Molecules A-C reflect hypothetical potential inhibitors that exhibit different inhibitory mechanisms.

For screening purposes, molecules with these positive attributes will be considered positive hits. As a control, it will be important to verify that the ThT response is specifically due to its interaction with the protein structure and not from interactions with the small molecule candidate in solution. Therefore, ThT fluorescence should also be measured in absence of protein, with just buffer components and candidate present. Interference with small molecule compounds has been observed before [62,63], and incidents like this could potentially generate false positives/negatives, or even prevent interpretation of the assay's data.

For this reason, it would be prudent to couple the fluorescence assay to another readout of aggregation. From a throughput perspective, light scattering (or turbidity) is easily adaptable, and has been utilized to measure protein aggregation [64], and even screen anti-amyloid molecules with β2m previously [63]. As described above, we know that small molecules can generate non-amyloid aggregates, which will also scatter light (and potentially generate false negatives). Thus, combining both assays will hopefully provide maximize the information output of a screen.

Through the work described in this dissertation, and with other members of the lab, we have developed a toolbox of assays and experiments that allow us to gain an insight into the effects of inhibitor molecules on amyloid formation. These types of experiments would be carried on a smaller pool of candidates that come out of a screen, as they are not feasible to do on a larger scale. Chiefly, electron microscopy should be the first priority in order to assess whether or not amyloid fibril structures are present in treated samples. Following the confirmation of no amyloid fibrils (whether there be no aggregates at all, or non-amyloid aggregates generated), characterization experiments to carry out would be similar to the techniques described in chapters 2 and 4, alongside complementary covalent labeling experiments to determine small molecule binding site information [65]. Furthermore, armed with our new knowledge of a heterogeneous tetramer system described in chapter 3, *in silico* docking could potentially be utilized to rationalize anti-amyloid activity.

6.2 References

[1] J.M. Wells, S.A. McLuckey, Collision-Induced Dissociation (CID) of Peptides and Proteins, in: Methods in Enzymology, Elsevier, 2005: pp. 148–185.

[2] S.A. McLuckey, M. Mentinova, Ion/Neutral, Ion/Electron, Ion/Photon, and Ion/Ion Interactions in Tandem Mass Spectrometry: Do We Need Them All? Are They Enough?, Journal of The American Society for Mass Spectrometry. 22 (2011) 3–12.

[3] J.L.P. Benesch, B.T. Ruotolo, D.A. Simmons, C.V. Robinson, Protein Complexes in the Gas Phase: Technology for Structural Genomics and Proteomics, Chemical Reviews. 107 (2007) 3544–3567.

[4] J.S. Cottrell, Protein identification using MS/MS data, Journal of Proteomics. 74 (2011) 1842–1851.

[5] B. Paizs, S. Suhai, Fragmentation pathways of protonated peptides, Mass Spectrometry Reviews. 24 (2005) 508–548.

[6] K.J. Light-Wahl, B.L. Schwartz, R.D. Smith, Observation of the Noncovalent Quaternary Associations of Proteins by Electrospray Ionization Mass Spectrometry, Journal of the American Chemical Society. 116 (1994) 5271–5278.

[7] B.L. Schwartz, J.E. Bruce, G.A. Anderson, S.A. Hofstadler, A.L. Rockwood, R.D. Smith, A. Chilkoti, P.S. Stayton, Dissociation of tetrameric ions of noncovalent streptavidin complexes formed by electrospray ionization, Journal of the American Society for Mass Spectrometry. 6 (1995) 459–465.

[8] J.C. Jurchen, E.R. Williams, Origin of Asymmetric Charge Partitioning in the Dissociation of Gas-Phase Protein Homodimers, Journal of the American Chemical Society. 125 (2003) 2817–2826.

[9] J.C. Jurchen, D.E. Garcia, E.R. Williams, Further studies on the origins of asymmetric charge partitioning in protein homodimers, Journal of the American Society for Mass Spectrometry. 15 (2004) 1408–1415.

[10] B.T. Ruotolo, Evidence for Macromolecular Protein Rings in the Absence of Bulk Water, Science. 310 (2005) 1658–1661.

[11] B.T. Ruotolo, S.-J. Hyung, P.M. Robinson, K. Giles, R.H. Bateman, C.V. Robinson, Ion Mobility–Mass Spectrometry Reveals Long-Lived, Unfolded Intermediates in the Dissociation of Protein Complexes, Angewandte Chemie International Edition. 46 (2007) 8001–8004.

[12] S. Mehmood, T.M. Allison, C.V. Robinson, Mass Spectrometry of Protein Complexes: From Origins to Applications, Annual Review of Physical Chemistry. 66 (2015) 453–474.

[13] J.D. Eschweiler, J.N. Rabuck-Gibbons, Y. Tian, B.T. Ruotolo, CIUSuite: A Quantitative Analysis Package for Collision Induced Unfolding Measurements of Gas-Phase Protein Ions, Analytical Chemistry. 87 (2015) 11516–11522.

[14] D.A. Polasky, S.M. Dixit, S.M. Fantin, B.T. Ruotolo, CIUSuite 2: Next-Generation Software for the Analysis of Gas-Phase Protein Unfolding Data, Analytical Chemistry. 91 (2019) 3147–3155.

[15] Y. Tian, L. Han, A.C. Buckner, B.T. Ruotolo, Collision Induced Unfolding of Intact Antibodies: Rapid Characterization of Disulfide Bonding Patterns, Glycosylation, and Structures, Analytical Chemistry. 87 (2015) 11509–11515.

[16] S.-J. Hyung, C.V. Robinson, B.T. Ruotolo, Gas-Phase Unfolding and Disassembly Reveals Stability Differences in Ligand-Bound Multiprotein Complexes, Chemistry & Biology. 16 (2009) 382–390.

[17] S. Niu, B.T. Ruotolo, Collisional unfolding of multiprotein complexes reveals cooperative stabilization upon ligand binding: Collisional Unfolding of Multiprotein Complexes, Protein Science. 24 (2015) 1272–1281.

[18] J.D. Eschweiler, R.M. Martini, B.T. Ruotolo, Chemical Probes and Engineered Constructs Reveal a Detailed Unfolding Mechanism for a Solvent-Free Multidomain Protein, Journal of the American Chemical Society. 139 (2017) 534–540.

[19] Y. Zhong, L. Han, B.T. Ruotolo, Collisional and Coulombic Unfolding of Gas-Phase Proteins: High Correlation to Their Domain Structures in Solution, Angewandte Chemie International Edition. 53 (2014) 9209–9212.

[20] S.I. Merenbloom, T.G. Flick, E.R. Williams, How Hot are Your Ions in TWAVE Ion Mobility Spectrometry?, Journal of The American Society for Mass Spectrometry. 23 (2012) 553–562.

[21] C.A. Scarff, V.J. Patel, K. Thalassinos, J.H. Scrivens, Probing hemoglobin structure by means of traveling-wave ion mobility mass spectrometry, Journal of the American Society for Mass Spectrometry. 20 (2009) 625–631.

[22] J. Seo, W. Hoffmann, S. Warnke, M.T. Bowers, K. Pagel, G. von Helden, Retention of Native Protein Structures in the Absence of Solvent: A Coupled Ion Mobility and Spectroscopic Study, Angewandte Chemie International Edition. 55 (2016) 14173–14176.

[23] Y. Sun, S. Vahidi, M.A. Sowole, L. Konermann, Protein Structural Studies by Traveling Wave Ion Mobility Spectrometry: A Critical Look at Electrospray Sources and Calibration Issues, Journal of The American Society for Mass Spectrometry. 27 (2016) 31–40.

[24] M.M. Maurer, G.C. Donohoe, S.J. Valentine, Advances in ion mobility-mass spectrometry instrumentation and techniques for characterizing structural heterogeneity, The Analyst. 140 (2015) 6782–6798.

[25] S.S. Jaswal, Biological insights from hydrogen exchange mass spectrometry, Biochimica et Biophysica Acta (BBA) - Proteins and Proteomics. 1834 (2013) 1188–1201.

[26] I.A. Kaltashov, C.E. Bobst, R.R. Abzalimov, Mass spectrometry-based methods to study protein architecture and dynamics: MS-Based Methods to Study Protein Architecture and Dynamics, Protein Science. 22 (2013) 530–544.

[27] L. Konermann, J. Pan, Y.-H. Liu, Hydrogen exchange mass spectrometry for studying protein structure and dynamics, Chem. Soc. Rev. 40 (2011) 1224–1234.

[28] T.E. Wales, J.R. Engen, Hydrogen exchange mass spectrometry for the analysis of protein dynamics, Mass Spectrometry Reviews. 25 (2006) 158–170.

[29] W. Paslawski, S. Mysling, K. Thomsen, T.J.D. Jørgensen, D.E. Otzen, Co-existence of Two Different α-Synuclein Oligomers with Different Core Structures Determined by Hydrogen/Deuterium Exchange Mass Spectrometry, Angewandte Chemie International Edition. 53 (2014) 7560–7563.

[30] C. Scavenius, S. Ghodke, D.E. Otzen, J.J. Enghild, Hydrogen exchange mass spectrometry as an analytical tool for the analysis of amyloid fibrillogenesis, International Journal of Mass Spectrometry. 302 (2011) 167–173.

[31] I. Kheterpal, K.D. Cook, R. Wetzel, Hydrogen/Deuterium Exchange Mass Spectrometry Analysis of Protein Aggregates, in: Methods in Enzymology, Elsevier, 2006: pp. 140–166.

[32] I. Kheterpal, R. Wetzel, Hydrogen/Deuterium Exchange Mass SpectrometryA Window into Amyloid Structure, Accounts of Chemical Research. 39 (2006) 584–593.

[33] S. Zhu, A. Shala, A. Bezginov, A. Sljoka, G. Audette, D.J. Wilson, Hyperphosphorylation of Intrinsically Disordered Tau Protein Induces an Amyloidogenic Shift in Its Conformational Ensemble, PLOS ONE. 10 (2015) e0120416.

[34] B. Serra-Vidal, L. Pujadas, D. Rossi, E. Soriano, S. Madurga, N. Carulla, Hydrogen/Deuterium Exchange-Protected Oligomers Populated during Aβ Fibril Formation Correlate with Neuronal Cell Death, ACS Chemical Biology. 9 (2014) 2678–2685.

[35] Y. Zhang, D.L. Rempel, J. Zhang, A.K. Sharma, L.M. Mirica, M.L. Gross, Pulsed hydrogen–deuterium exchange mass spectrometry probes conformational changes in amyloid beta (Aβ) peptide aggregation, Proceedings of the National Academy of Sciences. 110 (2013) 14604–14609.

[36] B. Zhou, Z.-Y. Zhang, Application of hydrogen/deuterium exchange mass spectrometry to study protein tyrosine phosphatase dynamics, ligand binding, and substrate specificity, Methods. 42 (2007) 227–233.

[37] K.D. Rand, M. Zehl, T.J.D. Jørgensen, Measuring the Hydrogen/Deuterium Exchange of Proteins at High Spatial Resolution by Mass Spectrometry: Overcoming Gas-Phase Hydrogen/Deuterium Scrambling, Accounts of Chemical Research. 47 (2014) 3018–3027.

[38] A.A. Makarov, R. Helmy, Combining size-exclusion chromatography with differential hydrogen–deuterium exchange to study protein conformational changes, Journal of Chromatography A. 1431 (2016) 224–230.

[39] K.D. Rand, S.D. Pringle, J.P. Murphy, K.E. Fadgen, J. Brown, J.R. Engen, Gas-Phase Hydrogen/Deuterium Exchange in a Traveling Wave Ion Guide for the Examination of Protein Conformations, Analytical Chemistry. 81 (2009) 10019–10028.

[40] U.H. Mistarz, S.A. Chandler, J.M. Brown, J.L.P. Benesch, K.D. Rand, Probing the Dissociation of Protein Complexes by Means of Gas-Phase H/D Exchange Mass Spectrometry, Journal of The American Society for Mass Spectrometry. 30 (2019) 45–57.

[41] S. Vahidi, B.B. Stocks, L. Konermann, Partially Disordered Proteins Studied by Ion Mobility-Mass Spectrometry: Implications for the Preservation of Solution Phase Structure in the Gas Phase, Analytical Chemistry. 85 (2013) 10471–10478.

[42] X. Lin, W. Zhao, X. Wang, Characterization of conformational changes and noncovalent complexes of myoglobin by electrospray ionization mass spectrometry, circular dichroism and fluorescence spectroscopy, Journal of Mass Spectrometry. (2010) 618-626.

[43] K.R. Babu, D.J. Douglas, Methanol-Induced Conformations of Myoglobin at pH 4.0, Biochemistry. 39 (2000) 14702–14710.

[44] F. Wang, X. Tang, Conformational Heterogeneity and Stability of Apomyoglobin Studied by Hydrogen/Deuterium Exchange and Electrospray Ionization Mass Spectrometry, Biochemistry. 35 (1996) 4069–4078.

[45] I.A. Kaltashov, A. Mohimen, Estimates of Protein Surface Areas in Solution by Electrospray Ionization Mass Spectrometry, Analytical Chemistry. 77 (2005) 5370–7379.

[46] J.W. Hudgens, E.S. Gallagher, I. Karageorgos, K.W. Anderson, J.J. Filliben, R.Y.-C. Huang, G. Chen, G.M. Bou-Assaf, A. Espada, M.J. Chalmers, E. Harguindey, H.-M. Zhang, B.T. Walters, J. Zhang, J.D. Venable, C. Steckler, I. Park, A. Brock, X. Lu, R.K. Pandey, A. Chandramohan, G.S. Anand, S.N. Nirudodhi, J.B. Sperry, J.C. Rouse, J.A. Carroll, K.D. Rand, U. Leurs, D.D. Weis, M.A. Al-Naqshabandi, T.S. Hageman, D. Deredge, P.L. Wintrode, M. Papanastasiou, J.D. Lambris, S. Li, S. Urata, Interlaboratory Comparison of Hydrogen-Deuterium Exchange Mass Spectrometry Measurements of the Fab fragment of NISTmAb, Analytical Chemistry. (2019) 7336-7345.

[47] J.A. Moroco, J.R. Engen, Replication in bioanalytical studies with HDX MS: aim as high as possible, Bioanalysis. 7 (2015) 1065–1067.

[48] J.R. Engen, T.E. Wales, Analytical Aspects of Hydrogen Exchange Mass Spectrometry, Annual Review of Analytical Chemistry. 8 (2015) 127–148.

[49] H. Mohammadiarani, V.S. Shaw, R.R. Neubig, H. Vashisth, Interpreting Hydrogen–Deuterium Exchange Events in Proteins Using Atomistic Simulations: Case Studies on Regulators of G-Protein Signaling Proteins, The Journal of Physical Chemistry B. 122 (2018) 9314–9323.

[50] R.G. McAllister, L. Konermann, Challenges in the Interpretation of Protein H/D Exchange Data: A Molecular Dynamics Simulation Perspective, Biochemistry. 54 (2015) 2683–2692.

[51] A.A. Petruk, L.A. Defelipe, R.G. Rodríguez Limardo, H. Bucci, M.A. Marti, A.G. Turjanski, Molecular Dynamics Simulations Provide Atomistic Insight into Hydrogen Exchange Mass Spectrometry Experiments, Journal of Chemical Theory and Computation. 9 (2013) 658–669.

[52] A.J. Doig, P. Derreumaux, Inhibition of protein aggregation and amyloid formation by small molecules, Current Opinion in Structural Biology. 30 (2015) 50–56.

[53] L.M. Young, J.C. Saunders, R.A. Mahood, C.H. Revill, R.J. Foster, L.-H. Tu, D.P. Raleigh, S.E. Radford, A.E. Ashcroft, Screening and classifying small-molecule inhibitors of amyloid formation using ion mobility spectrometry–mass spectrometry, Nature Chemistry. 7 (2015) 73–81.

[54] J.A. Hebda, M. Magzoub, A.D. Miranker, Small molecule screening in context: Lipid-catalyzed amyloid formation: Small Molecule Screening in Context, Protein Science. 23 (2014) 1341–1348.

[55] J. Chen, A.H. Armstrong, A.N. Koehler, M.H. Hecht, Small Molecule Microarrays Enable the Discovery of Compounds That Bind the Alzheimer's Aβ Peptide and Reduce its Cytotoxicity, Journal of the American Chemical Society. 132 (2010) 17015–17022.

[56] A.K. Buell, E.K. Esbjörner, P.J. Riss, D.A. White, F.I. Aigbirhio, G. Toth, M.E. Welland, C.M. Dobson, T.P.J. Knowles, Probing small molecule binding to amyloid fibrils, Physical Chemistry Chemical Physics. 13 (2011) 20044.

[57] L. Regazzoni, R. Colombo, L. Bertoletti, G. Vistoli, G. Aldini, M. Serra, M. Carini, R.M. Facino, S. Giorgetti, M. Stoppini, G. Caccialanza, E. De Lorenzi, Screening of fibrillogenesis inhibitors of β2-microglobulin: Integrated strategies by mass spectrometry capillary electrophoresis and in silico simulations, Analytica Chimica Acta. 685 (2011) 153–161.

[58] J. Habchi, S. Chia, R. Limbocker, B. Mannini, M. Ahn, M. Perni, O. Hansson, P. Arosio, J.R. Kumita, P.K. Challa, S.I.A. Cohen, S. Linse, C.M. Dobson, T.P.J. Knowles, M. Vendruscolo, Systematic development of small molecules to inhibit specific microscopic steps of Aβ42 aggregation in Alzheimer's disease, Proceedings of the National Academy of Sciences. 114 (2017) E200–E208.

[59] M.K. Gade, L.M. Blancas-Mejia, B. Weber, J. Buchner, M. Ramirez-Alvarado, H. Naiki, D. Otzen, ThT 101: a primer on the use of thioflavin T to investigate amyloid formation, Amyloid. 24 (2017) 1–16.

[60] A.I. Sulatskaya, A.V. Lavysh, A.A. Maskevich, I.M. Kuznetsova, K.K. Turoverov, Thioflavin T fluoresces as excimer in highly concentrated aqueous solutions and as monomer being incorporated in amyloid fibrils, Scientific Reports. 7 (2017) 2146.

[61] L.S. Wolfe, M.F. Calabrese, A. Nath, D.V. Blaho, A.D. Miranker, Y. Xiong, Protein-induced photophysical changes to the amyloid indicator dye thioflavin T, Proceedings of the National Academy of Sciences. 107 (2010) 16863–16868.

[62] F. Meng, P. Marek, K.J. Potter, C.B. Verchere, D.P. Raleigh, Rifampicin Does Not Prevent Amyloid Fibril Formation by Human Islet Amyloid Polypeptide but Does Inhibit Fibril Thioflavin-T Interactions: Implications for Mechanistic Studies of β-Cell Death, Biochemistry. 47 (2008) 6016–6024.

[63] L.A. Woods, G.W. Platt, A.L. Hellewell, E.W. Hewitt, S.W. Homans, A.E. Ashcroft, S.E. Radford, Ligand binding to distinct states diverts aggregation of an amyloid-forming protein, Nature Chemical Biology. 7 (2011) 730–739.

[64] R. Zhao, M. So, H. Maat, N.J. Ray, F. Arisaka, Y. Goto, J.A. Carver, D. Hall, Measurement of amyloid formation by turbidity assay—seeing through the cloud, Biophysical Reviews. 8 (2016) 445–471.

[65] T. Liu, T.M. Marcinko, P.A. Kiefer, R.W. Vachet, Using Covalent Labeling and Mass Spectrometry To Study Protein Binding Sites of Amyloid Inhibiting Molecules, Analytical Chemistry. 89 (2017) 11583–11591.

APPENDIX

SUPPLEMENTAL COMPUTATIONAL METHOD INFORMATION FOR

CHAPTER 3

Electronic Structure Calculation

To accurately predict the impact of the copper binding in different β2m oligomer

states, an advanced description of the β2m copper binding site is crucial to quantitatively

reproduce experiment observables. Due to the covalent nature of the interaction between a

copper ion and surrounding nitrogens participating in ion coordination, imposing pseudo-

bonds to restrain the geometry of the binding site is therefore needed. First, the starting

configuration of the β2m copper binding site was extracted from a crystal hexamer

structure (PDB: 3CIQ). Specifically, the initial structure containing a copper ion and four

surrounding residues (I1, Q2, H31, and D59) was energy minimized at the density

functional theory (DFT) level (B3LYP/LANL2DZ/6-31G(d)). The side chains of I1 and

Q2 were removed in electronic structural calculations since they do not directly

participate in copper binding. The partial charges of three surrounding nitrogens and the

copper ion were estimated by the Mulliken population analysis. All the electronic structure

calculations were performed using the ORCA 4.0 package [1].

The optimized structure is shown in Figure S1. Previous experimental studies

suggested that only the backbone nitrogen atoms of I1/Q2 and the side chain nitrogen of H31

participate in the copper coordination [2,3]. We then performed the bond scanning

calculations of three pseudo-bonds at the DFT level (Figure A1.1), in order to describe them

classically using harmonic potentials. The equilibrium bond lengths and the force constants

were summarized in Table A.1. The non-bonded Lennard-Jones parameters of copper were
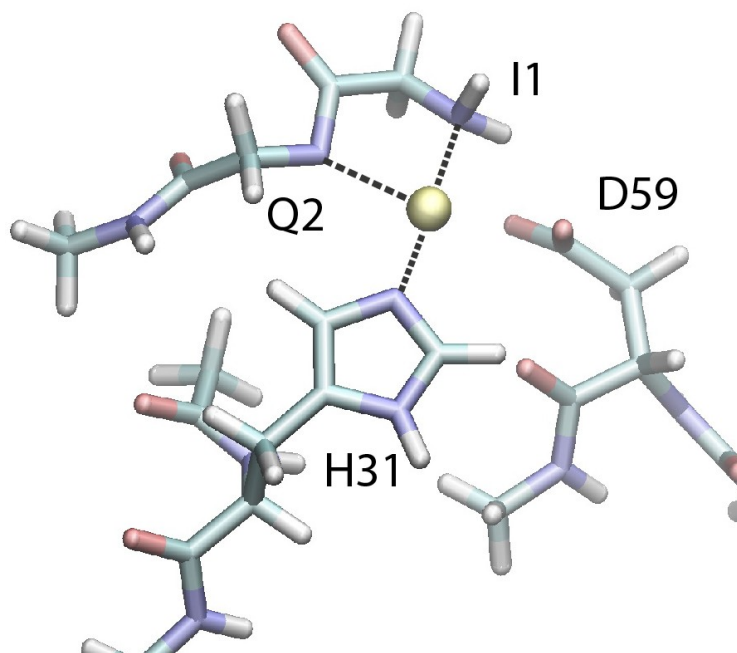
Figure A.1: The optimized geometry of the copper binding site in wild type β2m.

taken from a previous simulation study [4], and the Mulliken charges of the copper ion were summarized in Table A.2. Those bonded and non-bonded parameters that classically describe how the copper ion interacts with surrounding β2m residues were then used for molecular dynamics (MD) simulations described below.

Bond	Length (Å)	Force constant (kJ mol^{-1} Å^{-2})
N (I1) - Cu^{2+}	2.01	948.47
N (Q1) - Cu^{2+}	1.96	853.12
N (H31) - Cu^{2+}	1.94	1026.24

Table A.1: Summary of the bonded parameters for treating the β2m copper binding site.

Atom	σ (Å)	s (kJ mol^{-1})	charge (a.u)
N (I1)	CHARMM36m	CHARMM36m	0.34
N (Q2)	CHARMM36m	CHARMM36m	-0.62
N (H31)	CHARMM36m	CHARMM36m	-0.70
Cu^{2+}	2.63	0.134	0.40

Table A.2: Summary of the non-bonded parameters for treating the β2m copper binding site.

Molecular Dynamics simulation

Classical MD simulations using atomistic models were performed using the GROMACS 2018 package [5]. The CHARMM36m [6] force field and the TIP3P model [7] were chosen for modeling human β 2-microglobulin (β2m) and water molecules. For the monomer system, a β2m monomer was place in the center of a 6.0 nm cubic box and filled with ∼ 8,000 water molecules. For the dimer systems, two β2m monomers with the starting configurations as head-to-head and side-to-side arrangement were placed in the center of a 7.0 nm cubic box and filled with ∼ 10,000 water molecules. For the tetramer systems, four β2m monomers with the starting configurations as T1, T2, T3 and T4 arrangement were placed in the center of a 13 nm cubic box and filled with ∼ 80,000 water molecules. The protonation states of the titratable amino acid side chains and N-/C-terminus of β2m were chosen to reproduce the physiological condition at pH=7.

The initial configuration of the monomer system was extracted from the NMR deter- mined structure (PDB: 1JNJ). The initial configurations of the dimer systems was con- structed in the following steps. For constructing the head-to-head and side-to-side dimer systems, two protein chains (A/B and A/F) were extracted from the crystal structure of the β2m H13F mutant (PDB: 3CIQ), respectively. The residue F13 was transformed back to histidine to model the wide-type β2m. Then, after removing the first residue M0, for modeling the Cu(II)-bound states, the Cu(II) binding site was energy minimized using the bonded parameters derived from previous electronic structure calculations.

For modeling the Cu(II)-free states, the first residue Met and copper ions were simply removed. For con- structing the tetramer systems, the initial configurations of T1 and T2 were extracted from the crystal structure of the β2m H13F mutant (chain A/B/C/F). For T3 and T4, the initial structures were derived from the docking experiment which was described in the previous Method section. For modeling Cu(II)-bound/free

states, the same procedures were applied as for the dimer systems. For each system, after steepest descent energy minimization, an equilibration simulation was run after solvation at a constant temperature (300 K) and pressure coupled with the Berendsen method [8] for 10 ns. Then 10 ns NVT simulation was performed using velocity rescaling method [9] with an external heat bath at 300 K (coupling time 1 ps). After that, the system was assumed to be equilibrated.

During the production runs, the LINCS algorithm [10] was used to constrain bond lengths and angles of the protein, allowing an integration time step of 2 fs. Long-range electrostatic interactions beyond a cutoff of 1.2 nm were calculated by the Particle-Mesh-Ewald (PME) method [11] with a grid spacing of 0.12 nm. Short-range repulsive and attractive dispersion interactions were described with the Lennard-Jones potentials, using 1.2 nm for the cutoff length. The temperature of each replica was then controlled using the velocity rescaling method [9] with an external heath bath at target temperature with the coupling time of 1 ps. The volume of the simulation boxes was kept constant. The total production run for each system was 1 μs. All the simulations performed in this study are summarized in Table A.3.

Oligomer state	Cu(II) - state	number of runs	time/run (μs)	stability
Monomer	free	1	1	N/A
Dimer (head-to-head)	free	2	1	stable
Dimer (head-to-head)	bound	2	1	stable
Dimer (side-to-side)	free	2	1	dissociated
Dimer (side-to-side)	bound	2	1	stable
Tetramer (T1)	bound	1	1	stable
Tetramer (T2)	free	1	1	stable
Tetramer (T3)	free	1	1	stable
Tetramer (T4)	free	1	1	stable

Table A.3: Summary of the simulations performed in Chapter 3.

References

[1] F. Neese, Software update: the ORCA program system, version 4.0: Software update, Wiley Interdisciplinary Reviews: Computational Molecular Science. 8 (2018) e1327.

[2] R. Srikanth, V.L. Mendoza, J.D. Bridgewater, G. Zhang, R.W. Vachet, Copper Binding to β-2-Microglobulin and Its Pre-Amyloid Oligomers, Biochemistry. 48 (2009) 9871–9881.

[3] J. Dong, C.A. Joseph, N.B. Borotto, V.L. Gill, M.J. Maroney, R.W. Vachet, Unique Effect of Cu(II) in the Metal-Induced Amyloid Formation of β-2-Microglobulin, Biochemistry. 53 (2014) 1263–1274.

[4] V. Moses, Ö. Tastan Bishop, K.A. Lobb, The evaluation and validation of copper (II) force field parameters of the Auxiliary Activity family 9 enzymes, Chemical Physics Letters. 678 (2017) 91–97.

[5] M.J. Abraham, T. Murtola, R. Schulz, S. Páll, J.C. Smith, B. Hess, E. Lindahl, GROMACS: High performance molecular simulations through multi-level parallelism from laptops to supercomputers, SoftwareX. 1–2 (2015) 19–25.

[6] J. Huang, S. Rauscher, G. Nawrocki, T. Ran, M. Feig, B.L. de Groot, H. Grubmüller, A.D. MacKerell, CHARMM36m: an improved force field for folded and intrinsically disordered proteins, Nature Methods. 14 (2017) 71–73.

[7] W.L. Jorgensen, J. Chandrasekhar, J.D. Madura, R.W. Impey, M.L. Klein, Comparison of simple potential functions for simulating liquid water, The Journal of Chemical Physics. 79 (1983) 926–935.

[8] H.J.C. Berendsen, J.P.M. Postma, W.F. van Gunsteren, A. DiNola, J.R. Haak, Molecular dynamics with coupling to an external bath, The Journal of Chemical Physics. 81 (1984) 3684–3690.

[9] G. Bussi, D. Donadio, M. Parrinello, Canonical sampling through velocity rescaling, The Journal of Chemical Physics. 126 (2007) 014101.

[10] B. Hess, H. Bekker, H.J.C. Berendsen, J.G.E.M. Fraaije, LINCS: A linear constraint solver for molecular simulations, Journal of Computational Chemistry. 18 (1997) 1463–1472.

[11] T. Darden, D. York, L. Pedersen, Particle mesh Ewald: An $N \cdot \log(N)$ method for Ewald sums in large systems, The Journal of Chemical Physics. 98 (1993) 10089–10092.

BIBLIOGRAPHY

M.J. Abraham, T. Murtola, R. Schulz, S. Páll, J.C. Smith, B. Hess, E. Lindahl, GROMACS: High performance molecular simulations through multi-level parallelism from laptops to supercomputers, SoftwareX. 1–2 (2015) 19–25.

Alzheimer's and Dementia: Facts and Figures, (n.d.). https://www.alz.org/alzheimers-dementia/facts-figures.

A.E. Ashcroft, Mass spectrometry and the amyloid problem—How far can we go in the gas phase?, Journal of the American Society for Mass Spectrometry. 21 (2010) 1087–1096.

K. Antwi, M. Mahar, R. Srikanth, M.R. Olbris, J.F. Tyson, R.W. Vachet, Cu(II) organizes β-2-microglobulin oligomers but is released upon amyloid formation, Protein Science. 17 (2008) 748–759.

K.R. Babu, D.J. Douglas, Methanol-Induced Conformations of Myoglobin at pH 4.0, Biochemistry. 39 (2000) 14702–14710.

M.W. Beck, S.B. Oh, R.A. Kerr, H.J. Lee, S.H. Kim, S. Kim, M. Jang, B.T. Ruotolo, J.-Y. Lee, M.H. Lim, A rationally designed small molecule for identifying an in vivo link between metal–amyloid-β complexes and the pathogenesis of Alzheimer's disease, Chemical Science. 6 (2015) 1879–1886.

G. Bellesia, J.-E. Shea, Diversity of kinetic pathways in amyloid fibril formation, The Journal of Chemical Physics. 131 (2009) 111102.

J.L. Benesch, B.T. Ruotolo, Mass spectrometry: come of age for structural and dynamical biology, Current Opinion in Structural Biology. 21 (2011) 641–649.

J.L.P. Benesch, B.T. Ruotolo, D.A. Simmons, C.V. Robinson, Protein Complexes in the Gas Phase: Technology for Structural Genomics and Proteomics, Chemical Reviews. 107 (2007) 3544–3567.

F. Bernini, D. Malferrari, M. Pignataro, C.A. Bortolotti, G. Di Rocco, L. Lancellotti, M.F. Brigatti, R. Kayed, M. Borsari, F. del Monte, E. Castellini, Pre-amyloid oligomers budding: a metastatic mechanism of proteotoxicity, Scientific Reports. 6 (2016) 35865.

H.J.C. Berendsen, J.P.M. Postma, W.F. van Gunsteren, A. DiNola, J.R. Haak, Molecular dynamics with coupling to an external bath, The Journal of Chemical Physics. 81 (1984) 3684–3690.

S.L. Bernstein, N.F. Dupuis, N.D. Lazo, T. Wyttenbach, M.M. Condron, G. Bitan, D.B. Teplow, J.-E. Shea, B.T. Ruotolo, C.V. Robinson, M.T. Bowers, Amyloid-β protein oligomerization and the importance of tetramers and dodecamers in the aetiology of Alzheimer's disease, Nature Chemistry. 1 (2009) 326–331.

R. Beveridge, Q. Chappuis, C. Macphee, P. Barran, Mass spectrometry methods for intrinsically disordered proteins, The Analyst. 138 (2013) 32–42.

S. Bieler, L. Estrada, R. Lagos, M. Baeza, J. Castilla, C. Soto, Amyloid Formation Modulates the Biological Activity of a Bacterial Protein, Journal of Biological Chemistry. 280 (2005) 26880–26885.

J. Bieschke, J. Russ, R.P. Friedrich, D.E. Ehrnhoefer, H. Wobst, K. Neugebauer, E.E. Wanker, EGCG remodels mature α-synuclein and amyloid-β fibrils and reduces cellular toxicity, Proceedings of the National Academy of Sciences. 107 (2010) 7710–7715.

C. Bleiholder, M.T. Bowers, The Solution Assembly of Biological Molecules Using Ion Mobility Methods: From Amino Acids to Amyloid β-Protein, Annual Review of Analytical Chemistry. 10 (2017) 365–386.

C. Bleiholder, T.D. Do, C. Wu, N.J. Economou, S.S. Bernstein, S.K. Buratto, J.-E. Shea, M.T. Bowers, Ion Mobility Spectrometry Reveals the Mechanism of Amyloid Formation of Aβ(25–35) and Its Modulation by Inhibitors at the Molecular Level: Epigallocatechin Gallate and *Scyllo* -inositol, Journal of the American Chemical Society. 135 (2013) 16926–16937.

C. Bleiholder, N.F. Dupuis, T. Wyttenbach, M.T. Bowers, Ion mobility–mass spectrometry reveals a conformational conversion from random assembly to β-sheet in amyloid fibril formation, Nature Chemistry. 3 (2011) 172–177.

N.B. Borotto, Z. Zhang, J. Dong, B. Burant, R.W. Vachet, Increased β-Sheet Dynamics and D–E Loop Repositioning Are Necessary for Cu(II)-Induced Amyloid Formation by β-2-Microglobulin, Biochemistry. 56 (2017) 1095–1104.

L. Breydo, V.N. Uversky, Structural, morphological, and functional diversity of amyloid oligomers, FEBS Letters. 589 (2015) 2640–2648.

M. Brion, L. Lambs, and G. Berthon, Metal ion-tetracycline interactions in biological fluids. Part 6. Formation of copper(II) complexes with tetracycline and some of its derivatives and appraisal of their biological significance, Inorganica Chimica Actra. 123 (1986) 61–68.

L.E. Buchanan, M. Maj, E.B. Dunkelberger, P.-N. Cheng, J.S. Nowick, M.T. Zanni, Structural Polymorphs Suggest Competing Pathways for the Formation of

Amyloid Fibrils That Diverge from a Common Intermediate Species, Biochemistry. 57 (2018) 6470–6478.

A.K. Buell, E.K. Esbjörner, P.J. Riss, D.A. White, F.I. Aigbirhio, G. Toth, M.E. Welland, C.M. Dobson, T.P.J. Knowles, Probing small molecule binding to amyloid fibrils, Physical Chemistry Chemical Physics. 13 (2011) 20044.

M.F. Bush, Z. Hall, K. Giles, J. Hoyes, C.V. Robinson, B.T. Ruotolo, Collision Cross Sections of Proteins and Their Complexes: A Calibration Framework and Database for Gas-Phase Structural Biology, Analytical Chemistry. 82 (2010) 9557–9565.

G. Bussi, D. Donadio, M. Parrinello, Canonical sampling through velocity rescaling, The Journal of Chemical Physics. 126 (2007) 014101.

M.F. Calabrese, C.M. Eakin, J.M. Wang, A.D. Miranker, A regulatable switch mediates self-association in an immunoglobulin fold, Nature Structural & Molecular Biology. 15 (2008) 965–971.

M.F. Calabrese, A.D. Miranker, Formation of a Stable Oligomer of β-2 Microglobulin Requires only Transient Encounter with Cu(II), Journal of Molecular Biology. 367 (2007) 1–7.

C. Carazzone, R. Colombo, M. Quaglia, P. Mangione, S. Raimondi, S. Giorgetti, G. Caccialanza, V. Bellotti, E. De Lorenzi, Sulfonated molecules that bind a partially structured species of beta2-microglobulin also influence refolding and fibrillogenesis, Electrophoresis. 29 (2008) 1502–1510.

E. Cerasoli, M.G. Ryadnov, B.M. Austen, The elusive nature and diagnostics of misfolded Aβ oligomers, Frontiers in Chemistry. 3 (2015) 17.

J. Chen, A.H. Armstrong, A.N. Koehler, M.H. Hecht, Small Molecule Microarrays Enable the Discovery of Compounds That Bind the Alzheimer's Aβ Peptide and Reduce its Cytotoxicity, Journal of the American Chemical Society. 132 (2010) 17015–17022.

B. Cheng, H. Gong, H. Xiao, R.B. Petersen, L. Zheng, K. Huang, Inhibiting toxic aggregation of amyloidogenic proteins: A therapeutic strategy for protein misfolding diseases, Biochimica et Biophysica Acta (BBA) - General Subjects. 1830 (2013) 4860–4871.

X.R. Cheng, B.Y.H. Hau, A.J. Veloso, S. Martic, H.-B. Kraatz, K. Kerman, Surface Plasmon Resonance Imaging of Amyloid-β Aggregation Kinetics in the Presence of Epigallocatechin Gallate and Metals, Analytical Chemistry. 85 (2013) 2049–2055.

M.L. Choi, S. Gandhi, Crucial role of protein oligomerization in the pathogenesis of Alzheimer's and Parkinson's diseases, The FEBS Journal. 285 (2018) 3631–3644.

Y.-T. Choi, C.-H. Jung, S.-R. Lee, J.-H. Bae, W.-K. Baek, M.-H. Suh, J. Park, C.-W. Park, S.-I. Suh, The green tea polyphenol (-)-epigallocatechin gallate attenuates beta-amyloid-amyloid-induced neurotoxicity in cultured hippocampal neurons, Life Sciences. (2001) 603-614.

P. Cizas, R. Budvytyte, R. Morkuniene, R. Moldovan, M. Broccio, M. Lösche, G. Niaura, G. Valincius, V. Borutaite, Size-dependent neurotoxicity of β-amyloid oligomers, Archives of Biochemistry and Biophysics. 496 (2010) 84–92.

D.E. Clemmer, D.H. Russell, E.R. Williams, Characterizing the *Conformationome* : Toward a Structural Understanding of the Proteome, Accounts of Chemical Research. 50 (2017) 556–560.

M. Colombo, M. de Rosa, V. Bellotti, S. Ricagno, M. Bolognesi, A recurrent D-strand association interface is observed in β-2 microglobulin oligomers: β-2 microglobulin oligomeric interface, FEBS Journal. 279 (2012) 1131–1143.

J.S. Cottrell, Protein identification using MS/MS data, Journal of Proteomics. 74 (2011) 1842–1851.

Cristovao, J.S., Henriques, B.J., and Gomes, C.M., Biophysical and Spectroscopic Methods for Monitoring Protein Misfolding and Amyloid Aggregation, Methods in Molecular Biology. 1873 (2019) 3–18.

F. Danesh, L.T. Ho, Dialysis-Related Amyloidosis: History and Clinical Manifestations, Seminars in Dialysis. 14 (2001) 80–85.

T. Darden, D. York, L. Pedersen, Particle mesh Ewald: An $N \cdot \log(N)$ method for Ewald sums in large systems, The Journal of Chemical Physics. 98 (1993) 10089–10092.

K.A. Dill, H.S. Chan, From Levinthal to pathways to funnels, Nature Structural & Molecular Biology. 4 (1997) 10–19.

A.J. Doig, P. Derreumaux, Inhibition of protein aggregation and amyloid formation by small molecules, Current Opinion in Structural Biology. 30 (2015) 50–56.

J. Dong, C.A. Joseph, N.B. Borotto, V.L. Gill, M.J. Maroney, R.W. Vachet, Unique Effect of Cu(II) in the Metal-Induced Amyloid Formation of β-2-Microglobulin, Biochemistry. 53 (2014) 1263–1274.

T.B. Drüeke, Z.A. Massy, Beta2-Microglobulin, Seminars in Dialysis. 22 (2009) 378–380.

N.F. Dupuis, C. Wu, J.-E. Shea, M.T. Bowers, The Amyloid Formation Mechanism in Human IAPP: Dimers Have β-Strand Monomer−Monomer Interfaces, Journal of the American Chemical Society. 133 (2011) 7240–7243.

C.M. Eakin, F.J. Attenello, C.J. Morgan, A.D. Miranker, Oligomeric Assembly of Native-like Precursors Precedes Amyloid Formation by β-2 Microglobulin, Biochemistry. 43 (2004) 7808–7815.

C.M. Eakin, A.J. Berman, A.D. Miranker, A native to amyloidogenic transition regulated by a backbone trigger, Journal of Molecular Biology. 13 (2006) 202-208.

C.M. Eakin, J.D. Knight, C.J. Morgan, M.A. Gelfand, A.D. Miranker, Formation of a Copper Specific Binding Site in Non-Native States of β-2-Microglobulin, Biochemistry. 41 (2002) 10646–10656.

D.E. Ehrnhoefer, J. Bieschke, A. Boeddrich, M. Herbst, L. Masino, R. Lurz, S. Engemann, A. Pastore, E.E. Wanker, EGCG redirects amyloidogenic polypeptides into unstructured, off-pathway oligomers, Nature Structural & Molecular Biology. 15 (2008) 558–566.

D.E. Ehrnhoefer, M. Duennwald, P. Markovic, J.L. Wacker, S. Engemann, M. Roark, J. Legleiter, J.L. Marsh, L.M. Thompson, S. Lindquist, P.J. Muchowski, E.E. Wanker, Green tea (−)-epigallocatechin-gallate modulates early events in huntingtin misfolding and reduces toxicity in Huntington's disease models, Human Molecular Genetics. 15 (2006) 2743–2751.

T. Eichner, S.E. Radford, A Diversity of Assembly Mechanisms of a Generic Amyloid Fold, Molecular Cell. 43 (2011) 8–18.

T. Eichner, S.E. Radford, Understanding the complex mechanisms of β2-microglobulin amyloid assembly: β2-microglobulin fibrillogenesis at physiological pH, FEBS Journal. 278 (2011) 3868–3883.

J.R. Engen, T.E. Wales, Analytical Aspects of Hydrogen Exchange Mass Spectrometry, Annual Review of Analytical Chemistry. 8 (2015) 127–148.

J.D. Eschweiler, R.M. Martini, B.T. Ruotolo, Chemical Probes and Engineered Constructs Reveal a Detailed Unfolding Mechanism for a Solvent-Free Multidomain Protein, Journal of the American Chemical Society. 139 (2017) 534–540.

J.D. Eschweiler, J.N. Rabuck-Gibbons, Y. Tian, B.T. Ruotolo, CIUSuite: A Quantitative Analysis Package for Collision Induced Unfolding Measurements of Gas-Phase Protein Ions, Analytical Chemistry. 87 (2015) 11516–11522.

M. Fändrich, Oligomeric Intermediates in Amyloid Formation: Structure Determination and Mechanisms of Toxicity, Journal of Molecular Biology. 421 (2012) 427–440.

G. Fusco, M. Sanz-Hernandez, F.S. Ruggeri, M. Vendruscolo, C.M. Dobson, A. De Simone, Molecular determinants of the interaction of EGCG with ordered and disordered proteins, Biopolymers. 109 (2018) e23117.

V. Gabelica, A.A. Shvartsburg, C. Afonso, P. Barran, J.L.P. Benesch, C. Bleiholder, M.T. Bowers, A. Bilbao, M.F. Bush, J.L. Campbell, I.D.G. Campuzano, T. Causon, B.H. Clowers, C.S. Creaser, E. De Pauw, J. Far, F. Fernandez-Lima, J.C. Fjeldsted, K. Giles, M. Groessl, C.J. Hogan, S. Hann, H.I. Kim, R.T. Kurulugama, J.C. May, J.A. McLean, K. Pagel, K. Richardson, M.E. Ridgeway, F. Rosu, F. Sobott, K. Thalassinos, S.J. Valentine, T. Wyttenbach, Recommendations for reporting Ion Mobility Mass Spectrometry Measurements, Mass Spectrometry Reviews. 38 (2019) 291-320.

M.K. Gade, L.M. Blancas-Mejia, B. Weber, J. Buchner, M. Ramirez-Alvarado, H. Naiki, D. Otzen, ThT 101: a primer on the use of thioflavin T to investigate amyloid formation, Amyloid. 24 (2017) 1–16.

F. Gejyo, S. Odani, T. Yamada, N. Honma, H. Saito, Y. Suzuki, Y. Nakagawa, H. Kobayashi, Y. Maruyama, Y. Hirasawa, M. Suzuki, M. Arakawa, β2-microglobulin: A new form of amyloid protein associated with chronic hemodialysis, Kidney International. 30 (1986) 385–390.

S. Giorgetti, S. Raimondi, K. Pagano, A. Relini, M. Bucciantini, A. Corazza, F. Fogolari, L. Codutti, M. Salmona, P. Mangione, L. Colombo, A. De Luigi, R. Porcari, A. Gliozzi, M. Stefani, G. Esposito, V. Bellotti, M. Stoppini, Effect of Tetracyclines on the Dynamics of Formation and Destructuration of β2-Microglobulin Amyloid Fibrils, Journal of Biological Chemistry. 286 (2011) 2121–2131.

W.S. Gosal, I.J. Morten, E.W. Hewitt, D.A. Smith, N.H. Thomson, S.E. Radford, Competing Pathways Determine Fibril Morphology in the Self-assembly of β2-Microglobulin into Amyloid, Journal of Molecular Biology. 351 (2005) 850–864.

J. Habchi, S. Chia, R. Limbocker, B. Mannini, M. Ahn, M. Perni, O. Hansson, P. Arosio, J.R. Kumita, P.K. Challa, S.I.A. Cohen, S. Linse, C.M. Dobson, T.P.J. Knowles, M. Vendruscolo, Systematic development of small molecules to inhibit specific microscopic steps of Aβ42 aggregation in Alzheimer's disease, Proceedings of the National Academy of Sciences. 114 (2017) E200–E208.

T. Härd, C. Lendel, Inhibition of Amyloid Formation, Journal of Molecular Biology. 421 (2012) 441–465.

J.A. Hebda, M. Magzoub, A.D. Miranker, Small molecule screening in context: Lipid-catalyzed amyloid formation: Small Molecule Screening in Context, Protein Science. 23 (2014) 1341–1348.

H. Hernández, C.V. Robinson, Determining the stoichiometry and interactions of macromolecular assemblies from mass spectrometry, Nature Protocols. 2 (2007) 715–726.

N.H.H. Heegaard, J.W. Sen, N.C. Kaarsholm, M.H. Nissen, Conformational Intermediate of the Amyloidogenic Protein β $_2$ -Microglobulin at Neutral pH, Journal of Biological Chemistry. 276 (2001) 32657–32662.

B. Hess, H. Bekker, H.J.C. Berendsen, J.G.E.M. Fraaije, LINCS: A linear constraint solver for molecular simulations, Journal of Computational Chemistry. 18 (1997) 1463–1472.

W. Hoffmann, G. von Helden, K. Pagel, Ion mobility-mass spectrometry and orthogonal gas-phase techniques to study amyloid formation and inhibition, Current Opinion in Structural Biology. 46 (2017) 7–15.

M. Hora, M. Carballo-Pacheco, B. Weber, V.K. Morris, A. Wittkopf, J. Buchner, B. Strodel, B. Reif, Epigallocatechin-3-gallate preferentially induces aggregation of amyloidogenic immunoglobulin light chains, Scientific Reports. 7 (2017) 41515.

J. Huang, S. Rauscher, G. Nawrocki, T. Ran, M. Feig, B.L. de Groot, H. Grubmüller, A.D. MacKerell, CHARMM36m: an improved force field for folded and intrinsically disordered proteins, Nature Methods. 14 (2017) 71–73.

J.W. Hudgens, E.S. Gallagher, I. Karageorgos, K.W. Anderson, J.J. Filliben, R.Y.-C. Huang, G. Chen, G.M. Bou-Assaf, A. Espada, M.J. Chalmers, E. Harguindey, H.-M. Zhang, B.T. Walters, J. Zhang, J.D. Venable, C. Steckler, I. Park, A. Brock, X. Lu, R.K. Pandey, A. Chandramohan, G.S. Anand, S.N. Nirudodhi, J.B. Sperry, J.C. Rouse, J.A. Carroll, K.D. Rand, U. Leurs, D.D. Weis, M.A. Al-Naqshabandi, T.S. Hageman, D. Deredge, P.L. Wintrode, M. Papanastasiou, J.D. Lambris, S. Li, S. Urata, Interlaboratory Comparison of Hydrogen-Deuterium Exchange Mass Spectrometry Measurements of the Fab fragment of NISTmAb, Analytical Chemistry. (2019) 7336-7345.

S.-J. Hyung, A.S. DeToma, J.R. Brender, S. Lee, S. Vivekanandan, A. Kochi, J.-S. Choi, A. Ramamoorthy, B.T. Ruotolo, M.H. Lim, Insights into antiamyloidogenic properties of the green tea extract (-)-epigallocatechin-3-gallate toward metal-associated amyloid- species, Proceedings of the National Academy of Sciences. 110 (2013) 3743–3748.

S.-J. Hyung, C.V. Robinson, B.T. Ruotolo, Gas-Phase Unfolding and Disassembly Reveals Stability Differences in Ligand-Bound Multiprotein Complexes, Chemistry & Biology. 16 (2009) 382–390.

S.-J. Hyung, B.T. Ruotolo, Integrating mass spectrometry of intact protein complexes into structural proteomics, Proteomics. 12 (2012) 1547–1564.

M.G. Iadanza, M.P. Jackson, E.W. Hewitt, N.A. Ranson, S.E. Radford, A new era for understanding amyloid structures and disease, Nature Reviews Molecular Cell Biology. 19 (2018) 755–773.

S.S. Jaswal, Biological insights from hydrogen exchange mass spectrometry, Biochimica et Biophysica Acta (BBA) - Proteins and Proteomics. 1834 (2013) 1188–1201.

M. Jezowska-Bojczuk, L. Lambs, H. Kozlowski, G. Berthon, Metal ion-tetracycline interactions in biological fluids. 10. Structural investigations on copper(II) complexes of tetracycline, oxytetracycline, chlortetracycline, 4-(dedimethylamino)tetracycline, and 6-desoxy-6-demethyltetracycline and discussion of their binding modes, Inorganic Chemistry. 32 (1993) 428–437.

W.L. Jorgensen, J. Chandrasekhar, J.D. Madura, R.W. Impey, M.L. Klein, Comparison of simple potential functions for simulating liquid water, The Journal of Chemical Physics. 79 (1983) 926–935.

J.C. Jurchen, D.E. Garcia, E.R. Williams, Further studies on the origins of asymmetric charge partitioning in protein homodimers, Journal of the American Society for Mass Spectrometry. 15 (2004) 1408–1415.

J.C. Jurchen, E.R. Williams, Origin of Asymmetric Charge Partitioning in the Dissociation of Gas-Phase Protein Homodimers, Journal of the American Chemical Society. 125 (2003) 2817–2826.

N.M. Kad, S.L. Myers, D.P. Smith, D. Alastair Smith, S.E. Radford, N.H. Thomson, Hierarchical Assembly of β2-Microglobulin Amyloid In Vitro Revealed by Atomic Force Microscopy, Journal of Molecular Biology. 330 (2003) 785–797.

N.M. Kad, N.H. Thomson, D.P. Smith, D.A. Smith, S.E. Radford, β2-microglobulin and its deamidated variant, N17D form amyloid fibrils with a range of morphologies in vitro, Journal of Molecular Biology. 313 (2001) 559–571.

I.A. Kaltashov, C.E. Bobst, R.R. Abzalimov, Mass spectrometry-based methods to study protein architecture and dynamics: MS-Based Methods to Study Protein Architecture and Dynamics, Protein Science. 22 (2013) 530–544.

I.A. Kaltashov, A. Mohimen, Estimates of Protein Surface Areas in Solution by Electrospray Ionization Mass Spectrometry, Analytical Chemistry. 77 (2005) 5370–7379.

I.A. Kaltashov, J.W. Pawlowski, W. Yang, K. Muneeruddin, H. Yao, C.E. Bobst, A.N. Lipatnikov, LC/MS at the whole protein level: Studies of biomolecular structure and interactions using native LC/MS and cross-path reactive chromatography (XP-RC) MS, Methods. 144 (2018) 14–26.

T.K. Karamanos, A.P. Kalverda, G.S. Thompson, S.E. Radford, Visualization of Transient Protein-Protein Interactions that Promote or Inhibit Amyloid Assembly, Molecular Cell. 55 (2014) 214–226.

H. Katou, T. Kanno, M. Hoshino, Y. Hagihara, H. Tanaka, T. Kawai, K. Hasegawa, H. Naiki, Y. Goto, The role of disulfide bond in the amyloidogenic state of β2-microglobulin studied by heteronuclear NMR, Protein Science. 11 (2009) 2218–2229.

N. Khan, F. Afaq, M. Saleem, N. Ahmad, H. Mukhtar, Targeting Multiple Signaling Pathways by Green Tea Polyphenol (−)-Epigallocatechin-3-Gallate, Cancer Research. 66 (2006) 2500–2505.

I. Kheterpal, K.D. Cook, R. Wetzel, Hydrogen/Deuterium Exchange Mass Spectrometry Analysis of Protein Aggregates, in: Methods in Enzymology, Elsevier, 2006: pp. 140–166.

I. Kheterpal, R. Wetzel, Hydrogen/Deuterium Exchange Mass SpectrometryA Window into Amyloid Structure, Accounts of Chemical Research. 39 (2006) 584–593.

R. Kodali, R. Wetzel, Polymorphism in the intermediates and products of amyloid assembly, Current Opinion in Structural Biology. 17 (2007) 48–57.

L. Konermann, J. Pan, Y.-H. Liu, Hydrogen exchange mass spectrometry for studying protein structure and dynamics, Chem. Soc. Rev. 40 (2011) 1224–1234.

N.L. La Gruta, P.G. Thomas, A.I. Webb, M.A. Dunstone, T. Cukalac, P.C. Doherty, A.W. Purcell, J. Rossjohn, S.J. Turner, Epitope-specific TCR repertoire diversity imparts no functional advantage on the CD8+ T cell response to cognate viral peptides, Proceedings of the National Academy of Sciences. 105 (2008) 2034–2039.

F. Lanucara, S.W. Holman, C.J. Gray, C.E. Eyers, The power of ion mobility-mass spectrometry for structural characterization and the study of conformational dynamics, Nature Chemistry. 6 (2014) 281–294.

M.E. Larson, S.E. Lesné, Soluble Aβ oligomer production and toxicity: Soluble oligomeric Aβ production and toxicity, Journal of Neurochemistry. 120 (2012) 125–139.

N.B. Last, E. Rhoades, A.D. Miranker, Islet amyloid polypeptide demonstrates a persistent capacity to disrupt membrane integrity, Proceedings of the National Academy of Sciences. 108 (2011) 9460–9465.

S.S. Leal, H.M. Botelho, C.M. Gomes, Metal ions as modulators of protein conformation and misfolding in neurodegeneration, Coordination Chemistry Reviews. 256 (2012) 2253–2270.

S.J.C. Lee, E. Nam, H.J. Lee, M.G. Savelieff, M.H. Lim, Towards an understanding of amyloid-β oligomers: characterization, toxicity mechanisms, and inhibitors, Chemical Society Reviews. 46 (2017) 310–323.

J. Li, M. Zhu, S. Rajamani, V.N. Uversky, A.L. Fink, Rifampicin Inhibits alpha-Synuclein Fibrillation and Disaggregates Fibrils, Chemistry & Biology. 11 (2004) 1513–1521.

Y. Liang, M.O. Ore, S. Morin, D.J. Wilson, Specific Disruption of Transthyretin(105–115) Fibrilization Using "Stabilizing" Inhibitors of Transthyretin Amyloidogenesis, Biochemistry. 51 (2012) 3523–3530.

K.J. Light-Wahl, B.L. Schwartz, R.D. Smith, Observation of the Noncovalent Quaternary Associations of Proteins by Electrospray Ionization Mass Spectrometry, Journal of the American Chemical Society. 116 (1994) 5271–5278.

X. Lin, W. Zhao, X. Wang, Characterization of conformational changes and noncovalent complexes of myoglobin by electrospray ionization mass spectrometry, circular dichroism and fluorescence spectroscopy, Journal of Mass Spectrometry. (2010) 618-626.

T. Liu, T.M. Marcinko, P.A. Kiefer, R.W. Vachet, Using Covalent Labeling and Mass Spectrometry To Study Protein Binding Sites of Amyloid Inhibiting Molecules, Analytical Chemistry. 89 (2017) 11583–11591.

N. Lorenzen, S.B. Nielsen, Y. Yoshimura, B.S. Vad, C.B. Andersen, C. Betzer, J.D. Kaspersen, G. Christiansen, J.S. Pedersen, P.H. Jensen, F.A.A. Mulder, D.E. Otzen, How Epigallocatechin Gallate Can Inhibit α-Synuclein Oligomer Toxicity *in Vitro*, Journal of Biological Chemistry. 289 (2014) 21299–21310.

J. Lu, Q. Cao, C. Wang, J. Zheng, F. Luo, J. Xie, Y. Li, X. Ma, L. He, D. Eisenberg, J. Nowick, L. Jiang, D. Li, Structure-Based Peptide Inhibitor Design of Amyloid-β Aggregation, Frontiers in Molecular Neuroscience. 12 (2019) 1-10.

D.R. Madden, J.C. Gorga, J.L. Strominger, D.C. Wiley, The three-dimensional structure of HLA-B27 at 2.1 Å resolution suggests a general mechanism for tight peptide binding to MHC, Cell. 70 (1992) 1035–1048.

A.A. Makarov, R. Helmy, Combining size-exclusion chromatography with differential hydrogen–deuterium exchange to study protein conformational changes, Journal of Chromatography A. 1431 (2016) 224–230.

S. Makin, The amyloid hypothesis on trial, Nature. 559 (2018) S4–S7.

T.M. Marcinko, J. Dong, R. LeBlanc, K.V. Daborowski, R.W. Vachet, Small molecule-mediated inhibition of β-2-microglobulin-based amyloid fibril formation, Journal of Biological Chemistry. 292 (2017) 10630–10638.

E.G. Marklund, M.T. Degiacomi, C.V. Robinson, A.J. Baldwin, J.L.P. Benesch, Collision Cross Sections for Structural Proteomics, Structure. 23 (2015) 791–799.

K.E. Marshall, R. Marchante, W.-F. Xue, L.C. Serpell, The relationship between amyloid structure and cytotoxicity, Prion. 8 (2014) 192–196.

A.T. Marvian, D.J. Koss, F. Aliakbari, D. Morshedi, T.F. Outeiro, *In vitro* models of synucleinopathies: informing on molecular mechanisms and protective strategies, Journal of Neurochemistry. 150 (2019) 535-565.

D. Matthes, V. Gapsys, J.T. Brennecke, B.L. de Groot, An Atomistic View of Amyloidogenic Self-assembly: Structure and Dynamics of Heterogeneous Conformational States in the Pre-nucleation Phase, Scientific Reports. 6 (2016) 33156.

M.M. Maurer, G.C. Donohoe, S.J. Valentine, Advances in ion mobility-mass spectrometry instrumentation and techniques for characterizing structural heterogeneity, The Analyst. 140 (2015) 6782–6798.

R.G. McAllister, L. Konermann, Challenges in the Interpretation of Protein H/D Exchange Data: A Molecular Dynamics Simulation Perspective, Biochemistry. 54 (2015) 2683–2692.

S.A. McLuckey, M. Mentinova, Ion/Neutral, Ion/Electron, Ion/Photon, and Ion/Ion Interactions in Tandem Mass Spectrometry: Do We Need Them All? Are They Enough?, Journal of The American Society for Mass Spectrometry. 22 (2011) 3–12.

V.J. McParland, N.M. Kad, A.P. Kalverda, A. Brown, P. Kirwin-Jones, M.G. Hunter, M. Sunde, S.E. Radford, Partially Unfolded States of β 2 -Microglobulin and Amyloid Formation in Vitro, Biochemistry. 39 (2000) 8735–8746.

S. Mehmood, T.M. Allison, C.V. Robinson, Mass Spectrometry of Protein Complexes: From Origins to Applications, Annual Review of Physical Chemistry. 66 (2015) 453–474.

V.L. Mendoza, K. Antwi, M.A. Barón-Rodríguez, C. Blanco, R.W. Vachet, Structure of the Preamyloid Dimer of β-2-Microglobulin from Covalent Labeling and Mass Spectrometry, Biochemistry. 49 (2010) 1522–1532.

V.L. Mendoza, M.A. Barón-Rodríguez, C. Blanco, R.W. Vachet, Structural Insights into the Pre-Amyloid Tetramer of β-2-Microglobulin from Covalent Labeling and Mass Spectrometry, Biochemistry. 50 (2011) 6711–6722.

F. Meng, P. Marek, K.J. Potter, C.B. Verchere, D.P. Raleigh, Rifampicin Does Not Prevent Amyloid Fibril Formation by Human Islet Amyloid Polypeptide but Does Inhibit Fibril Thioflavin-T Interactions: Implications for Mechanistic Studies of β-Cell Death [†], Biochemistry. 47 (2008) 6016–6024.

S.I. Merenbloom, T.G. Flick, E.R. Williams, How Hot are Your Ions in TWAVE Ion Mobility Spectrometry?, Journal of The American Society for Mass Spectrometry. 23 (2012) 553–562.

U.H. Mistarz, S.A. Chandler, J.M. Brown, J.L.P. Benesch, K.D. Rand, Probing the Dissociation of Protein Complexes by Means of Gas-Phase H/D Exchange Mass Spectrometry, Journal of The American Society for Mass Spectrometry. 30 (2019) 45–57.

H. Mohammad-Beigi, F. Aliakbari, C. Sahin, C. Lomax, A. Tawfike, N.P. Schafer, A. Amiri-Nowdijeh, H. Eskandari, I.M. Møller, M. Hosseini-Mazinani, G. Christiansen, J.L. Ward, D. Morshedi, D.E. Otzen, Oleuropein derivatives from olive fruit extracts reduce α-synuclein fibrillation and oligomer toxicity, Journal of Biological Chemistry. 294 (2019) 4215–4232.

H. Mohammadiarani, V.S. Shaw, R.R. Neubig, H. Vashisth, Interpreting Hydrogen–Deuterium Exchange Events in Proteins Using Atomistic Simulations: Case Studies on Regulators of G-Protein Signaling Proteins, The Journal of Physical Chemistry B. 122 (2018) 9314–9323.

C.J. Morgan, M. Gelfand, C. Atreya, A.D. Miranker, Kidney dialysis-associated amyloidosis: a molecular role for copper in fiber formation, Journal of Molecular Biology. 309 (2001) 339–345.

J.A. Moroco, J.R. Engen, Replication in bioanalytical studies with HDX MS: aim as high as possible, Bioanalysis. 7 (2015) 1065–1067.

G.P. Morris, I.A. Clark, B. Vissel, Inconsistencies and Controversies Surrounding the Amyloid Hypothesis of Alzheimer's Disease, Acta Neuropathologica Communcations. 2 (2014) 135.

V. Moses, Ö. Tastan Bishop, K.A. Lobb, The evaluation and validation of copper (II) force field parameters of the Auxiliary Activity family 9 enzymes, Chemical Physics Letters. 678 (2017) 91–97.

S. Nakano, S. Megro, T. Hase, T. Suzuki, M. Isemura, Y. Nakamura, S. Ito, Computational Molecular Docking and X-ray Crystallographic Studies of Catechins in New Drug Design Strategies, Molecules. 23 (2018) 2020.

A. Napp, V. Houbart, A. Demelenne, M. Merville, J. Crommen, M. Dumoulin, G. Garraux, A. Servais, M. Fillet, Separation and determination of alpha-synuclein monomeric and oligomeric species using two electrophoretic approaches, Electrophoresis. 39 (2018) 3022–3031.

A. Nath, D.E. Schlamadinger, E. Rhoades, A.D. Miranker, Structure-Based Small Molecule Modulation of a Pre-Amyloid State: Pharmacological Enhancement of IAPP Membrane-Binding and Toxicity, Biochemistry. 54 (2015) 3555–3564.

F. Neese, Software update: the ORCA program system, version 4.0: Software update, Wiley Interdisciplinary Reviews: Computational Molecular Science. 8 (2018) e1327.

A. Negri, V. Naponelli, F. Rizzi, S. Bettuzzi, Molecular Targets of Epigallocatechin—Gallate (EGCG): A Special Focus on Signal Transduction and Cancer, Nutrients. 10 (2018) 1936.

R. Nelson, M.R. Sawaya, M. Balbirnie, A.Ø. Madsen, C. Riekel, R. Grothe, D. Eisenberg, Structure of the cross-β spine of amyloid-like fibrils, Nature. 435 (2005) 773–778.

S. Niu, B.T. Ruotolo, Collisional unfolding of multiprotein complexes reveals cooperative stabilization upon ligand binding: Collisional Unfolding of Multiprotein Complexes, Protein Science. 24 (2015) 1272–1281.

J.M. Nussbaum, M.E. Seward, G.S. Bloom, Alzheimer disease: A tale of two prions, Prion. 7 (2013) 14–19.

T. Ookoshi, K. Hasegawa, Y. Ohhashi, H. Kimura, N. Takahashi, H. Yoshida, R. Miyazaki, Y. Goto, H. Naiki, Lysophospholipids induce the nucleation and extension of 2-microglobulin-related amyloid fibrils at a neutral pH, Nephrology Dialysis Transplantation. 23 (2008) 3247–3255.

T. Ozdal, E. Capanoglu, F. Altay, A review on protein–phenolic interactions and associated changes, Food Research International. 51 (2013) 954–970.

B. Paizs, S. Suhai, Fragmentation pathways of protonated peptides, Mass Spectrometry Reviews. 24 (2005) 508–548.

W. Paslawski, S. Mysling, K. Thomsen, T.J.D. Jørgensen, D.E. Otzen, Co-existence of Two Different α-Synuclein Oligomers with Different Core Structures Determined by Hydrogen/Deuterium Exchange Mass Spectrometry, Angewandte Chemie International Edition. 53 (2014) 7560–7563.

A.T. Petkova, R.D. Leapman, Z. Guo, W.-M. Yau, M.P. Mattson, R. Tycko, Self-Propagating, Molecular-Level Polymorphism in Alzheimer's B-Amyloid Fibrils, Science. 307 (2005) 262–265.

A.A. Petruk, L.A. Defelipe, R.G. Rodríguez Limardo, H. Bucci, M.A. Marti, A.G. Turjanski, Molecular Dynamics Simulations Provide Atomistic Insight into Hydrogen Exchange Mass Spectrometry Experiments, Journal of Chemical Theory and Computation. 9 (2013) 658–669.

J.D. Pham, B. Demeler, J.S. Nowick, Polymorphism of Oligomers of a Peptide from β-Amyloid, Journal of the American Chemical Society. 136 (2014) 5432–5442.

G.W. Platt, S.E. Radford, Glimpses of the molecular mechanisms of β_2-microglobulin fibril formation in vitro: Aggregation on a complex energy landscape, FEBS Letters. 583 (2009) 2623–2629.

D.A. Polasky, S.M. Dixit, S.M. Fantin, B.T. Ruotolo, CIUSuite 2: Next-Generation Software for the Analysis of Gas-Phase Protein Unfolding Data, Analytical Chemistry. 91 (2019) 3147–3155.

A. Politis, A.Y. Park, S.-J. Hyung, D. Barsky, B.T. Ruotolo, C.V. Robinson, Integrating Ion Mobility Mass Spectrometry with Molecular Modelling to Determine the Architecture of Multiprotein Complexes, PLoS ONE. 5 (2010) e12080.

N.E. Pryor, M.A. Moss, C.N. Hestekin, Unraveling the Early Events of Amyloid-β Protein (Aβ) Aggregation: Techniques for the Determination of Aβ Aggregate Size, International Journal of Molecular Sciences. 13 (2012) 3038–3072.

M. Quaglia, C. Carazzone, S. Sabella, R. Colombo, S. Giorgetti, V. Bellotti, E. De Lorenzi, Search of ligands for the amyloidogenic protein β2-microglobulin by capillary electrophoresis and other techniques, Electrophoresis. 26 (2005) 4055–4063.

K. Rajabi, A.E. Ashcroft, S.E. Radford, Mass spectrometric methods to analyze the structural organization of macromolecular complexes, Methods. 89 (2015) 13–21.

R.N. Rambaran, L.C. Serpell, Amyloid fibrils: Abnormal protein assembly, Prion. 2 (2008) 112–117.

K.D. Rand, S.D. Pringle, J.P. Murphy, K.E. Fadgen, J. Brown, J.R. Engen, Gas-Phase Hydrogen/Deuterium Exchange in a Traveling Wave Ion Guide for the Examination of Protein Conformations, Analytical Chemistry. 81 (2009) 10019–10028.

K.D. Rand, M. Zehl, T.J.D. Jørgensen, Measuring the Hydrogen/Deuterium Exchange of Proteins at High Spatial Resolution by Mass Spectrometry: Overcoming Gas-Phase Hydrogen/Deuterium Scrambling, Accounts of Chemical Research. 47 (2014) 3018–3027.

R.M. Rasia, C.W. Bertoncini, D. Marsh, W. Hoyer, D. Cherny, M. Zweckstetter, C. Griesinger, T.M. Jovin, C.O. Fernandez, Structural characterization of copper(II) binding to -synuclein: Insights into the bioinorganic chemistry of Parkinson's disease, Proceedings of the National Academy of Sciences. 102 (2005) 4294–4299.

L. Regazzoni, R. Colombo, L. Bertoletti, G. Vistoli, G. Aldini, M. Serra, M. Carini, R.M. Facino, S. Giorgetti, M. Stoppini, G. Caccialanza, E. De Lorenzi, Screening of fibrillogenesis inhibitors of β2-microglobulin: Integrated strategies by mass spectrometry capillary electrophoresis and in silico simulations, Analytica Chimica Acta. 685 (2011) 153–161.

E. Rennella, A. Corazza, S. Giorgetti, F. Fogolari, P. Viglino, R. Porcari, L. Verga, M. Stoppini, V. Bellotti, G. Esposito, Folding and Fibrillogenesis: Clues from β2-Microglobulin, Journal of Molecular Biology. 401 (2010) 286–297.

H.E. Revercomb, E.A. Mason, Theory of plasma chromatography/gaseous electrophoresis. Review, Analytical Chemistry. 47 (1975) 970–983.

C.V. Robinson, E.W. Chung, B.B. Kragelund, J. Knudsen, R.T. Aplin, F.M. Poulsen, C.M. Dobson, Probing the Nature of Noncovalent Interactions by Mass Spectrometry. A Study of Protein−CoA Ligand Binding and Assembly, Journal of the American Chemical Society. 118 (1996) 8646–8653.

B.T. Ruotolo, K. Giles, I. Campuzano, A.M. Sandercock, R.H. Bateman, C.V Robinson, Evidence for Macromolecular Protein Rings in the Absence of Bulk Water, Science. 310 (2005) 1658–1661.

B.T. Ruotolo, S.-J. Hyung, P.M. Robinson, K. Giles, R.H. Bateman, C.V. Robinson, Ion Mobility–Mass Spectrometry Reveals Long-Lived, Unfolded Intermediates in the Dissociation of Protein Complexes, Angewandte Chemie International Edition. 46 (2007) 8001–8004.

B.T. Ruotolo, J.L.P. Benesch, A.M. Sandercock, S.-J. Hyung, C.V. Robinson, Ion mobility–mass spectrometry analysis of large protein complexes, Nature Protocols. 3 (2008) 1139–1152.

Ruysschaert, J.M., Raussens, V., ATR-FTIR Analysis of Amyloid Proteins, Methods in Molecular Biology. 1777 (2018) 69–81.

K. Saeki, S. Hayakawa, S. Nakano, S. Ito, Y. Oishi, Y. Suzuki, M. Isemura, In Vitro and In Silico Studies of the Molecular Interactions of Epigallocatechin-3-O-gallate (EGCG) with Proteins That Explain the Health Benefits of Green Tea, Molecules. 23 (2018) 1295.

M. Sakono, T. Zako, Amyloid oligomers: formation and toxicity of Aβ oligomers: Formation of toxic Aβ oligomers, FEBS Journal. 277 (2010) 1348–1358.

C.J. Sarell, S.R. Wilkinson, J.H. Viles, Substoichiometric Levels of Cu $^{2+}$ Ions Accelerate the Kinetics of Fiber Formation and Promote Cell Toxicity of Amyloid-β from Alzheimer Disease, Journal of Biological Chemistry. 285 (2010) 41533–41540.

K. Sasahara, H. Yagi, H. Naiki, Y. Goto, Heat-induced Conversion of β2-Microglobulin and Hen Egg-white Lysozyme into Amyloid Fibrils, Journal of Molecular Biology. 372 (2007) 981–991.

C.A. Scarff, V.J. Patel, K. Thalassinos, J.H. Scrivens, Probing hemoglobin structure by means of traveling-wave ion mobility mass spectrometry, Journal of the American Society for Mass Spectrometry. 20 (2009) 625–631.

R. Scarpioni, M. Ricardi, V. Albertazzi, S. De Amicis, F. Rastelli, L. Zerbini, Dialysis-related amyloidosis: challenges and solutions, International Journal of Nephrology and Renovascular Disease. Volume 9 (2016) 319–328.

C. Scavenius, S. Ghodke, D.E. Otzen, J.J. Enghild, Hydrogen exchange mass spectrometry as an analytical tool for the analysis of amyloid fibrillogenesis, International Journal of Mass Spectrometry. 302 (2011) 167–173.

B.L. Schwartz, J.E. Bruce, G.A. Anderson, S.A. Hofstadler, A.L. Rockwood, R.D. Smith, A. Chilkoti, P.S. Stayton, Dissociation of tetrameric ions of noncovalent streptavidin complexes formed by electrospray ionization, Journal of the American Society for Mass Spectrometry. 6 (1995) 459–465.

U. Sengupta, A.N. Nilson, R. Kayed, The Role of Amyloid-β Oligomers in Toxicity, Propagation, and Immunotherapy, EBioMedicine. 6 (2016) 42–49.

J. Seo, W. Hoffmann, S. Warnke, M.T. Bowers, K. Pagel, G. von Helden, Retention of Native Protein Structures in the Absence of Solvent: A Coupled Ion Mobility and

Spectroscopic Study, Angewandte Chemie International Edition. 55 (2016) 14173–14176.

J. Seo, W. Hoffmann, S. Warnke, X. Huang, S. Gewinner, W. Schöllkopf, M.T. Bowers, G. von Helden, K. Pagel, An infrared spectroscopy approach to follow β-sheet formation in peptide amyloid assemblies, Nature Chemistry. 9 (2017) 39–44.

B. Serra-Vidal, L. Pujadas, D. Rossi, E. Soriano, S. Madurga, N. Carulla, Hydrogen/Deuterium Exchange-Protected Oligomers Populated during Aβ Fibril Formation Correlate with Neuronal Cell Death, ACS Chemical Biology. 9 (2014) 2678–2685.

M. Shahnawaz, C. Soto, Microcin Amyloid Fibrils A Are Reservoir of Toxic Oligomeric Species, Journal of Biological Chemistry. 287 (2012) 11665–11676.

N. Shanmugam, M.O.D.G. Baker, S.R. Ball, M. Steain, C.L.L. Pham, M. Sunde, Microbial functional amyloids serve diverse purposes for structure, adhesion and defence, Biophysical Reviews. 11 (2019) 287-302.

T. Sheynis, A. Friediger, W.-F. Xue, A.L. Hellewell, K.W. Tipping, E.W. Hewitt, S.E. Radford, R. Jelinek, Aggregation Modulators Interfere with Membrane Interactions of β2-Microglobulin Fibrils, Biophysical Journal. 105 (2013) 745–755.

A.A. Shvartsburg, R.D. Smith, Fundamentals of Traveling Wave Ion Mobility Spectrometry, Analytical Chemistry. 80 (2008) 9689–9699.

B.N. Singh, S. Shankar, R.K. Srivastava, Green tea catechin, epigallocatechin-3-gallate (EGCG): Mechanisms, perspectives and clinical applications, Biochemical Pharmacology. 82 (2011) 1807–1821.

D.P. Smith, T.W. Knapman, I. Campuzano, R.W. Malham, J.T. Berryman, S.E. Radford, A.E. Ashcroft, Deciphering Drift Time Measurements from Travelling Wave Ion Mobility Spectrometry-Mass Spectrometry Studies, European Journal of Mass Spectrometry. 15 (2009) 113–130.

D.P. Smith, S.E. Radford, A.E. Ashcroft, Elongated oligomers in β2-microglobulin amyloid assembly revealed by ion mobility spectrometry-mass spectrometry, Journal of the American Chemical Society. 136 (2010) 5432–5442.

D.P. Smith, L.A. Woods, S.E. Radford, A.E. Ashcroft, Structure and Dynamics of Oligomeric Intermediates in β2-Microglobulin Self-Assembly, Biophysical Journal. 101 (2011) 1238–1247.

D.D. Soto-Ortega, B.P. Murphy, F.J. Gonzalez-Velasquez, K.A. Wilson, F. Xie, Q. Wang, M.A. Moss, Inhibition of amyloid-β aggregation by coumarin analogs can

be manipulated by functionalization of the aromatic center, Bioorganic & Medicinal Chemistry. 19 (2011) 2596–2602.

R. Srikanth, V.L. Mendoza, J.D. Bridgewater, G. Zhang, R.W. Vachet, Copper Binding to β-2-Microglobulin and Its Pre-Amyloid Oligomers, Biochemistry. 48 (2009) 9871–9881.

M. Stefani, Structural features and cytotoxicity of amyloid oligomers: Implications in Alzheimer's disease and other diseases with amyloid deposits, Progress in Neurobiology. 99 (2012) 226–245.

J.C. Stroud, C. Liu, P.K. Teng, D. Eisenberg, Toxic fibrillar oligomers of amyloid-B have cross-B structure, Proceedings of the National Academy of Sciences. 109 (2012) 7717–7722.

S. Sudhakar, E. Mani, Rapid dissolution of amyloid β fibrils by silver nanoplates, Langmuir. 35 (2019) 6962-6970.

A.I. Sulatskaya, A.V. Lavysh, A.A. Maskevich, I.M. Kuznetsova, K.K. Turoverov, Thioflavin T fluoresces as excimer in highly concentrated aqueous solutions and as monomer being incorporated in amyloid fibrils, Scientific Reports. 7 (2017) 2146.

Y. Sun, S. Vahidi, M.A. Sowole, L. Konermann, Protein Structural Studies by Traveling Wave Ion Mobility Spectrometry: A Critical Look at Electrospray Sources and Calibration Issues, Journal of The American Society for Mass Spectrometry. 27 (2016) 31–40.

H. Tachibana, K. Koga, Y. Fujimura, K. Yamada, A receptor for green tea polyphenol EGCG, Nature Structural & Molecular Biology. 11 (2004) 380–381.

T. Takahashi, S. Nagatoishi, D. Kuroda, K. Tsumoto, Thermodynamic and computational analyses reveal the functional roles of the galloyl group of tea catechins in molecular recognition, PLOS ONE. 13 (2018) e0204856.

T. Tanaka, T. Ishii, D. Mizuno, T. Mori, R. Yamaji, Y. Nakamura, S. Kumazawa, T. Nakayama, M. Akagawa, (−)-Epigallocatechin-3-gallate suppresses growth of AZ521 human gastric cancer cells by targeting the DEAD-box RNA helicase p68, Free Radical Biology and Medicine. 50 (2011) 1324–1335.

W.M. Tay, D. Huang, T.L. Rosenberry, A.K. Paravastu, The Alzheimer's Amyloid-β(1–42) Peptide Forms Off-Pathway Oligomers and Fibrils That Are Distinguished Structurally by Intermolecular Organization, Journal of Molecular Biology. 425 (2013) 2494–2508.

Y. Tian, L. Han, A.C. Buckner, B.T. Ruotolo, Collision Induced Unfolding of Intact Antibodies: Rapid Characterization of Disulfide Bonding Patterns, Glycosylation, and Structures, Analytical Chemistry. 87 (2015) 11509–11515.

T. Tomiyama, A. Shoji, K. Kataoka, Y. Suwa, S. Asano, H. Kaneko, N. Endo, Inhibition of Amyloid Protein Aggregation and Neurotoxicity by Rifampicin: its possible function as a hydroxyl radical scavenger, Journal of Biological Chemistry. 271 (1996) 6839–6844.

B.H. Toyama, J.S. Weissman, Amyloid Structure: Conformational Diversity and Consequences, Annual Review of Biochemistry. 80 (2011) 557–585.

R. Tycko, Amyloid Polymorphism: Structural Basis and Neurobiological Relevance, Neuron. 86 (2015) 632–645.

R. Tycko, Physical and structural basis for polymorphism in amyloid fibrils: Amyloid Polymorphism, Protein Science. 23 (2014) 1528–1539.

R. Tycko, R.B. Wickner, Molecular Structures of Amyloid and Prion Fibrils: Consensus versus Controversy, Accounts of Chemical Research. 46 (2013) 1487–1496.

S. Vahidi, B.B. Stocks, L. Konermann, Partially Disordered Proteins Studied by Ion Mobility-Mass Spectrometry: Implications for the Preservation of Solution Phase Structure in the Gas Phase, Analytical Chemistry. 85 (2013) 10471–10478.

T.E. Wales, J.R. Engen, Hydrogen exchange mass spectrometry for the analysis of protein dynamics, Mass Spectrometry Reviews. 25 (2006) 158–170.

M.A. Wälti, J. Steiner, F. Meng, H.S. Chung, J.M. Louis, R. Ghirlando, V. Tugarinov, A. Nath, G.M. Clore, Probing the mechanism of inhibition of amyloid-β(1–42)–induced neurotoxicity by the chaperonin GroEL, Proceedings of the National Academy of Sciences. 115 (2018) E11924–E11932.

F. Wang, X. Tang, Conformational Heterogeneity and Stability of Apomyoglobin Studied by Hydrogen/Deuterium Exchange and Electrospray Ionization Mass Spectrometry, Biochemistry. 35 (1996) 4069–4078.

J.M. Wells, S.A. McLuckey, Collision-Induced Dissociation (CID) of Peptides and Proteins, in: Methods in Enzymology, Elsevier, 2005: pp. 148–185.

D.M. Williams, T.L. Pukala, Novel insights into protein misfolding diseases revealed by ion mobility-mass spectrometry, Mass Spectrometry Reviews. 32 (2013) 169–187.

L.S. Wolfe, M.F. Calabrese, A. Nath, D.V. Blaho, A.D. Miranker, Y. Xiong, Protein-induced photophysical changes to the amyloid indicator dye thioflavin T, Proceedings of the National Academy of Sciences. 107 (2010) 16863–16868.

L.A. Woods, G.W. Platt, A.L. Hellewell, E.W. Hewitt, S.W. Homans, A.E. Ashcroft, S.E. Radford, Ligand binding to distinct states diverts aggregation of an amyloid-forming protein, Nature Chemical Biology. 7 (2011) 730–739.

L.A. Woods, S.E. Radford, A.E. Ashcroft, Advances in ion mobility spectrometry–mass spectrometry reveal key insights into amyloid assembly, Biochimica et Biophysica Acta (BBA) - Proteins and Proteomics. 1834 (2013) 1257–1268.

L.M. Young, J.C. Saunders, R.A. Mahood, C.H. Revill, R.J. Foster, L.-H. Tu, D.P. Raleigh, S.E. Radford, A.E. Ashcroft, Screening and classifying small-molecule inhibitors of amyloid formation using ion mobility spectrometry–mass spectrometry, Nature Chemistry. 7 (2015) 73–81.

R. Zhao, M. So, H. Maat, N.J. Ray, F. Arisaka, Y. Goto, J.A. Carver, D. Hall, Measurement of amyloid formation by turbidity assay—seeing through the cloud, Biophysical Reviews. 8 (2016) 445–471.

T.O. Zhang, A.M. Alperstein, M.T. Zanni, Amyloid β-Sheet Secondary Structure Identified in UV-Induced Cataracts of Porcine Lenses using 2D IR Spectroscopy, Journal of Molecular Biology. 429 (2017) 1705–1721.

Y. Zhang, D.L. Rempel, J. Zhang, A.K. Sharma, L.M. Mirica, M.L. Gross, Pulsed hydrogen–deuterium exchange mass spectrometry probes conformational changes in amyloid beta (Aβ) peptide aggregation, Proceedings of the National Academy of Sciences. 110 (2013) 14604–14609.

T. Zhang, J. Zhang, P. Derreumaux, Y. Mu, Molecular Mechanism of the Inhibition of EGCG on the Alzheimer Aβ $_{1-42}$ Dimer, The Journal of Physical Chemistry B. 117 (2013) 3993–4002.

Y. Zhong, L. Han, B.T. Ruotolo, Collisional and Coulombic Unfolding of Gas-Phase Proteins: High Correlation to Their Domain Structures in Solution, Angewandte Chemie International Edition. 53 (2014) 9209–9212.

B. Zhou, Z.-Y. Zhang, Application of hydrogen/deuterium exchange mass spectrometry to study protein tyrosine phosphatase dynamics, ligand binding, and substrate specificity, Methods. 42 (2007) 227–233.

S. Zhu, A. Shala, A. Bezginov, A. Sljoka, G. Audette, D.J. Wilson, Hyperphosphorylation of Intrinsically Disordered Tau Protein Induces an Amyloidogenic Shift in Its Conformational Ensemble, PLOS ONE. 10 (2015) e0120416.